N O T I C E

THIS DOCUMENT HAS BEEN REPRODUCED FROM MICROFICHE. ALTHOUGH IT IS RECOGNIZED THAT CERTAIN PORTIONS ARE ILLEGIBLE, IT IS BEING RELEASED IN THE INTEREST OF MAKING AVAILABLE AS MUCH INFORMATION AS POSSIBLE

NASA CR-159699

National Aeronautics and
Space Administration

CF6 JET ENGINE PERFORMANCE IMPROVEMENT - NEW FAN

by

W.A. Fasching

GENERAL ELECTRIC COMPANY

(NASA-CR-159699) CF6 JET ENGINE PERFORMANCE IMPROVEMENT: NEW FAN (General Electric Co.) 202 p HC A10/MF A01 CSCL 21E

N80-23309

Unclas
G3/07 19330

Prepared For

National Aeronautics and Space Administration

NASA Lewis Research Center
Contract NAS3-20629

MAY 1980
RECEIVED
NASA STI FACILITY
ACCESS DEPT.

FOREWORD

The work was performed by the CF6 Engineering Department of General Electric's Aircraft Engine Group, Aircraft Engine Engineering Division, Cincinnti, Ohio. The program was conducted for the National Aeronautics and Space Administration, Lewis Research Center, Cleveland, Ohio, under Subtask 2.1 of the CF6 Jet Engine Performance Improvement Program, Contract Number NAS3-20629. The Performance Improvement Program is part of the Engine Component Improvement (ECI) Project, which is part of the NASA Aircraft Energy Efficiency (ACEE) Program. The NASA Project Engineer for the New Fan Program was D.C. Reemsnyder. The program was initiated in August 1977 and completed in May 1979.

The report was prepared by W.A. Fasching, General Electric Program Manager, with the assistance of D.B. Eastep, J.L. Gross, F.J. Klaus, H.J. Macke, D.G. Salyards, B.E. Safriet, M.L. Miller and R.M. Strock.

PRECEDING PAGE BLANK NOT FILMED

TABLE OF CONTENTS

PRECEDING PAGE BLANK NOT FILMED

TABLE OF CONTENTS (Concluded)

1.0 SUMMARY

As part of the NASA-sponsored Engine Component Improvement (ECI) Program, a new fan package has been developed to reduce fuel consumption of current CF6 turbofan engines for today's wide-bodied commercial aircraft. The new fan package consists of a modified fan blade, reduced fan tip clearance due to a fan case stiffener, and a smooth casing tip shroud (microballoon epoxy in open-cell aluminum honeycomb). The new CF6 Fan Program included full scale engine and component testing and monitoring of aircraft flight tests. Full scale CF6-50 engine testing included back-to-back performance and acoustic tests, a power management test, a crosswind test, and a cyclic endurance test. Component tests consisted of a model fan rotor photoelastic stress test and a full-size fan blade bench fatigue test.

Back-to-back sea level and simulated altitude engine performance tests demonstrated the predicted improvement in altitude cruise specific fuel consumption (sfc) of 1.8% for the improved fan compared to the original fan. Subsequent sea level production engine and aircraft flight tests confirmed this cruise sfc improvement. Based on this demonstrated cruise sfc improvement of 1.8%, a 2.0% block fuel saving per aircraft is projected for a new CF6 engine with the improved fan for the longest U.S. domestic and international missions. The improved fan offers an annual fuel savings per aircraft up to 1.37 million liters (0.36 million gallons).

Back-to-back engine acoustic tests established that the improved and original fans will have comparable community noise exposure. The FAA has accepted the acoustic equivalency of the improved and original CF6 fans. The improved fan has a significant reduction in multiple pure tones (buzz saw noise) compared to the original fan which should significantly reduce aircraft passenger compartment noise levels during aircraft takeoff and initial climbout.

Power management tests of the CF6-50 engine with the improved fan defined the fan speed/engine thrust relationship for the DC-10-30, B747-200, and A300B aircraft. Full scale fan nozzle thrust and flow coefficients were determined from instrumented engine ground tests and correlated with aircraft flight tests.

Several component and engine tests were conducted to confirm the structural integrity of the improved fan. Component photoelastic and blade bench fatigue tests demonstrated that the stresses and fatigue margins of the improved fan blade are similar to the original CF6 fan blade. Engine crosswind testing demonstrated that the improved fan blade has similar crosswind/distortion characteristics to the original blade. The improved fan operated successfully without exceeding vibratory stress limits with both the DC-10-30 and Boeing 747-200 inlets at allowable takeoff crosswinds up to 35 knots. A previous bird ingestion engine test demonstrated that the improved fan blade is as rugged as the original CF6 fan blade. Fan tip rub button tests indicated that the fan case stiffener provided a significant improvement in fan casing roundness compared to the unstiffened case. This permits reduced operating fan tip clearances and improved fan efficiency.

The CF6-50 engine cyclic endurance test demonstrated a basic life capability of the improved fan blade and the fan case stiffener in over 1000 simulated flight cycles without any sign of distress. A separate blade/shroud interaction rub test indicated no evidence of blade and casing interaction due to heavy rubs into the smooth microballoon casing tip shroud material.

Aircraft flight tests with the improved fan were considered. The improved fan has been certified by the FAA for use in the CF6-50C2/E2 engines and is now in commercial service on the Boeing 747-200, Douglas DC-10-30, and Airbus Industrie A300B aircraft. The improved fan will also be incorporated in the CF6-6D2C and -6K engines, and provides a basis for performance improvement in the CF6-80 and -32 engines. The improved fan will make a very substantial contribution to reduced fuel consumption in commercial aviation through the balance of the century.

2.0 INTRODUCTION

National energy demand has outpaced domestic supply creating an increased U.S. dependence on foreign oil. This increased dependence was dramatized by the OPEC oil embargo in the winter of 1973 to 1974. In addition, the embargo triggered a rapid rise in the cost of fuel which, along with the potential of further increases, brought about a changing economic circumstance with regard to the use of energy. These events, of course, were felt in the air transport industry as well as other forms of transportation. As a result of these experiences, the Government, with the support of the aviation industry, has initiated programs aimed at both the supply and demand aspects of the problem. The supply problem is being investigated by looking at increasing fuel availability from such sources as coal and oil shale. Efforts are currently underway to develop engine combustor and fuel systems that will accept fuels with broader specifications.

Reduced fuel consumption is the other approach to deal with the overall problem. A long-range effort to reduce fuel consumption is to evolve new technology which will permit development of a more energy efficient turbofan or the use a different propulsive cycle, such as a turboprop. Although studies have indicted large reductions in fuel usage are possible (e.g., 15% to 40%), any significant impact of this approach is at least 15 years away. In the near term, the only practical propulsion approach is to improve the fuel efficiency of current engines. Examination of this approach has indicated that a 5% fuel reduction goal starting in the 1980 to 1982 time period is feasible for a current commercial engines. These engines will continue to be significant fuel users for the next 15 to 20 years.

Accordingly, NASA is sponsoring the Aircraft Energy Efficient (ACEE) Program (based on a congressional request) which is directed at reduced fuel consumption of commercial air transports. The Engine Component Improvement (ECI) Program is the element of the ACEE Program directed at reducing fuel consumption of current commercial aircraft engines. The ECI Program consists of two parts: engine diagnostics and performance improvement. The engine diagnostics effort is to provide information to identify the sources and causes of engine deterioration. The performance improvement effort is directed at developing engine components having performance improvement and retention characteristics which can be incorporated into new production and existing engines.

The performance improvement effort was initiated with a feasibility analysis which identified performance improvement concepts and then assessed the technical and economic merits of these concepts. This assessment included a determination of airline acceptability, the probability of introducing the concepts into production by the 1980 to 1982 time period, and their retrofit potential. The study was conducted in cooperation with Boeing and Douglas aircraft companies and American and United Airlines, and is reported in Reference 1.

In the feasibility analysis, the new CF6 fan performance improvement concept was selected for development and evaluation because of its fuel savings potential and attractive airline payback period. The objective of the new fan program was to develop technology and to verify the predicted fuel savings by engine ground tests. Inititally, the new fan concept consisted of an improved CF6 fan blade, reduced fan tip clearances due to a new fan case stiffener, and a revised fan operating line change by increasing the fan nozzle area. An improvement in cruise sfc of about 1.8% was estimated due to the new fan on the CF6-50 engine.

The new fan program was a 20-month effort that included model, component, and full scale engine testing. Model fan rotor photoelastic stress tests and full-size fan blade bench fatigue tests were conducted. CF6-50 engine testing included performance, acoustic, power management, crosswind, and cyclic endurance tests of the improved fan, and comparison of results with the original CF6 production fan. Additional GE-funded CF6-50 engine tests, including bird ingestion and performance and aircraft flight tests, were also conducted and are reported herein. An overview of the new fan program is presented in Reference 2.

3.0 INITIAL NEW FAN DESIGN AND TESTING

Initially, the new CF6 fan concept consisted of improved fan blade aerodynamic design, a 1.50 mm (0.060 in.) reduction in fan tip clearance due to a new fan case stiffener and optimization of the fan cruise operating line. Together, these improvement items offered a potential reduction in CF6-50 engine sfc at cruise of 1.8% (Reference 1). This potential sfc reduction is achieved with a modest weight increase of 13 kg (29 lb) and a forward center of gravity shift of 0.8 cm (0.3 in.). A maintenance cost reduction (lower DOC) is projected, resulting from the lower turbine gas temperatures that accompany the improved engine performance. An improvement in cruise sfc of about 1.6% was estimated for the new fan on the CF6-6 engine.

The improvement in aerodynamic performance of the fan has been achieved largely by way of a more forwrad throat location (more camber in the forward portion of airfoil) and aft location of the part-span shroud, resulting in an improvement in the entire chordwise and spanwise efficiency. Reduced fan tip clearances, further improving performance, are achieved by stiffening the fan case. Optimization of the cycle is achieved by adjusting the fan operating line so that it passes through the region of peak efficiency. The total predicted improvement in fan efficiency was 4.7% at cruise-equivalent power which is projected to be a 2.7% sfc improvement at sea level static cruise equivalent power. This translates into the altitude cruise sfc improvement of 1.8%.

3.1 EARLY DESIGN STUDIES

Since the CF6 engine powers the DC-10-10, DC-10-30, B747, and A300B aircraft, it will continue to be a significant fuel user for the next 15 to 20 years. In mid-1975, a GE study was initiated to consider an aerodynamic redesign of the fan blade for the CF6-6 and CF6-50 engines. It was the objective of this study to further fan technology development to significantly improve the performance of these two high bypass ratio engines without compromising structural integrity, maintenance cost, or reliability. The study indicated that the CF6 fan could potentially be improved up to 2.0 points in fan efficiency if the blockage due to the part span shroud could be reduced. The detailed fan aerodynamic and mechanical designs were established; initial bench testing for blade vibratory frequencies, nodal patterns, and stress distributions was performed; fan stress and aerodynamic mapping was done on an actual engine; and initial engine performance improvement was evaluated through CF6-50 back-to-back testing. In addition, rotating rig bird ingestion tests were conducted to establish blade/bird strike integrity.

A cross section of the CF6-50 engine showing the proposed fan performance improvements is presented in Figure 1. The CF6-50 engine has a full diameter, single-stage fan and three low pressure compressor stages which boost the flow into the core engine (Figure 2). These booster stages allow higher thrust

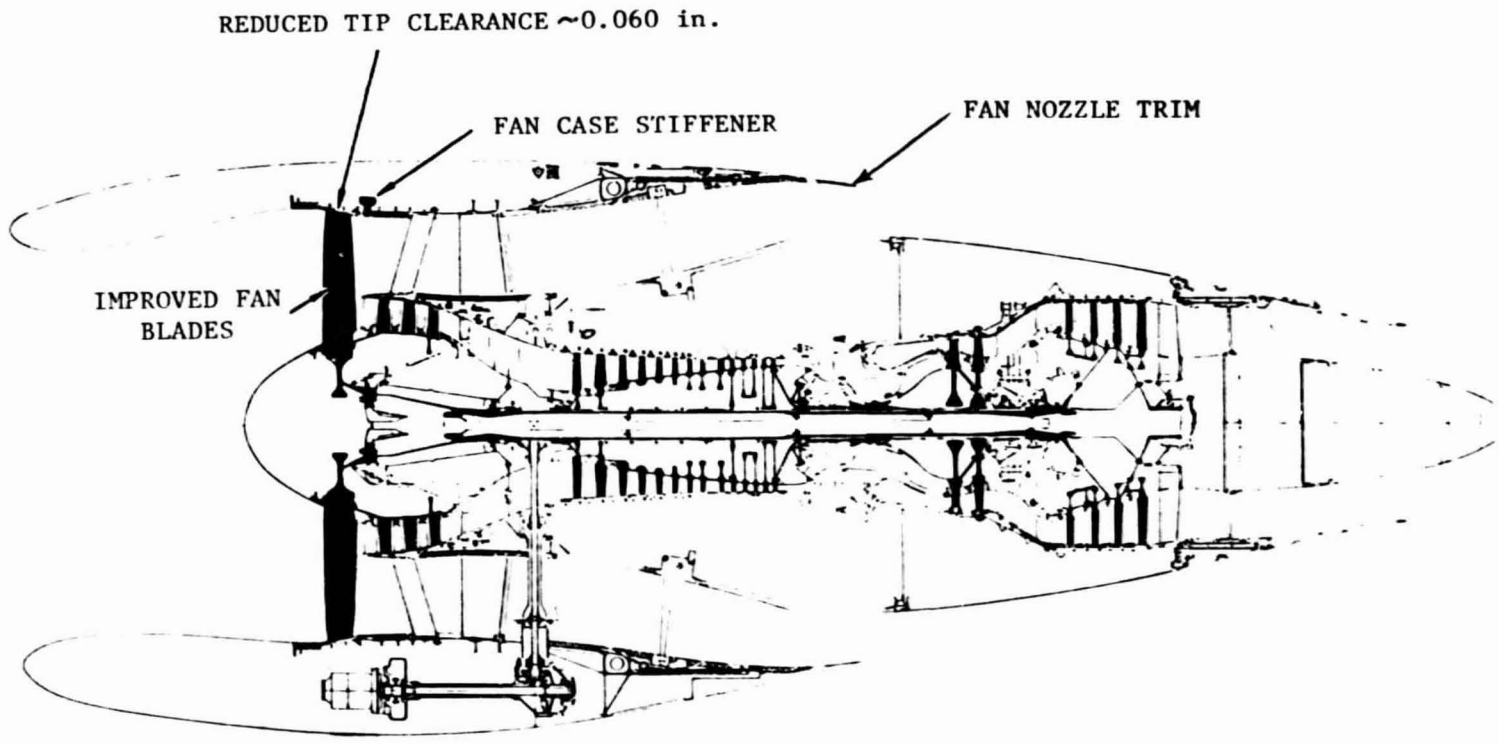

Figure 1. CF6-50 Engine: Initial Fan Performance Improvement Concept.

ORIGINAL PAGE IS
OF POOR QUALITY

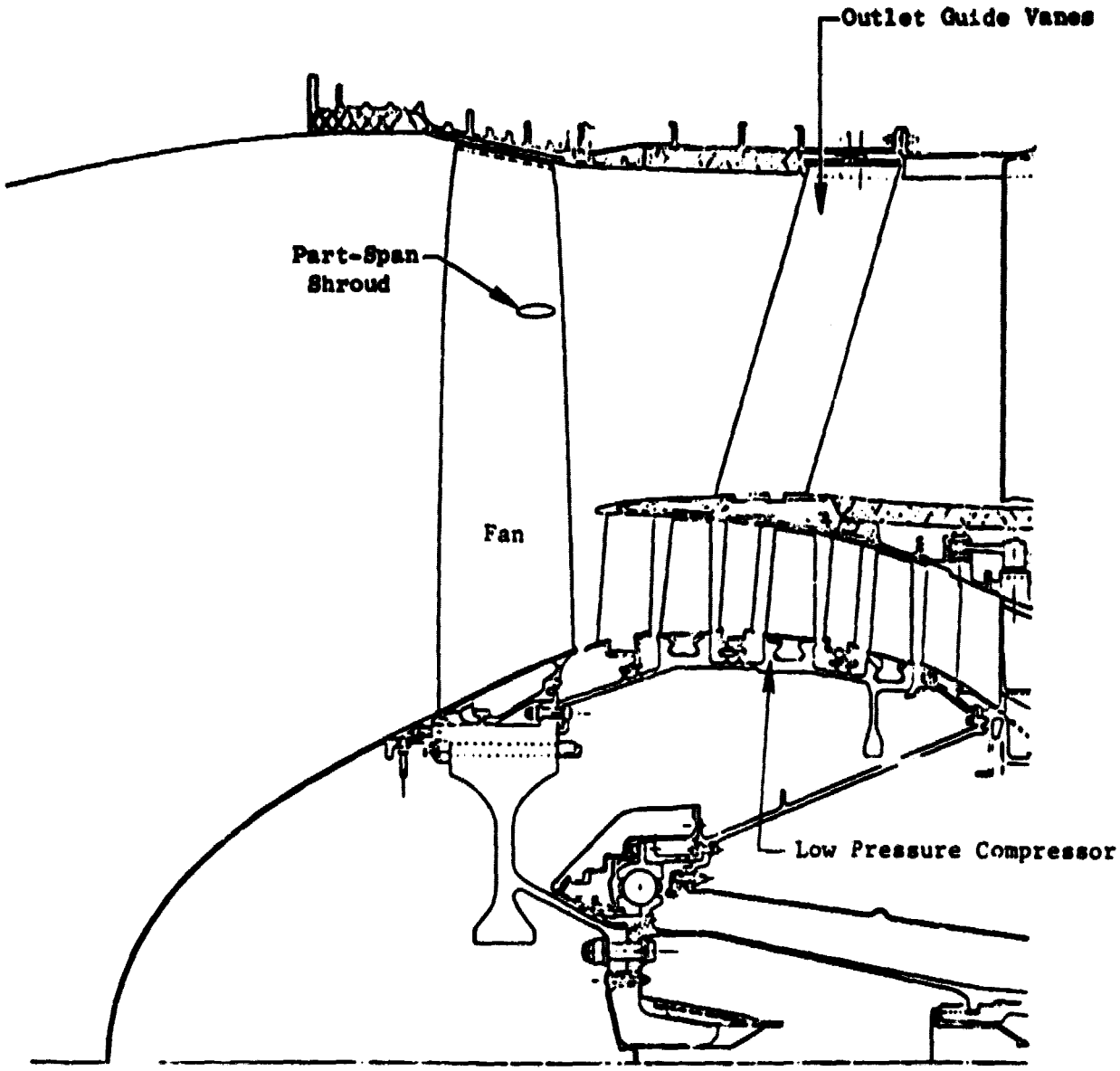

Figure 2. CF6-50 Engine; Fan and Three-stage Low Pressure Compressor.

with minimum overall engine envelope and weight. The lower thrust, CF6-6 engine, Figure 3, consists of a full diameter, single-stage fan followed by a single-stage, low pressure compressor to boost the flow into the core engine.

3.1.1 Fan Aerodynamic Design

An analytical study of the detailed aerodynamic flow characteristics was made of the CF6 fan versus the first stage with part-span shroud of a two-stage NASA fan. This study indicated areas of potential efficiency improvement significantly greater than initially forecast. Procedures were developed which permitted the assessment of spanwise blockage effects on airfoil surfaces (such as the part-span shroud). This assessment revealed that throat margins in the vicinity of the shroud were more subcritical than initially considered. A comparative assessment of the NASA part-span shroud fan blade revealed that throat margins in the shroud vicinity were not subcritical. It was deduced that the NASA design obtained the throat margin in two ways. First, the passage throat was forward relative to the current CF6 fan. A more forward throat location was achieved in the redesign by putting more camber in the forward portion of the airfoil. Second, the part-span shroud was located aft toward the trailing edge of the airfoil resulting in reduced throat blockage. In turn, the leading edge of the shroud operates in a region of lower Mach number flow within the passage. Removal of the subcritical throats from the redesigned fan eliminated the large radial flow shift and permitted the blade to operate as designed. The entire spanwise efficiency level increased with little effect on the shroud wake. Moving the passage throat forward, by putting more camber forward in the airfoil, unloaded the trailing edge and resulted in more effective camber. A photograph of the original production and the improved CF6 fan blade is presented in Figure 4.

In addition to the above redesign considerations, additional camber was put into the airfoil to raise the peak efficiency at pressure ratios corresponding to the current CF6-50 cruise operating level throughout the speed range.

3.1.2 Fan Mechanical Design

The most obvious change in the mechanical design of the improved performance fan blade is the movement of the part-span shroud aft on the airfoil. A comparison of the part-span shrouds for the original and the improved fan blades is shown in Figure 5. Some small but important differences between the two part-span shroud designs are (1) a 41° pressure-face angle with the engine axis for the redesign versus a 39° angle for the original design; this change corresponds with the stagger angle change of the airfoil at its shroud section, and (2) a larger radius blending to airfoil for improved support and increased stiffness for the redesign.

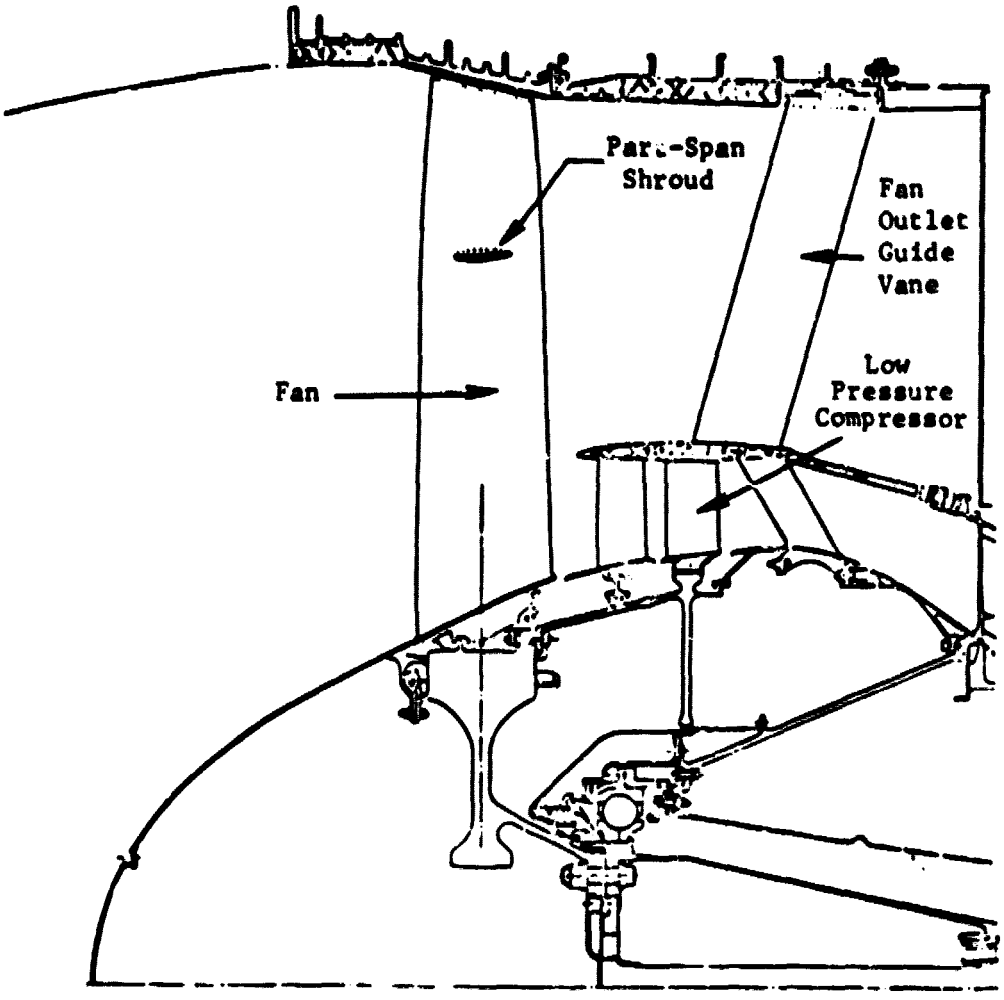

Figure 3. CF6-6 Engine: Fan and Single-Stage Low Pressure Compressor.

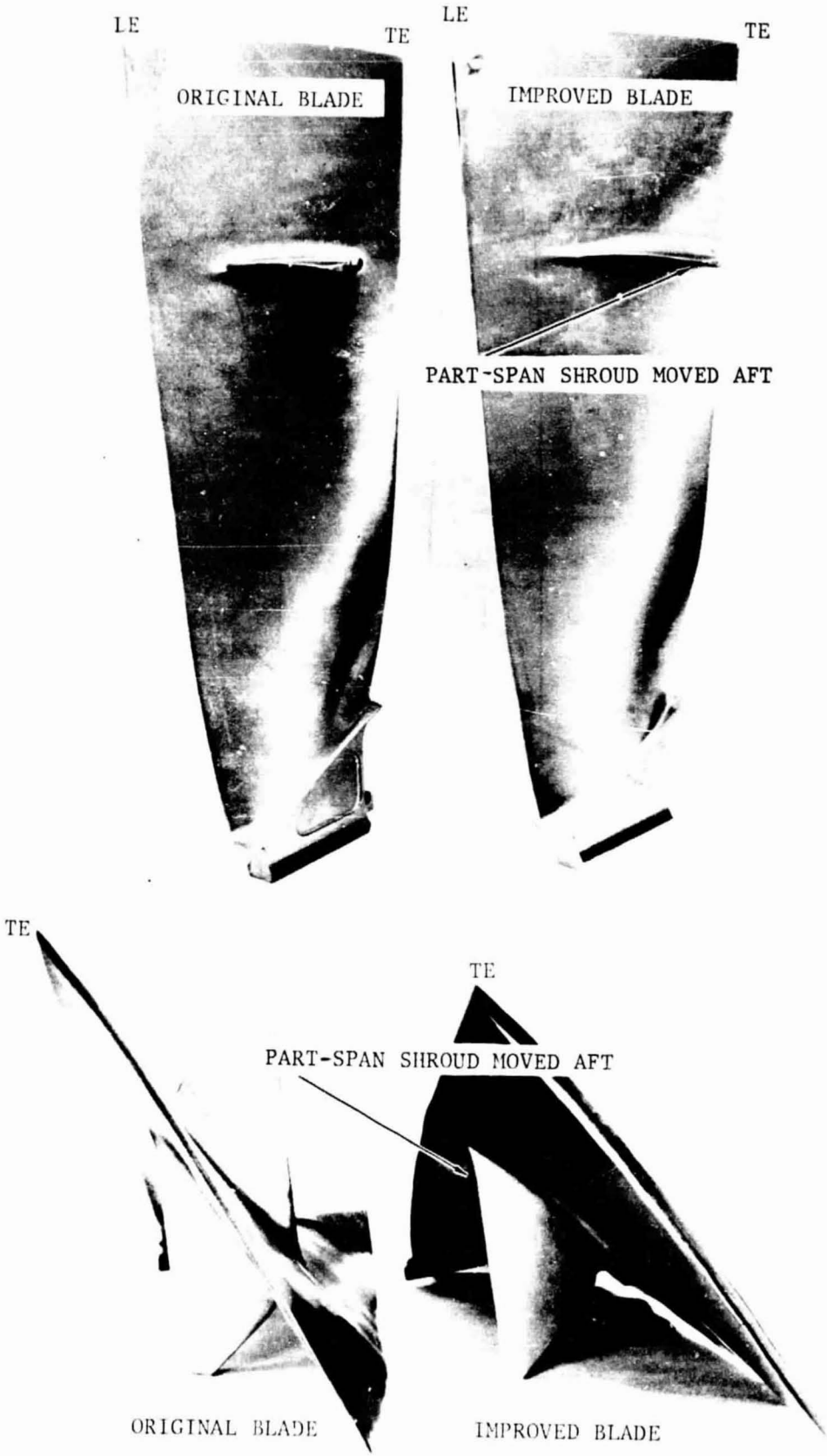

Figure 4. CF6 Original Production and Improved Fan Blades.

ORIGINAL PAGE IS
OF POOR QUALITY

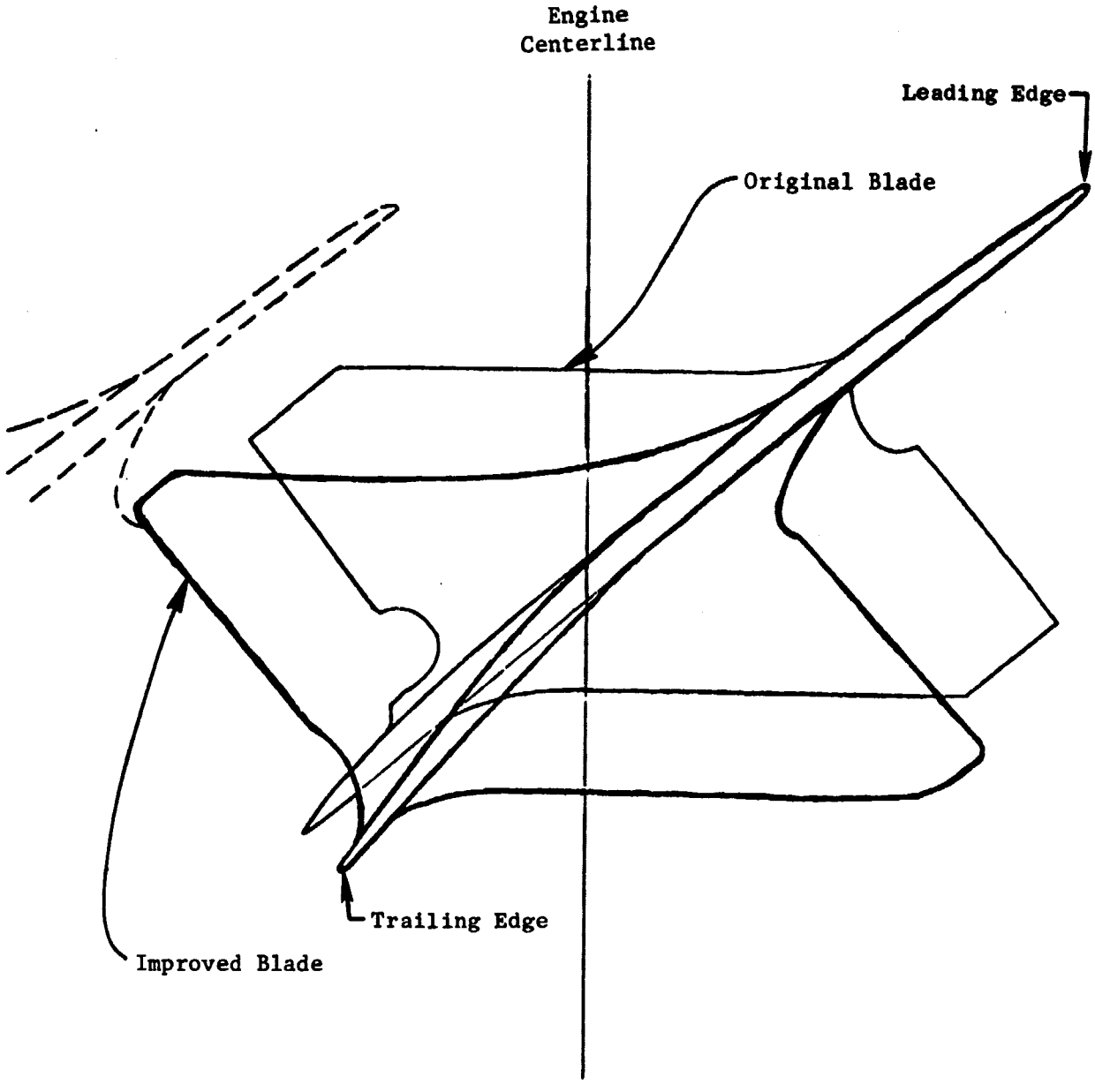

Figure 5. CF6 Fan Blade Part-Span Shroud Comparison.

Other features of the shroud design are nearly identical, such as span location, weight, thickness, and cross-sectional streamline shape.

The original and improved fan blades have identical design chord and thickness, as shown in Figure 6. However, the orientation angle of the chordline (complement of stagger angle) of the improved fan blade is more open over the inner portion of the span and about 1.5° more closed in the outer tip portion, as shown in Figure 7. During the fan performance tests reported herein (Section 7.0), the blade part-span shroud interlocks were subsequently modified (restaggered) to close the running blade stagger angle by about 1.5° at the part-span shroud to fine-tune the fan-engine match.

Camber angle is larger for the redesigned airfoil of the improved fan (as shown in Figure 8) than for the original design. The dovetail is identical for the redesign to facilitate interchangeability by sets and thereby take advantage of the improved performance with minimum hardware change.

3.1.3 Fan Case Stiffener Ring

A clearance reduction between the fan blade tip and casing tip shroud provides potential for further performance improvement. The radial clearance reduction potential relative to original production configuration is 1.5 mm (0.060 in.), based on observation of revenue service hardware and analysis, provided fan casing roundness could be improved. This clearance reduction has a theoretical payoff of 1.1 points in fan efficiency. However, in order to take advantage of this payoff, it was concluded that the fan case must be stiffened to raise the critical interaction frequencies of the fan rotor and fan case above the maximum operating fan speed. These critical interaction points occur at the intersection of the case harmonics with the respective rotor backward traveling wave harmonics as shown in Figure 9. Only the backward-traveling rotor waves are critical in that an excitation rub by the case is a backwards excitation on the rotor relative to its travel direction. The original production configuration avoided these phenomena via sufficient clearances to eliminate rubbing and/or negate the coupling from buildups between the rotor and case.

Figure 9 also shows the case resonant frequencies when the stiffener ring is added. The interaction points are well beyond the maximum fan speed operating range so the fan clearances can be closed down 1.5 mm (0.06 in.) with confidence. These results and the stiffening ring shown in Figure 10 are largely the result of experimental investigations. In parallel with the experimental programs, analytical modeling was also accomplished.

An analytical model of the fan case structural elements was extended to include a wing and tail engine inlet adapter (Figure 11). Boundary conditions which are defined at the frame strut locations include variable axial stiffness based on the fan case mode shape in order to obtain correlation with component test. Good correlation was obtained between analysis and test for the

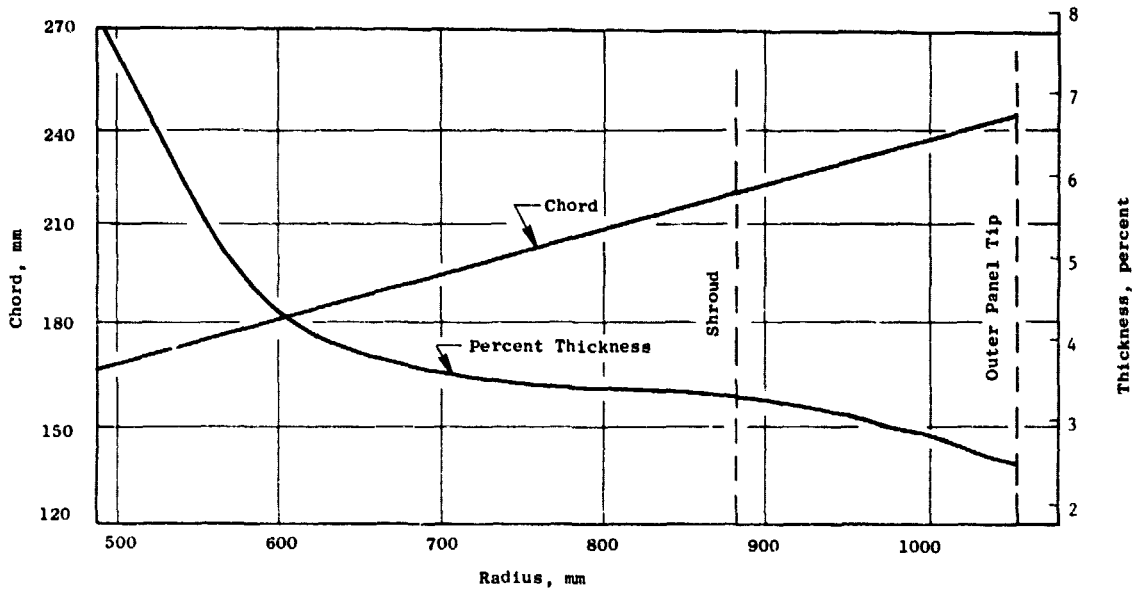

Figure 6. CF6 Original and Improved Fan Blades, Chord and Percent Thickness Radial Distribution.

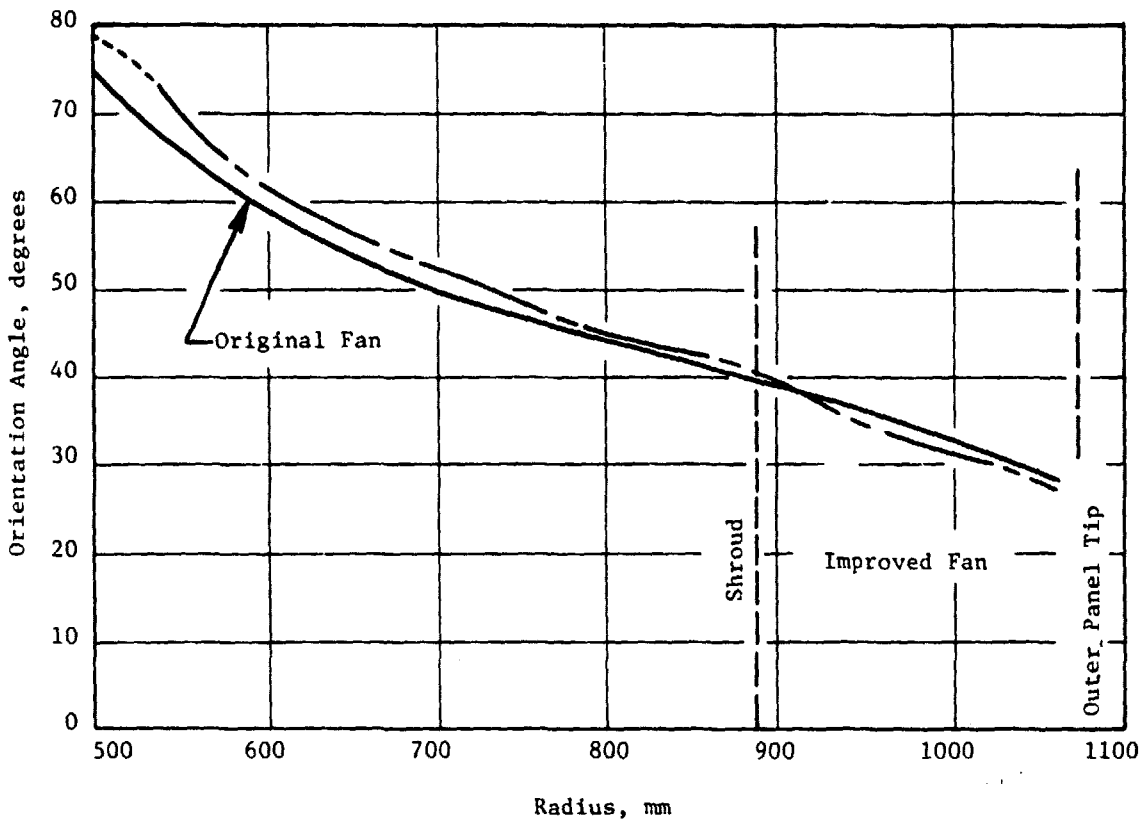

Figure 7. CF6 Original and Improved Fan Blades: Orientation Angle of Chord Line Radial Distribution.

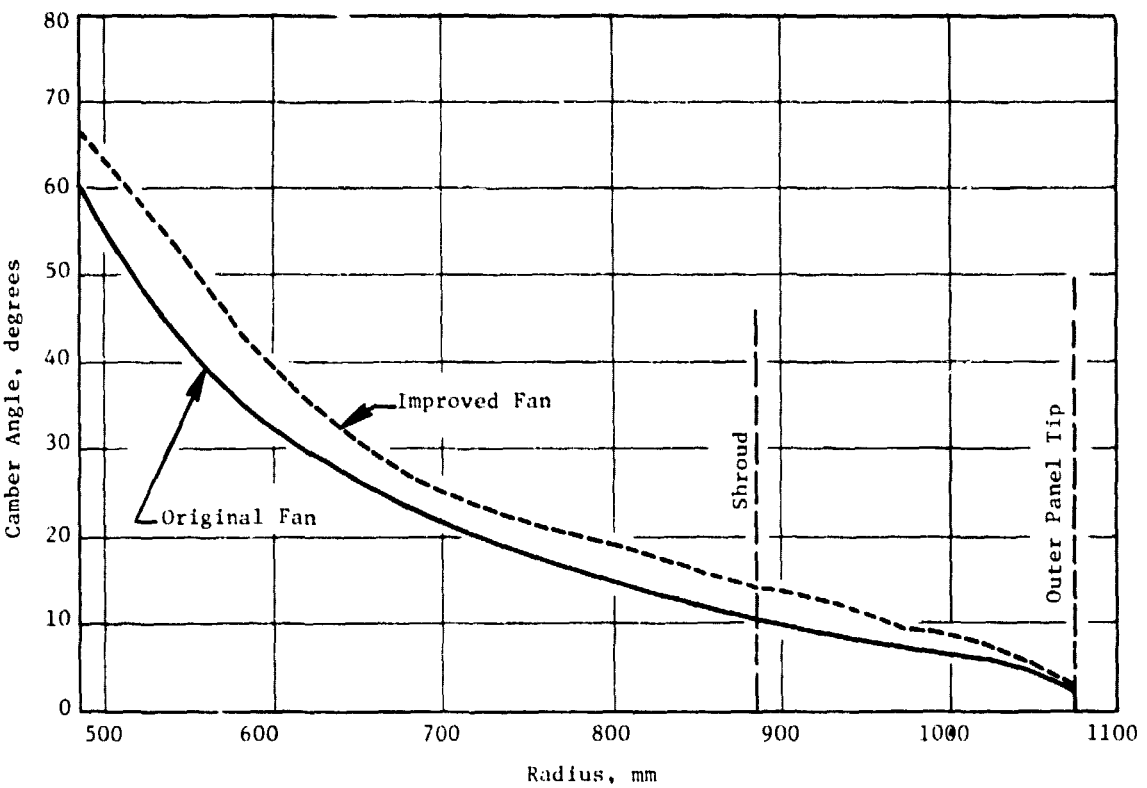

Figure 8. CF6 Original and Improved Fan Blades: Camber Angle Radial Distribution.

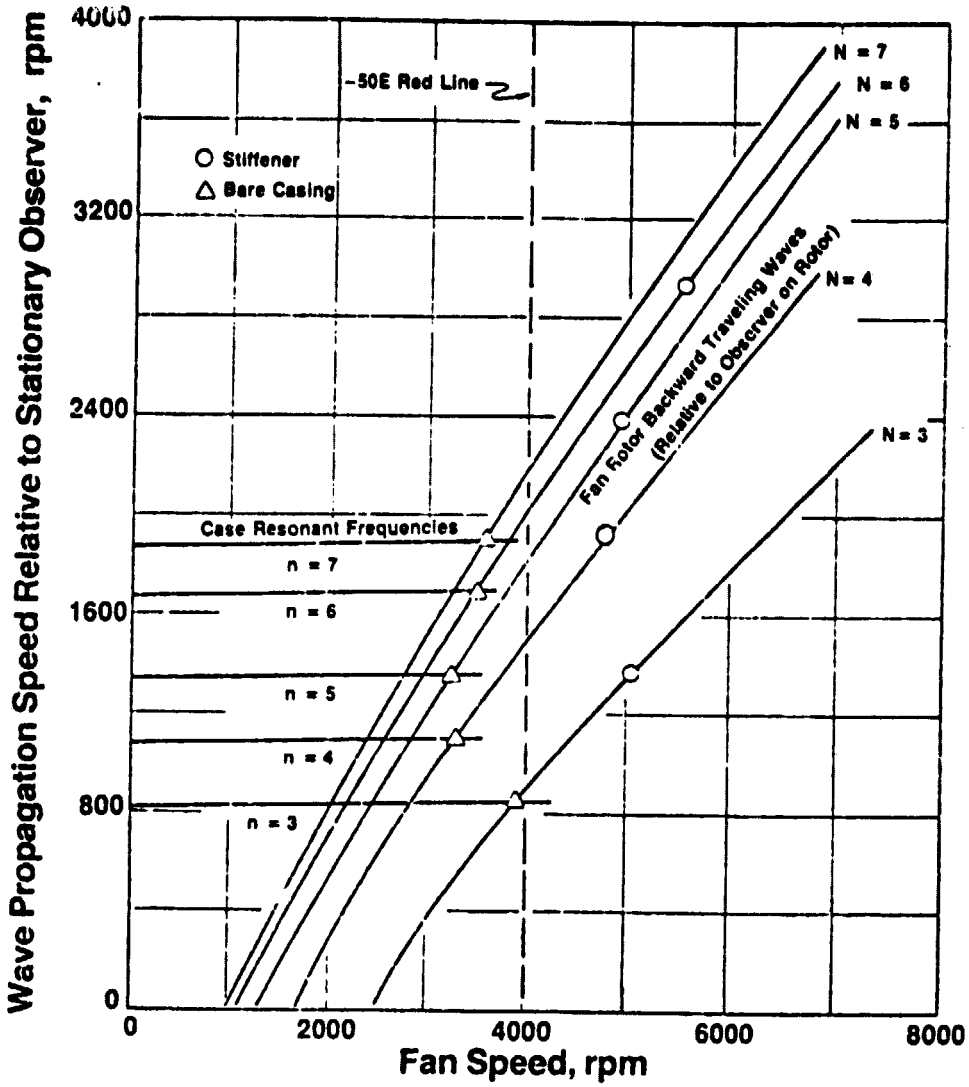

Figure 9. CF6-50 Campbell Diagram, DC-10 Tail Engine.

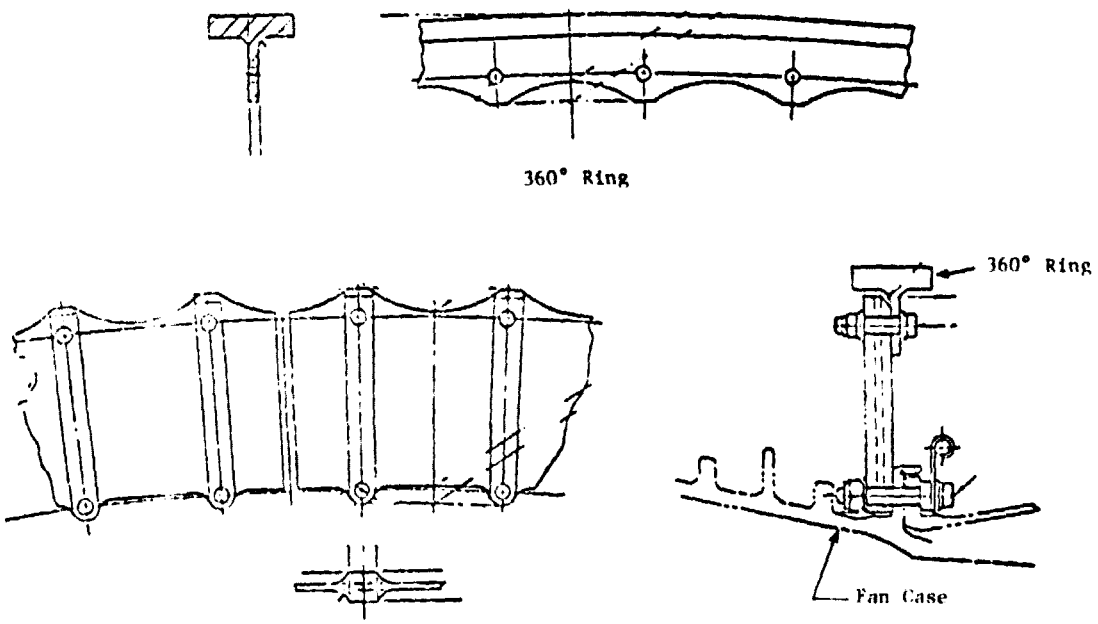

Figure 10. CF6-50 Fan Case Stiffener.

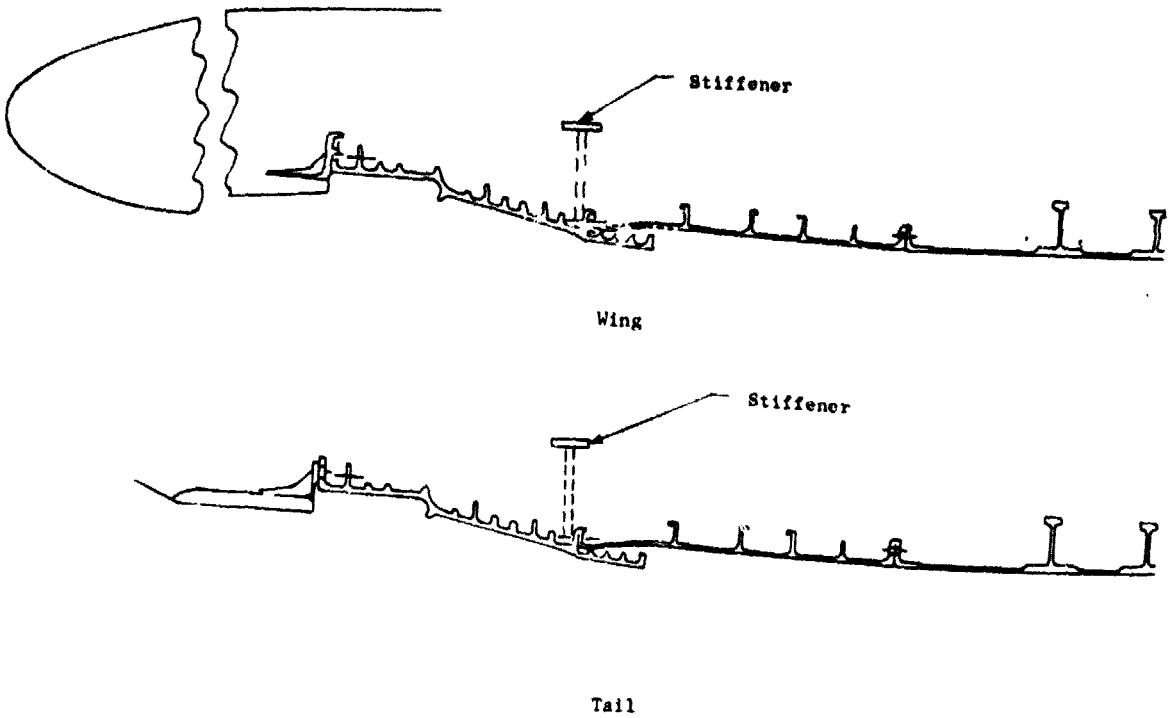

Figure 11. Engine Inlet Adapter.

wing inlet and duct inlet adapters for an unstiffened case configuration. For a stiffened fan case configuration, the correlation was not as consistent between analysis and test for the wing inlet.

The orignial CF6 fan casing tip shroud was open cell aluminum honeycomb. During the performance testing, the tip shrouds were modified by installing microballoon epoxy in the honeycomb and grinding it smooth.

3.1.4 Fan Operating Line

Cycle optimization studies had indicated that the fan operating line of the improved fan would have to be lowered for improved efficiency at cruise operation. This was to be accomplished by trimming the fan nozzle as shown in Figure 12. The performance tests demonstrated that the improvements for an increase in fan exit area are not sufficient to warrant a nozzle area change (see Section 7.7).

3.2 PREVIOUS ENGINE DEVELOPMENT TESTS

Two key requirements for an operationally serviceable fan are the ability to withstand FAA prescribed bird ingestion damage and to function over the full operating range with acceptable vibration stress levels. Analytical design assessment for these two items is very difficult and empirical data are required. Because of the significant development cost and the importance of these two considerations, it was decided to perform an early screening before proceeding into the full fan development program. The first of these efforts was a fan stress mapping test which was performed on the first set of blades prior to the start of the NASA-sponsored program. The second test was a bird ingestion test that was conducted in parallel during the early phase of the NASA-sponsored program. To provide a comprehensive overview of the fan development, these tests are also documented in this report.

3.2.1 Engine Performance and Fan Mapping Test

The fan mapping test was conducted with a CF6-50 engine equipped with the improved fan blades. This engine had an adjustable fan nozzle to control the fan operating line. Aerodynamic instrumentation was utilized forward and aft of the fan stage to measure pressures, airflow rates, and temperatures. Strain gages were also installed at key locations on the fan blade to measure vibratory stress on the airfoil, shroud and shank/dovetail. The fan was operated through the entire speed range at various operating lines up to and including full stall. From this testing, it was possible to define a complete fan map, including the stall line. Stresses measured on all the various operating lines were very similar to stresses measured on the original CF6 fan blade. Aeromechanical performance of the improved fan blade was very similar to the original blade. Two resonant points occurred on both blades at 2500 and 3350 rpm. Vibratory stresses even in resonance are low. The vibratory stress of the fan blade in stall was less than 100% of the infinite life limits. The stall margin of the improved fan blade was within 1% of the stall margin on the original fan blade.

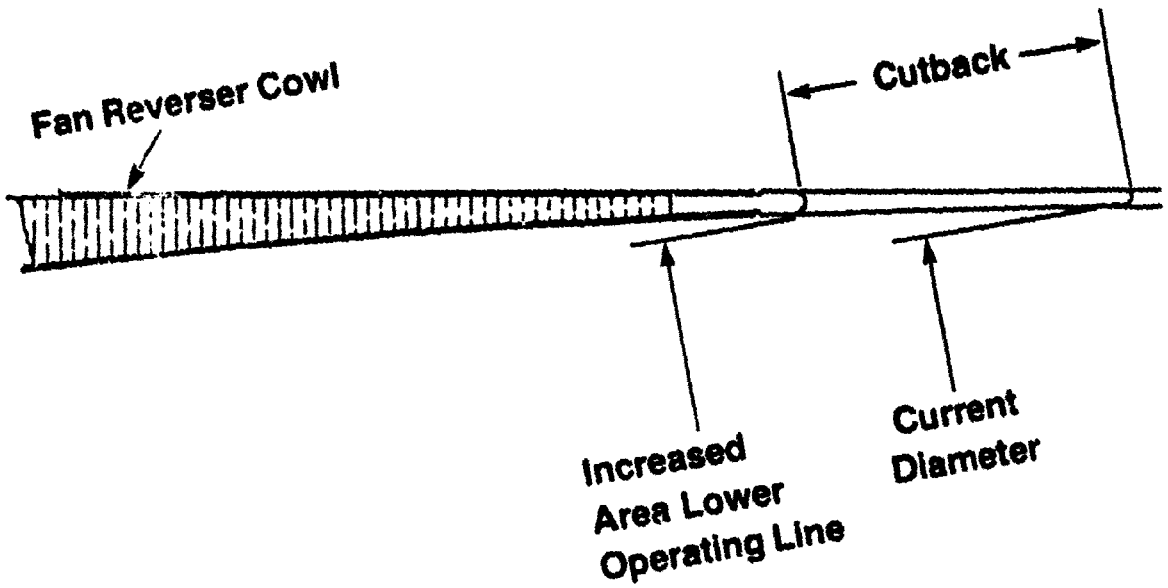

Figure 12. Increased Fan Nozzle Area.

ORIGINAL PAGE IS
OF POOR QUALITY

3.2.2 Bird Ingestion Engine Test

A bird ingestion test with the improved fan blades was conducted to simulate typical bird ingestion incidents that can occur during ground roll or first segment climb. Conditions simulating this condition were set up by using a wind tunnel ahead of the engine to produce a wind velocity of 54.9 m/sec (180 ft/sec). An aircraft inlet was installed on the CF6-50 engine. Three 25.4 cm (10 in.) diameter guns were used to inject a total of eight 0.68 kg (1.5 lb) seagulls into the engine inlet. Two of the birds struck the spinner, four of the birds struck the fan blade at the splitter, and two of the birds struck the outer panel. The guns were placed far enough ahead of the engine to allow the bird to take a natural position with wings spread prior to striking the fan blade. The purpose of this setup was to simulate an encounter with a flock of birds.

After such an ingestion, the engine is required to demonstrate at least 75% of takeoff thrust for 5 minutes. The 75% thrust was demonstrated for 5 minutes, and a higher thrust setting of over 91% thrust was demonstrated additionally. Damage to the fan blades was limited mostly to the outer panel strikes. Bending of the fan blade in-board of the shroud was very small. There was no damage to the spinner, the root of the fan blade, or the booster from the birds that struck the spinner. Unbalance due to the bird strikes was low. There were no cracks or fragmentation of fan blades from the bird strike. Based on the favorable experience, the improved fan blade was concluded to be as rugged or better than the original CF6 fan blade and no design modification was required prior to proceeding through further development.

3.3 DESIGN CONSIDERATIONS

3.3.1 Installation

The fan case stiffener ring was initially installed on a mockup to identify installation interference problems with the aircraft equipment installed in this area of the fan case. Modifications to engine buildup hardware and supporting brackets were identified and fabricated to complete the mockup. The primary interference problems were with the electrical harness routing and modification of brackets and several leads to provide some added length.

The hydraulic system required rework involving tube redesign, lengthened hoses, and bracket redesign, none of which were extensive. Some repositioning of the fuel inlet hose and throttle cable routing was made without rework. Figure 13 shows a typical installation in the area of the fan case stiffener.

3.3.2 Safety

The improved performance fan blade has been designed to operate under the same conditions as the original fan blade. Steady-state and vibratory stress levels throughout the blade, part-span shroud, shank, and dovetail are very

similar for the improved fan blade as for the original fan blade. The same margin of safety has been built into the improved blade as exists for the original blade. The manufacturing process used for the improved blade is the same process as that used for the original blade. Blade materials and the coatings used in the dovetail and the part-span shroud at wear points are the same for both blades.

Factory endurance testing has been completed on the new fan blade simulating airline flight cycles. Factory testing of 2034 cycles and approximately 1000 hours has been completed. All postvisual and fluorescent penetrant inspections of the improved fan blade after engine testing have shown no distress.

Three flight test programs of the improved fan have been completed. These flight tests were conducted by Airbus Industrie on the A300B, by Douglas on the DC-10-30, and by Boeing on the 747-200 aircraft. In all of these programs, the mechanical performance of the fan blade was equivalent to the original fan blade with no distress of any kind.

3.3.3 Reliability

The improved fan blade has been designed to achieve a total useful life with repairs of at least 30,000 hours or 30,000 flight cycles, whichever occurs first. This is the same technical objective used in the design of the original fan blade.

All the maneuver load conditions, such as yaw and pitch velocity, have been used in analyzing the new fan blade. Loads imposed on the blade under these maneuver load conditions are very similar to the loads imposed on the original fan blade. Stresses for such conditions are comparable between the two designs. The improved fan blade is not limiting in low cycle fatigue life. None of the conditions in the factory testing, such as crosswind testing or fan mapping, showed any measured stresses as high as the endurance limit of the fan blade material. There have never been any fatigue failures in the original CF6 fan blade in more than 10 million flight hours of experience. Based on comparable stress levels between the new blade and the original design, this same level of reliability is expected for the improved fan blade.

3.3.4 Maintainability

The same maintainability features have been designed into the improved performance fan blade as exist for the original fan blade. It is possible to install or remove a single fan blade from the disk without affecting any of the adjacent blades. This can be done when the engine is installed in the aircraft by removing the spinner and disassembling the fan blade retainers. The fan blade edge thickness for the improved blade is the same as that on the original fan blade. The experience gained to date shows comparable tolerance

to foreign object damage, such as birds and small objects, that are typically ingested. It is expected that larger objects such as tire tread and hand tools can be ingested by the new blade without doing extensive damage. This ruggedness has been previously demonstrated on the original fan blade. The fan blades are paired by moment weight to facilitate the replacement of a damaged blade without requiring trim balance of the engine. The wear life of the blade coatings is expected to be the same for the improved blade as the original blade based on calculated bearing stresses and the experience gained in the factory and flight test programs.

4.0 FAN ROTOR PHOTOELASTIC TEST

The principal objective of the photoelastic test was to obtain a detailed stress analysis of the fan blades and disk, especially in areas where stresses are considered likely to be limiting. The photoelastic method has the greatest value in analyzing locations of complex stress concentration which are difficult to analyze by other means.

4.1 ROTATING STRESS-FREEZING TEST FACILITY

The Rotating Stress-Freezing Test Facility consists of an environmental chamber with vacuum, heating, and cooling capabilities and a variable speed motor drive for rotating model tests. The facility is capable of operation at pressures from ambient to 1 mm of Hg and temperatures from 20° to 180° C. The chamber has a full opening door with an observation panel. The chamber floor has a removable bottom plate for drilling and tapping, and installation of various supports. A photograph of the improved fan photoelastic model installed in the test facility is shown in Figure 13.

Because of the large size and weight of the model, a special rugged bearing support structure was used for the test, and large radiation screens were added to aid in maintaining a uniform model temperature in a vacuum. A slip ring assembly was mounted on the shaft to permit monitoring of thermocouples in representative thick and thin parts of the model itself for temperature control.

For the photoelastic analysis of model slices, several polariscopes were used. Other conventional lab and shop equipment was used in manufacturing the models, slicing, polishing, etc.

4.2 TEST CONFIGURATION

Test hardware included a 0.6 scale model of the CF6-50 fan disk and a full set of improved fan blades. Three types of blade shanks were used: full shank (no pocket), half-pocket shank (original design), and full pocket shank (Figure 14). All airfoil sections and part-span shrouds were identical on all blades. As shown in Figure 15, the blades were held in place by means of retainers made of metal and nylon in such a way that their weight matched the properly scaled weight of the production design retainers.

The fan disk was a scaled model of the production CF6 fan disk, except that the flange on the aft ends of the posts was omitted. It was mounted in the test rig so that it was cantilevered from the aft flange.

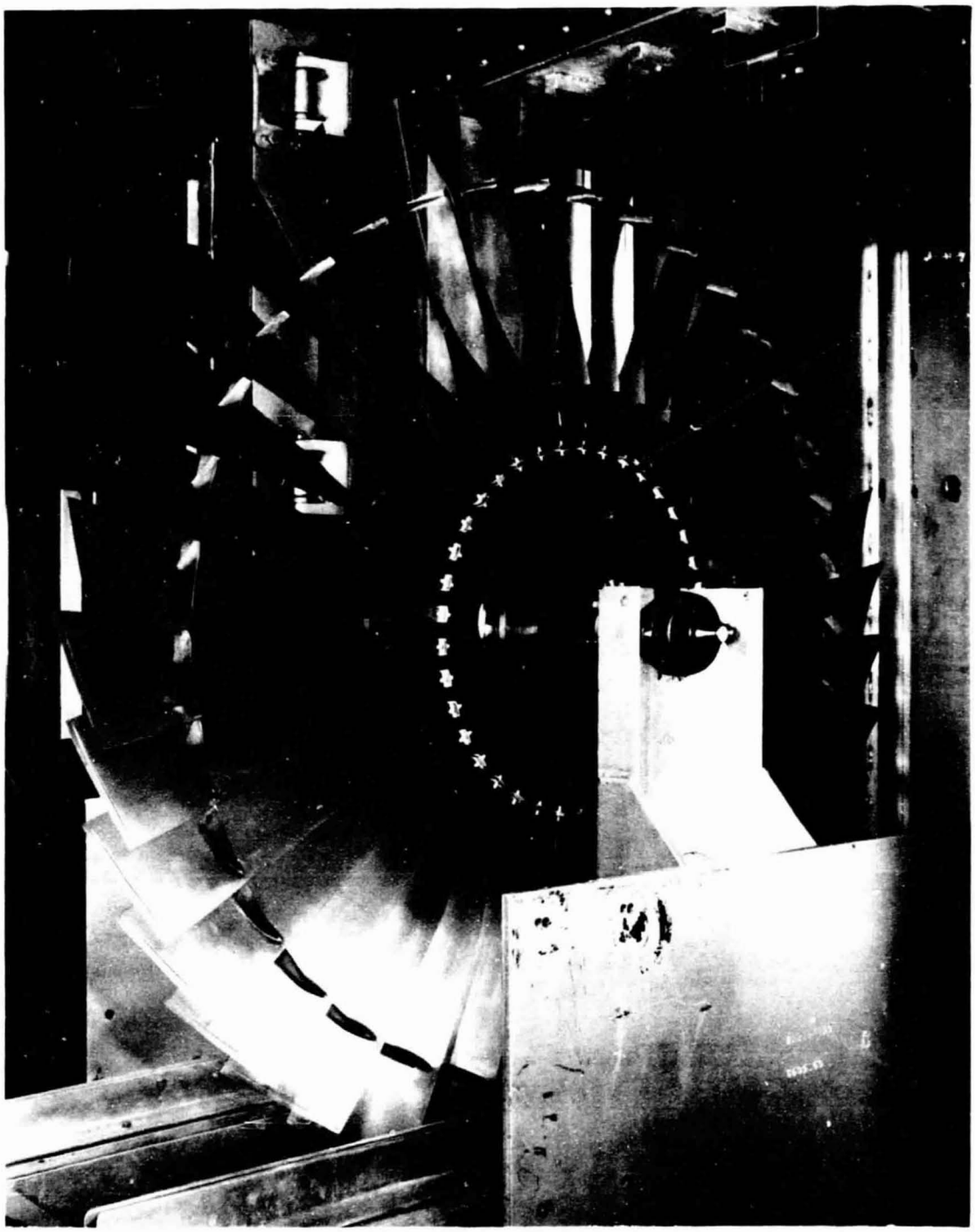

Figure 13. Photoelastic Model of Improved Fan Mounted in Rotating Stress-Freezing Test Facility.

ORIGINAL PAGE IS
OF POOR QUALITY

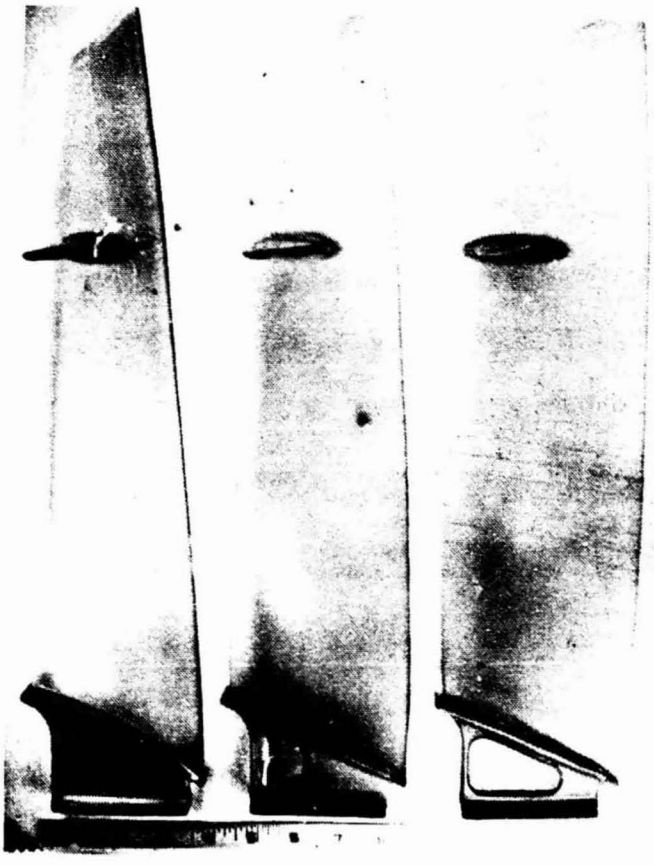

Full Shank Half-Pocket Shank Full Pocket Shank

Figure 14. Photoelastic Models of Fan Bladed With Three Types of Blade Shanks: Full Shank, Half-Pocket Shank, and Full Pocket Shank.

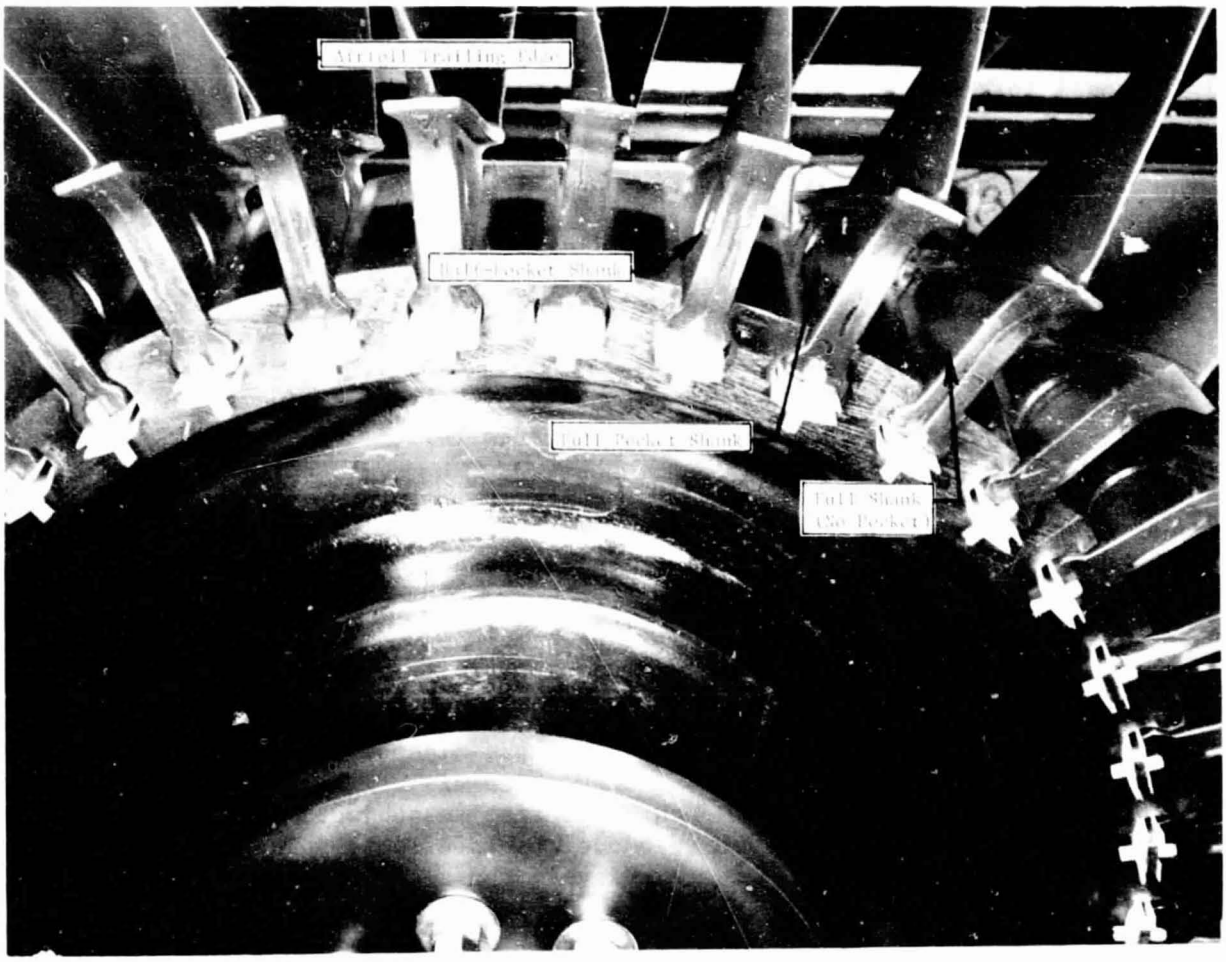

Figure 15. Closeup View of Blade Shrouds Showing Buildup to Prevent "Shingling".

ORIGINAL PAGE IS
OF POOR QUALITY

In order to prevent "shingling" of the blade part-span shrouds, the shroud contact faces of alternate blades were built up with an epoxy paste material, as shown in Figure 16. This modification was found necessary after the first attempt to stress-freeze the model had to be aborted due to shroud shingling. The second attempt ran successfully after the blades were annealed and modified as shown.

4.3 INSTRUMENTATION

Model instrumentation consisted of five thermocouples mounted at the following locations:

1. Tip of blade located in Disk Slot 1.
2. Tip of blade located in Disk Slot 3.
3. Shroud of blade located in Disk Slot 3.
4. Inside rim post near disk OD.
5. Inside disk hub 19 mm (0.75 in.) from ID.

These thermocouples were used to monitor temperatures in the extreme locations (thinnest-outermost at the blade tips and thickest-innermost at the disk hub) to assure that model temperature remained uniform within approximately 3° C.

4.4 TEST PROCEDURE

Stress-freezing is possible because of the diphase behavior of many polymeric solids. The molecules of these materials are held together by primary and secondary bonds. When such a material is subject to loads at room temperature, both sets of molecular bonds are in effect; however, as the temperature is increased to a certain level, the secondary bonds relax and the primary bonds must carry the entire applied load. At this temperature, relatively large, but still elastic, deformations occur. When polarized light is passed through the solid, double refraction occurs with the relative retardation of the two light components (or fringe order) being linearly proportional to the principal stress difference. When the temperature is again lowered to room temperature with the loads still applied, the secondary molecular bonds re-form and lock in the deformations, as well as the above photoelastic effect, just as it existed at the stress-freezing temperature. Since this "thawing" and "freezing" occur on a molecular scale, thin slices may be cut out of the solid model for analysis without disturbing the deformation or the double refraction properties. Epoxy resins, such as Araldite, are commonly used for photoelastic stress-freezing.

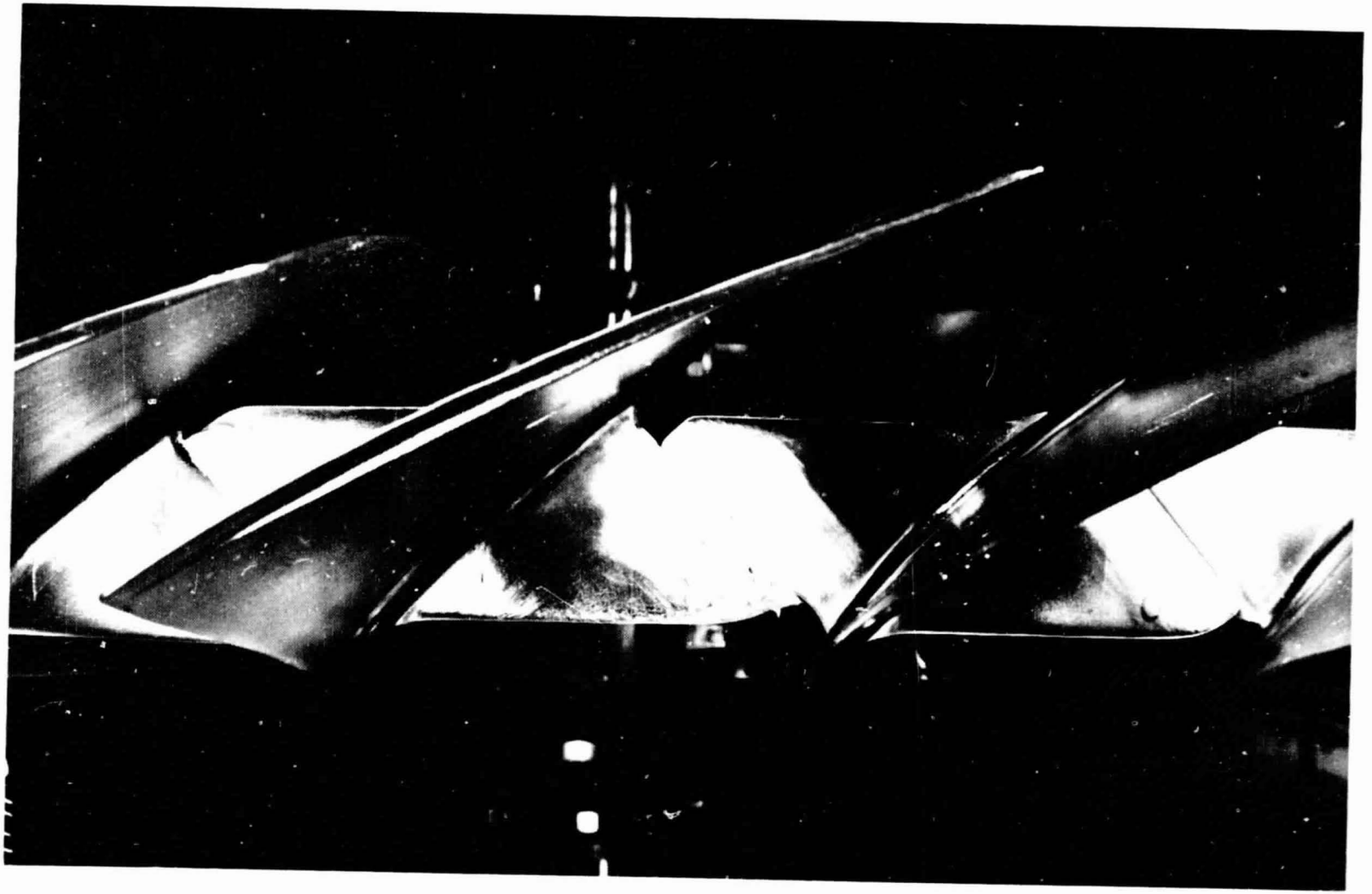

Figure 16. Closeup View of Blade Shrouds Showing Buildup to Prevent "Shingling".

Epoxy models of compressor and turbine rotor parts, such as bladed disks, may have rotational stresses frozen into them by means of a specially designed oven. When mounted in such a facility, the model is first turned slowly by the variable speed motor as the temperature is slowly increased. Temperature gradients are carefully minimized by monitoring thermocouples mounted in a thick and a thin section of a dummy plastic part and adjusting the rate of heating so as to limit the temperature differential. When the stress-freezing temperature is nearly reached, the oven is evacuated to eliminate air loads and the motor speed is brought up to the desired rpm to reach a preselected deformation and stress level. After stabilization, the oven temperature is slowly reduced, again with continuous monitoring and control based on the thermocouple readings from the dummy part. When the temperature dropped below the stress-freezing temperature, the vacuum is slowly released and the motor is stopped.

After the oven reaches room temperature, the model is removed and analysis begins. Thin slices are cut along planes where stresses are desired, and fringe orders and stress directions are determined in a polariscope. Depending on the size and shape of the slices, a diffused-light polariscope or a magnifying slice analysis polariscope or a polarizing microscope may be used for this analysis. Micrometer measurement of slice thickness is also required. Since rotating models usually have a geometric pattern that is repeated many times, several sets of slices may be cut with different orientations using identical model areas in order to completely define the state of stress, and/or duplicate slices may be cut in identical areas for confirmation of results. Stresses in the slices are calculated by conventional photoelastic techniques with the aid of a "fringe constant" determined from a bending or tensile calibration bar.

The rotating stress freezing test was conducted according to the cycle shown in Figure 17. After conclusion of the stress-freezing cycle, the optical effects of the frozen stresses were viewed with polarized light. For example, overall fringe patterns of the three types of blade shanks tested are shown in Figure 18 as viewed in a diffused-light polariscope with cross polarizer and analyzer.

The fan blades were sliced and analyzed in four areas (Figure 19):

1. Part-span shroud region (70% of span)

2. Airfoil - at Section G-G, 271 mm (10.66 in.) above the dovetail base (40% of span)

3. Airfoil root (airfoil - platform fillet tangency point)

4. Dovetail and shank.

Most of the analyses were done on four blades, one full shank (Blade A2), two half-pocket shanks (Blades B20 and B23), and one full pocket shank (Blade C19). All of these blades were analyzed in the dovetail and shank, but not all blades were analyzed in the other three areas.

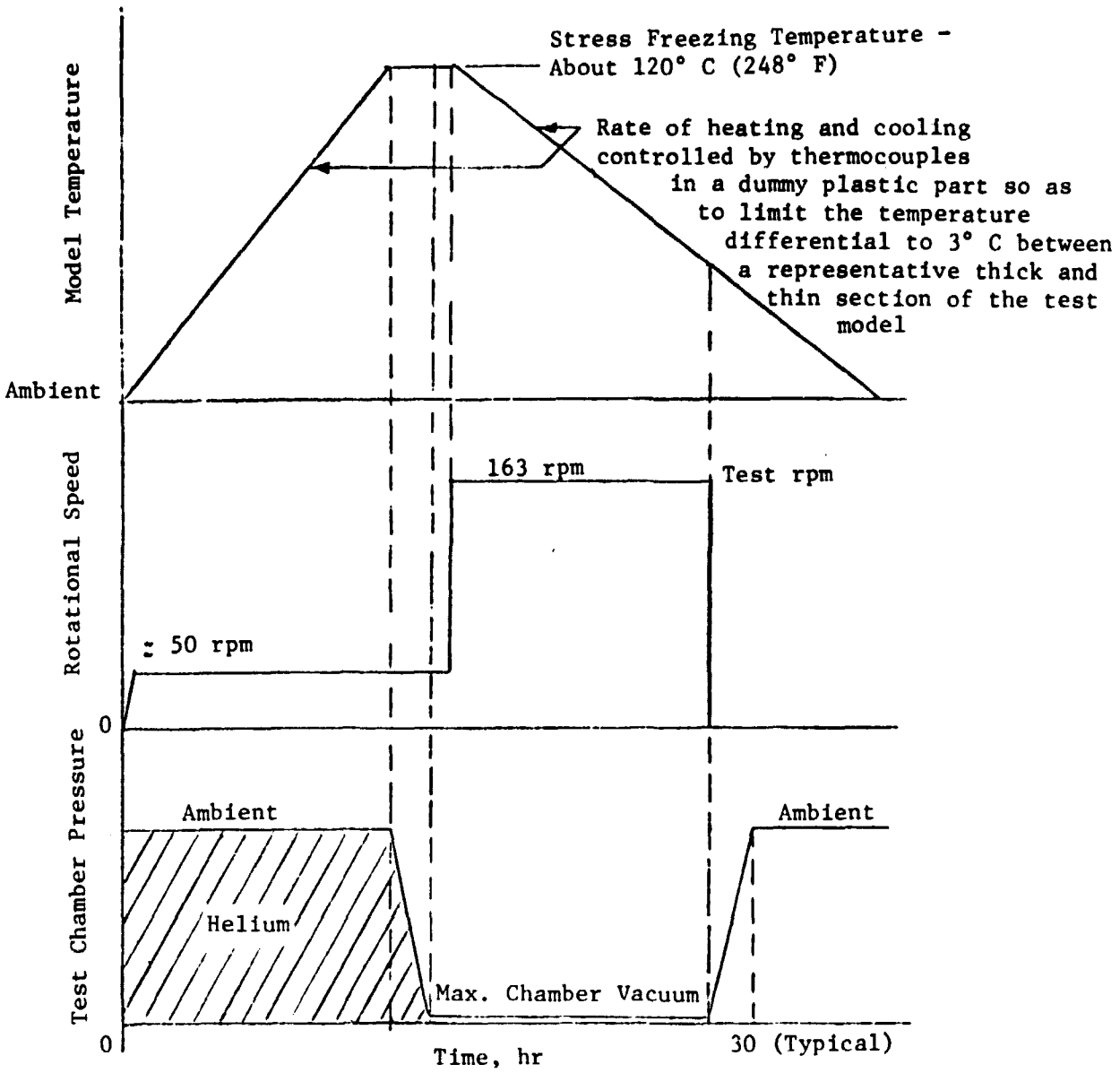

Figure 17. Rotating Stress-Freezing Cycle for Fan Model.

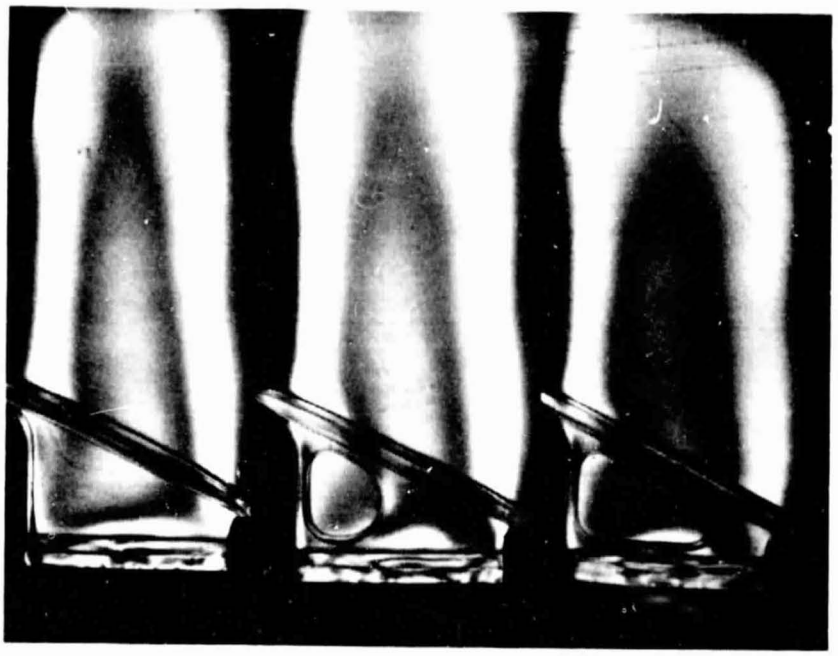

Figure 18. Overall Dark Field Frozen Stress Fringe Patterns in the Three Types of Blade Shanks.

A typical slicing diagram is shown in Figure 19 for the shank, airfoil root, and upper airfoil for blade B20. Except for the airfoil root slices, all slices (including shroud slices) were oriented perpendicular to the blade midchord and in a radial direction. The airfoil root slices were oriented perpendicular to the platform, as indicated in Figure 19, to conform to the usual convention for orientation of strain gages in blade end-effects testing. Shroud slices from Blade B20 located in Disk Slot 28 are shown in Figure 20.

Isochromatic fringe patterns of a typical set of shank/dovetail slices from Blade 23 are shown in Figure 21.

4.5 TEST RESULTS AND DISCUSSION

Stress data in the part-span shroud member adjacent to the airfoil fillet region are shown on the slice profile diagrams of Figure 22. The maximum shroud photoelastic (compression) stress (concave side of airfoil and on the radially outboard surface) of -521 MPa (-76,000 psi) in Slice 4 agrees well in location with peak values found in instrumented engine tests and also with finite element analysis, but it is about 50% higher in magnitude. The maximum shroud photoelastic (tension) stress (convex side of airfoil and on the radially inboard surface) of 501 MPa (73,000 psi) in Slice 10 is similarly about 50% higher than both the theoretical analysis and strain gage experimental results. Figure 23 shows these photoelastic data compared with the finite element analysis of this blade and the similarity of the data distribution trends can be noted. The data for the shroud region on the concave side of the airfoil, which is in tension (the radially inboard surface), are in very good agreement with the finite element analysis.

The spanwise airfoil stress distribution data at a section 270.8 mm (10.66 in.) above the dovetail base (reference Section G-G, Figure 19), are shown in Figure 24 for Blade A2 (full-shank blade). Blades S20 (half-pocket shank blade) and C19 (full pocket shank blade) were also sliced and photoelastically analyzed at this section; those data were almost identical to that shown. Figure 24 shows the photoelastic results compared with the finite element analysis of the blade. The data trends between the photoelastic test and the theoretical analysis are in excellent agreement, though the maximum photoelastic stress on the convex surface (at 0.4 fraction of airfoil chord location) of 568 MPa (82,500 psi) is about 25% higher in magnitude than the theoretical value. Figure 25 shows the spanwise stress data at Section G-G from Blade C19 along with theoretical "twisted blade program" analyses of this blade with (a) shrouds "free" and (b) shrouds "locked up".

The airfoil root stress data distribution from Blade B20 is shown in Figure 26 along with the results of the finite element analysis of the blade. Agreement between these data is good; maximum stress in the airfoil root region does not exceed 400 MPa (58,000 psi). Figure 27 shows these same photoelastic data along with results from end-effects testing of a full scale metal blade. The photoelastic data and the metal blade strain gage data, from the pure radial pull test for which the load conditions are similar (but obviously not identical), are for the most part in good agreement. The

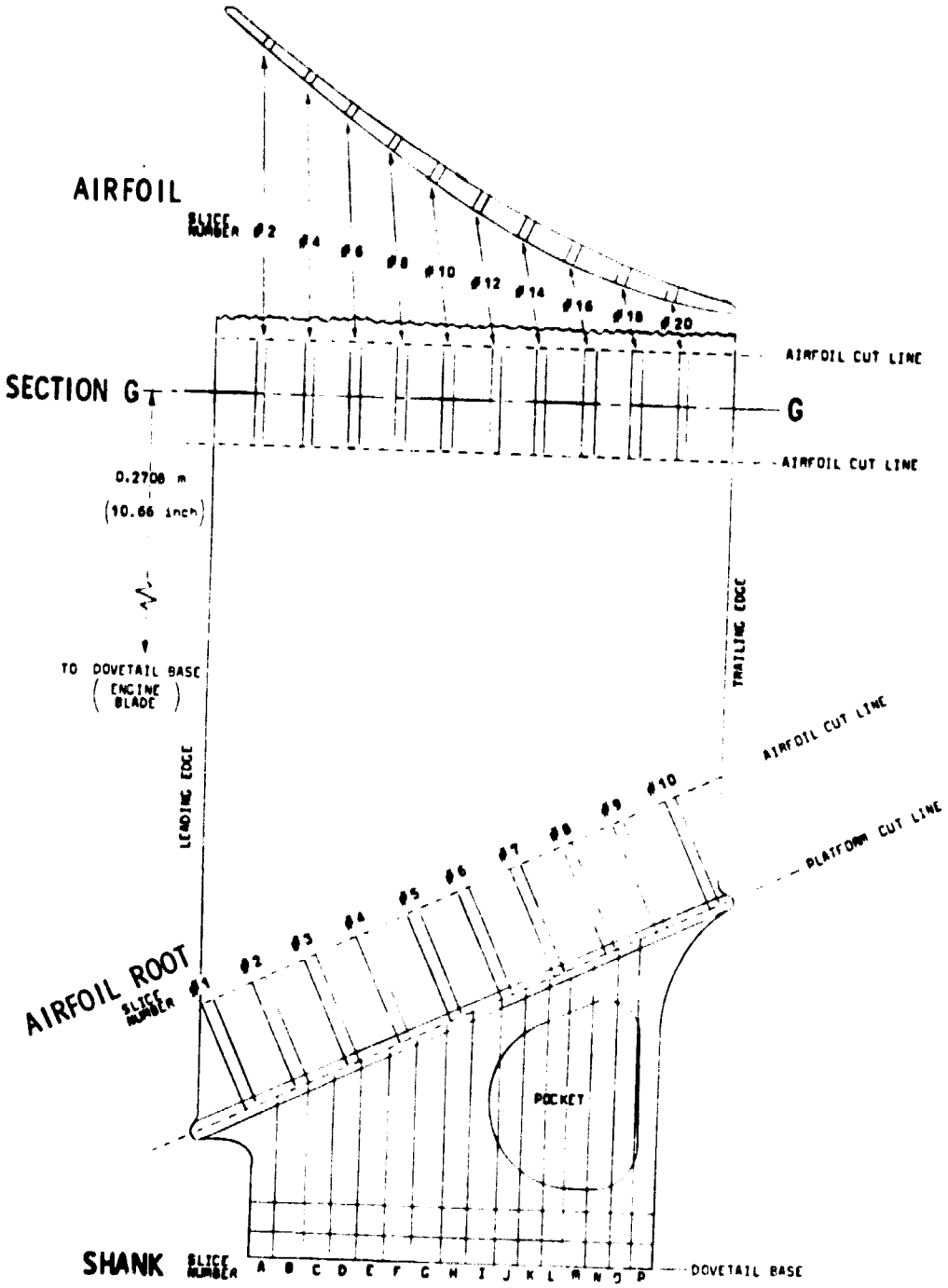

Figure 19. Slicing Diagram for Blade B-20 for Dovetail and Shank, Airfoil Root, and Upper Airfoil.

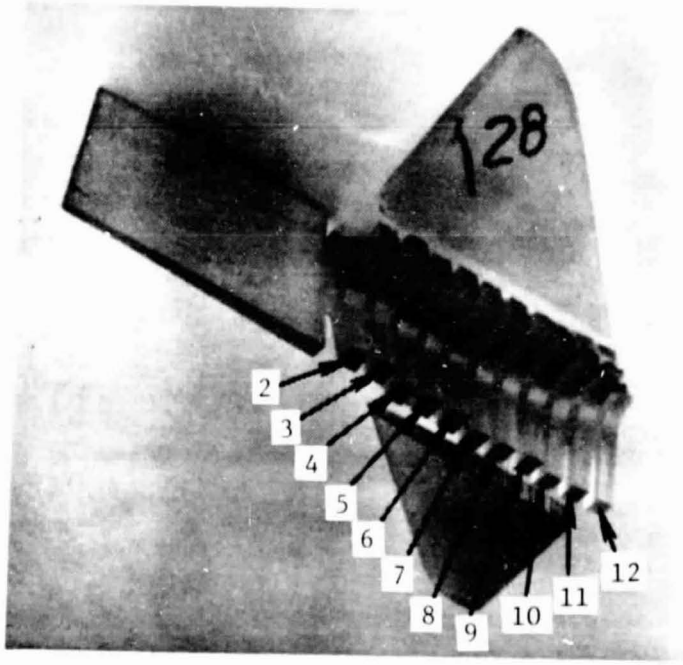

(a) Slices Reassembled with Airfoil Leading Edge and Shroud Tips.

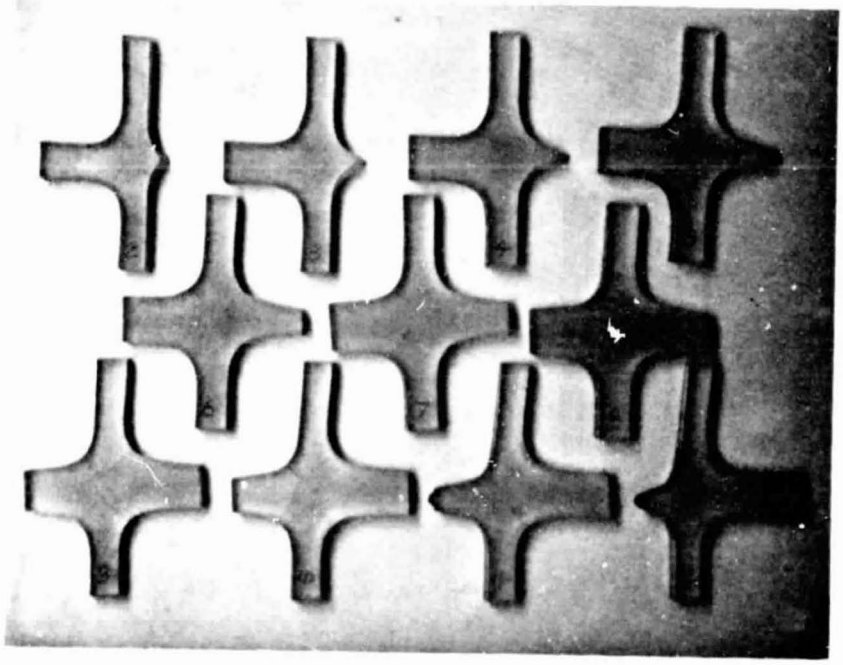

(b) Slices Arranged and Numbered Consecutively from Forward to Aft.

Figure 20. Shroud Slices from Blade B20.

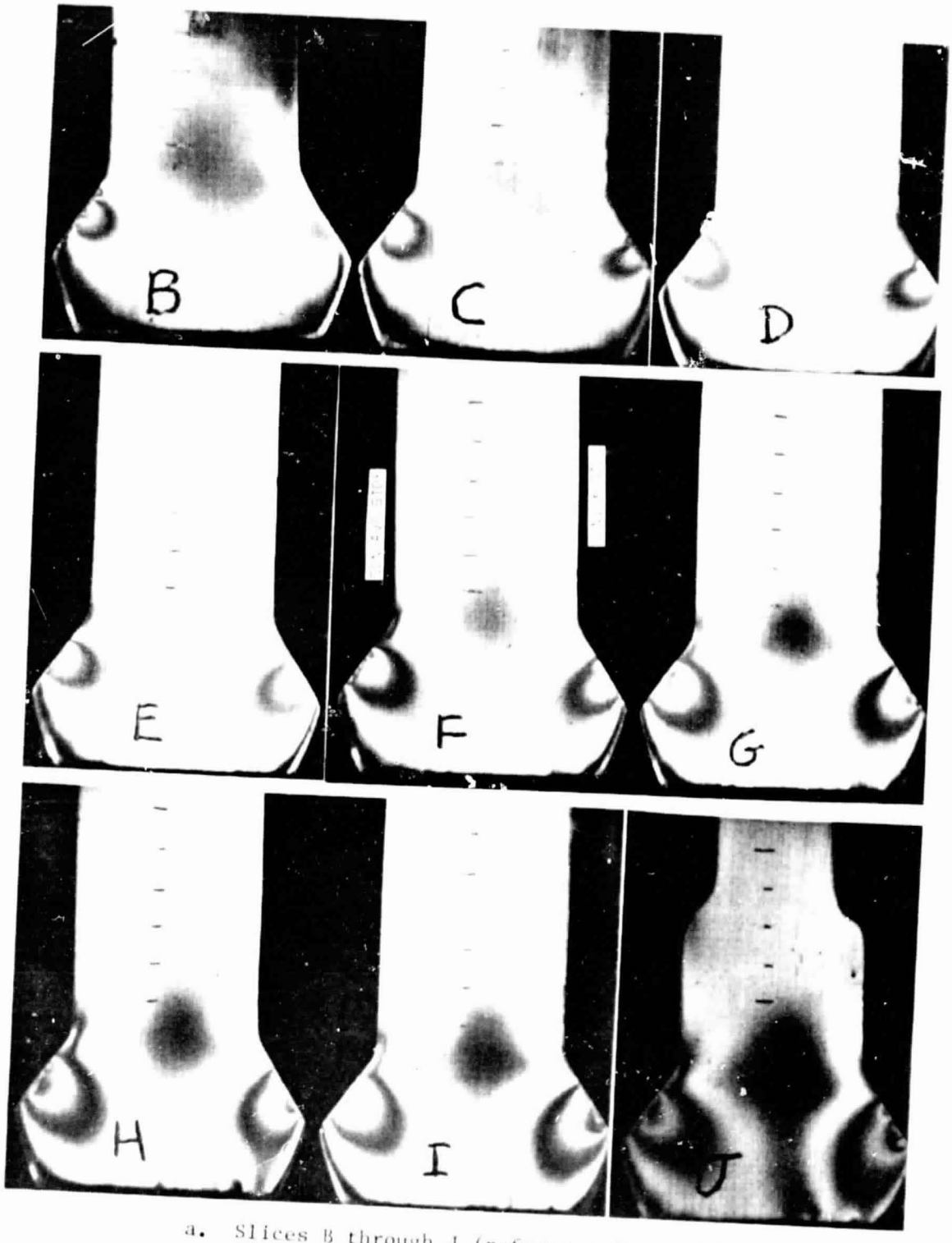

a. Slices B through J (reference Figure 19)

Figure 21. Photographs of Shank-Dovetail Photoelastic (Dark Field) Isochromatic Fringe Patterns, Forward Looking Aft, Half-Pocket Shank Blade B23.

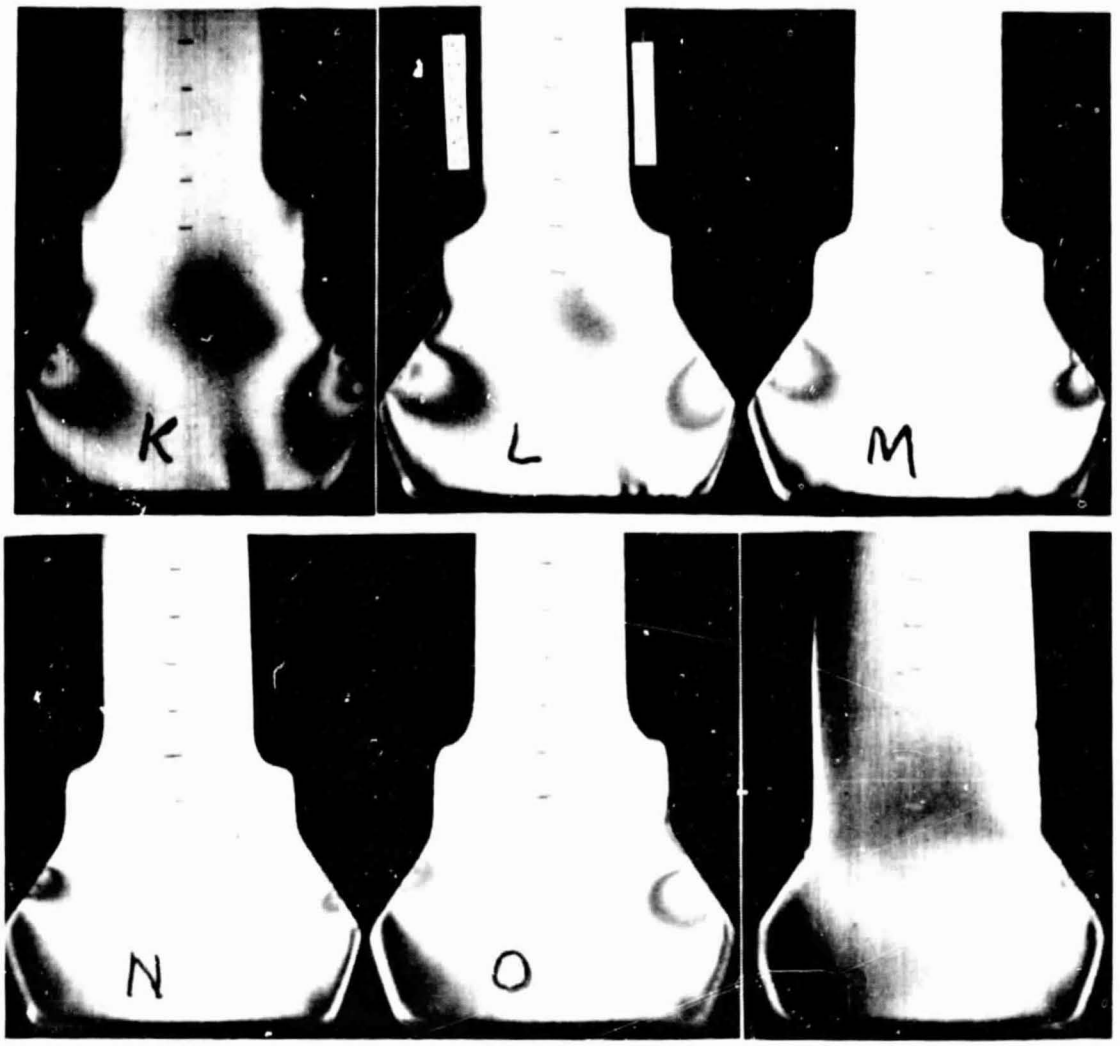

b. Slices K through P (reference Figure 19)

Figure 21. Photographs of Shank-Dovetail Photoelastic (Dark Field) Isochromatic Fringe Patterns, Forward Looking Aft, Half-Pocket Shank Blade B23 (Concluded).

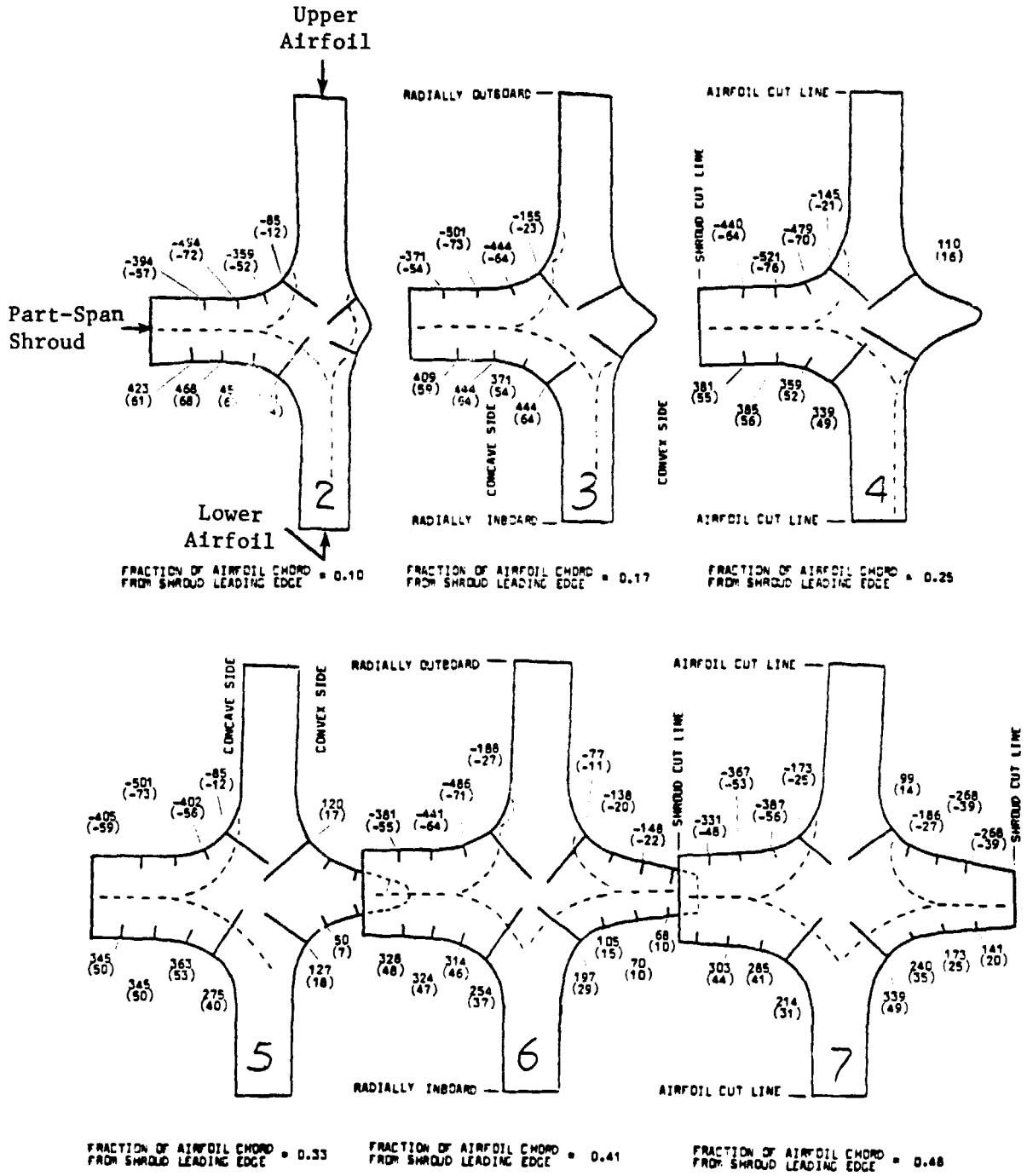

a. Slices 2 through 7 (See Figure 20a. for location)

Figure 22. Airfoil Shroud Region Surface Stress Distribution, 3785 RPM.

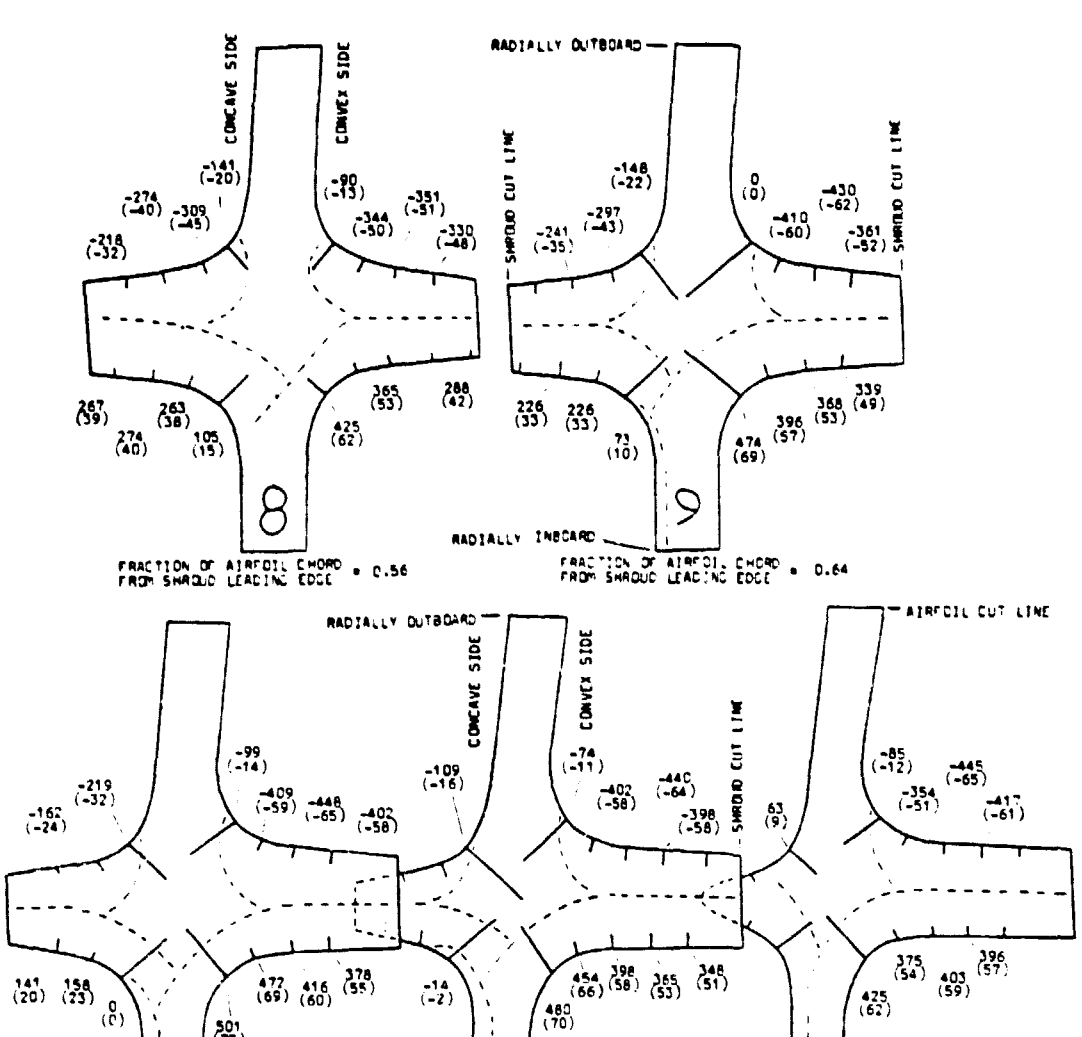

b. Slices 8 through 12 (See Figure 20a. for location)

Figure 22. Airfoil Shroud Region Surface Stress Distribution, 3785 RPM (Concluded).

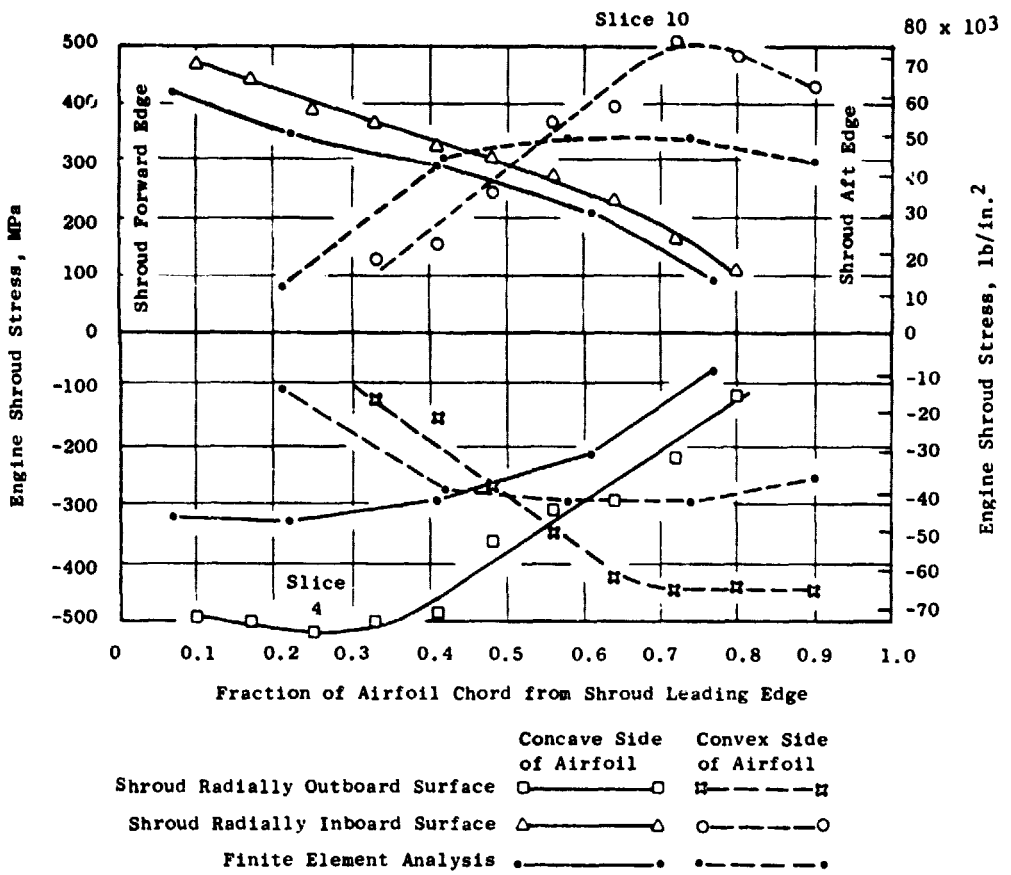

Figure 23. CF6 Improved Fan Blade: Airfoil Part-Span Shroud Region Stress Distribution, 3785 RPM at Sea Level.

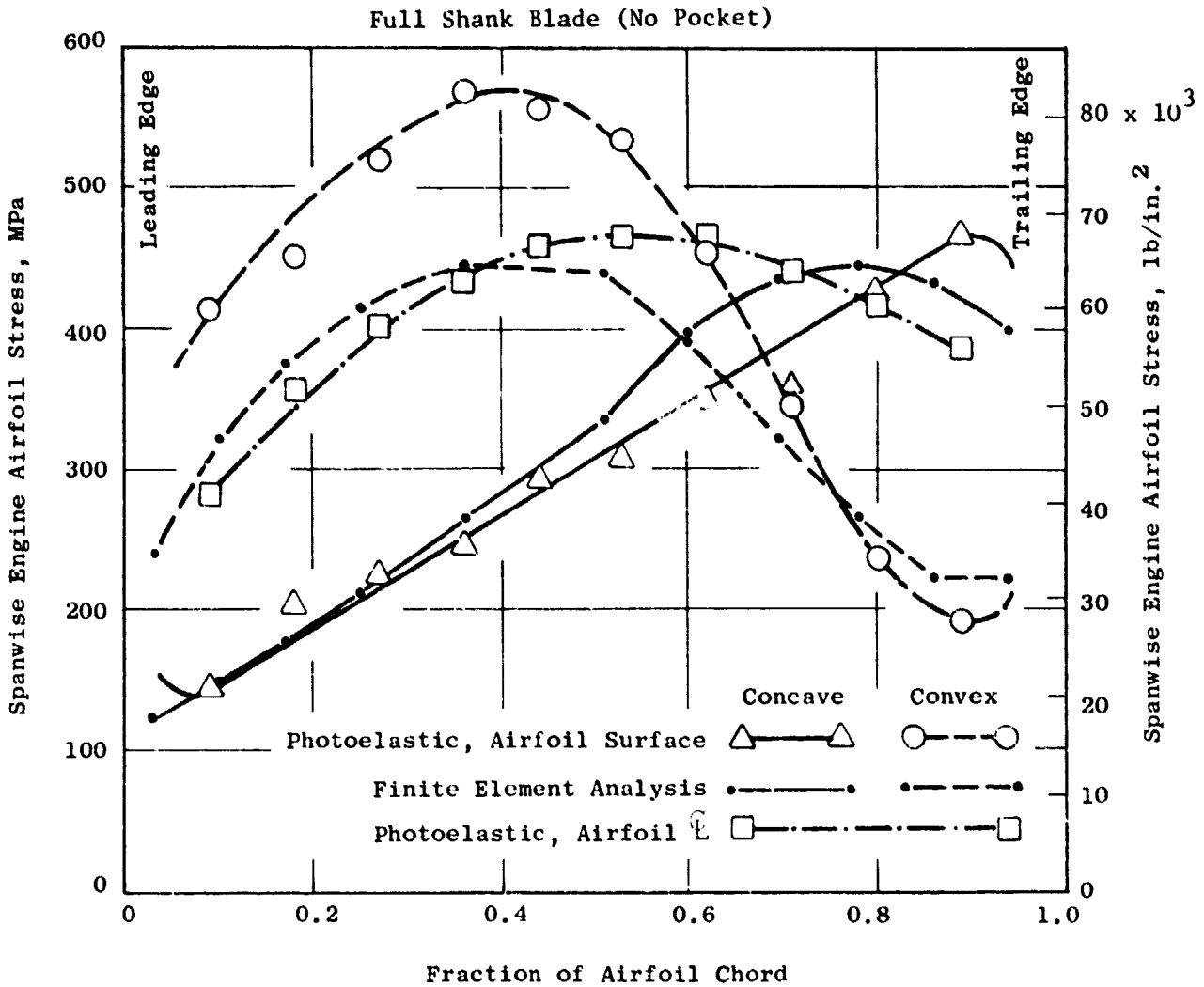

Figure 24. CF6 Improved Fan Blade A2, Spanwise Stress in Airfoil at Section G-G, 0.2708 m (10.66 Inches) Above Dovetail Base, 3785 RPM at Sea Level.

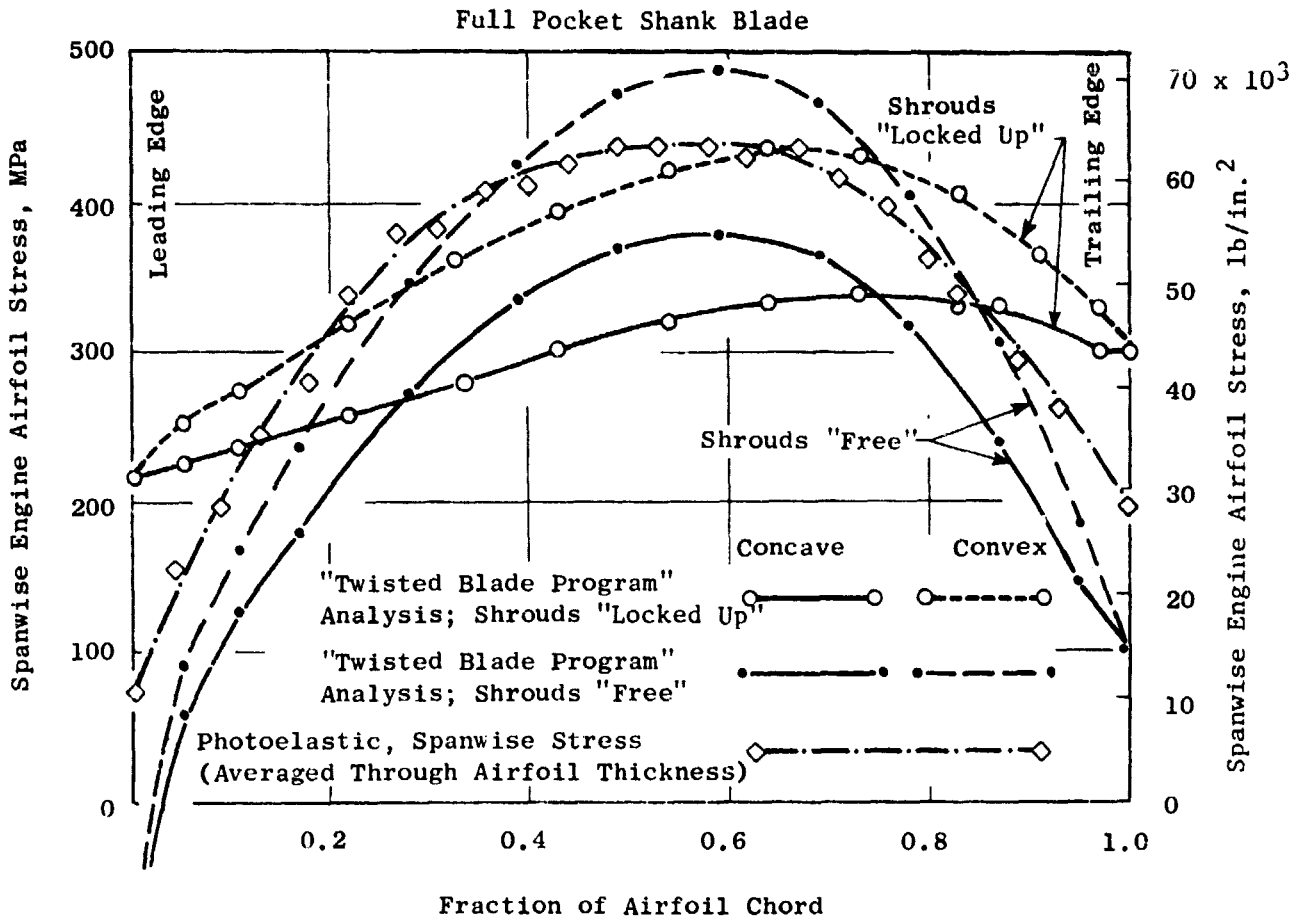

Figure 25. CF6 Improved Fan Blade C19, Spanwise Stress in Airfoil at Section G-G 0.2708 m (10.66 Inches) Above Dovetail Base, 3785 RPM at Sea Level.

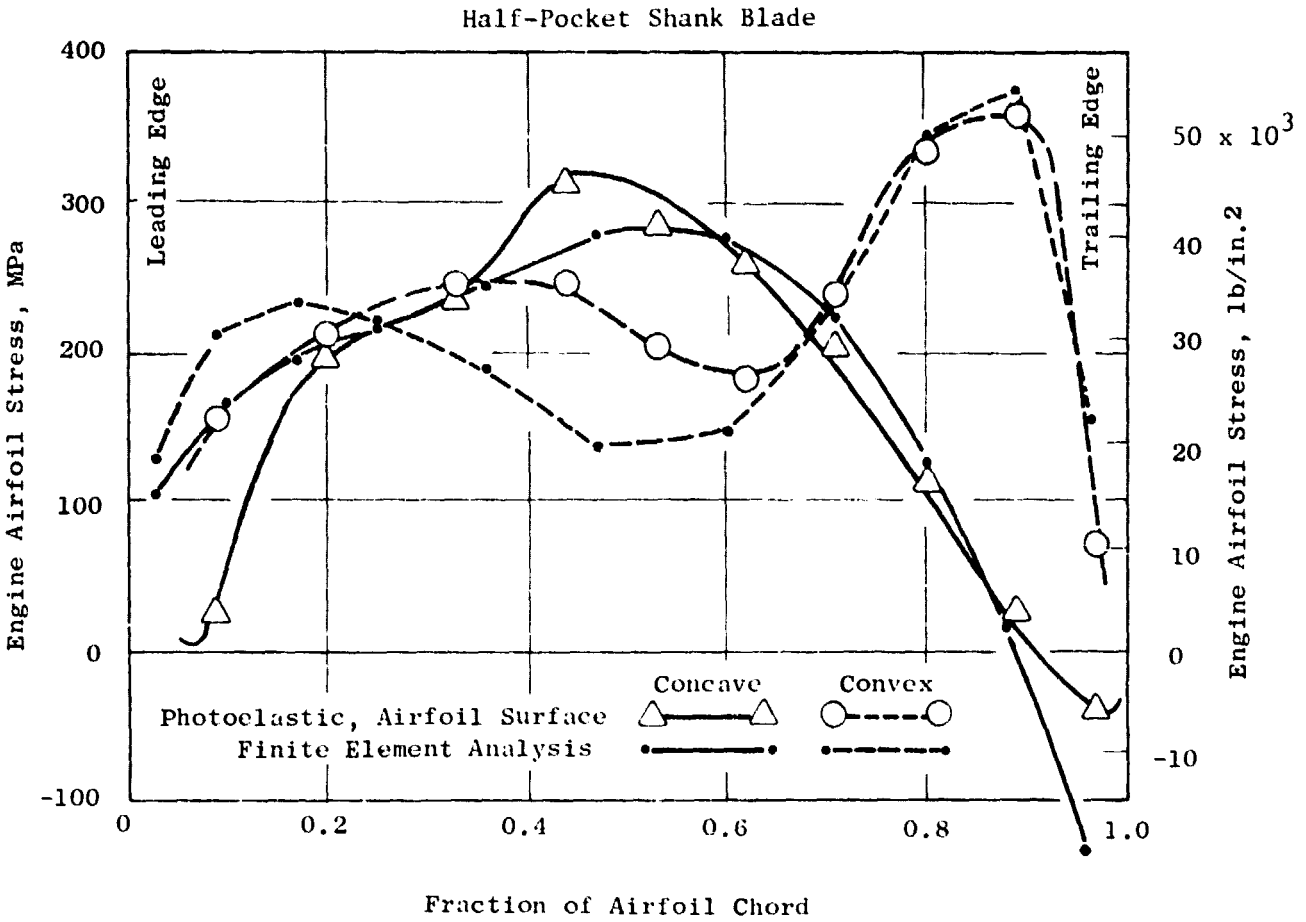

Figure 26. CF6 Improved Fan Blade B20, 3785 RPM at Sea Level.

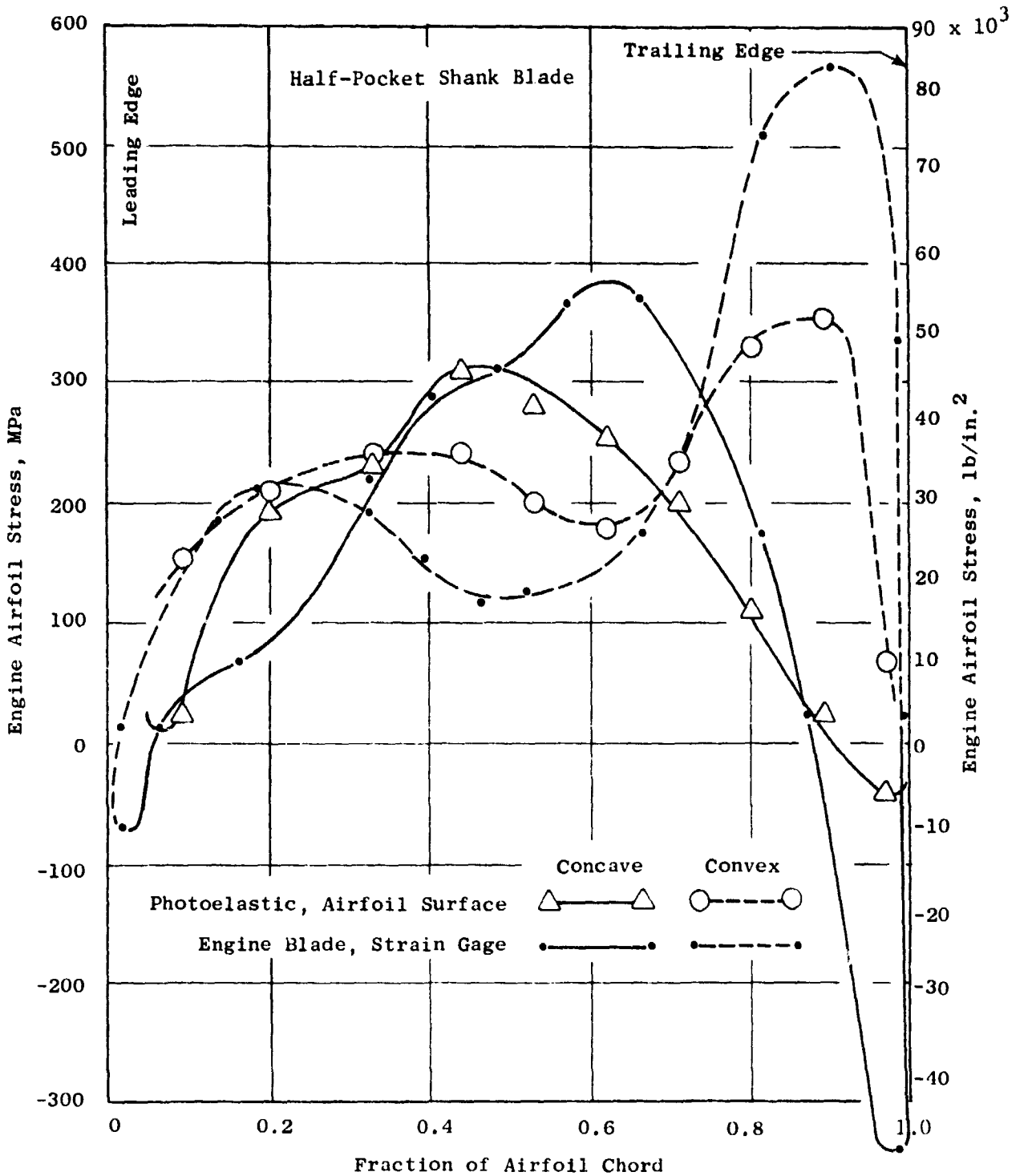

Figure 27. CF6-50 Improved Fan Blade B20, Engine Airfoil Root Stress Distribution, 3785 RPM at Sea Level.

plotted photoelastic stresses were taken at a height above the platform corresponding to the strain gage locations and were oriented perpendicular to the platform, as were the strain gages. The true maximum stress for each slice was not plotted, because it generally did not exceed the value at the strain gage location by more than 10%. Blade C19 was also analyzed in the airfoil root region and those data are compared to Blade B20 in Figure 28; again, agreement between these data is excellent.

For the four blades analyzed, stresses were determined from shank slices cut as shown in Figure 19. Stresses obtained included: (1) the maximum dovetail fillet stresses, (2) maximum pocket fillet stresses (for Blades B20 and C19), (3) surface stresses at a reference section 21.6 mm (0.86 in.) above the dovetail base on both (concave and convex side) surfaces (all discussions are given in terms of full-size blade geometry rather than 0.6X model geometry), and (4) shank centerline stresses at a reference section 38.1 mm (1.50 in.) above the dovetail base. Stresses were also read at a section 15.8 mm (0.624 in.) above the dovetail base, but this value was always close to the peak value in the dovetail fillet. The 15.8 mm (0.624 in.) and 21.8 mm (0.86 in.) dimensions corresponded to locations which were used for strain gage placement in end-effects testing of metal blades, while the 38.1 mm (1.50 in.) dimension was chosen as a convenient reference location near the base but out of the stress concentration. It serves to define the location of a nominal stress when stress concentrations are desired or to relate photoelastic results to finite-element results. Figures 29, 30, and 31 are plots of stress ratios, or stress concentrations, for the dovetail fillets. These concentrations are defined as the ratio of maximum dovetail fillet stress to the reference shank centerline stress at 38.1 mm (1.50 in.) above the dovetail base and are given in this form for generalized application to different design conditions.

All stresses shown on the various figures are presented as the actual values for a full size titanium 6-4 blade rotating at 3785 rpm. Equations used to calculate the stresses from the photoelastic fringe orders are given below.

The model stress was calculated from

$$\sigma m = \frac{fn}{t} \tag{1}$$

where

σ_m = model stress (MPa)

f = fringe constant for the model material (MPa/m)

n = fringe order

t = slice thickness (m)

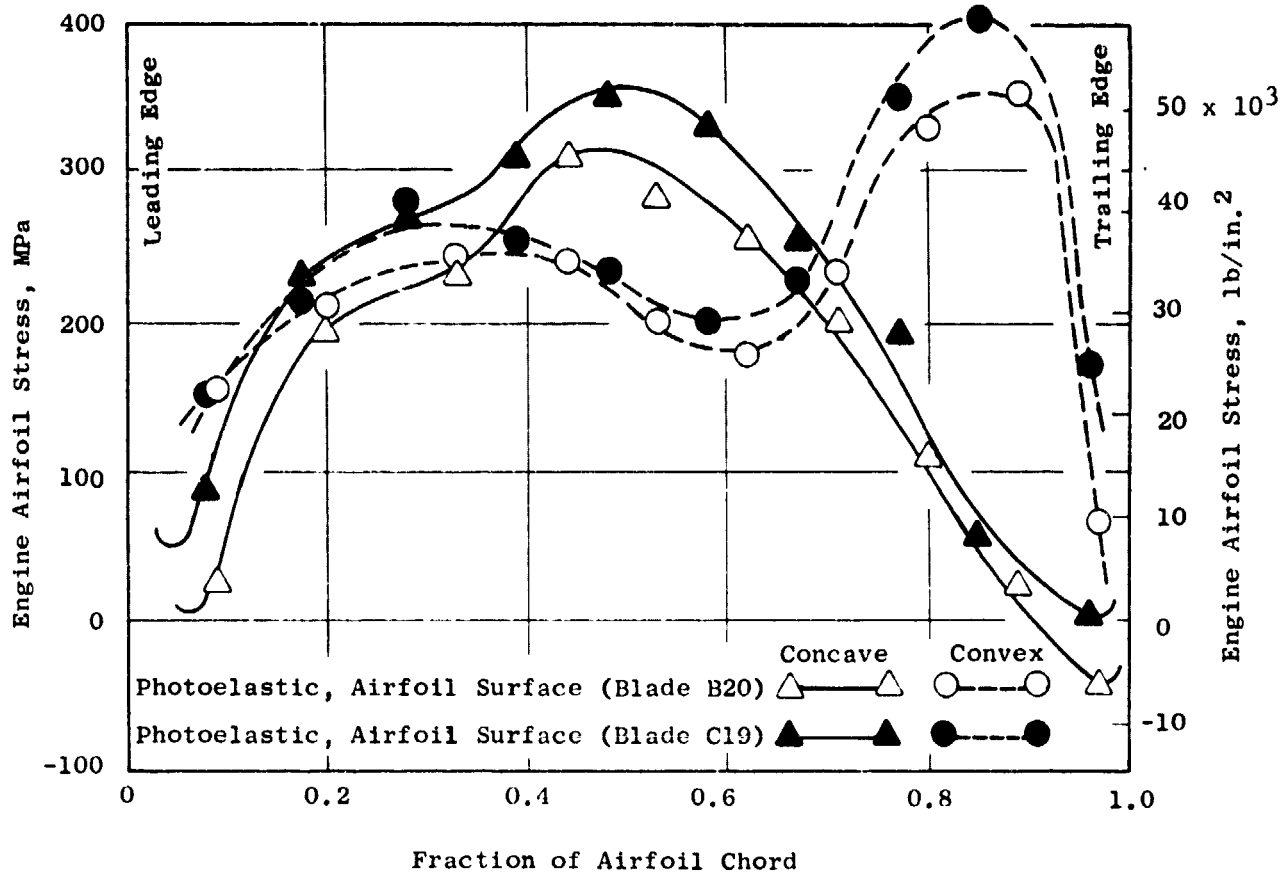

Figure 28. CF6 Improved Fan Blades B20 and C19, Engine Airfoil Root Stress Distribution, 3785 RPM at Sea Level.

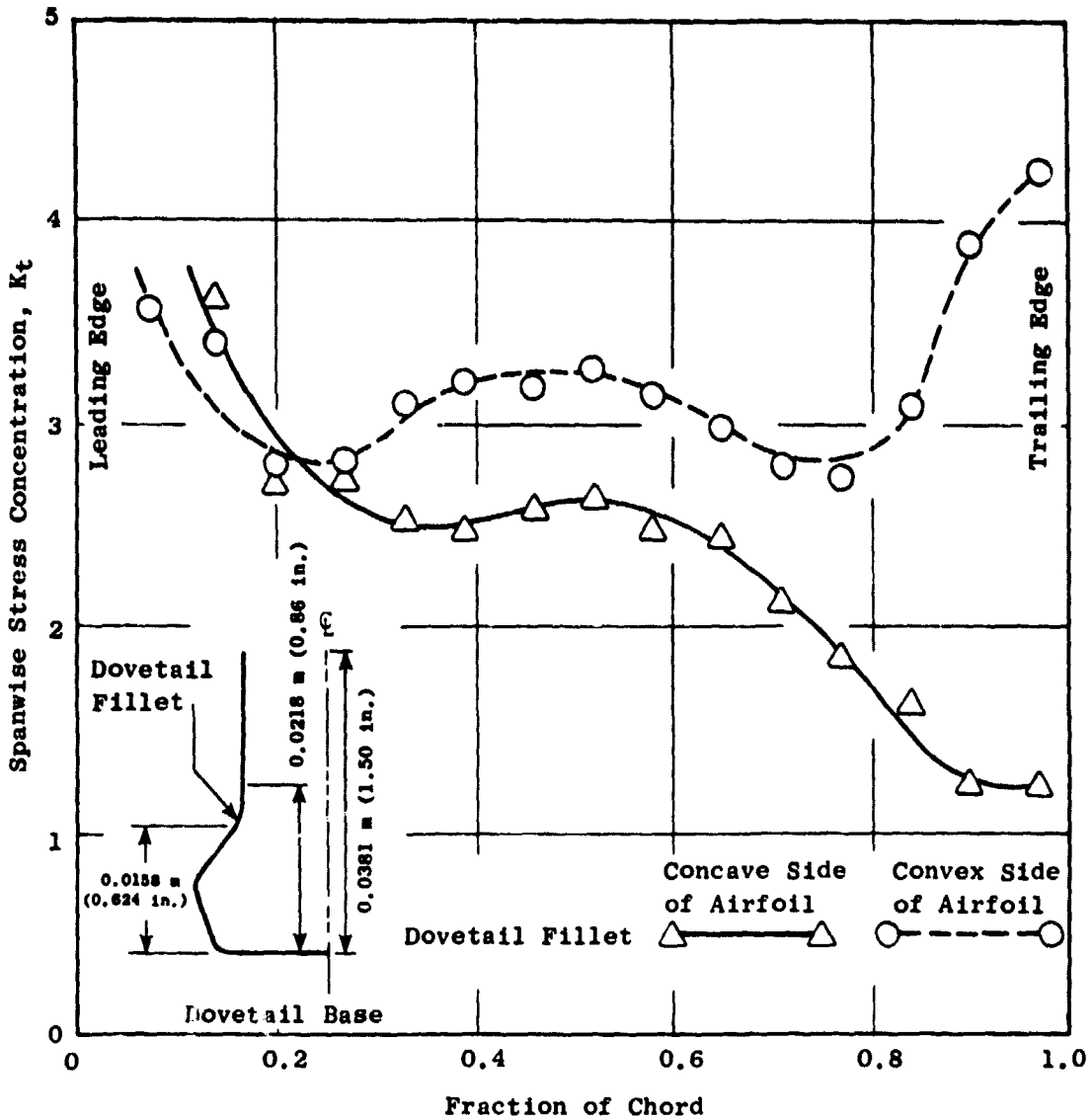

Figure 29. Dovetail Fillet Stress Concentration K_t for Full Shank Blade A2, 3785 RPM at Sea Level.

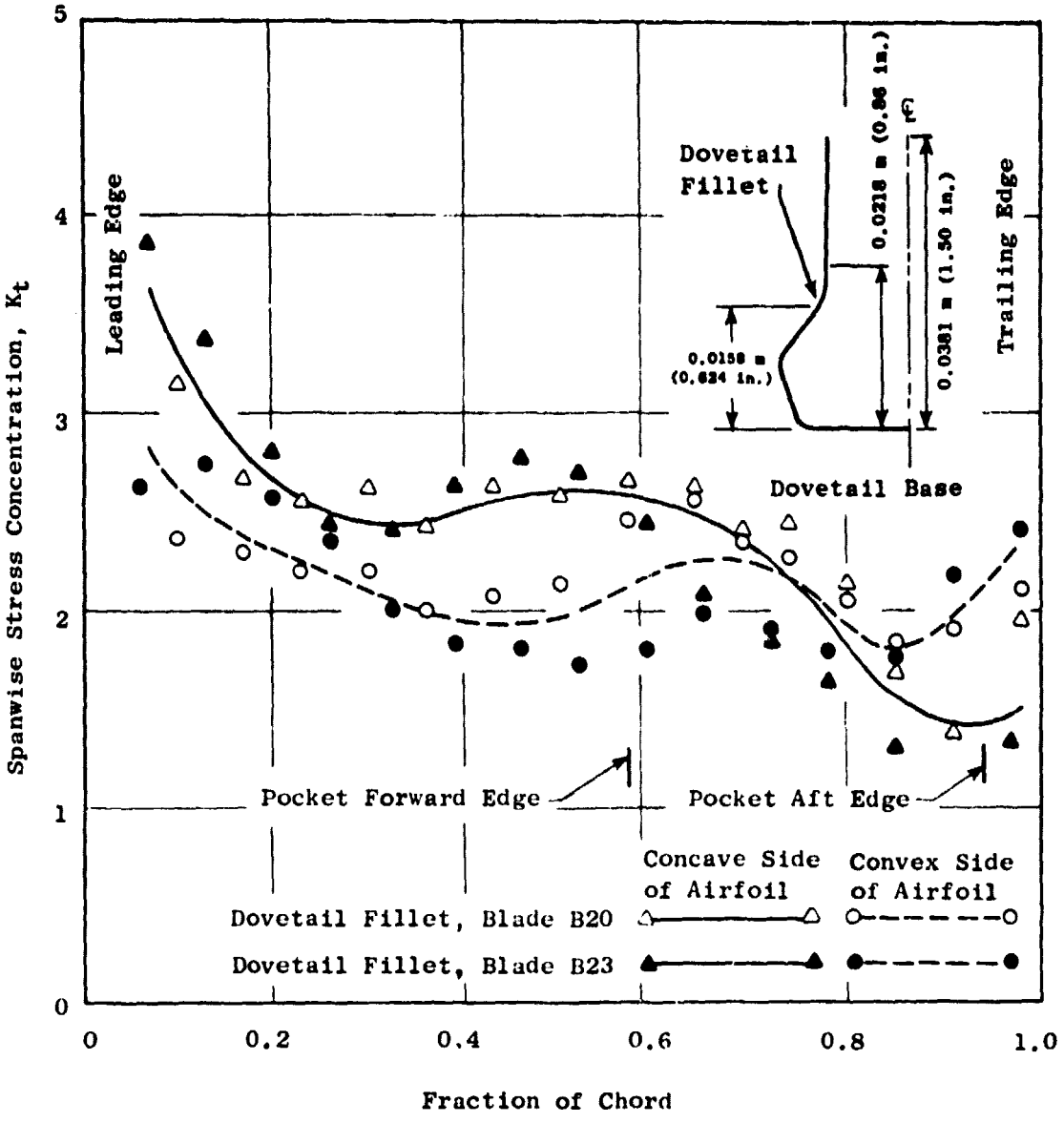

Figure 30. Dovetail Fillet Stress Concentration K_t for Half-Pocket Shank Blades B20 and B23, 3785 RPM at Sea Level.

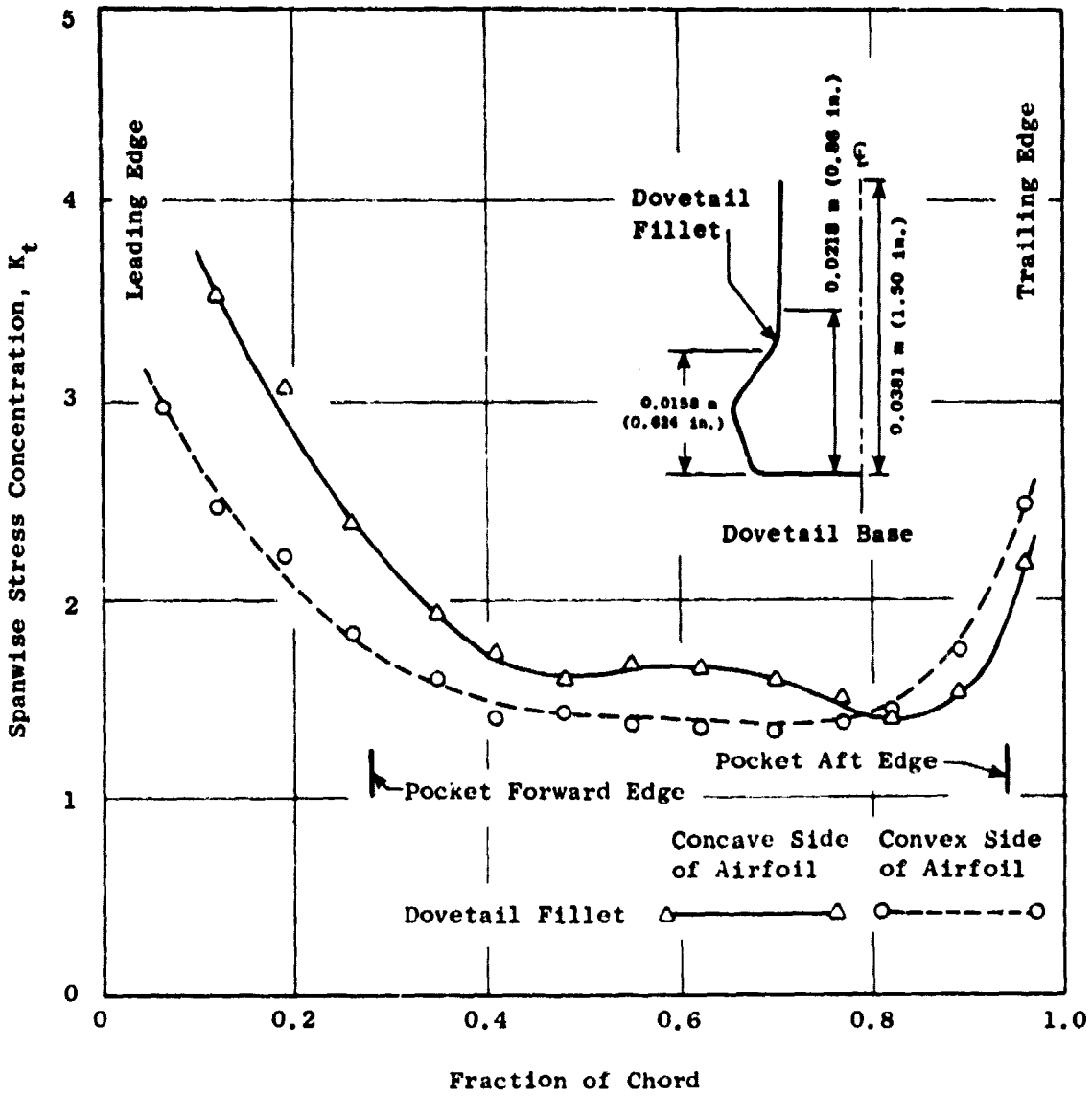

Figure 31. Dovetail Fillet Stress Concentration K_t for Full Pocket Shank Blade C19, 3785 RPM at Sea Level.

The prototype stress was calculated from

$$\sigma_p = \sigma_m \left(\frac{\gamma_p}{\gamma_m}\right) \left(\frac{\omega_p}{\omega_m}\right)^2 \left(\frac{\ell_p}{\ell_m}\right)^2 \quad (2)$$

where

σ_p = engine part stress (MPa)

γ_p = material density of engine part (g/m^3)

γ_m = density of model material (g/m3)

ω_p = rotational speed (3785 rpm) of engine parts (rad/sec)

ω_m = rotational speed (163 rpm) of model (rad/sec)

ℓ_p = characteristic length of engine part (m)

ℓ_m = characteristic length of model (m)

The geometric scale factor is

$$\frac{\ell_m}{\ell_p} = 0.6 \quad (3)$$

Equation (2) for the prototype stress eventually reduces to

$$\sigma_p = k \frac{n}{t} \text{ (MPa) at 3785 rpm} \quad (4)$$

where k is a constant factor, the value of which depends upon the material, physical properties, and units used to express the other quantities in the equation.

Model to prototype strain ratio (ϵ_m/ϵ_p) was calculated from

$$\frac{\epsilon_m}{\epsilon_p} = \left(\frac{E_p}{E_m}\right) \left(\frac{\gamma_m}{\gamma_p}\right) \left(\frac{\ell_m}{\ell_p}\right)^2 \left(\frac{\omega_m}{\omega_p}\right)^2 = \left(\frac{E_p}{E_m}\right) \frac{f}{k} \quad (5)$$

where

E_p = Young's modulus of engine part

E_m = Young's modulus of model at critical temperature

For this test, Equation (5) reduces to

$$\frac{\epsilon_m}{\epsilon_p} = 1.20$$

Poisson's ratio for the model is 0.5.

Some unforseen problems were encountered in this test, most of which were caused in one way or another by the unusual large size of the photoelastic model, and some of which warrant further investigation.

For example, the problem of part-span shroud "shingling" was noted, and corrective action was taken which solved the problem. Yet, the shrouds did not lock up as expected by theoretical analysis of blade untwist and as observed in engine test. In the photoelastic test, all shrouds were observed to be fully closed (and presumed locked up) at the stress-freezing (or critical) temperature; but as the chamber temperature was slowly decreased, some small gaps appeared and moved around among the blades. This implies a loss of lockup and some undesirable relative motion of the blades. Photoelastic spanwise airfoil stresses at reference Section G-G, 270.8 mm (10.66 in.) above the dovetail base, were compared with theoretical results for both "locked" and "unlocked" shrouds (see Figure 25). It should be noted that the photoelastic stress results fell midway between the two, possibly indicating a loss of that lockup.

For this stress-freeze test, the choice was made to rotate the model at an rpm corresponding approximately to a 1:1 strain ratio with the full-size engine component. This was done primarily to achieve realistic blade stresses, especially those due to untwist, and presumably to achieve realistic shroud lockup. Several undesirable side-effects of this choice affected the accuracy of the results:

- Fringe orders were low, magnifying the relative value of any residual stresses or reading inaccuracies. This was partially overcome by taking relatively thick slices.

- Gravity load effects during rotation were relatively large compared to the centrifugal load. The gravity force also produced a 1/rev cycle which is considered undesirable during a stress-freeze.

- Model defects in such things as dovetail pressure-face fitup would be expected to show up in an exaggerated manner.

Results shown in Figures 29, 30, and 31 show successively reduced concentration factors with increased pocket size. However, this does not necessarily mean that the peak stress decreases, since the "nominal" stress is increasing at the same time. There does appear to be some shielding of the dovetail fillet by the proximity of the pocket, but this benefit may be offset locally by the flow of stress around the ends of the pockets.

5.0 FAN BLADE BENCH FATIGUE TEST

Objectives of the improved fan blade bench fatigue tests were to demonstrate that (1) the design has no stress risers at the airfoil edges, around the part-span shroud, in the airfoil root platform shank dovetail area, or elsewhere; (2) the manufacturing processes produce a fan blade whose fatigue strength is in accordance with the material specifications; and (3) adequate design margin exists between measured stress levels in engine testing, such that no field fatigue problems would be anticipated.

5.1 TEST SETUP AND TEST CONFIGURATIONS

A bench test setup was utilized for these tests. An inner panel section of the fan blade was clamped at the dovetail and supported as a cantilever beam as shown in Figure 32. The fan blades were excited using a siren which produced air pulses by air flowing through a slotted disk rotating at controlled variable speeds. Pulse frequency was adjusted to coincide with the test parts fundamental vibratory mode frequency by varying the rotational speed of the slotted disk. Test component tip amplitude was measured through a calibrated microscope. Siren frequency and input were held constant during the fatigue test. Component failure was determined by a decrease in blade amplitude and resonant frequency.

Fan blade forgings and finished blades were used in this test. Test bars were machined from production forgings in the areas shown in Figure 33. Two notched specimens were machined from the dovetail area of the forging for low cycle fatigue testing, and two smooth specimens were machined from the midspan shroud area of the forging for high cycle fatigue testing. All test bars were unpeened.

Production fan blades were cut 127 mm (5 in.) below the midspan shroud. The lower blade half, consisting of the dovetail and the inner panel, was used for the inner panel test as-is. The upper blade half, consisting of the outer panel, midspan shroud and the inner panel stub below the midspan, was used for the outer panel test and the shroud test. For the outer panel test, a "kirksite" block was cast around the inner panel stub up to the top of the shroud. For the shroud test, a similar block was cast around the convex side of the airfoil. The blocks were machined square and used for clamping during the test.

5.2 INSTRUMENTATION

No instrumentation was applied to the notched low cycle fatigue test bars nor to the smooth high cycle fatigue test bars. These tests were conducted in the Materials Laboratory where applied axial loads for low cycle fatigue tests and bending moments for high cycle fatigue tests are accurately measured.

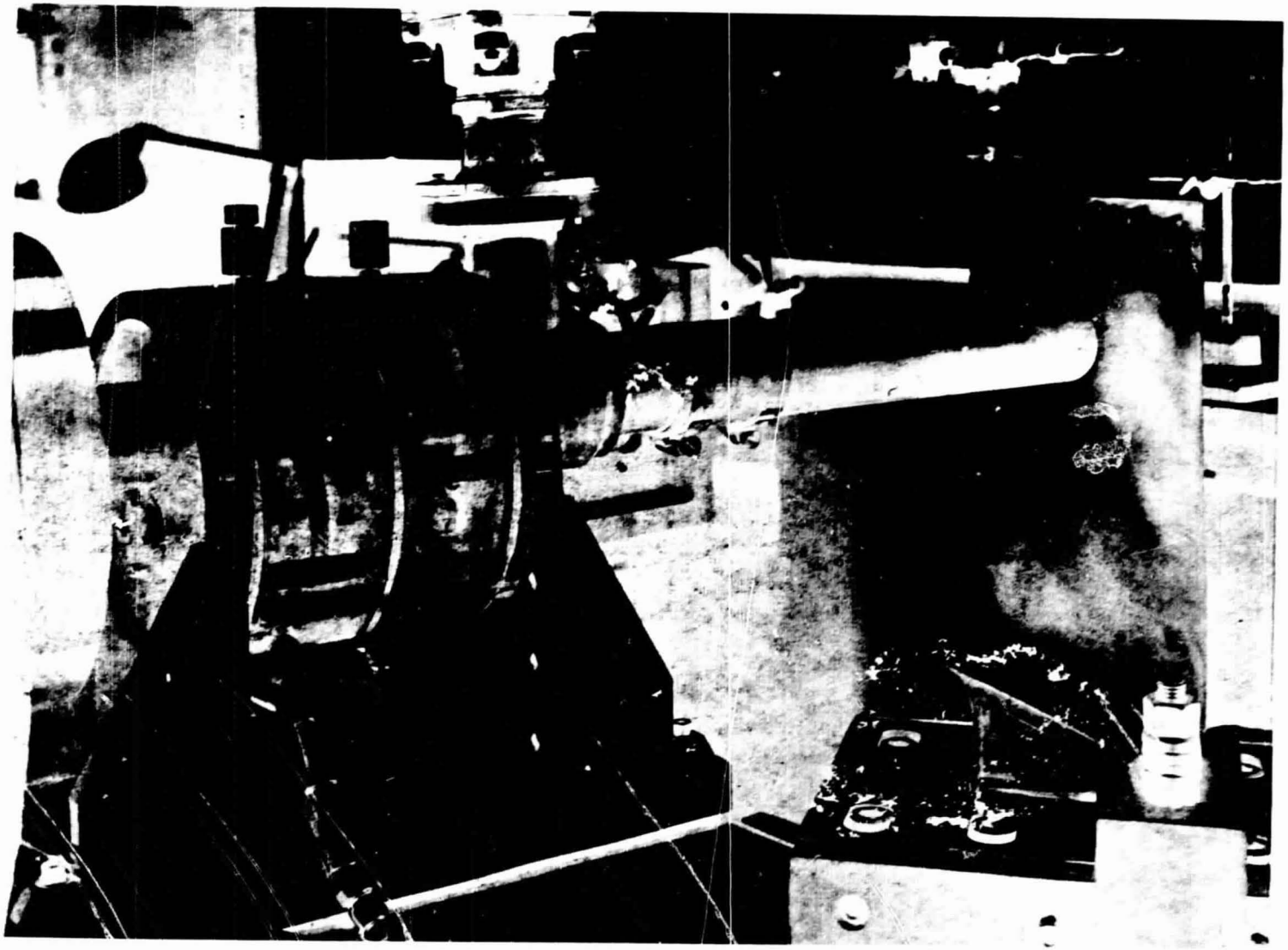

Figure 32. Inner Panel Test Setup.

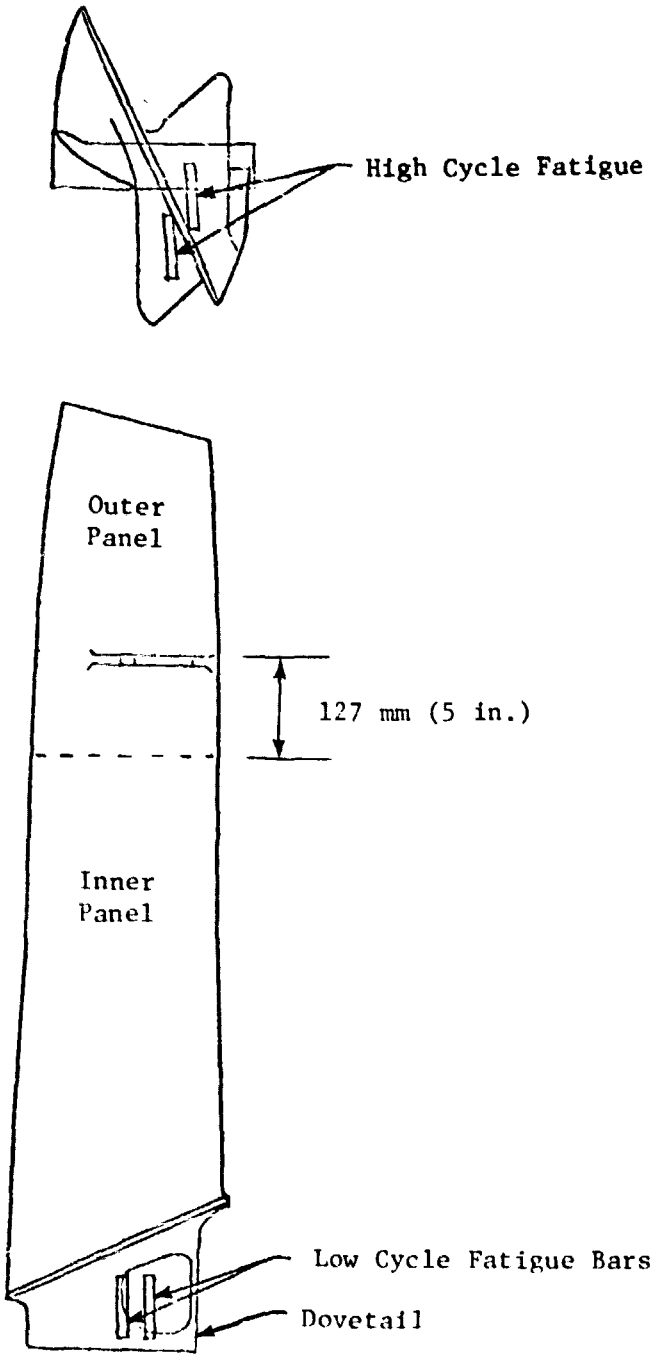

Figure 33. Location of Test Bars Taken From Forging.

For the inner panel fatigue tests, eight strain gages were used, all on the concave side of the blade and shank at the leading edge, as shown in Figure 34. The gages were positioned to be in the area of highest stress. Locating this area was based on previous dynamic stress distribution testing and on failure initiation from previous fatigue tests on similar fan blades. Four gages were used on the airfoil. The first airfoil gage was right at the fillet tangency point. The next three gages were spaced 25.4 mm (1 in.) apart. The four shank gages were located at the edge of the corner radius tangency point. The spacing of these gages was as close to the adjacent gage as possible. Grid sizes of all gages used were 1.6 mm and 0.8 mm.

Five strain gages were used on the outer panel fatigue tests, as shown in Figure 35. Selection of these locations was based on the same previous fatigue test discussed above. The gages were always located on the fillet tangency point and perpendicular to the tangency line. Failure initiation was always very close to the strain gage.

Eight strain gages were used on the concave shroud fatigue tests as shown in Figure 36. Gages were placed back-to-back on the top and bottom sides of the shroud. The fillet tangency point was consistently used as the locator from the edge or airfoil. It was not possible to drive the shroud to an amplitude that would produce failure, so it is not known how the instrumentation corresponded to the fatigue initiation points. However, previous tests on similar fan blades indicated that the middle gage in the group of three was the initiation point.

5.3 TEST PROCEDURE

For the low cycle fatigue bars taken from the shank section of the forging, an axial load to produce a stress level of 62,055 N/cm^2 (90,000 $lb/in.^2$) was applied to the notched bars. The load was then cycled from 0 to 62,055 N/cm^2 (90,000 $lb/in.^2$) for the entire test until the bar failed.

A moment was applied to the first smooth bar, taken from the shroud section of the forging. This stress was cycled from a compressive to a tensile stress at the 37,922 N/cm^2 (55,000 $lb/in.^2$) level. Since the first bar tested did not fail in 10.6×10^6 cycles, the second bar was loaded to give a stress level of 44,817 N/cm^2 (65,000 $lb/in.^2$). The second bar sustained 15.5×10^6 cycles without failure.

The inner panel fatigue testing was accomplished by clamping the cutoff inner panel of the blade on the dovetail pressure face. The blade was then vibrated with an air siren at its first flexural frequency. The highest reading strain gage was on the airfoil. Previous tests with a similar blade had shown the maximum stress to be on the shank; that blade though had a larger pocket in the shank and that difference probably explains the difference in stress distribution. The siren air pressure was then increased until the highest reading strain gage read 46,450 N/cm^2 (67,368 $lb/in.^2$). The blade did not fail after 5×10^6 cycles were accrued. The stress level was then increased to 49,988 N/cm^2 (72,500 $lb/in.^2$). When the part still did not

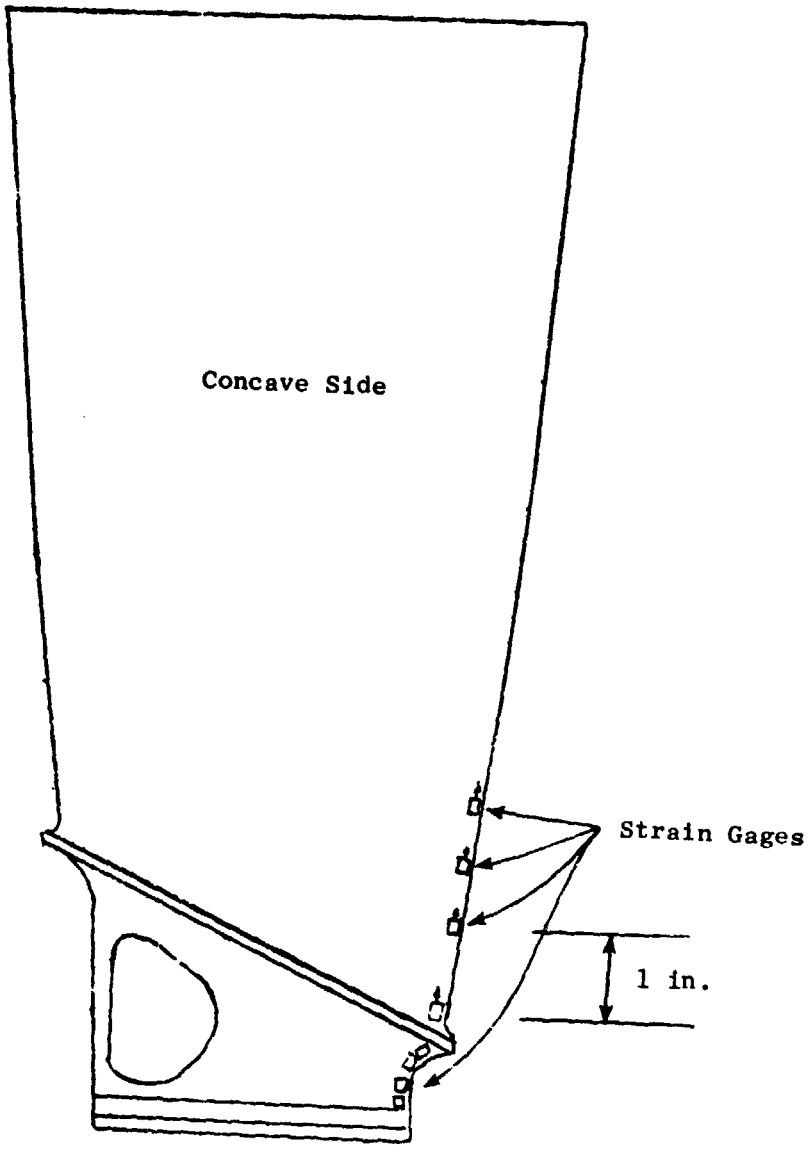

Figure 34. Inner Panel Instrumentation.

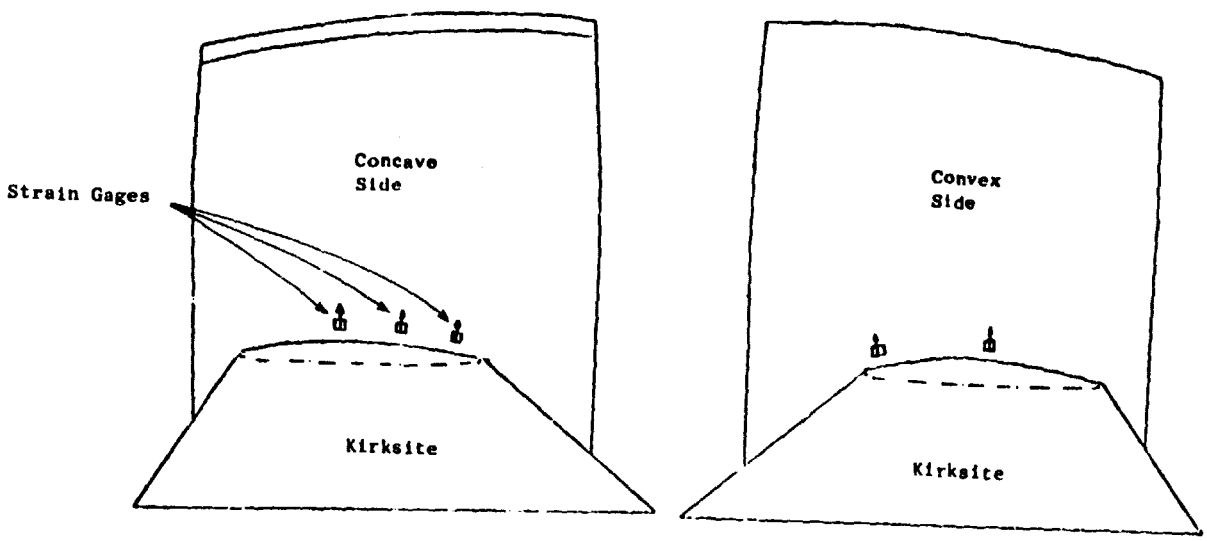

Figure 35. Outer Panel Instrumentation.

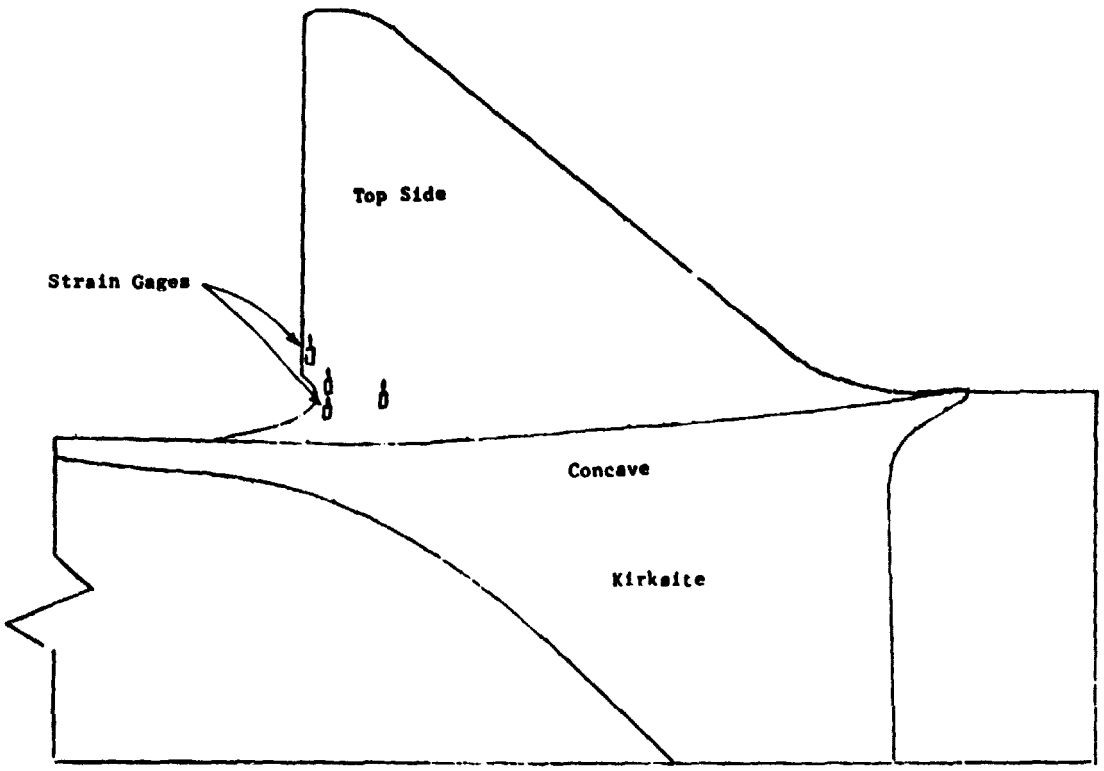

Figure 36. Concave Side Shroud Instrumentation.

fail after 10^6 cycles, the level was increased to 53,436 N/cm^2 (77,500 lb/in.^{2}) for another 10^6 cycles - again without failure. Finally, the level was increased to 56,883 N/cm^2 (82,500 lb/in.^{2}) and failure occurred prior to 10^4 cycles. The same procedure was followed on another inner panel specimen, except the test was started at 49,988 N/cm^2 (72,500 lb/in.^{2}) for the first 5×10^6 cycles and failure finally occurred at 60,330 N/cm^2 (87,500 lb/in.^{2}) in under 10^4 cycles.

The outer panel fatigue testing was conducted by clamping the kirksite block, which had been cast around the inner panel below the part-span shroud. The blade was driven in its first flexural mode of vibration by an air siren. The maximum strain gage reading of 46,540 N/cm^2 (69,500 lb/in.^{2}) was attained for 5×10^6 cycles without failure. The stress level was then increased to 49,988 N/cm^2 (72,500 lb/in.) for 10^6 cycles without failure, then to 53,436 N/cm^2 (77,500 lb/in.^{2}) for 10^6 cycles without failure. Finally, at 56,883 N/cm^2 (82,500 lb/in.), failure occurred in under 10^4 cycles. Another outer panel specimen was tested. The initial stress level of 49,988 N/cm^2 (72,500 lb/in.^{2}) for 5×10^6 cycles was completed without failure; the part failed at a level of 53,436 N/cm^2 (72,500 lb/in.^{2}) in under 10^4 cycles.

The concave side shroud fatigue test was conducted by clamping the kirksite block that had been poured around the convex side shroud and airfoil and driving the shroud with an air siren at its first flexural natural frequency. The stress level on the highest reading strain gage was 46,540 N/cm^2 (67,500 lb/in.^{2}). At this level, 5×10^6 cycles were accrued without failure. The amplitude was then increased to 49,988 N/cm^2 (72,500 lb/in.^{2}), where 10^7 cycles were accrued without failure. Since the siren was incapable of driving the shroud to a higher amplitude, the testing was terminated.

5.4 TEST RESULTS AND COMPARISON TO PREDICTIONS

Results of the round bar low cycle fatigue test are shown in the room temperature fatigue diagram in Figure 37. Both bars were tested at 62,055 N/cm^2 (90,000 lb/in.^{2}) peak stress or 31,027 N/cm^2 (45,000 lb/in.^{2}) alternating stress. The first test bar failed in 15,528 cycles. The second bar failed in 23,192 cycles. The average of these two test points would be 19,360 cycles. This compares with a material specification average life of 20,000 cycles, or a -3σ standard deviation life of 6000 cycles. These results are in good agreement with the average life and the material low cycle fatigue characteristics appear to meet all life requirements required of the fan blade.

High cycle round bar test results are shown on the Goodman diagram in Figure 38. The first test specimen was run at 37,922 N/cm^2 (55,000 lb/in.^{2}) alternating stress. This bar did not fail after 10^7 cycles. The second bar was tested at 44,817 N/cm^2 (65,000 lb/in.) and it did not fail after 15×10^6 cycles. These results compare well to the average materials specifications high cycle fatigue strength at an "A" ratio (alternating stress divided by mean stress) of infinity. The average high cycle fatigue material strength

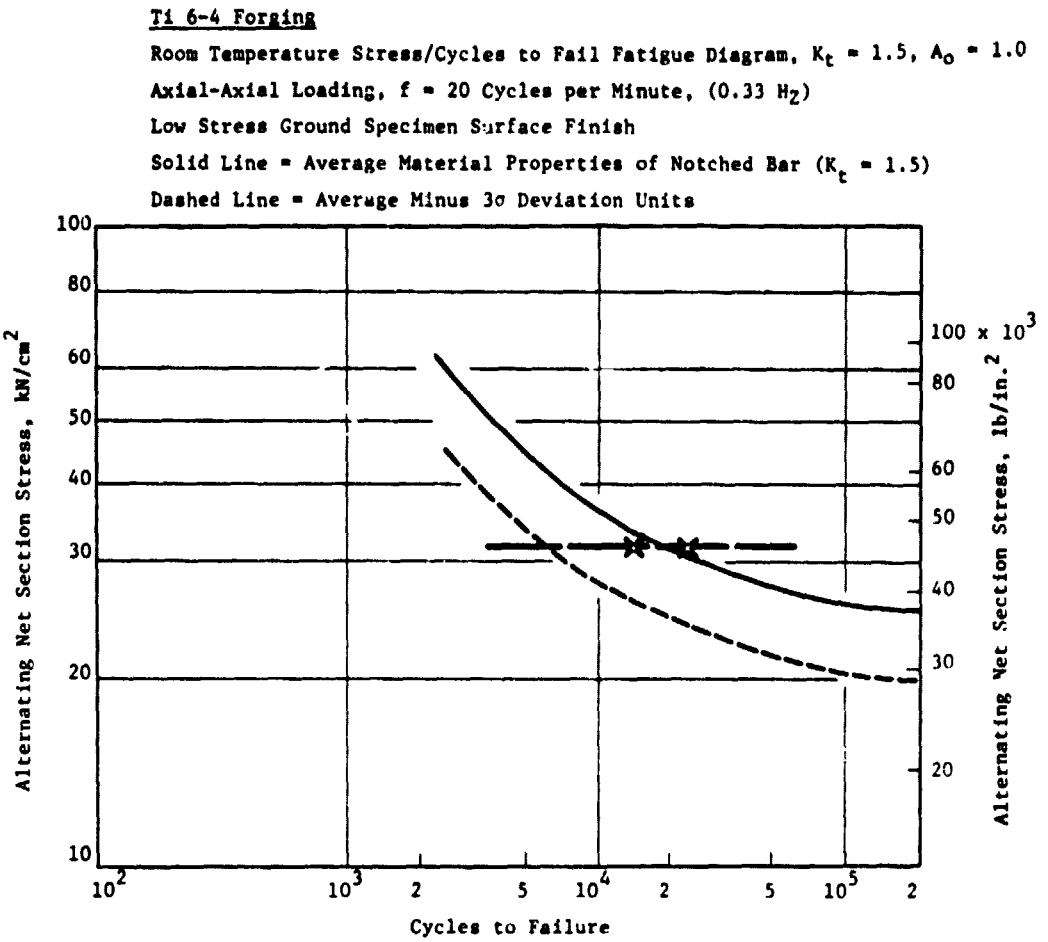

Figure 37. Fatigue Characteristics of Titanium LCF Specimens Made from Fan Blade Forgings in Dovetail Area.

Ti-6Al-4V Forging

Room Temperature Goodman Fatigue Diagram

Solid Line = Average Material Properties of Smooth Bar

Dashed Line = Average Minus 3σ Deviation Units

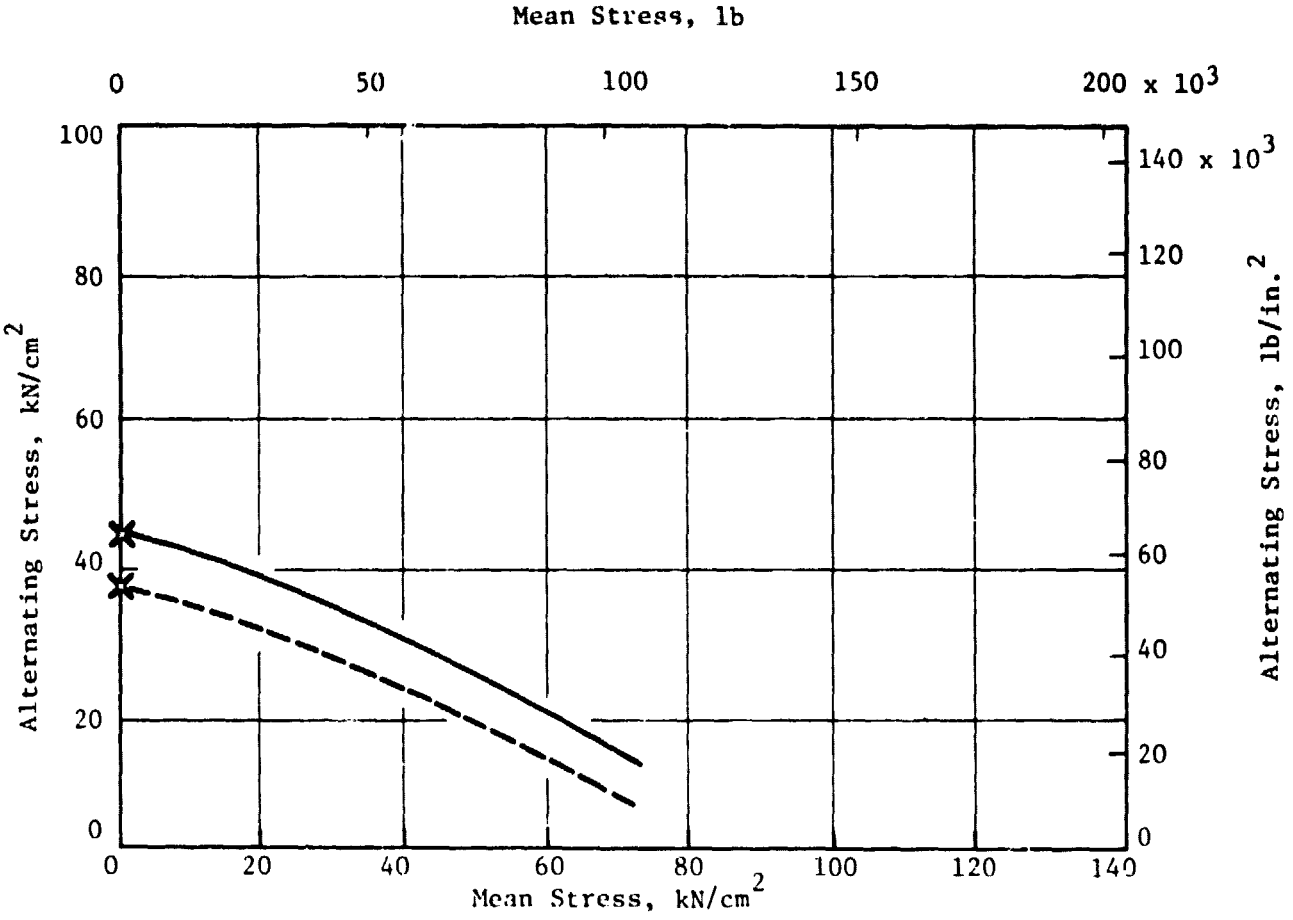

Figure 38. Goodman Diagram for Titanium HCF Specimens Made from Fan Blade Forgings in the Midspan Shroud Area.

is 44,128 N/cm^2 (64,000 lb/in.^{2}) and the -3σ standard deviation strength is 37,233 N/cm^2 (54,000 lb/in.^{2}).

Inner panel fatigue test results are shown in Figure 39 and are represented by the circles. The level of the first test was initiated at 46,540 N/cm^2 (67,500 lb/in.^{2}) and increased in increments of 3450 N/cm^2 (5,000 lb/lb/in.^{2}) until the part finally failed at 56,883 N/cm^2 (82,500 lb/in.^{2}). The second specimen was tested at an initial 49,988 N/cm^2 (72,500 lb/in.^{2}) and also increased in 3450 N/cm^2 (5000 lb/in.^{2}) increments until failure at 60,330 N/cm^2 (87,500 lb/in.^{2}). These results compare well with the materials S-N curve that shows an average runout of 51,000 N/cm^2 and a -3σ standard deviation strength of 43,440 N/cm^2 (63,000 lb/in.^{2}).

Outer panel fatigue test results on finished blades are also shown in Figure 39 and are represented by the triangles. The same levels were tested and increased incrementally the same as for the inner panel test. The first test specimen failed at 56,883 N/cm^2 (82,500 lb/in.^{2}) and the second at 53,436 N/cm^2 (77,500 lb/in.^{2}). The outer panel points plot the same as the inner panel on the Goodman diagram in Figure 40.

Part-span shroud fatigue test results are shown in Figure 39 by the rectangular symbols. A level of 46,540 N/cm^2 (67,368 lb/in.^{2}) was run without failing the shroud. The test was terminated without experiencing a shroud fatigue crack because of the limitations of the air siren.

Bench fatigue test results with both the round bar test specimens and the finished airfoil demonstrated that the improved fan blade design is equal in fatigue margin to the current CF6 fan blade. The current CF6 fan blade has never experienced a fatigue failure in over 12 million flight hours. The fatigue testing demonstrated that the improved fan blade has no high stress concentrations to degrade the fatigue strength of the design. A substantial margin exists between measured engine stresses and the fatigue capability of the design.

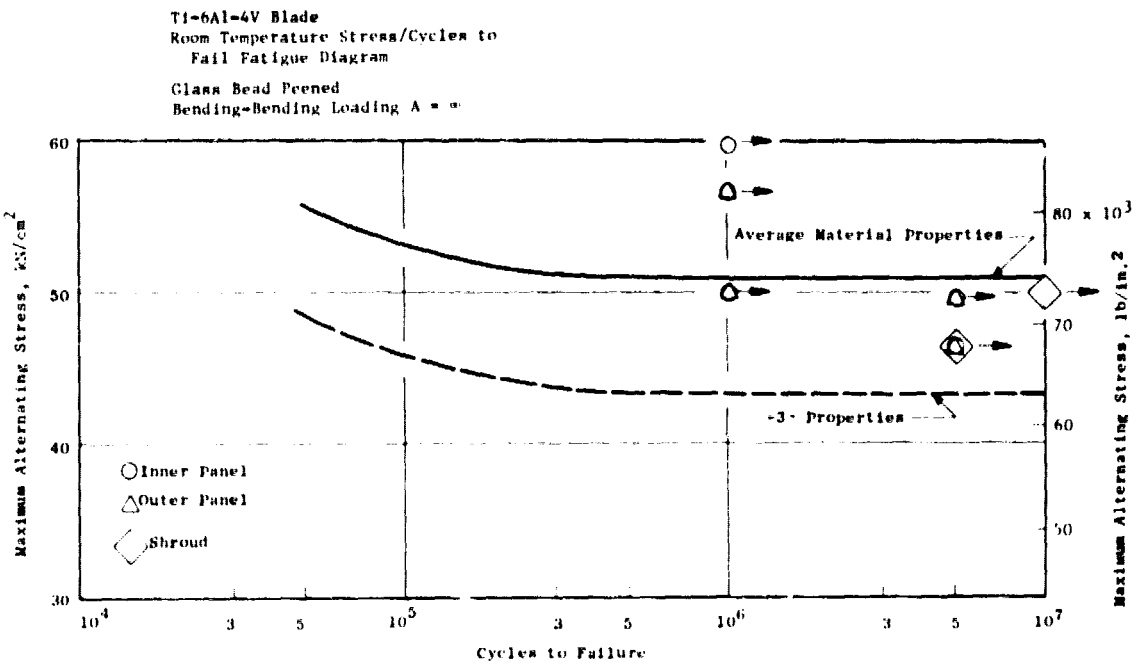

Figure 39. Fatigue Characteristics of Fan Blade Inner and Outer Panels and Part-Span Shroud.

Ti-6Al-4V Blade
RT Fatigue Limit Diagram
Glass Bead Peened
Estimated Condition: 6-12 N, No. 98 Bead, 125%

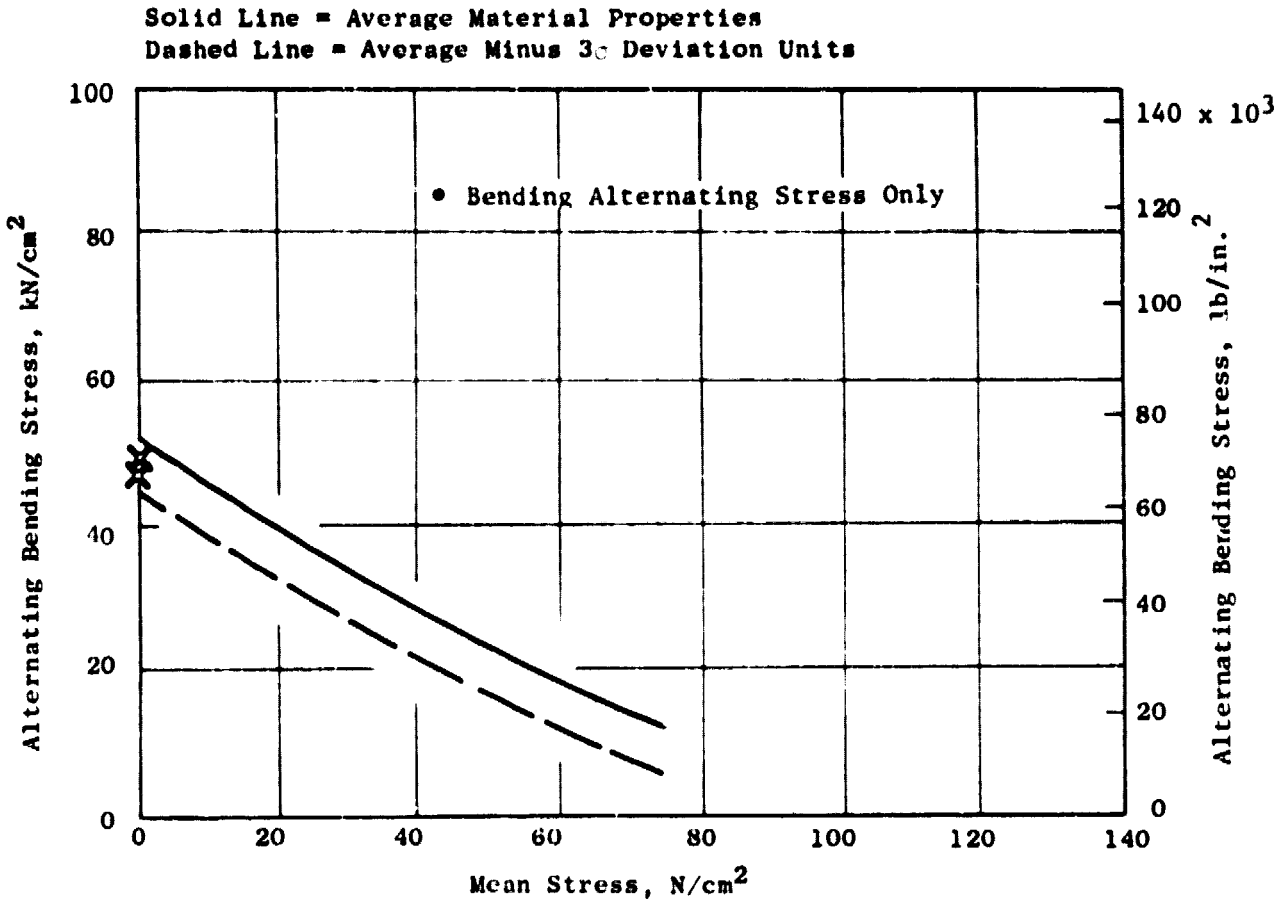

Figure 40. Goodman Diagram for Improved Fan Blade Inner and Outer Panels and Part-Span Shroud.

6.0 ENGINE CROSSWIND TEST

Objectives of the crosswind test were to evaluate the performance of the improved fan blade on a CF6-50 engine under the influence of inlet distortion induced by 90° crosswinds and to demonstrate the aeromechanical operation of the improved fan blade using both the Douglas DC-10-30 and the Boeing 747 inlets at crosswind velocities up to 64.8 to 74.1 km/hr (35 to 40 kn).

6.1 CROSSWIND TEST FACILITY AND CONFIGURATIONS

The test was conducted in the outdoor crosswind test facility shown in Figure 41. A bridge-type structure supports a turntable thrust frame for overhead engine mounting. Crosswinds up to 185 km/hr (100 kn) for a stationary engine centerline and up to 157 km/hr (85 kn) at angles between 0° and 90° can be created by the thirteen 5664 m^3/min (200,000 cfm) two-stage axial flow variable pitch fans driven by 150 kw electric motors in this facility. Automatic data handling in the adjacent control blockhouse can be processed on an Evendale time-sharing computer.

Test vehicles for the DC-10-30 inlet and B747 inlet tests were CF6-50 engines. The fan configuration was the same for each test and consisted of the following:

- Improved fan blades with fan case stiffener to permit tip clearance to be set at 2.92 mm (0.115 in.)
- Open cell aluminum honeycomb fan casing tip shrouds
- Inlet rake system which replaced the standard spinner with a split spinner to provide support for the rakes.

6.2 INSTRUMENTATION

6.2.1 Strain Gages

The strain gages used for measuring fan blade stresses were 1.6 mm (1/16 in.) grid, dynamic type, with 350 ohm resistance. Strain signals were routed out through a forward slip ring and displayed on oscilloscopes as well as recorded on magnetic tapes.

Four fan blades were instrumented with a total of 16 strain gages at four different locations. These blades were installed in Disk Slots 1, 10, 19 and 29. Figure 42 is a schematic of blade strain gage locations. These gage locations were chosen to insure a relatively high level of response to all anticipated vibratory modes.

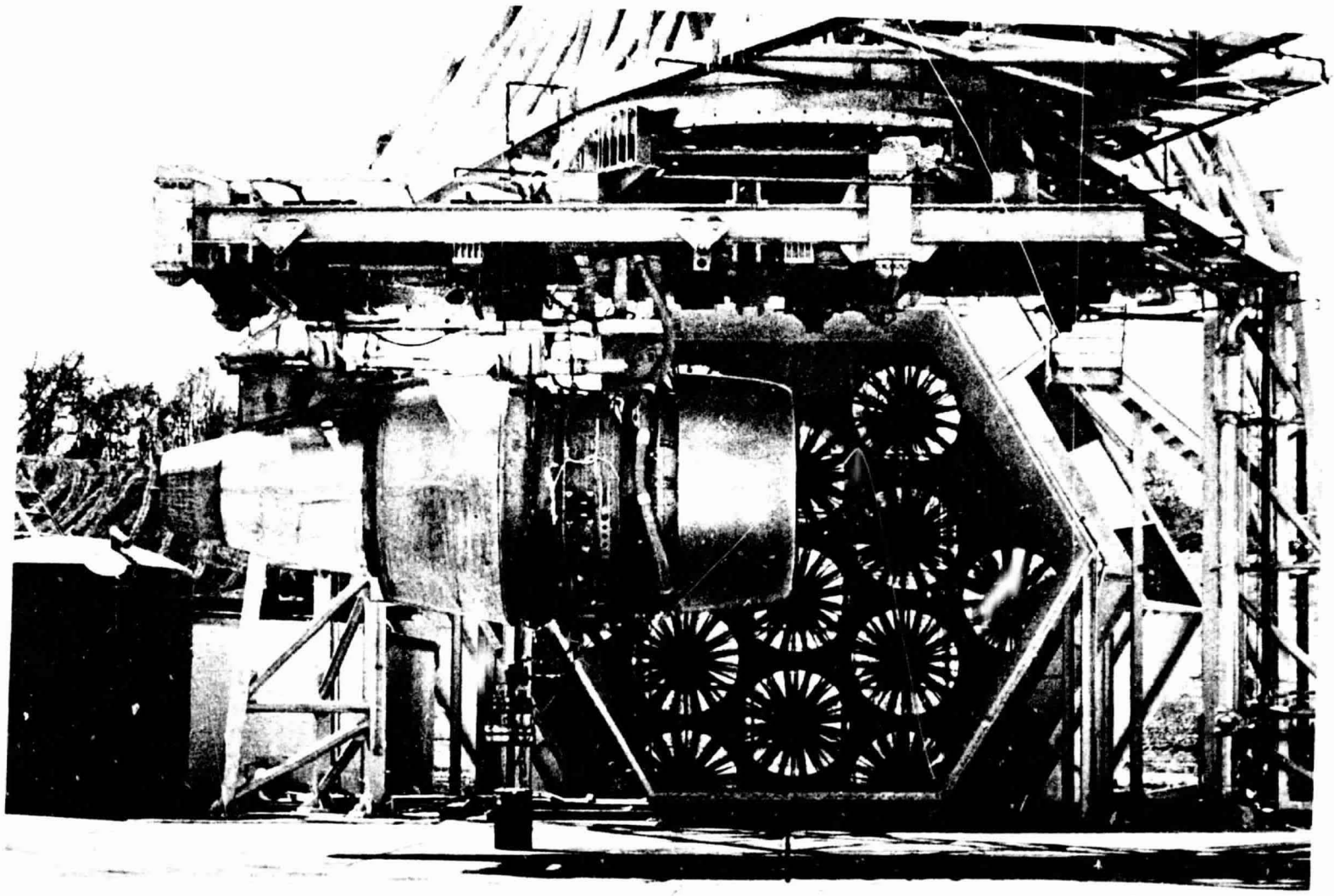

Figure 41. Engine Crosswind Test Facility.

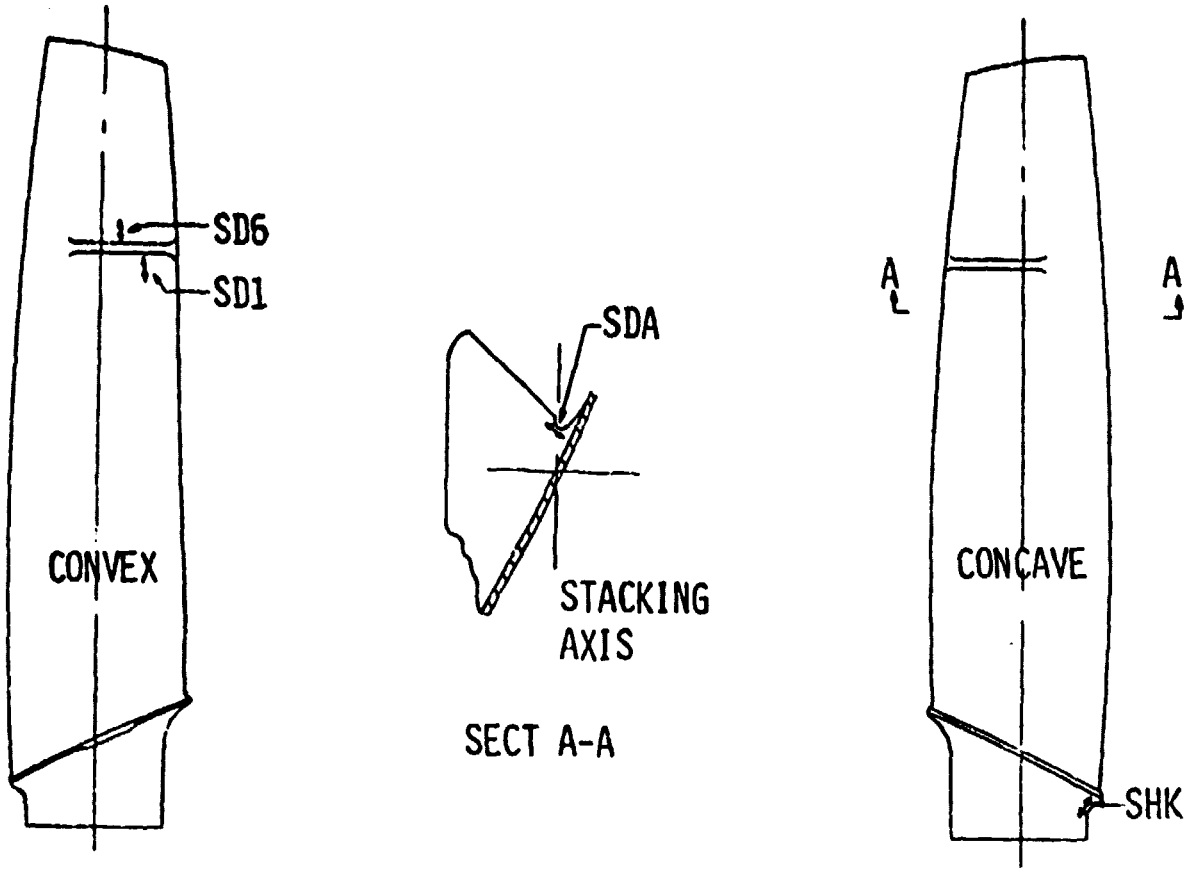

Blade	Disk Slot	Gages
1	1	SHK, SD1, SD6, SDA
2	10	SHK, SD6, SD1, SDA
3	19	SHK, SD1, SD6, SDA
4	29	SHK, SD6, SD1, SDA

Figure 42. Fan Blade Strain Gage Instrumentation.

6.2.2 Fan Inlet Aerodynamic Instrumentation

Fan inlet aerodynamic distortion was monitored and measured in the circumferential and radial directions by steady-state pressure and temperature probes mounted on rakes as illustrated in Figure 43.

The steady-state instrumentation was located slightly forward of the fan and consisted of six rakes spaced circumferentially clockwise (aft looking forward) at 38°, 98°, 158°, 218°, 278°, and 338°. Each rake contained six total pressure probes, six static pressure taps, and five temperature probes.

There were also two boundary layer rakes located at 55° and 270°. Each boundary layer rake contained nine total pressure probes located off the wall at immersions of 5.1 mm (0.2 in.), 10.2 mm (0.4 in.), 15.3 mm (0.6 in.), 20.4 mm (0.8 in.), 25.4 mm (1.0 in.), 38.1 mm (1.5 in.), 50.8 mm (2.0 in.), 63.5 mm (2.5 in.) and 76.2 mm (3.0 in.).

There were also two dynamic pressure transducers in the fan discharge wall. The test instrumentation which was used to monitor engine operation is shown in Figure 44.

6.3 TEST PROCEDURE

The engine with the DC-10-30 or B747 inlet was installed in the test stand and set up with the engine oriented with the crosswind from the left (aft looking forward) at an angle of 90° with the engine axis. Instrumentation was connected. The following test sequence was performed:

1. Perform normal prefire checks, including a leak check.

2. Start the engine and stabilize for 5 minutes at ground idle.

3. Perform the mechanical checkout and break-in run.

4. Set fan speed at flight idle, and slowly turn on the required number of facility fans, one at a time, to obtain the desired crosswind velocity.

5. Slowly accelerate engine to the desired corrected fan speed, stabilize 3 minutes, and take data. If maximum fan speed cannot be reached because of fan stalls or high vibrations, back off 100 rpm, stabilize 3 minutes, and record data.

6. Record the fan speed at which the inlet flow reattached; and define the inlet separation, inlet distortion, and engine stability for each crosswind condition.

The engine with the DC-10-30 inlet was tested for about 35 hours in order to complete the following crosswind test points:

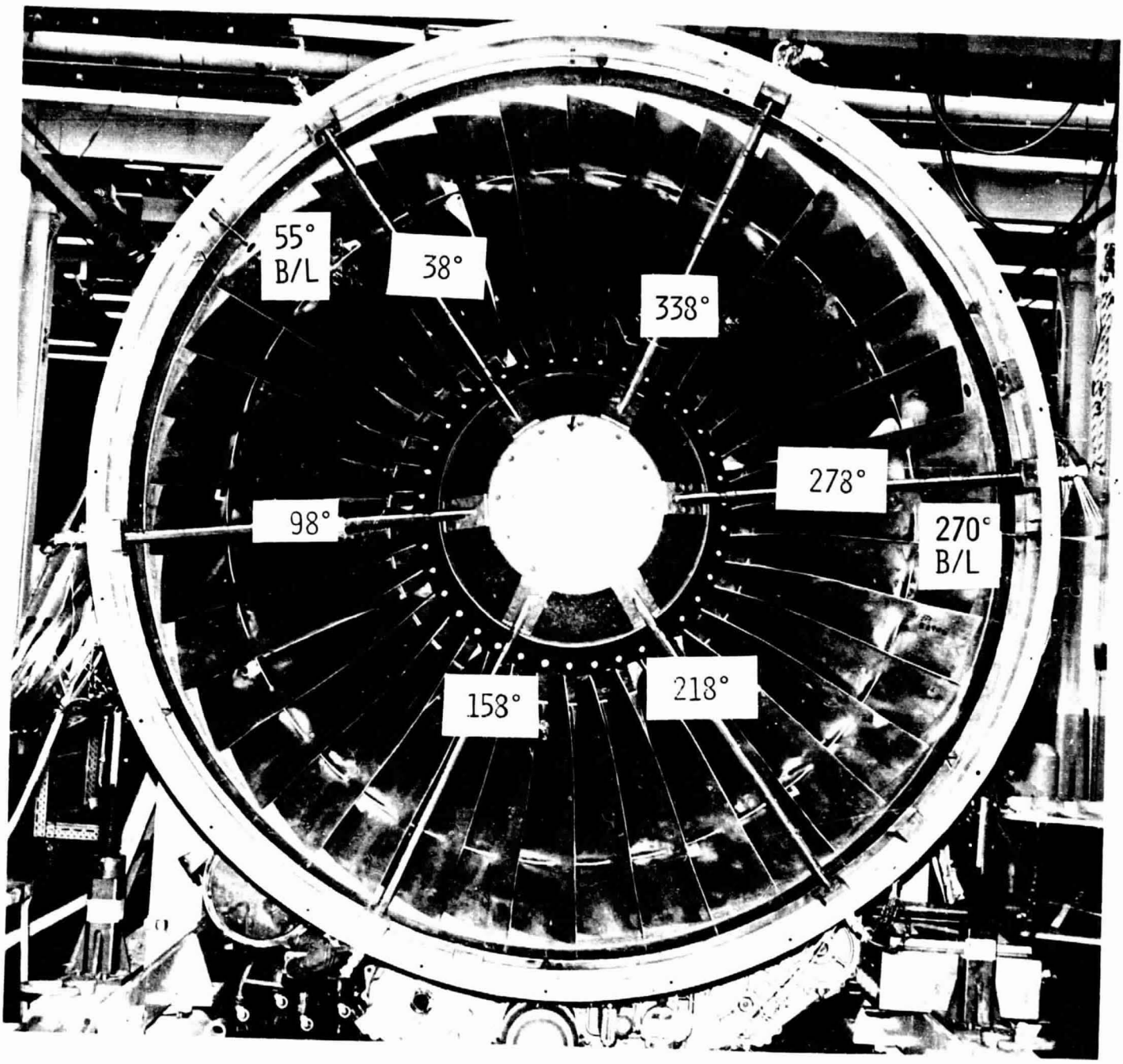

Figure 43. Fan Inlet Instrumentation for Crosswind Test.

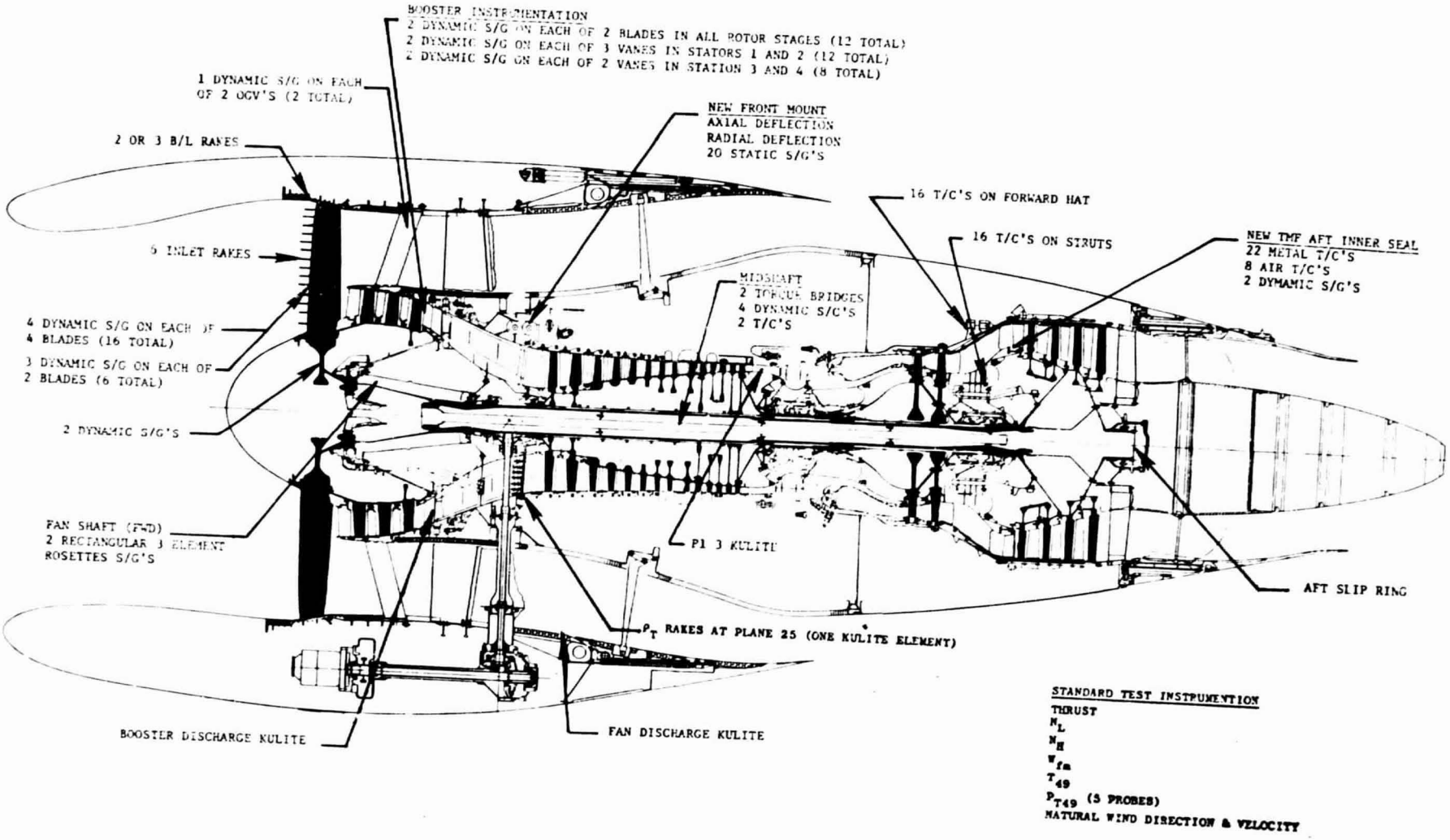

Figure 44. CF6-50 Engine - Instrumentation for Crosswind Test.

Fan Speed		Crosswind Facility[1] No. of Fans/Average Crosswind Velocity, km/hr				
rpm	%	0/0	4/33.9	5/42.6	7/60.0	9/65.8
Ground Idle		X				
Flight Idle		X	X	X	X	X
2500	72.8	X	X	X	X	X
2746	80.0	X	X			
3350	97.6	X	X	X	X	X
3670	106.0	X	X	X	X	X[2]
3783	110.2	X				
3900	113.6	X	X	X	X	X[2]

(1) Figure 45 identifies the facility fans in operation
(2) Not completed because of facility failure

6.3.1 DC-10-30 Inlet - Baseline Test Procedure

The baseline test was run with an ambient tailwind gusting up to 9.6 km/hr (6 mph). The engine was operated from ground idle to 3900 rpm corrected fan speed. The following steady-state speeds were set and held for a period of 5 minutes:

- Flight Idle
- 2500 rpm
- 2746 rpm
- 3350 rpm
- 3670 rpm
- 3783 rpm
- 3900 rpm

6.3.2 DC-10-30 Inlet - 90° Crosswind Test Procedure

With four facility fans on, the engine was operated from ground idle to 3900 rpm corrected fan speed. The following steady-state speeds were set and held for a period of 5 minutes:

- Flight Idle
- 2500 rpm

No. of Fans	DC-10-30 Inlet Tests Average Crosswind Velocity		Fans in Operation
	km/hr	knots	
4	33.9	18.3	4,5,9,10
5	42.6	23.0	4,5,7,9,10
6	51.0	27.5	3,4,5,7,9,10
7	60.0	32.4	3,4,5,7,9,10,11
9	65.8	35.5	3,4,5,6,7,8,9,10,11
10	72.5	39.1	2,3,4,5,6,7,8,9,10,11
13	92.3	49.8	All

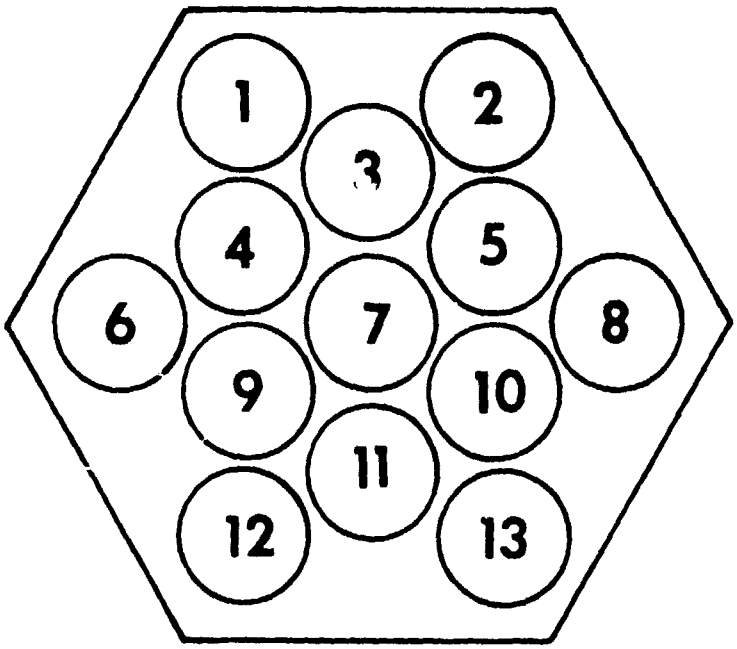

Looking Upstream

Figure 45. Identification of Facility Fans for Crosswind Test.

- 2746 rpm
- 3350 rpm
- 3670 rpm
- 3900 rpm

This procedure was repeated, except for the 2746 rpm, with five and seven facility fans on. With nine facility fans on, the engine was operated from ground idle to 3580 rpm physical speed. The following steady-state speeds were set and held for a period of 5 minutes:

- Flight Idle
- 2500 rpm
- 3350 rpm

While taking data at the 3350 rpm point, two facility fans failed resulting in foreign object damage to the test fan blades which terminated the test.

New facility fans were installed prior to the engine testing with the B747 inlet. The new facility fans generated less crosswind velocity than the original fans. Four facility fans generated 33.9 km/hr (18.3 kn) while the DC-10-30 inlet was being tested, whereas four facility fans only generated 29.6 km/hr (16 kn) when the B747 inlet was being tested. This explains why there was some difference between the two tests in the velocities used even though the same number of facility fans was used.

The engine with the B747 inlet was tested for about 15 hours in order to determine inlet separation, inlet distortion, and engine stability for the following crosswind test points:

Fan Speed		Crosswind Facility(1) No. of Fans/Average Crosswind Velocity, km/hr					
rpm	%	0/0	4/29.6	5/35.2	7/40.8	9/59.3	12/79.7
Ground Idle		X	X	X	X	X	X
2500	72.8	X	X	X	X	X	X
2800	81.6				X	X	X
3350	97.6	X	X	X			
3600	104.9	X	X				
3898	113.6	X					

(1) Figure 45 identifies the facility fans in operation

6.3.3 B747 Inlet - Baseline Test Procedure

The baseline test was run with an ambient tailwind gusting up to 6.4 km/hr (4 mph). The engine was operated from ground idle to 3898 rpm physical fan speed. The following steady-state speeds were set and held long enough to collect stress data:

- 2500 rpm
- 3350 rpm
- 3600 rpm

6.3.4 B747 Inlet - 90° Crosswind Test Procedure

With sufficient facility fans to supply 29.6 km/hr (16 kn) crosswind, the engine was operated from ground idle to 3550 rpm physical fan speed. The following steady-state speeds were set and held long enough to collect stress data:

- 2500 rpm
- 3350 rpm
- 3550 rpm

With 35.2 km/hr (19 kn) crosswind, the engine was operated from ground idle to 3400 rpm physical fan speed. Steady-state speeds of 2500 rpm and 3350 rpm were set and held long enough to collect stress data.

The fan speed was limited to 2800 rpm for the remainder of the test. This fan speed is sufficient to provide breakaway power levels required to achieve forward aircraft speed for initiating takeoff and inlet cleanup. This is consistent with the rolling takeoffs practiced in airline service.

With 40.8 km/hr (22 kn) crosswind, the engine was operated from ground idle to 2800 rpm physical fan speed. Steady-state speeds of 2500 rpm and 2800 rpm were set and held long enough to collect stress data. This sequence was repeated with 59.3 km/hr (32 kn) crosswind and repeated again with 79.7 km/hr (43 kn) crosswind.

6.4 TEST RESULTS AND DISCUSSION

6.4.1 Modes of Vibration

Modes of vibration and levels of response of the improved fan blade were observed throughout the engine operating speed range for various levels of distortion. Blade characteristic vibratory modes and corresponding infinite

life stress limits associated with the strain gage locations were determined and an analysis of the vibratory behavior of the fan rotor assemblies as a system was conducted.

Significant system vibratory modes observed in the fan are: first 3-diametral, second 6-diametral and second 5-diametral, given in the order of occurrence from ground idle to maximum fan speed as shown in Figure 46.

In system modes, the blades respond in phase with each other. A system mode of the N-diametral type for a rotating system is usually characterized by a vibratory wave which travels in the direction opposite to that of the system rotation. Thus, when the system speed and the vibratory speed are equal, the vibratory motion appears standing still to a stationary observer. This occurs when the frequency curve of the N-diametral mode crosses the N-cycle per revolution line. The speed at which this occurs is referred to as the N-diametral critical speed. This is the only speed at which this mode can be excited to any significant stress level. The first 2-diametral mode has also been observed at high engine operating speeds. Since the frequency curve for this mode does not cross the 2/rev line in the engine operating speed range, the observed levels have been low.

The other type of vibration observed on the fan blades is out-of-phase mode vibration. During this type of vibration, blades tend to behave independently of each other. Figure 47 is an out-of-phase Campbell diagram for the advanced fan blade. The only significant out-of-phase modes observed on the fan blade have been first flexural, first torsional, and second flexural modes. Peak response of these modes generally occur at the crossover point of frequency curve and the N-cycle per revolution lines.

Vibratory characteristics of the improved fan blade are very similar to the current CF6 production fan blade.

6.4.2 Stress Limits

Infinite life stress limits were calculated for each vibratory mode at each strain gage location where significant stresses occur in that particular mode.

The meaning of infinite life stress limit is that, as long as the stress at a particular gage location in a particular mode does not exceed this limit, the maximum stress experienced in the part is less than the endurance strength of the material, and the part will operate safely for an infinite time at this condition. The limits include factors to account for: (1) sharp corners, fillets and other discontinuities when necessary, (2) blade-to-blade variations, and (3) electronics accuracy limit.

Infinite life stress limits for the principal vibratory modes of the improved fan blade are presented in Table I and Figures 48 through 51.

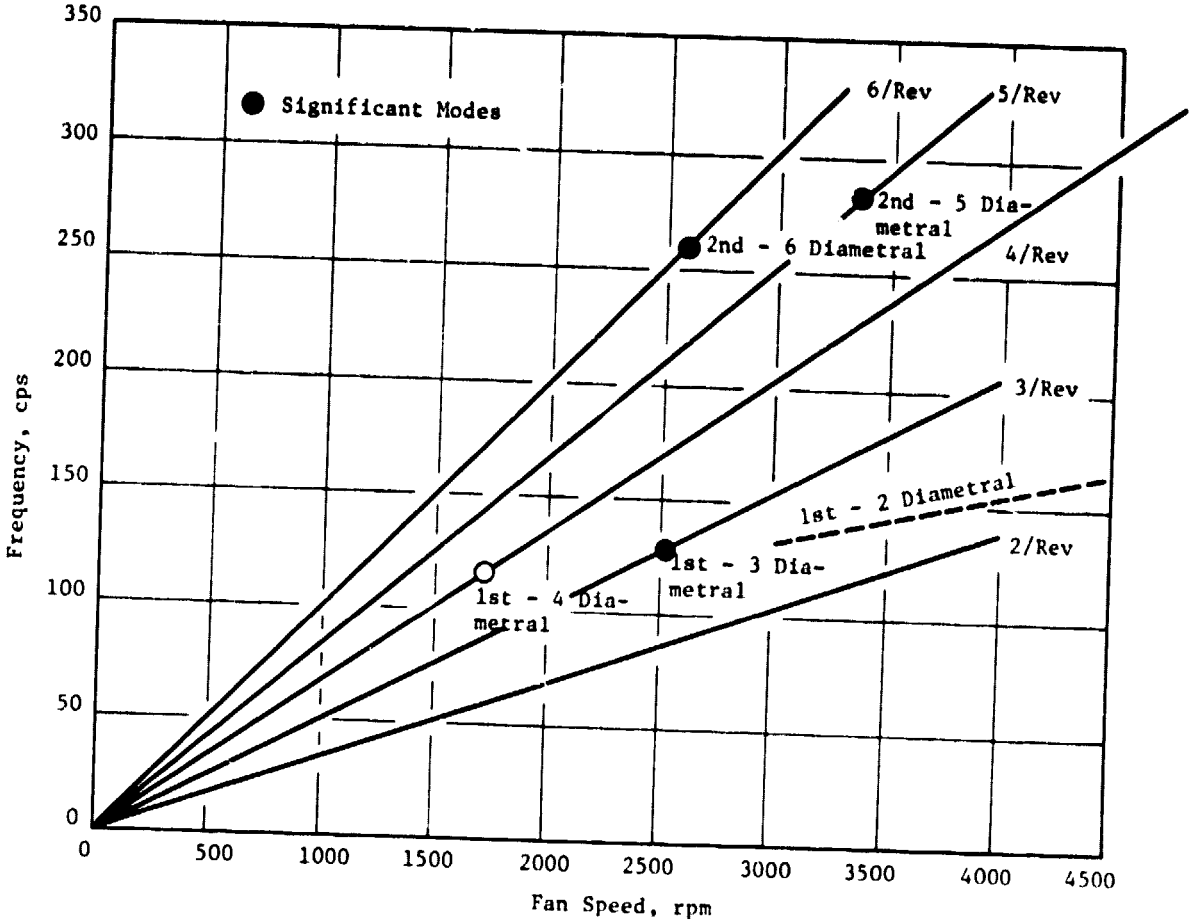

Figure 46. CF6-50 Engine, Improved Fan Rotor Blade System Modes Campbell Diagram.

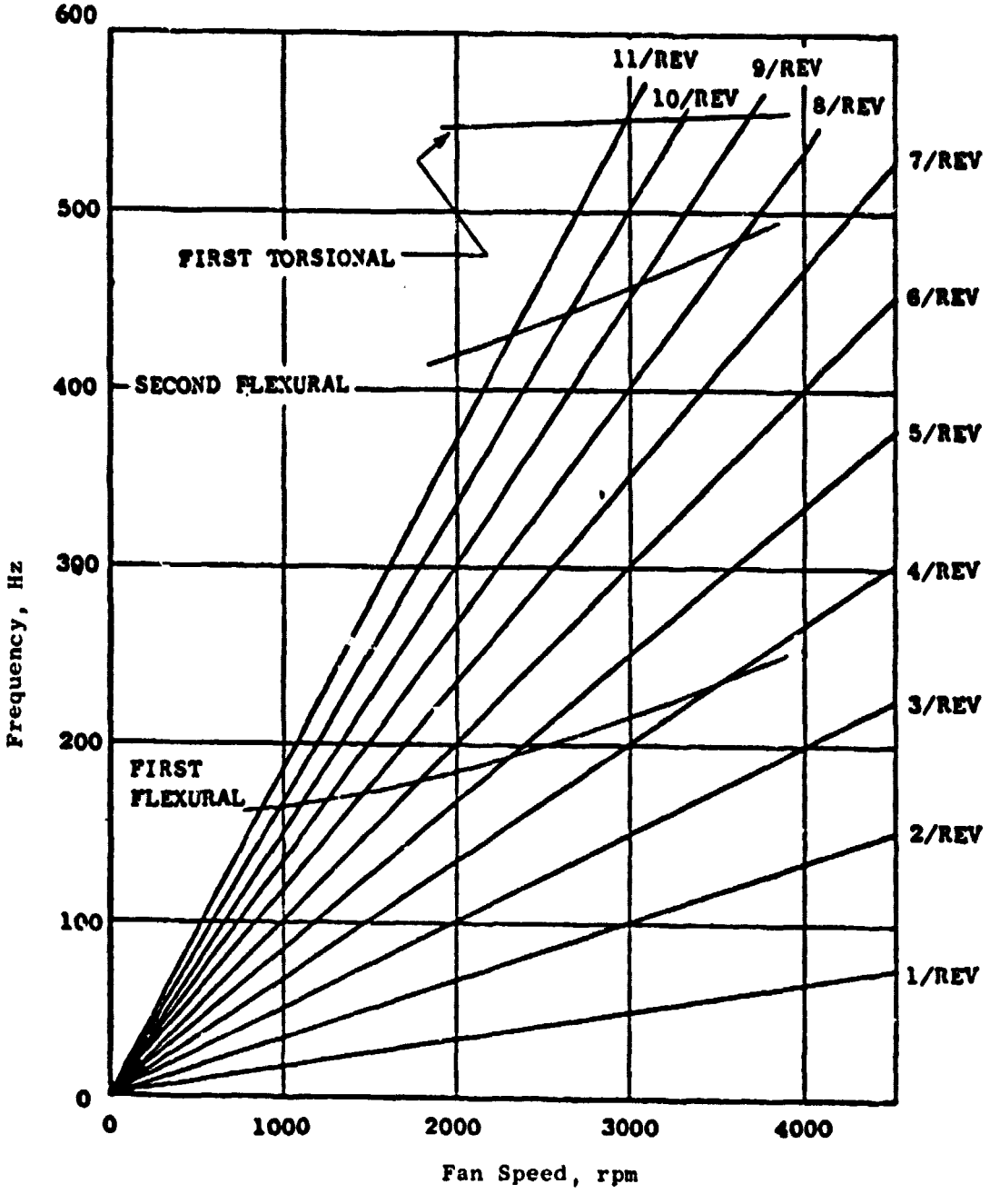

Figure 47. Fan Campbell Diagram Out-of-Phase Modes, Improved Fan Blade.

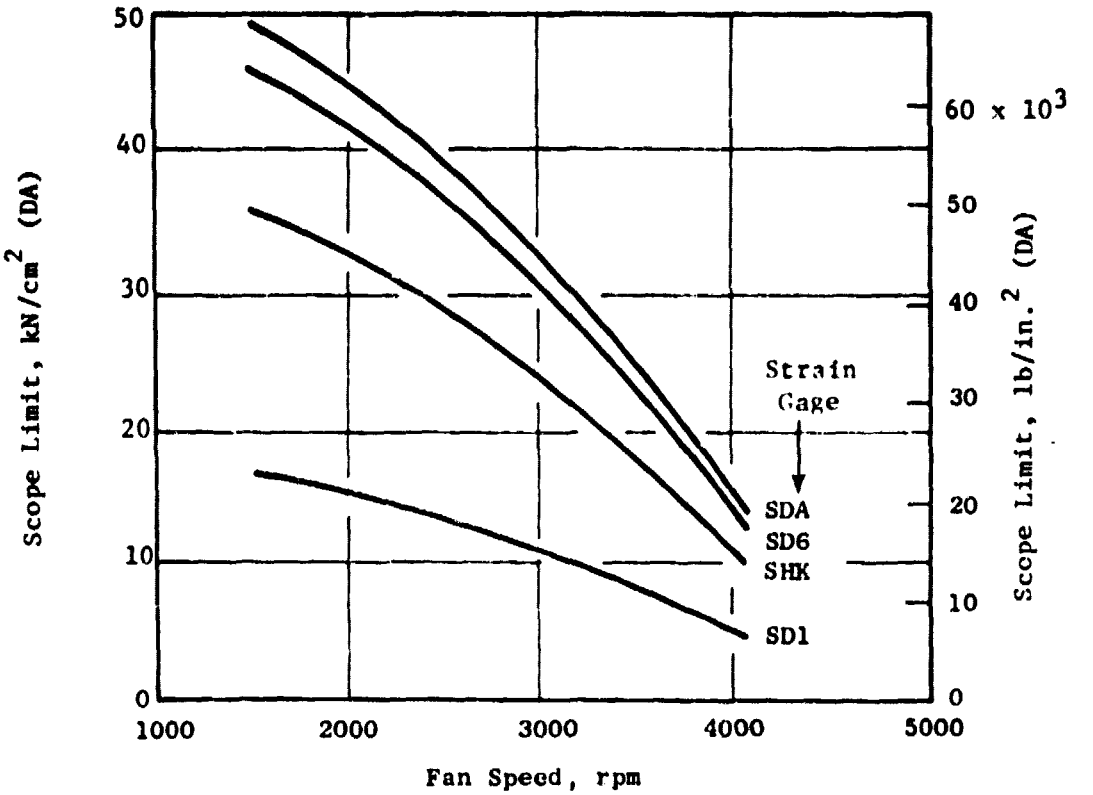

Figure 48. Improved Fan Blade Scope Limits, First Two-Diametral System Mode.

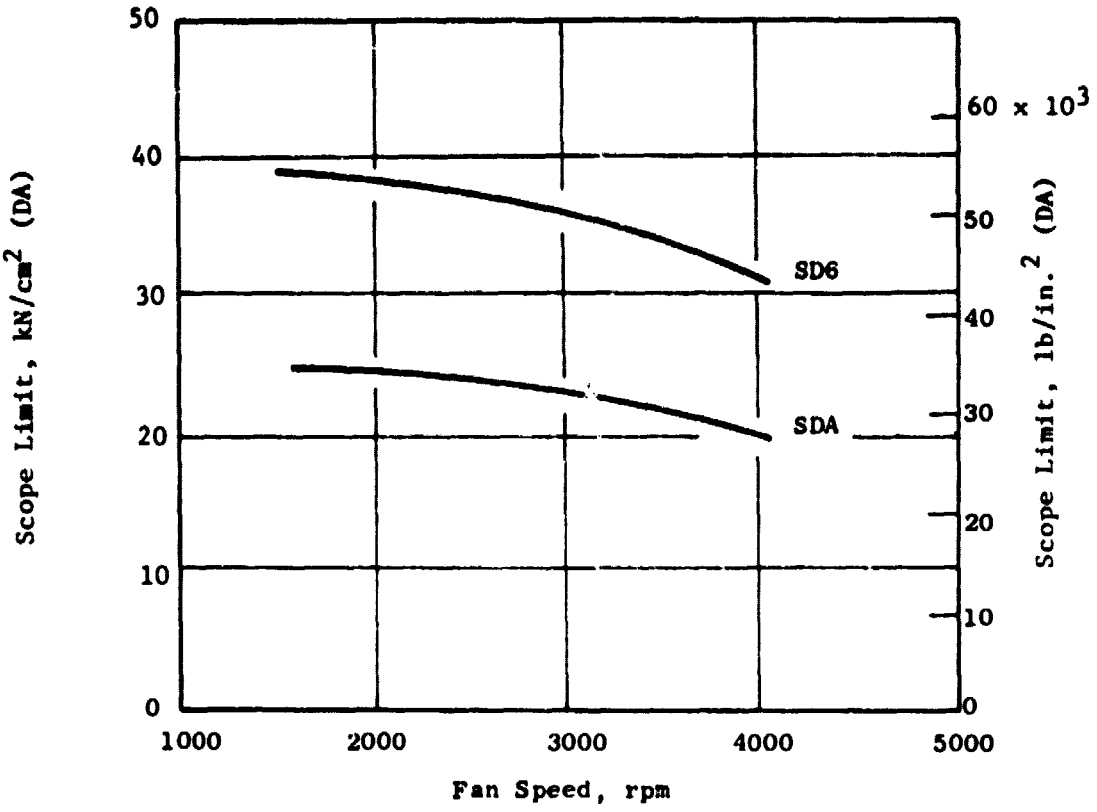

Figure 49. Improved Fan Blade Scope Limits, First Flexural Mode.

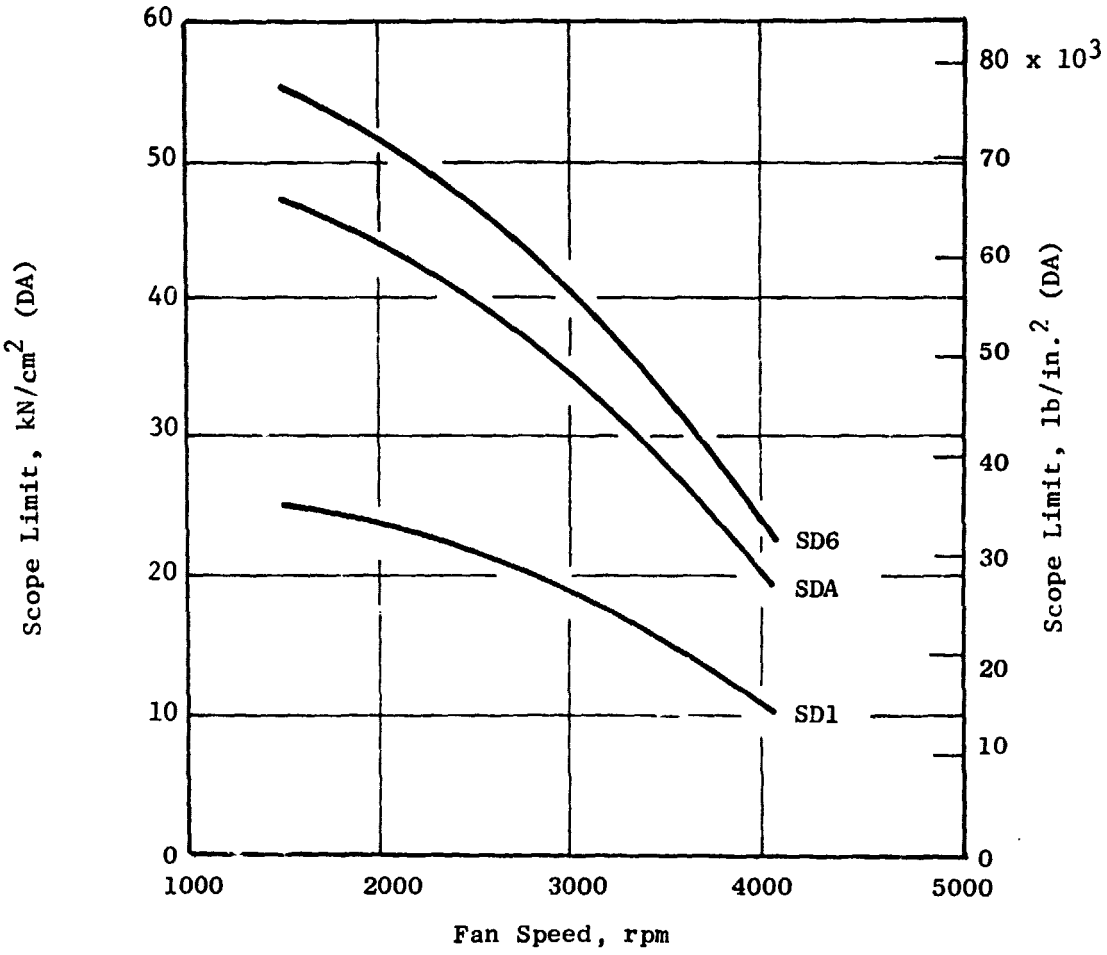

Figure 50. Improved Fan Blade Scope Limits, First Torsional Mode.

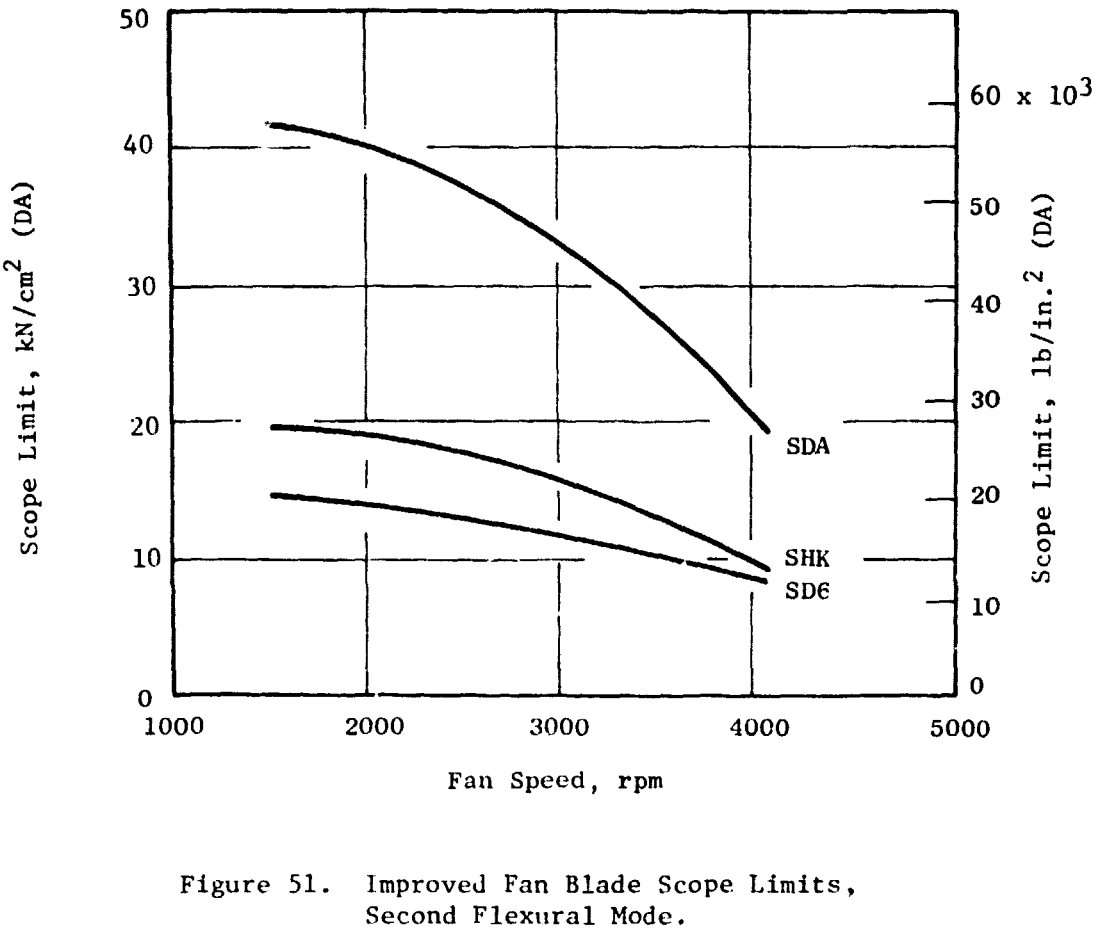

Figure 51. Improved Fan Blade Scope Limits, Second Flexural Mode.

Table I. Improved Fan Blade System Infinite Life Stress Limits for Several Vibratory Modes.

Mode	Frequency, Hz	Speed, rpm	Stress Limits N/cm^2 ($lb/in.^2$) for Strain Gage			
			SHK	SD1	SD6	SDA
First 2-Diametral				See Figure 48		
First 3-Diametral	126	2520	25,230 (36,600)	12,061 (17,500)	35,164 (51,000)	37,302 (54,100)
Second 6-Diametral	283	3400	9,374 (13,600)	---	29,780 (43,200)	22,415 (32,600)
Second 6-Diametral	250	2500	11,031 (16,000)	---	31,987 (46,400)	23,024 (33,400)

6.4.3 DC-10-30 Inlet - Actual Stresses

Baseline Test

Stresses observed during this test with the DC-10-30 inlet were well within infinite life stress limits. The maximum stress levels for each gage location were as follows:

Gage[1] Location	Overall[2] Stress (N/cm^2)	Stress Limit at Gage Point, %	Fan Speed, rpm	Wind
SHK	9,992	19	2500	Gusting Tailwind
SHK	6,109	12	2500	Slight Tailwind
SD1	7,933	18	2500	Gusting Tailwind
SD1	5,167	12	2500	Slight Tailwind
SD6	14,826	29	2500	Gusting Tailwind
SD6	8,619	17	2500	Slight Tailwind
SDA	7,933	17	2500	Gusting Tailwind
SDA	5,167	11	2500	Slight Tailwind

(1) See Figure 42
(2) Double Amplitude (DA)

As shown in the above tabulation, the maximum stress for each gage occurred at 2500 rpm fan speed. The predominant vibratory modes are first 3-diametral and second 6-diametral system modes. The ambient wind was a slight tailwind 3.7-5.6 km/hr (2-3 kn) gusting to 9.3 km/hr (5 kn). The data reduction clearly shows an increase in stress for the gusting condition. Since the lower stresses are more representative of baseline stresses, both conditions are listed here. For 2500 rpm, the infinite life stress limit at the critical point on the blade is 44% for the gusting tailwind and 25.6% for the lower tailwind (Table II).

90° Crosswind Distortion Testing

The engine was operated to 3900 rpm fan speed with up o 60 km/hr (32.4 kn) crosswind, and to 3580 rpm with 65.8 km/hr (35.5 kn) crosswind. The test was terminated at this point because of the aforementioned facility failure. The conditions tested exceed the aircraft operational limits in a crosswind environemnt. All fan blade stresses were well within infinite life limits (Table II).

Plots representative of the fan face total pressure distortion patterns observed in this test are shown in Figures 52 and 53. Distortion levels were generally low. Separation was encountered at 1180 rpm with 60 km/hr (32.4 kn)

Table 1I. Improved Fan Blade Crosswind Test, Douglas DC-10-30 Inlet, Measured Stresses and Life Limits.

Crosswind Velocity Velocity (km/hr)	No. Facility Fans On	Attachment Fan Speed 1)	Fan Speed (rpm)											
			1500 (Flight Idle)		2500		2746		3350		3670		3783		3900	
			Overall Stress N/cm^2	Life Limits (%)	Overall Stress N/cm^2	Life Limits (%)	Overall Stress N/cm^2	Life Limits (%)	Overall Stress N/cm^2	Life Limits (%)	Overall Stress N/cm^2	Life Limits (%)	Overall Stress N/cm^2	Life Limits (%)	Overall Stress N/cm^2	Life Limits (%)
Baseline	0	-	2755	7.7	14,826 8,619	44.0 25.6	7,23b 4,481	21.1 13.1	9,649 5,510	28.2 18.5	7,580 4,138	21.0 15.0	6207	18.3	5,510	20.8
33.9	4	1000	4138	12.2	16,895	49.8	10,002	29.0	18,268	56.6	10,688	28.6			7,923	26.4
42.6	5	930	5167	11.4	17,238	50.4			18,611	57.9	11,718	30.5			9,305	34.7
60.0	7	1460	5863	21.5												
60.0	7	1460	4481	16.4	18,611	54.4			18,611	57.2	11,031	23.4			12,061	36.5
65.8	9	1630	7933	29.4												
65.8	9	1630	5510	17.6	16,199	47.0			17,582	53.7	13,444	41.2				

NOTES: 1) Attachment fan speed is the speed at which the flow attaches to the inlet lip. Flow is separated from the inlet lip below this speed.

2) Highest measured overall dynamic stress at given speed - double amplitude values (DA).

3) Life limits percent of allowable dynamic stress for infinite life at critical point.

4) Peak levels include effect of 9.3 km/hr tailwind. Lower levels ignore peaks due to tailwind and are more representative of baseline stresses.

Seven Facility Fans: N_1 = 3887 rpm
Crosswind Velocity = 32.4 knots

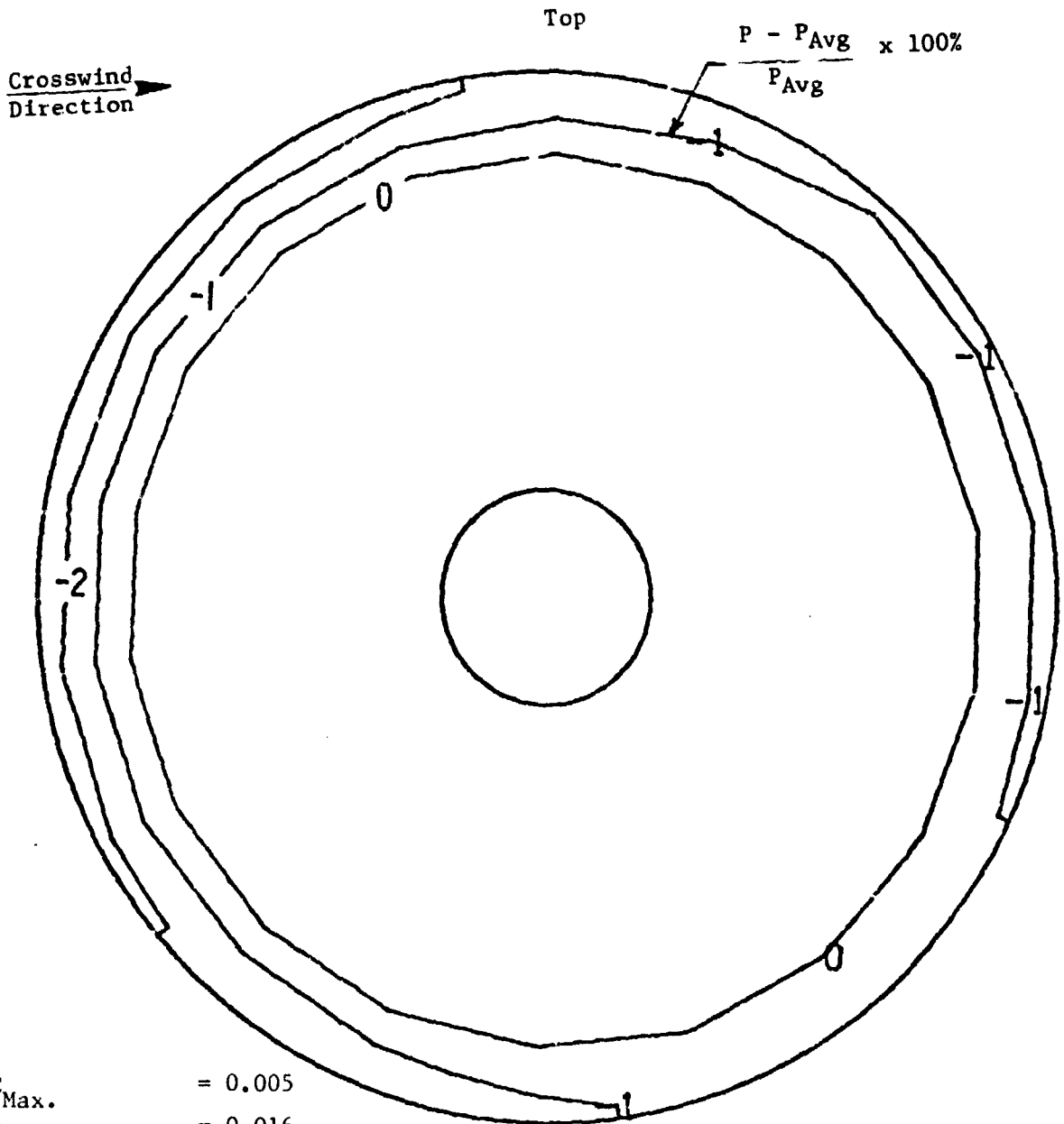

$IDC_{Max.}$ = 0.005

$IDR_{Max.}$ = 0.016

$\frac{P_{Max.} - P_{Min.}}{P_{Avg.}}$ = 2.8%

Looking Upstream - ALF

Figure 52. CF6-50 Engine With Improved Fan and DC-10-30 Inlet: Fan Face Total Pressure Distortion Patterns for 90° Crosswind at 32.4 Knots, 3887 RPM (Attached Inlet Flow).

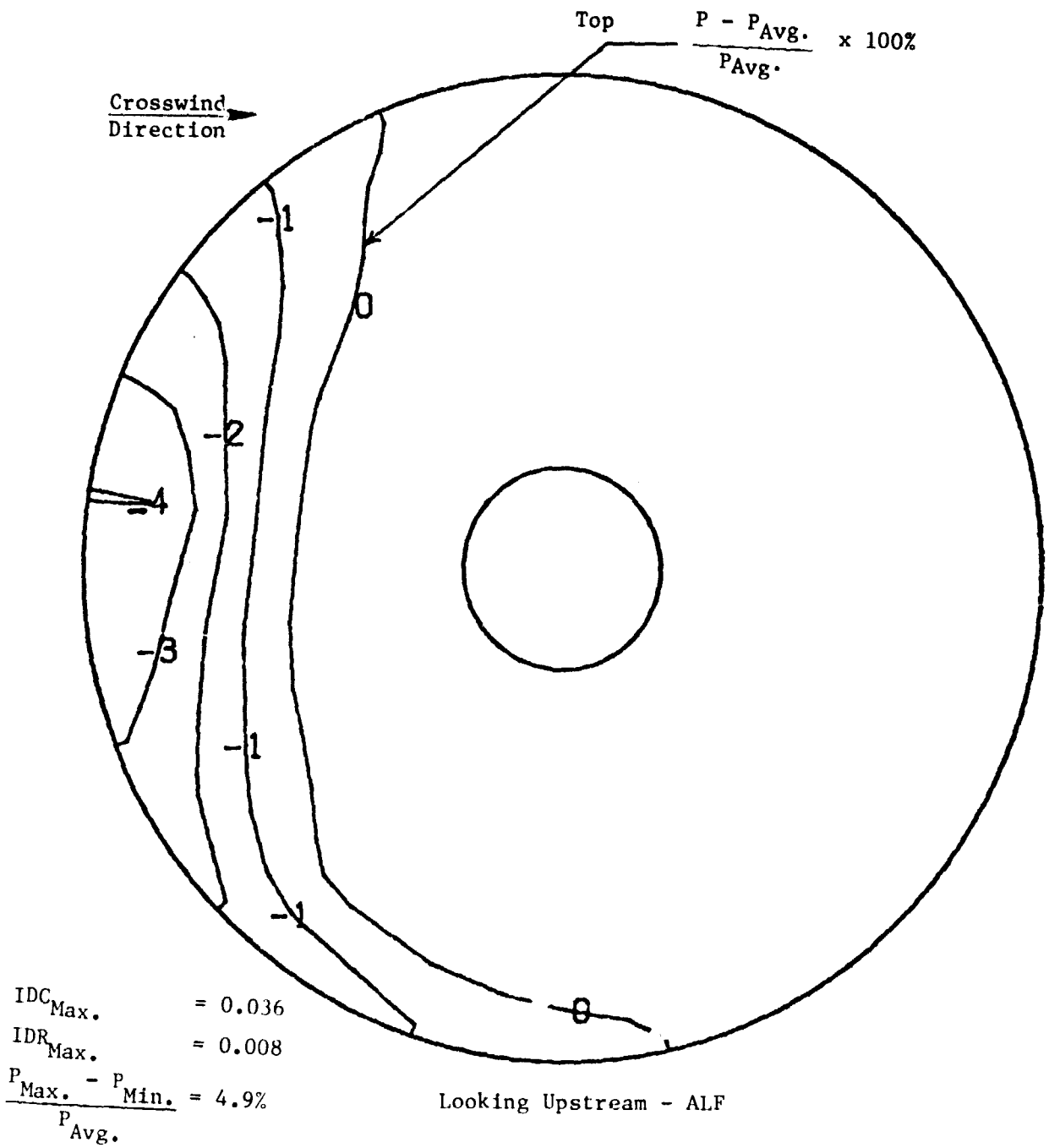

Figure 53. CF6-50 Engine With Improved Fan and DC-10-30 Inlet: Fan Face Total Pressure Distortion Patterns for 90° Crosswind at 35.5 Knots, 1556 R.M (Separated Inlet Flow).

crosswind and at 1400 rpm with 65.8 km/hr (35.5 kn) crosswind. Flow reattached at 1460 rpm and 1630 rpm, respectively. No separation was encountered at higher fan speeds. The maximum stress levels for each gage location were as follows:

Gage(1) Location	Overall(2) Stress (N/cm^2)	Stress Limit at Gage Point, %	Fan Speed, rpm	Crosswind, km/hr
SHK	14,483	28	2500	42.6
SD1	13,100	30	2500	60.0
SD6	18,611	39	3380	42.6
	18,611	36	2500	60.0
	18,611	39	3380	60.0
SDA	16,542	35	2500	60.0

(1) See Figure 42
(2) Double Amplitude (DA)

The maximum stress observed was 18,611 N/cm^2 DA on gage SD6 at 3350 rpm with 42.6 km/hr (23 kn) crosswind. The predominant mode was second 5-diametral system mode. At this condition, the infinite life stress limit at the critical point was 57.2%. This was the highest limit seen in the test.

6.4.4 B747 Inlet - Actual Stresses

Baseline Test

Stresses observed during this test with the B747 inlet were well within infinite life stress limits. The maximum stress levels measured at each gage location were as follows:

Gage(1) Location	Overall(2) Stress (N/cm^2)	Stress Limit at Gage Point, %	Fan Speed, rpm
SHK	6207	12	2500
SD1	7580	17	2500
SD6	9992	21	3350
SD6	8619	17	2500
SDA	7236	15	2500

(1) See Figure 42
(2) Double Amplitude (DA)

The predominant vibratory modes at 2500 rpm are first 3-diametral, and second 6-diametral system modes, and the infinite life stress limit at the critical point on the blade is 24.8%. The vibration mode at 3350 rpm is almost entirely second 5-diametral system mode, and the infinite life stress limit at the critical point is 33.5%. The data reduction for gage SD6 shows the effect of gusting wind at the 9992 N/cm^2 DA reading. A stress of 7236 N/cm^2 DA is more representative of the baseline at 3350 rpm, making the infinite life limit 24%.

90° Crosswind Distortion Testing

The engine was operated up to 3350 rpm with 29.6 km/hr (16 kn) crosswind, up to 3400 rpm with 19 knots crosswind, and up to 2800 rpm with up to 79.7 km/hr (43 kn) crosswind. This test sequence is consistent with the operation of the aircraft in service. Rolling takeoffs and aircraft velocity during maneuvers prevent high crosswind distortion without sufficient axial flow to clean up the inlet.

All fan blade stresses were well within infinite life limits as shown in Table III. Maximum stresses measured on this test are slightly less than those measured during similar testing on the original fan blade.

Plots representative of the fan face total pressure distortion patterns observed in this test are presented in Figures 54 and 55.

The maximum stress levels for each gage location were as follows:

Gage[1] Location	Overall[2] Stress (N/cm^2)	Stress Limit at Gage Point, %	Fan Speed, rpm	Crosswind, km/hr
SHK	7,923	15	2500	59.3 and 79.7
SD1	9,649	22	2500	59.3
SD6	13,787	27	2500	79.7
SDA	11,718	25	2500	79.7

(1) See Figure 42
(2) Double Amplitude (DA)

The maximum stress first observed in the test was 13,787 N/cm^2 DA on gage SD6 at 2500 rpm with 79.7 km/hr (43 kn) crosswind. The predominant vibratory modes are first 3-diametral and second 6-diametral system modes. At this condition, the percent of infinite life stress limits at the critical point was 40.2%. This was the highest life limit seen in the test.

Table III. Improved Fan Blade Crosswind Test, Boeing 747 Inlet, Measured Stresses and Life Limits.

Crosswind Velocity (km/hr)	No. Facility Fans	Separation Fan Speed (rpm) 1)	1500 (Flight Idle)		Fan Speed (rpm)									
			Overall Stress 2) N/cm^2	Life Limits 3) (%)	Overall Stress N/cm^2	Life Limits (%)	Overall Stress N/cm^2	Life Limits (%)	Overall Stress N/cm^2	Life Limits (%)	Overall Stress N/cm^2	Life Limits (%)	Overall Stress N/cm^2	Life Limits (%)
Baseline	0	-	1725	4.8	8,619	24.8			9992	33.5	5,167	17.4	6207	18.0
29.6	4	3200	2069	6.0	6,550	19.0			8619	28.8	8,962	28.6		
35.2	5	2800	2755	7.9	7,580	22.0	4,481	13.2	9305	31.2	12,747	40.2		
40.7	7	Separated Up To 2830 rpm (Max) Speed This Point	3451	10.0	10,688	31.0	9,649	28.5						
59.3	10	"	4138	12.1	11,374	33.1	10,345	30.6						
79.7	13	"	4824	13.9	13,787	40.2	11,374	34.0						

NOTES: 1) Separation fan speed is the high speed point at which the flow separates from the inlet lip.

2) Highest measured overall dynamic stress at given speed - double amplitude values (DA)

3) Percent of allowable dynamic stress for infinite life at critical point.

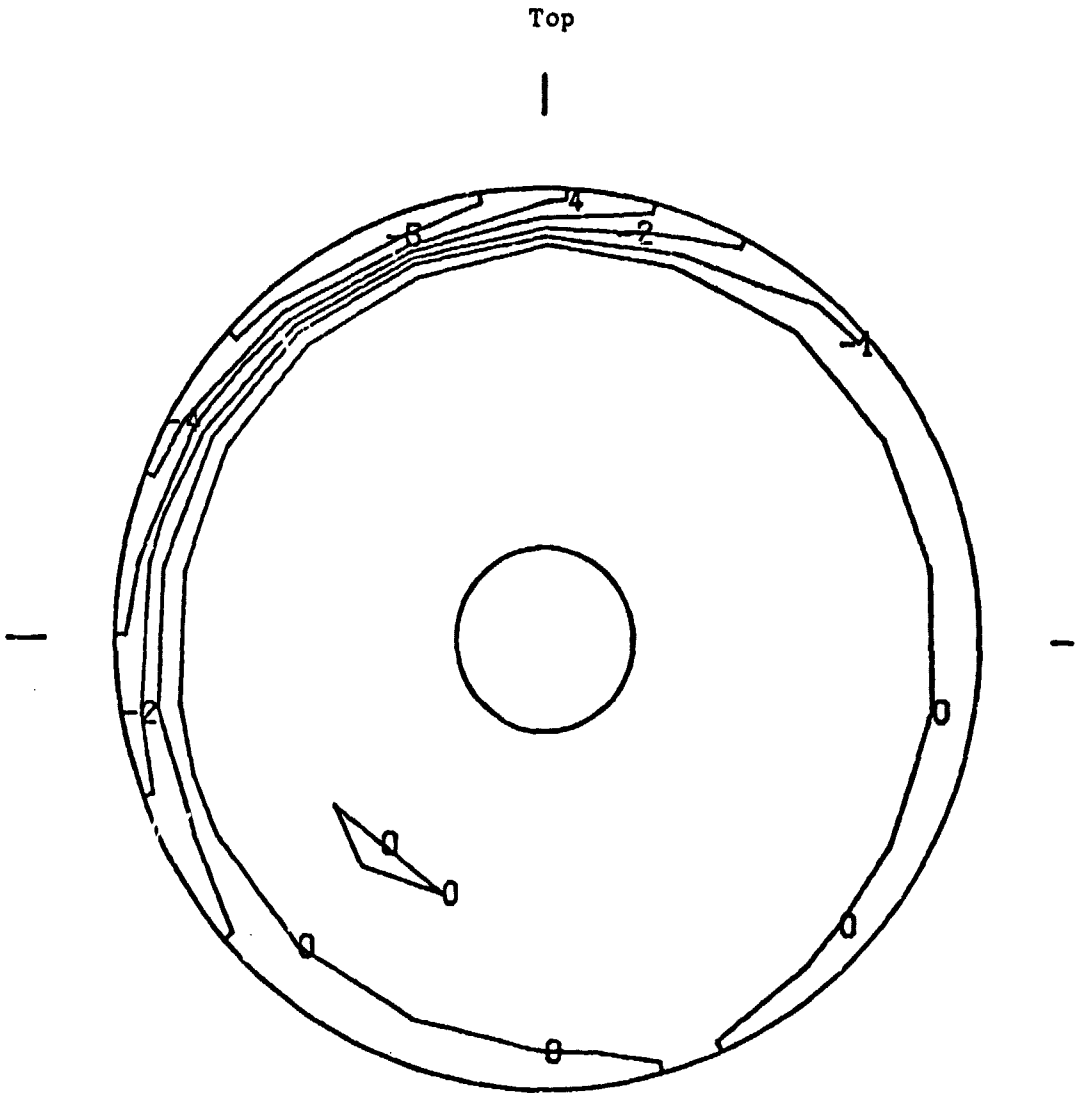

$IDC_{Max.}$ = 0.022

$\frac{P_{Max.} - P_{Min.}}{P_{Avg.}}$ = 6.6%

Steady-state Pattern - ALF

Figure 54. CF6-50 Engine With Improved Fan and 747 Inlet: Fan Face Total Pressure Distortion Patterns for 90° Crosswind at 22 Knots, N_1 = 3899 RPM (Attached Inlet Flow).

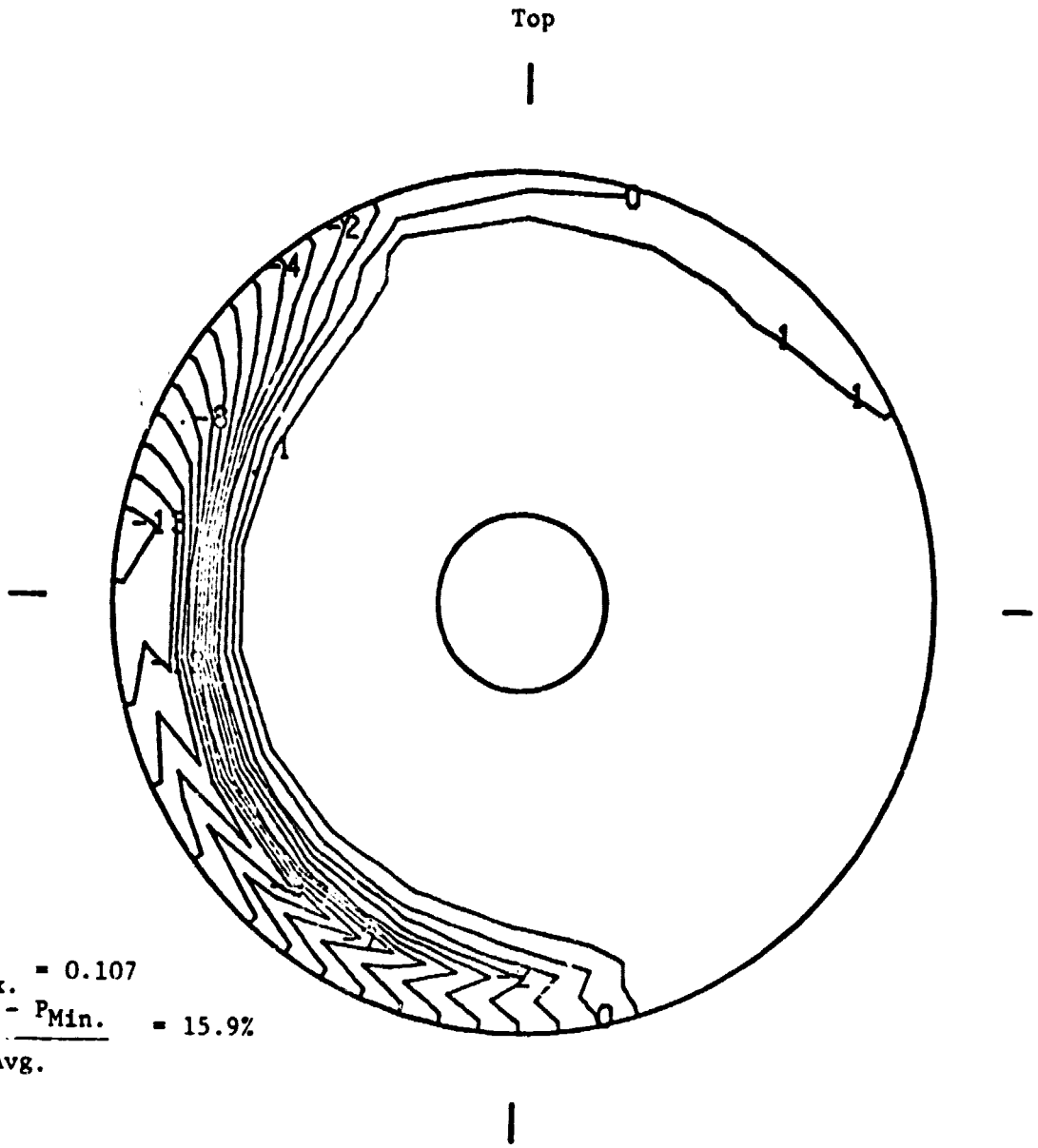

Figure 55. CF6-50 Engine With Improved Fan and 747 Inlet: Fan Face Total Pressure Distortion Patterns for 90° Crosswind at 43 Knots, N_1 = 2814 RPM (Separated Inlet Flow).

Engine crosswind testing demonstrated that the improved fan blade has similar crosswind/distortion characteristics as the original CF6 fan blade which has a very satisfactory record for operation under crosswind conditions or high inlet distortion without any problems. Results indicate that the new fan blade can operate successfully without exceeding vibratory stress limits with both the DC-10-30 and B747 inlets at allowable takeoff crosswinds up to 64.8 km/hr (35 kn).

7.0 ENGINE PERFORMANCE TEST

The objective of the back-to-back engine performance testing was to measure the performance improvement that results from replacing the original production CF6-50 fan with the improved fan stage. Performance improvement was measured at sea level and during simulated altitude operation. Modification to the improved fan package was required to achieve the predicted sfc performance improvement. Testing included evaluation of improved fan blades, a fan case stiffener for improved roundness, reduced fan tip clearance, fan casing tip shroud configuration, and fan nozzle area variation.

In addition to the back-to-back engine performance test results discussed in this section, production engine and aircraft flight test results with the final improved fan package are presented in Section 11.0.

7.1 ENGINE TEST FACILITY

7.1.1 Test Cell

Back-to-back engine testing was conducted in indoor test cells which contain engine mounting facilities, overhead air inlet with turning vanes, and an exhaust stack. The engine is normally mounted in a test cowling which forms the fan exhaust nozzle and mates with the primary exhaust nozzle. Figure 56 shows the engine test configuration for both sea level and simulated altitude performance tests. Altitude cruise was simulated by testing with fan and core exhaust nozzle diffusers to create choked exhaust nozzle operating conditions on a sea level test stand.

7.1.2 Special Test Equipment

Due to the requirements of this test to measure performance at sea level and simulated altitude conditions, special test hardware was provided. Special test equipment included an inlet bellmouth, a modified CF6-50 fan reverser, a fan nozzle diffuser, and a primary nozzle and diffuser extension for simulated altitude operation.

Bellmouth - Initial testing was conducted with a bellmouth without an inlet screen. This bellmouth differs from the conventional development bellmouth in that it mounts to the engine front flange, instead of being facility mounted, in order to simulate the weight of the flight inlet. Initial testing showed unacceptable inlet temperature measurements with the bellmouth-mounted thermocouple rakes. Consequently, a conventional development test bellmouth with inlet screen-mounted air thermocouples was utilized for inlet temperature measurements. Inasmuch as this bellmouth was facility-mounted, inlet weight simulation was provided by attachment of a dummy weight to the fan casing.

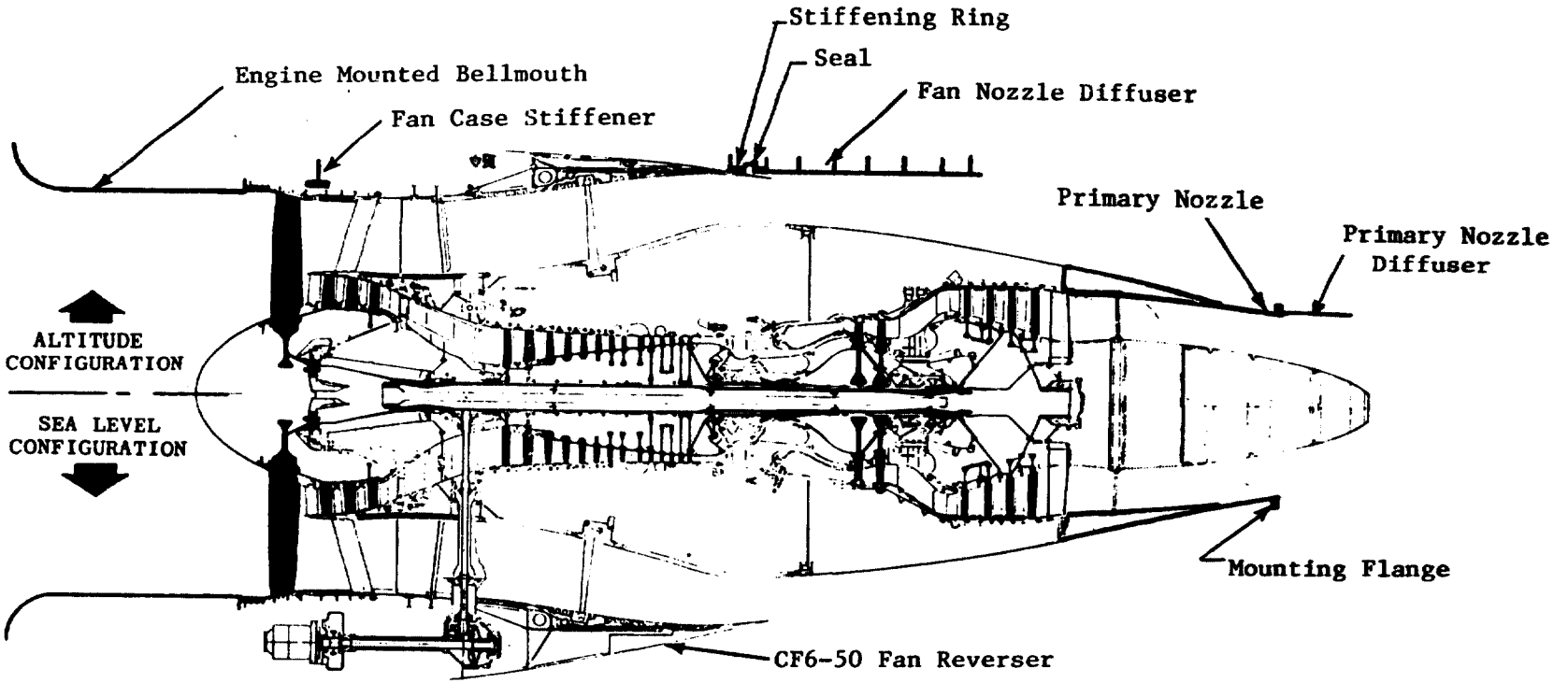

Figure 56. CF6-50 Engine Test Configurations for Sea Level and Simulated Altitude Performance Test.

C-2

ORIGINAL PAGE IS POOR QUALITY

Fan Reverser - A CF6-50 fan reverser with standard fan nozzle was used for the back-to-back testing. The reverser had been modified for an ejector seal and by the addition of a stiffening ring near the aft end of the translating cowl to take the extra load imposed by the fan exhaust diffuser for simulated altitude operation. The fan nozzle area was varied by trimming the fan reverser trailing edge.

Fan Nozzle Diffuser - The fan nozzle diffuser is a 48-inch cylindrical extension to the fan nozzle (Figure 56). The diffuser causes the fan nozzle exit static pressure to be reduced below choking pressure providing a simulation of the cruise operating line of the fan. The diffuser is hinged to the pylon to permit opening for engine access. The diffuser is sealed to the reverser by a flexible seal between the forward end of the diffuser and the stiffening ring on the reverser. Figure 57 shows the diffuser, fan reverser, and core cowl door attached to the test pylon.

Primary Nozzle and Diffuser - For these tests, a special primary nozzle has been constructed with the inner flowpath contour identical to a CF6-50 turbine reverser and a mounting flange for a diffuser extension (Figure 56). Installing the primary nozzle diffuser extension causes the primary nozzle to choke at a lower pressure ratio to simulate altitude operation. Figure 58 shows the primary nozzle with the diffuser extension attached. This special primary nozzle was replaced with a conventional nozzle without the diffuser mounting flange for sea level testing. Early testing has shown that the flange had a marked effect on primary nozzle flow coefficient without the diffuser installed.

7.1.3 Data Acquisition System

The system basically consists of a cell system and a site system. The cell system performs steady-state and transient data acquisition, conversion to engineering units, quick-look performance calculations, and short term storage. Converted data are automatically transmitted to site system for further on-line processing, graphic display, and hard-copy output. The site system utilizes a data base concept for efficient storage, retrieval, and reprocessing of current and historical data. In addition, data may be transmitted to the General Electric Evendale time-sharing computer center for further processing such as cycle deck analysis and comparison.

Data acquisition capability consists of 400 pressure channels, 400 temperature channels, 10 frequency channels, and 128 dc voltages such as: load cells, individual pressure transducers, position potentiometers, etc. The pressure system consists of ten 40-port scan values with available pressure ranges from ± 0.7 kg/cm^2 gage (± 10 psig) through ± 35.15 kg/cm^2 gage (± 500 psig). The system incorporates autoranging and multiple sampling capability for all data channels to assure optimal resolution and precision in addition to variable averaging time for frequency measurements. Data may be achieved and processed in either a steady-state or transient mode. Typical steady-state acquisition time is 30 seconds with each parameter sampled 49 times over the 30-second time period. Transient acquisition rates are

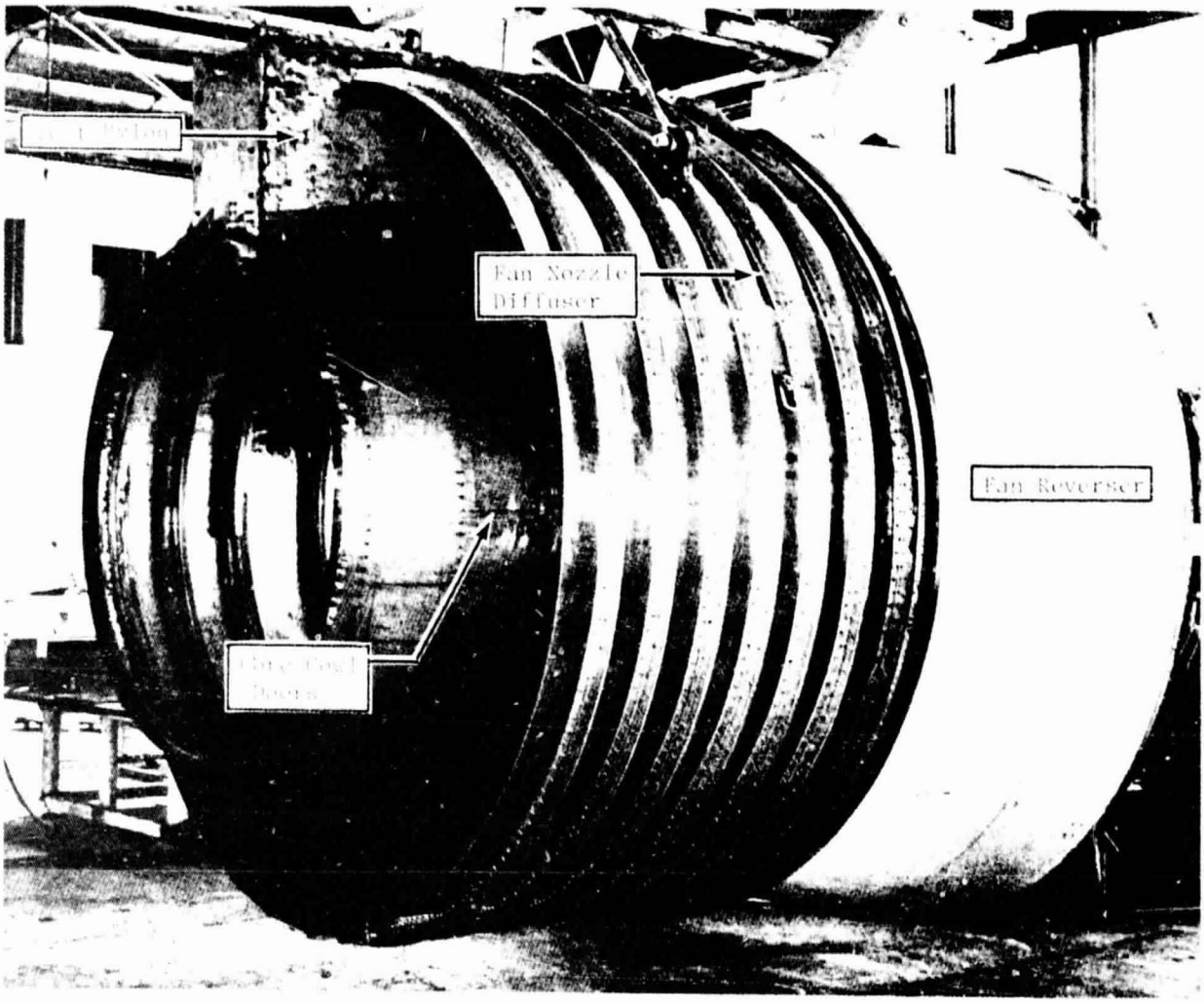

Figure 57. Fan Reverser with Fan Nozzle Diffuser Installed.

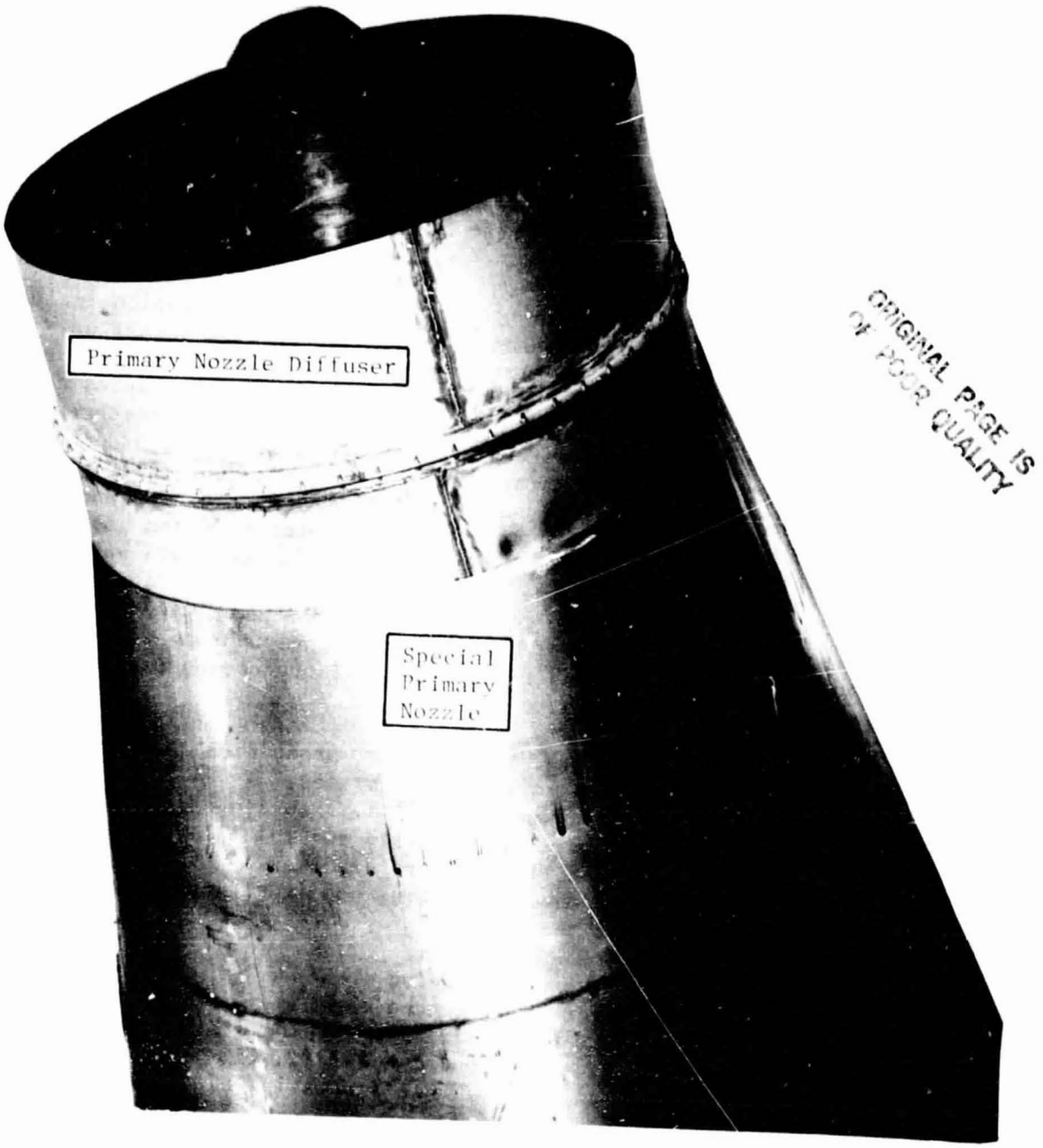

ORIGINAL PAGE IS OF POOR QUALITY

Figure 58. CF6-50 Primary Nozzle and Diffuser for Simulated Altitude Performance Testing.

variable from one sample per second per channel to 250 samples per second per channel. Redundant measurements are made of key parameters such as fuel flow, fan speed, and thrust. Automatic data rejection techniques, ratio of redundant measurements, and on-line system verification analysis further enhance overall data quality.

7.2 ENGINE TEST CONFIGURATIONS

Initial testing was performed using a CF6-50 development engine. The intent, in selecting hardware for this engine, was to build an engine with performance equivalent to a new engine that had been subject to initial performance deterioration.

Significant features of the initial engine test configuration included: fan booster, high pressure turbine and low pressure turbine rotors were assembled primarily from parts used on a previous build; the high pressure compressor rotor had new blades which had been ground to provide clearances consistent with the engine new front mount configuration; the high pressure compressor stator had a refurbished forward casing and the aft casing used on the previous build; vanes were used parts; the high pressure turbine tip shrouds were new production configuration and were ground to obtain clearances slightly open from nominal; and the low pressure turbine stator had been used on the previous build except that the tip shrouds and interstage seals were new.

For the baseline performance tests, the CF6-50 engine was run with a set of original production fan blades. The fan casing tip shroud was open-cell aluminum honeycomb and was ground to the original production minimum tip clearance of 4.45 mm (0.175 in.).

Following the baseline tests, the original production fan blades were replaced with a full set of the improved fan blades. A new forward fan case and the fan case stiffener ring were installed. New fan casing tip shrouds of open-cell aluminum honeycomb were installed and initially ground to a minimum tip clearance of 2.92 mm (0.115 in.), a reduction of 1.52 mm (0.060 in.). Refer to Figure 1 for the improved fan engine configuration and to Section 3.0 for a detailed description of the improved fan.

Improved fan blade sets were fabricated in-house by General Electric and by an outside vendor. In order to fine tune the fan engine match to obtain the predicted sfc improvement, the blade part-span shroud interlocks were subsequently modified (restaggered) to close the running blade stagger angle by about 1.5° at the part-span shroud. The fan casing tip shroud was also modified by installing microballoon epoxy in open cell aluminum honeycomb to provide a smooth casing tip shroud. The tip shrouds were then ground to provide tighter fan tip clearances down to about 2.16 mm (0.085 in.), a reduction of 2.29 mm (0.090 in.).

A second new CF6-50 engine was utilized in order to complete the improved fan performance test program in an expeditious manner. A third (production) CF6-50 E2 engine was also used to test the restaggered improved fan blades back-to-back against production-type improved fan blades.

7.3 INSTRUMENTATION AND DATA REDUCTION

Engine performance instrumentation included pressure and temperature measurements at the inlet and exit of the fan, booster and high pressure compressor, and at the exit of the high pressure and low pressure turbines. Inlet bellmouth instrumentation was provided to determine fan inlet airflow. In addition, both fan and core rotor speeds, fuel flow, and engine thrust were measured.

Test instrumentation used to measure fan performance and to monitor engine operation is broken down into two groups: general instrumentation and aerodynamic instrumentation (Figure 59).

7.3.1 General Instrumentation

- Barometric Pressure - The local barometric pressure measured using a recording microbarograph.
- Humidity - The absolute humidity measured in grains of moisture per pound of dry air using a humidity indicator.
- Cell Static Pressure - Test cell static pressure measured at four locations in the cell.
- Fan Speed - Low pressure rotor speed measured using two fan case-mounted, fan speed sensors.
- Core Speed - High pressure rotor speed measured using engine core speed sensor driven off the end of the lube and scavenge pump.
- Main Fuel Flow - Volumetric flowmeter, facility-mounted.
- Verification Fuel Flow - Second fuel flowmeter mounted in series with the main fuel flowmeter.
- Fuel Temperature - Temperature of fuel measured at the facility flowmeter using a single chromel/alumel probe in the fuel line.
- Fuel Sample Specific Gravity - Specific gravity of the fuel sample measured using a hydrometer.
- Fuel Sample Temperature - Fuel sample temperature measured during the specific gravity measurement.
- Fuel Lower Heating Value - Lower heating value of the fuel sample as determined by a bomb calorimeter.
- Thrust - Thrust frame, axial force measurement using three strain gage-type load cells for redundant measurements.

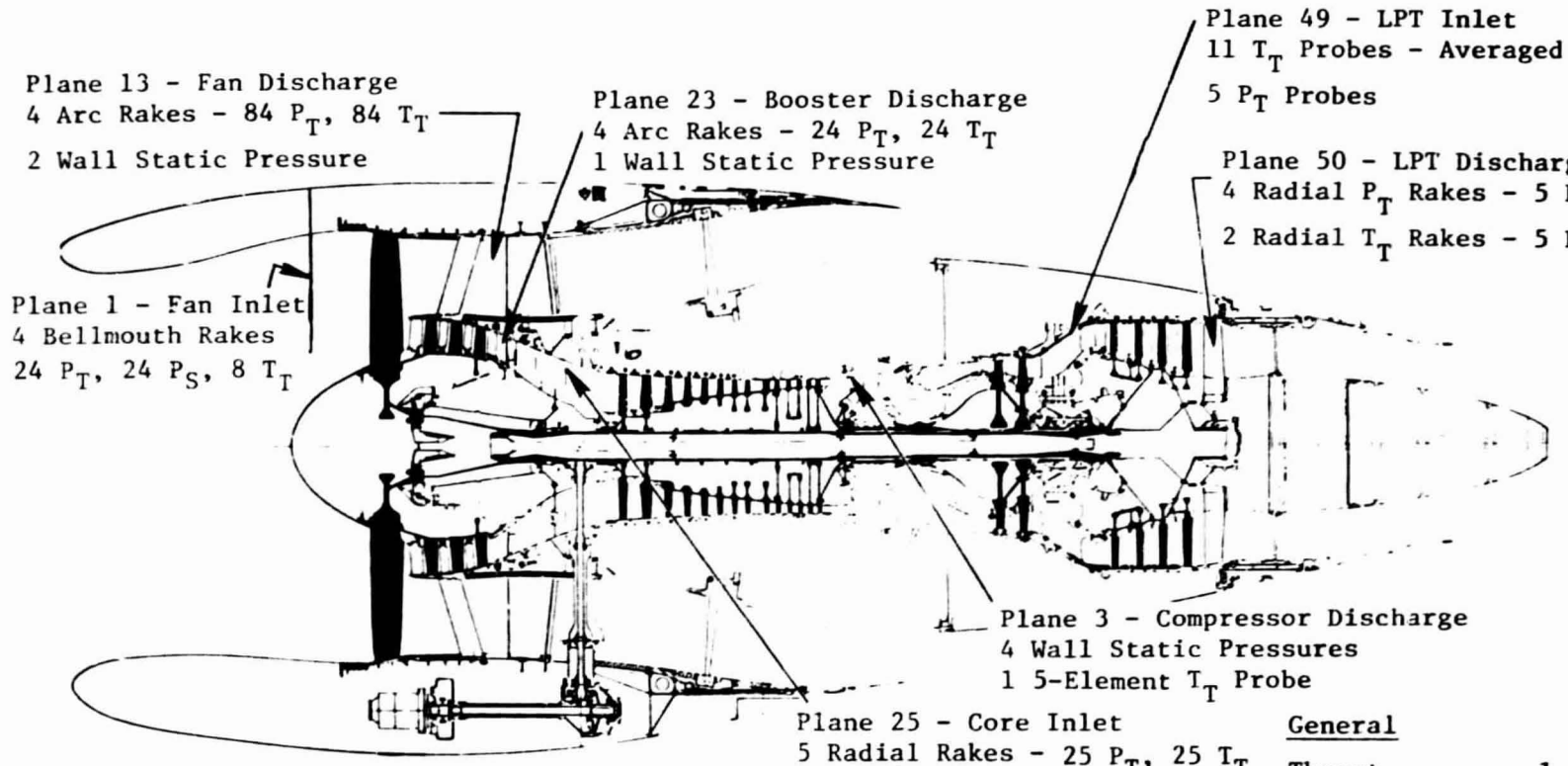

General	
Thrust	1
Fan Speed	2
Core Speed	1
Fuel Flow	2
Fuel Temp.	1
Throttle Angle	1
VSV Position	1
VBV Position	1
Humidity	1
Barometer	1

Figure 59. CF6-50 Engine: Instrumentation for Fan Performance Test.

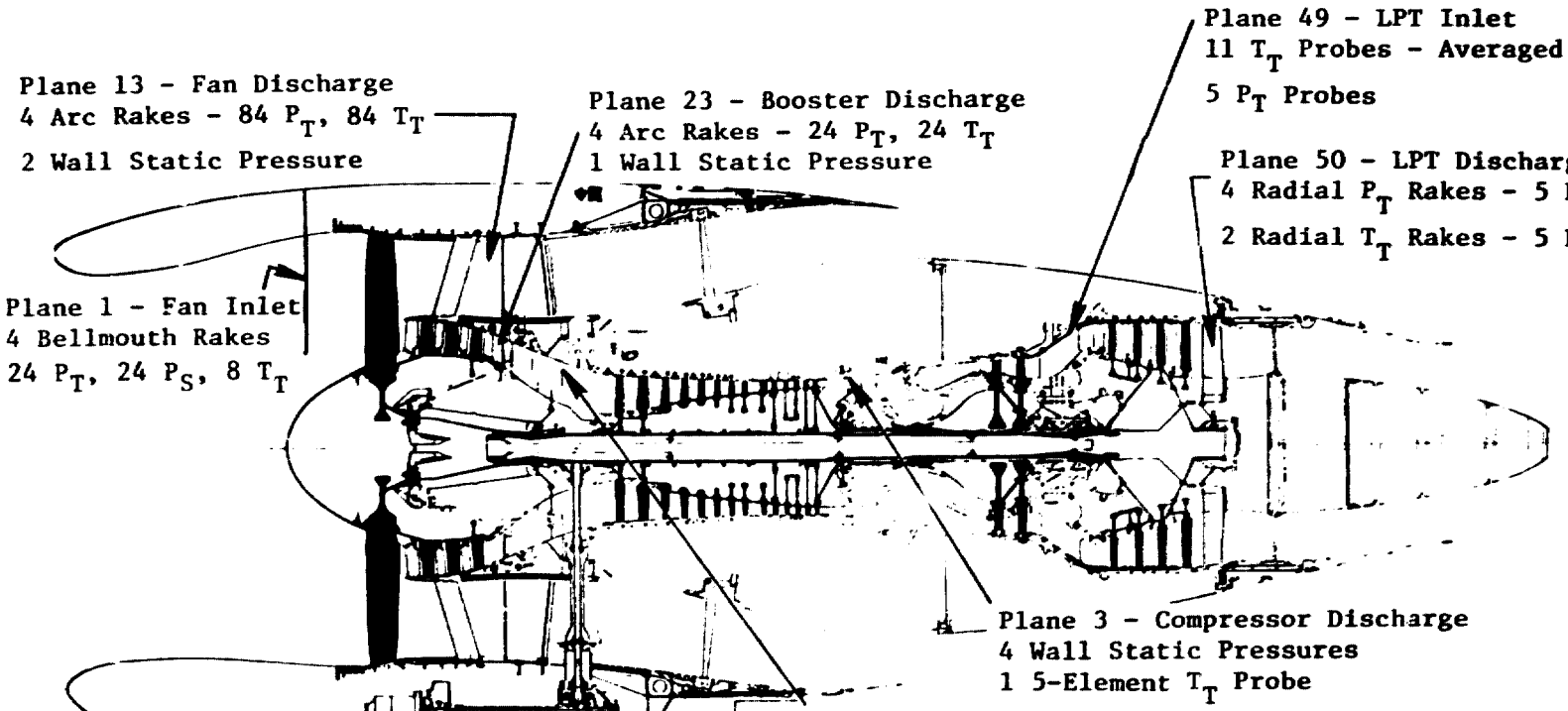

General	
Thrust	1
Fan Speed	2
Core Speed	1
Fuel Flow	2
Fuel Temp.	1
Throttle Angle	1
VSV Position	1
VBV Position	1
Humidity	1
Barometer	1

Figure 59. CF6-50 Engine: Instrumentation for Fan Performance Test.

- Variable Stator Vane Position - Readout of the linear variable differential transformer attached to the high pressure compressor variable stator pump handle.

- Variable Bleed Valve Position - Readout of the linear variable differential transformer attached to the variable bleed valve actuation mechanism.

7.3.2 Aerodynamic Instrumentation

The following rakes, probes, and static pressure taps were installed to measure airflow, temperature, and pressure as required to define component performance:

Fan Inlet (Station 1)

Bellmouth rakes were installed to measure static pressure, total pressure, and total temperature at the fan inlet. Four rakes each having six total pressure probes, six static pressure probes, and two total temperature probes were used.

Fan Discharge (Station 13)

Four arc rakes with 21 probes/rake were installed in the aft fan case to measure total pressure and total temperature. Seven different radial immersions with three elements per immersion were sampled for a total of 84 temperature and 84 pressure probes. Two pressure taps were installed in the aft fan case to measure fan discharge static pressure.

Booster Discharge (Station 23)

Four arc rakes each having six temperature and six pressure probes were installed to measure booster discharge total temperature and total pressure. A single tap was installed to measure booster discharge static pressure.

Compressor Inlet (Station 25)

Core inlet pressure and temperature were measured using five rakes and five elements per rake. Five flowpath wall static pressure taps were also installed.

Compressor Discharge (Station 3)

Four of the borescope port plugs in the compressor rear frame were modified to permit compressor discharge static pressure measurement. A single 5-element thermocouple probe was used to measure compressor discharge temperature.

Low Pressure Turbine Inlet (Station 49)

Temperature in this plane was measured by a production configuration EGT harness consisting of 11 dual element thermocouple probes electrically averaged. Pressure was measured using five probes each having five elements all feeding a single fitting.

Low Pressure Turbine Discharge (Station 5)

Low pressure turbine discharge pressure was measured using four rakes having five elements each. Temperature was measured by two rakes having five elements each.

7.3.3 Data Reduction

Preliminary performance calculations were done on-line by the "quick-look" data reduction program. This program is part of the cell data acquisition and processing system described in an earlier section. Test measurements, calibration curves, configuration constants, and fixed data inputs are combined in these calculations.

Most parameters of interest are calculated in the quick-look program. However, detailed cycle analysis was augmented by design point studies using the status cycle deck. This technique has the capability of providing a balanced cycle evaluation of any test point. The user has the option of selecting between redundant measurements for input to the cycle match while letting the cycle calculation provide parameter estimates where measurements are not available.

7.4 TEST PROCEDURE AND HISTORY

Performance improvements associated with the improved fan package were determined by back-to-back performance calibrations that were conducted by testing a CF6-50 engine with the original production CF6 fan replacing the fan with the improved fan and repeating the test. Performance calibrations consisted of two automatic data recordings at each of 12 power settings from the maximum takeoff rating to ground idle. This performance calibration was then repeated in each case. Additional data were occasionally required if any uncertainty in performance levels existed after completion of the two power calibrations. For simulated altitude operation, the fan and primary nozzle diffusers were installed.

Based on the previous test results, the original fan blade part-span shroud was reworked to improve blade resistance to foreign object damage (FOD). Initial back-to-back engine performance tests established that the part-span rework would be common to both the original and improved fan blades. Additional engine tests were conducted to check out the operational characteristics of the fan and primary nozzle diffusers.

A list of the fan performance tests on the first engine is presented in Table IV. The flight condition and the engine configuration are indicated.

A second new CF6-50 engine was introduced into the improved fan performance test program while repairs were being made to the first installation. A back-to-back test of the original to the General Electric fabricated improved fan blades was run to establish a baseline on the second engine. A list of tests completed on this engine is shown in Table V. Test procedures, instrumentation, and data reduction were similar to those with the original engine, and this testing was completed in a similar test cell. The engine was tested in a slave cowling with a slave primary nozzle. Most special instrumentation was removed from the original engine and installed in the second engine, except for the booster discharge rakes.

Additional testing was done to evaluate the performance of improved performance fan blades which had been vendor-fabricated. Testing was also accomplished define a further reduction in tip clearance below the 1.5 mm (0.060 in.) reductions already incorporated with the fan case stiffener. A further reduction in clearance of 1.0 mm (0.040 in.) with a smooth-surfaced shroud material in place of the open-celled honeycomb was tested.

7.5 DISCUSSION OF RESULTS

The predicted performance improvement of the improved fan package, including the 1.5 mm (0.060 in.) reduction in fan tip clearance, is shown in Table VI. Predicted cruise sfc improvements and equivalent values for ground testing are shown in this table. Sea level performance comparisons in Table VI and subsequent curves are made at a sea level static thrust of 17,800 daN (40,000 lb) which corresponds to a typical altitude cruise power setting. As shown, the improved fan provides a significant improvement in part-speed efficiency at cruise power settings. This provides a significant fuel savings, particularly at the intermediate power settings typical of altitude cruise.

The early portion of the test series evaluated the improved fan blade with 1.50 mm (0.060 in.) tip clearance reduction compared to the original fan configuration. Results of Tests 1 to 4 are shown on Figures 60 through 67. Initial testing with the original fan blades in the sea level and the simulated altitude cruise configurations with exhaust diffusers showed expected engine operating characteristics. The diffusers provided choked exhaust nozzles for an effective simulation of altitude cruise engine operating lines. Actual sfc performance is plotted on an absolute sfc scale, and the curves show the incremental improvement in absolute sfc. The $\%\Delta$sfc improvement is

Table IV. CF6-50 Engine 1 - Fan Performance Tests.

Test No.	Flight Condition	Fan Blades/ Fabricator	Fan Case Stiffener Ring	Casing Tip Shroud	Tip Clearance mm (in.)	Fan Nozzle Area, A_{18}	Comments
1	SLS	Orig./GE Prod.	No	Open Cell Aluminum Honeycomb	4.45(0.175)	Nom.	
2	Sim. Altitude	Orig./GE Prod.	No	↓	↓	Nom. + Fan Diffuser	
3	Sim. Altitude	Improved/GE	Yes	↓	2.92(0.115)	Nom. + Fan Diffuser	
4	SLS	Improved/GE	↓	↓	↓	Nom.	
5	↓	Orig./GE	↓	↓	4.45(0.175)	↓	Data N.G., VSV Opened 2°
6	↓	Improved/GE	↓	↓	2.92(0.115)	↓	High Flow Booster
7	↓	↓	↓	↓	↓	Nom.	Std. Booster
8	SLS	↓	↓	↓	↓	Nom. + 1%	
9	Sim. Altitude	Improved/GE	↓	↓	↓	Nom. + 1% + Fan Diffuser	
10	Sim. Altitude	Improved/ Vendor	↓	↓	↓	Nom. + 1% + Fan Diffuser	Data N.G., Failed Core Cowl Doors
11	SLS	Improved/ Vendor	↓	↓	↓	Nom. + 1%	
12	SLS	Restaggered Imp./Vendor	↓	↓	↓	↓	
13	SLS	Orig./GE Prod.	Yes	Open Cell Aluminum Honeycomb	2.92(0.115)	Nom. + 1%	

Table V. CF6-50 Engine 2 - Fan Performance Tests.

Test No.	Flight Condition	Fan Blades/ Fabricator	Fan Case Stiffener Ring	Casing Tip Shroud	Tip Clearance mm (in.)	Fan Nozzle Area, A_{18}
14	SLS	Improved/GE	Yes	Open Cell Aluminum Honeycomb	2.92(0.115)	Nom.
15	↓	Orig./GE	↓	Open Cell Aluminum Honeycomb	4.45(0.175)	↓
16		Imp./Vendor		Open Cell Aluminum Honeycomb	4.45(0.175)	
17		Restaggered Imp./Vendor		Oval Grind Open Cell Aluminum Honeycomb	2.92(0.115) 2.16(0.085) Min.	Nom.
18	↓	Restaggered Imp./Vendor	↓	Oval Grind Open Cell Aluminum Honeycomb	2.92(0.115) 2.16(0.085) Min.	Nom. + 1%
19	SLS	Restaggered Imp./Vendor	Yes	Smooth Micro-balloon Epoxy in Open Cell Aluminum Honeycomb	2.29(0.090)	Nom. + 1%

Table VI. Improved Fan Predicted Performance Improvement.

Item	Predicted Improvement % Δ Cruise sfc	Equivalent % Δ sfc at SLS, 17,800 daN (40,000 lb)FN
Improved Fan Blade	-1.0	-1.9
Reduced Fan Clearance 1.5 mm (0.060 in.)	-0.6	-0.8
1% Increased Fan Nozzle Area (A_{18})	-0.2	0
TOTAL	-1.8	-2.7

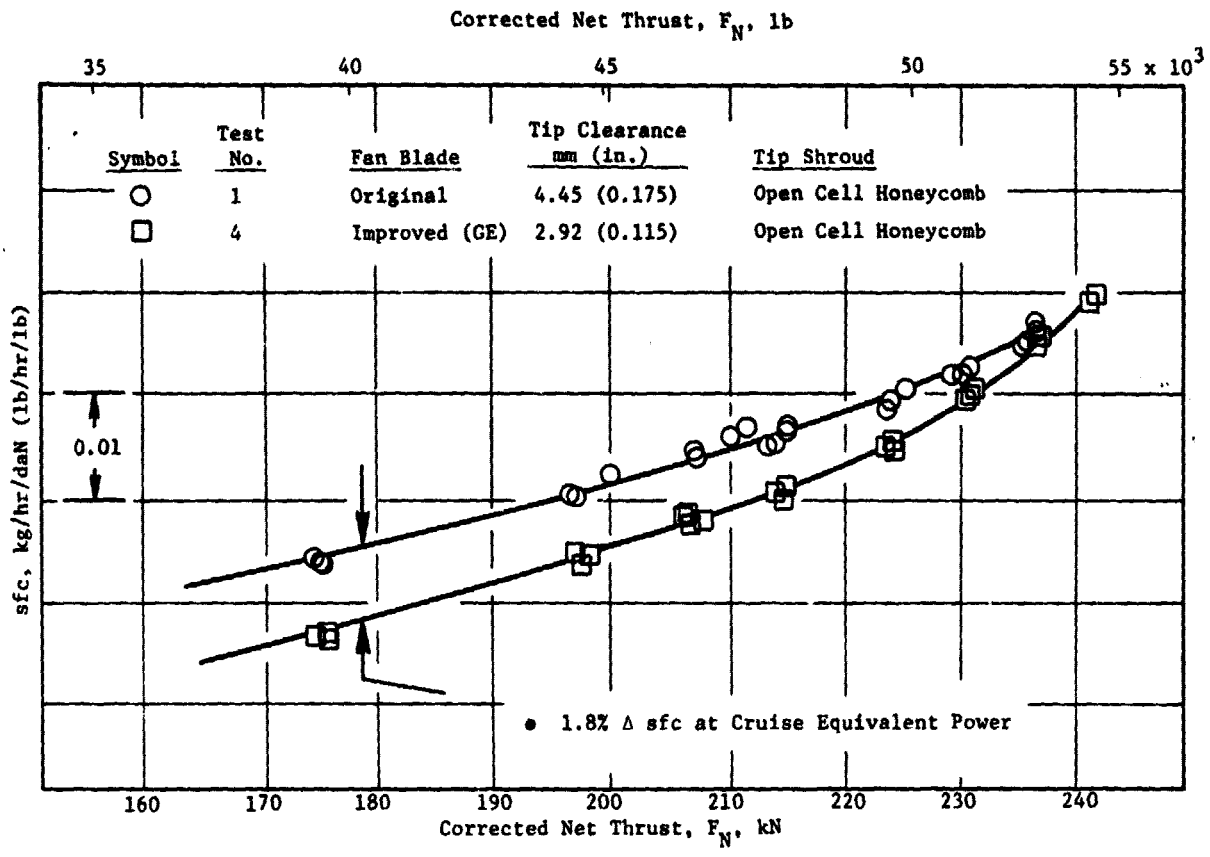

Figure 60. CF6-50 Engine: SFC Performance Versus Net Thrust for Original and Improved Fans, Sea Level Static, Initial Testing.

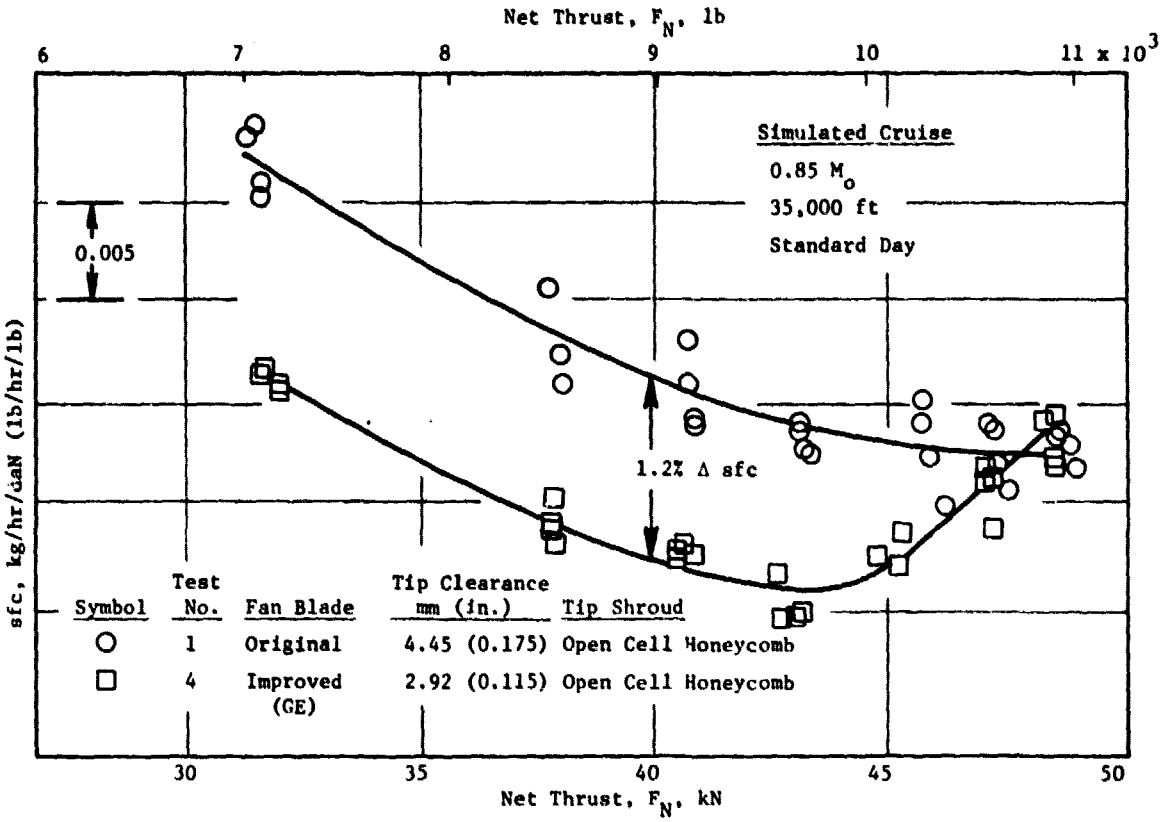

Figure 61. CF6-50 Engine Simulated Cruise SFC Performance Versus Net Thrust for Original and Improved Fans.

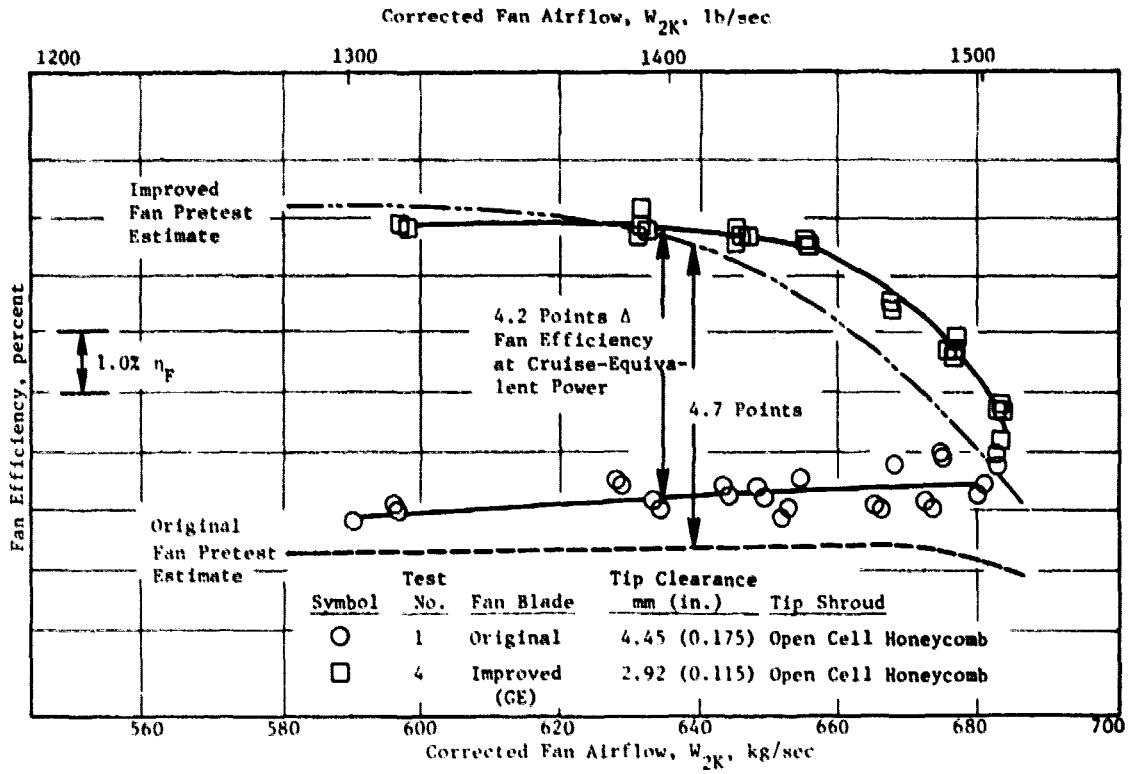

Figure 62. CF6-50 Engine Fan Efficiency Improvement Versus Fan Airflow for Original and Improved Fans, Sea Level Static, Initial Testing.

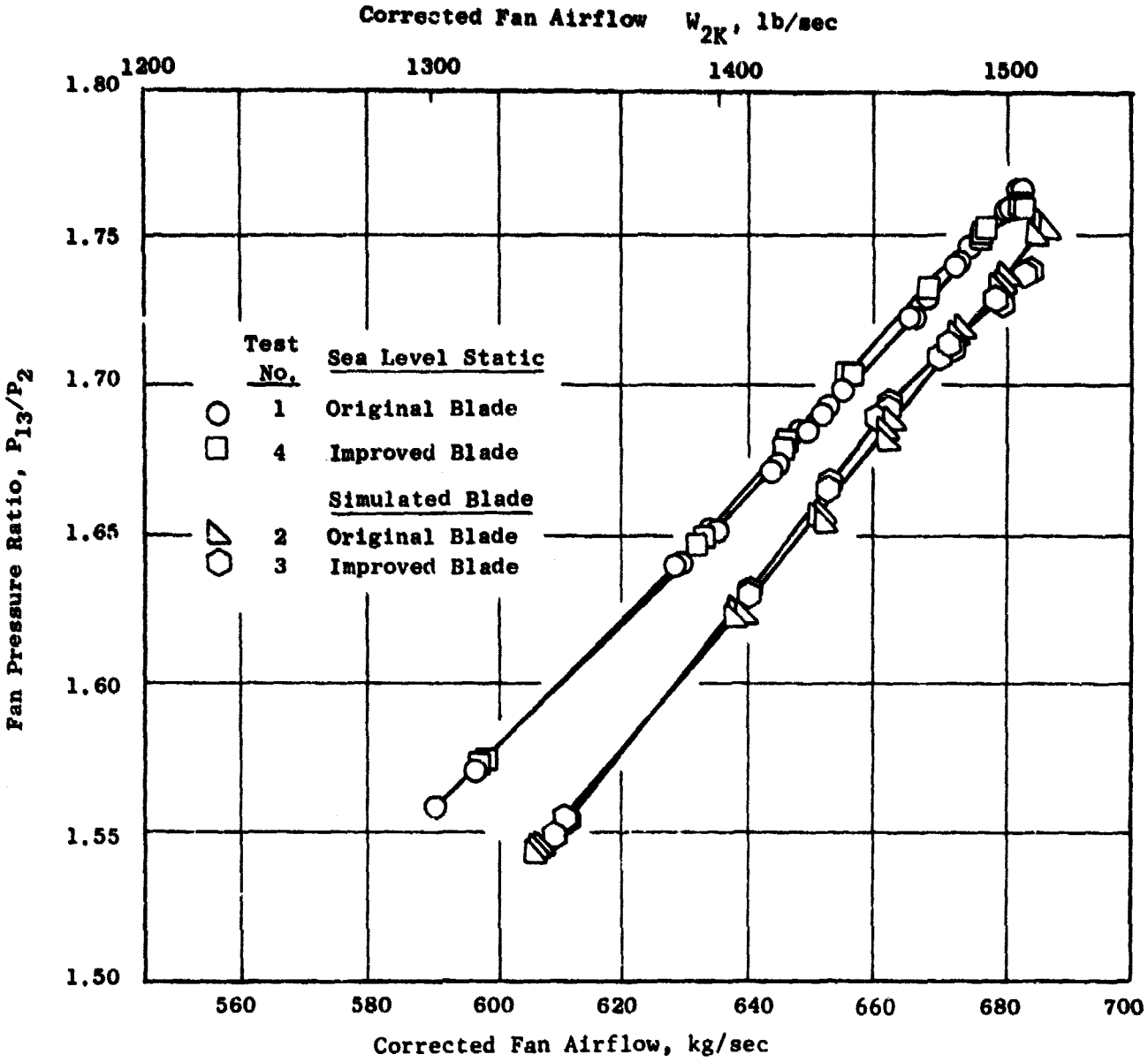

Figure 63. CF6-50 Engine Fan Operating Lines for SLS and Simulated Altitude Operation With the Original and Improved Fans.

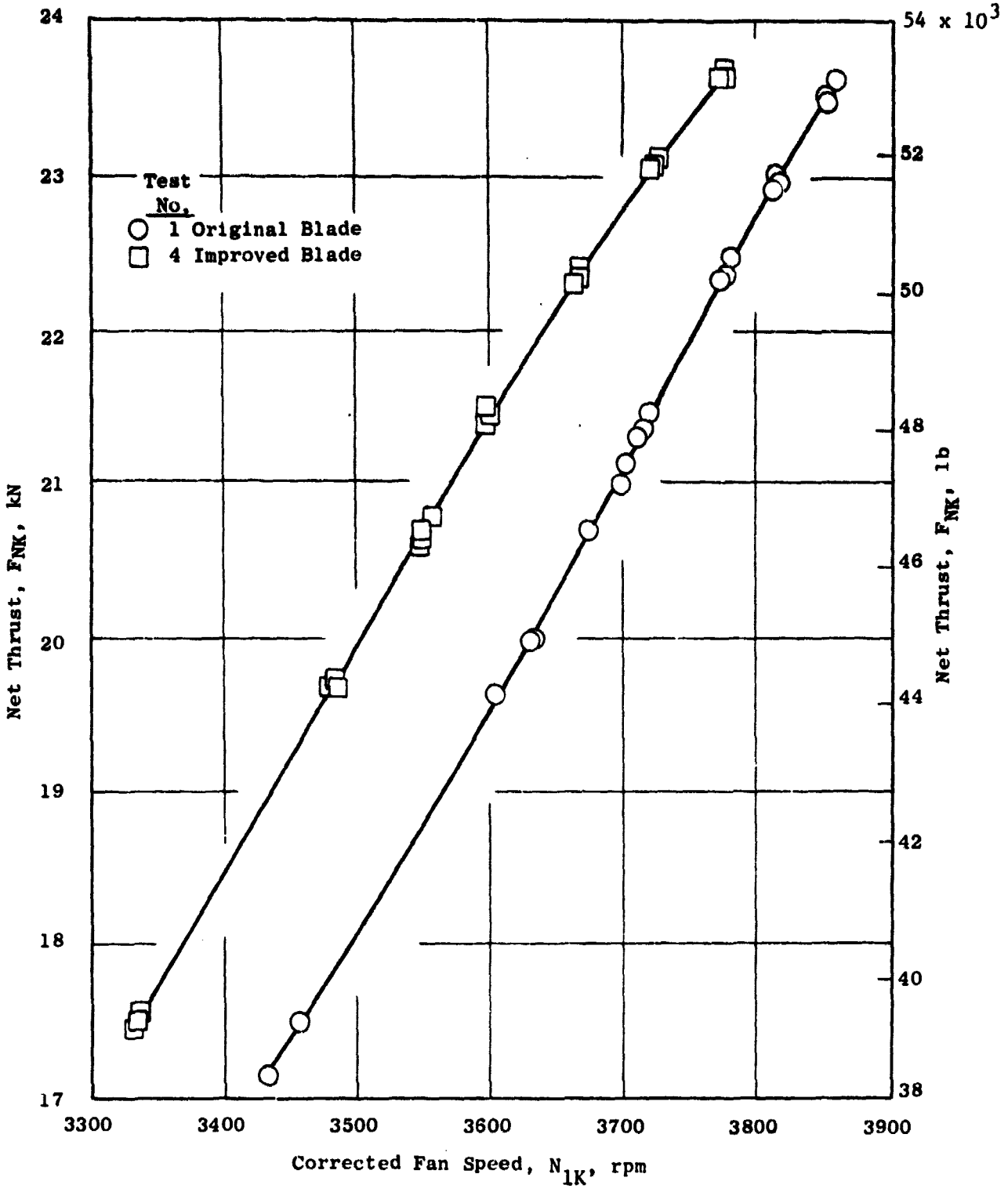

Figure 64. CF6-50 Engine SLS Thrust-Speed Characteristics With Original and Improved Fans.

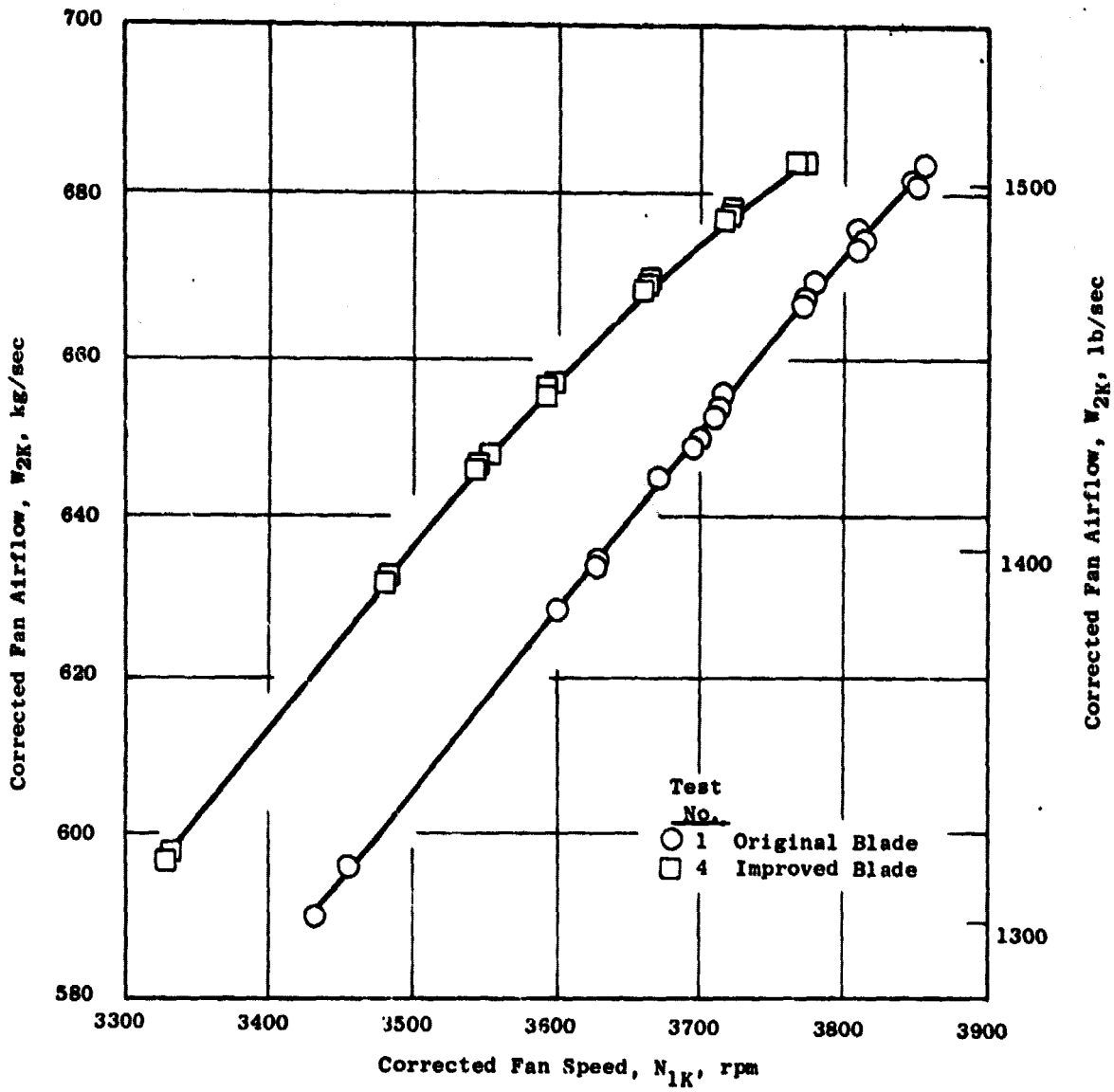

Figure 65. CF6-50 Engine Fan Airflow Characteristics, Sea Level Static with Original and Improved Fans.

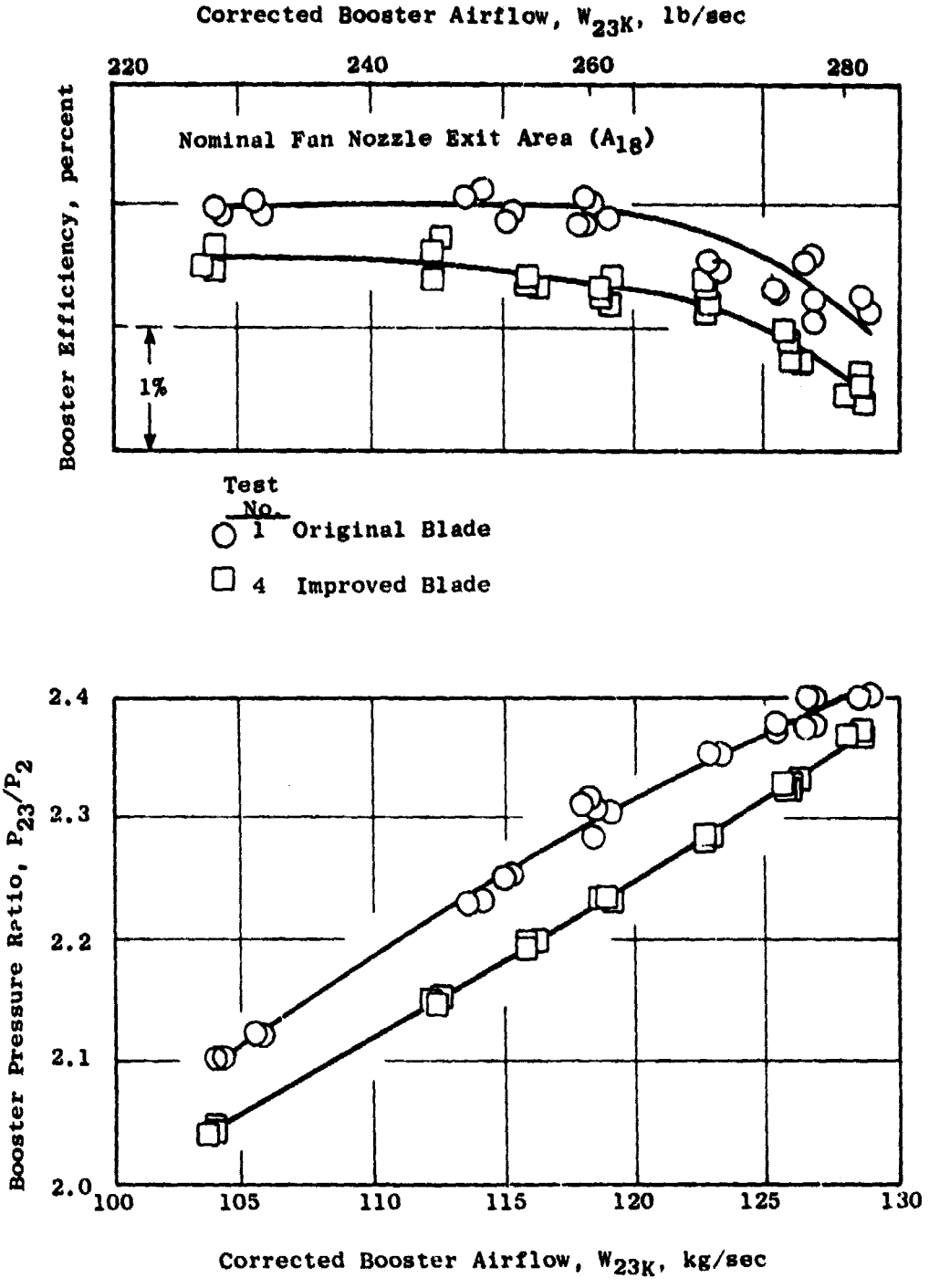

Figure 66. CF6-50 Engine Booster Performance, Sea Level Static With Original and Improved Fans.

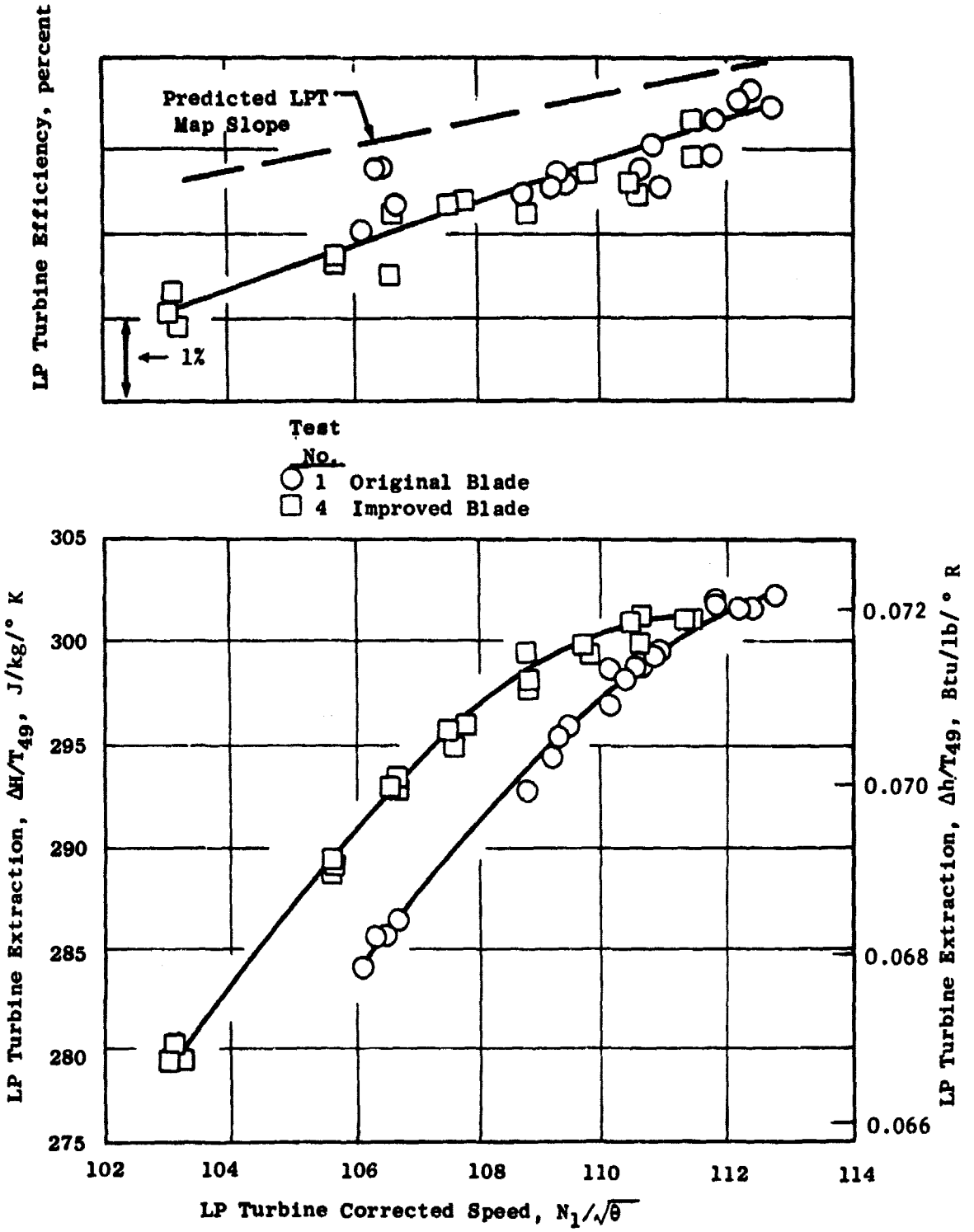

Figure 67. CF6-50 Engine Low Pressure Turbine Performance, Sea Level Static With Original and Improved Fans.

indicated for the cruise power setting for both sea level and simulated altitude conditions.

Figures 60 and 61 show sfc improvements at both sea level and simulated cruise from the initial engine tests with the improved fan blade. At a sea level static thrust equivalent to altitude cruise power, an improvement of 1.8% was obtained, which represented approximately two-thirds of the improvement required to achieve a 1.8% improvement at altitude cruise conditions. The curves indicate that significant fuel consumption improvements had been demonstrated but were not consistent with the observed fan efficiency increases shown on Figure 62. The measured fan efficiency increase of 4.2 points was within 0.5 point of expectations. On the basis of performance sensitivities, this would have been expected to produce a much larger improvement in engine fuel consumption. Detailed analysis of the engine cycle revealed that the fan efficiency improvement was not reflected directly in improved sfc but was offset to a significant degree by losses in the booster and low pressure turbine efficiencies.

Fan operating lines are shown in Figure 63 for the sea level and simulated altitude runs on both fan blades. An unexpected rollover in the fan operating line occurred at higher airflows with the improved fan blade. The original fan blades were reinstalled and tested to check out the instrumentation and measured performance. This testing indicated that a "pressure correlation" is required to be applied to the measured pressures to determine true average station pressure with the new fan blade. These adjustments do not affect sea level sfc results where performance is based on measured thrust, but they are needed for the performance assessment for the simulated altitude tests with the exhaust nozzle diffusers where thrust must be calculated from exhaust nozzle pressure.

As had been expected based on prior testing of the improved fan blade on an earlier engine, the thrust and airflow characteristics versus fan speed show a considerably lower fan speed requirement for equivalent thrusts with the improved fan. These higher flow pumping characteristics at a given speed are shown on Figures 64 and 65 for the improved fan.

Data analysis and design point cycle studies showed that the higher flow pumping characteristic of the improved fan resulted in performance penalties in the booster and low pressure turbine, detracting from the fuel savings projected for the fan efficiency improvement. Figures 66 and 67 show these deviations from the expected performance in the booster and low pressure (LP) turbine. The lower required fan speed to produce a given thrust caused the booster and LP turbine to operate at lower speed and lower efficiencies compared to operation with the original fan. Prior engine testing had given an indication from limited instrumentation that increased booster supercharging with the increased hub camber on the improved fan blade could essentially recover the booster operating line from the loss that would be expected from the required low rotor speed. Figure 66 shows that this did not occur on Test 4, which had complete booster discharge instrumentation. The lower booster operating line resulted in a loss of operating booster efficiency of

0.5 to 0.75 point. Although some loss in LP turbine efficiency was expected due to off-design operation with the lower turbine speed, the data indicated that the LP turbine efficiency loss was more than expected by about 0.6 point. These data showed tht further cycle improvements could be obtained by improved matching of the new fan and other engine components.

The 1.0% increased fan nozzle area, A_{18}, was then tested with the improved fan blade at sea level and simulated cruise (Tests 8 and 9). Specific fuel consumption results are shown on Figures 68 and 69. The improvements were not considered sufficient to warrant the change, since the calculations actually showed a slight loss (0.2%) at cruise with the open A_{18}. These small fractions of a percent are within the ability to calculate performance from nozzle pressures.

The major testing needed to identify additional performance improvements for the improved fan performance engine was directed to the second CF6-50 engine. The fan discharge arc rakes were removed from the first engine and installed in the second engine. The back-to-back SLS test of the original to General Electric-fabricated improved fan blades showed a 2.3% sfc improvement at the cruise-equivalent power of 17,800 daN, which was somewhat better than the 1.8% sfc improvement observed on the first engine but still less than the objective 2.7% at SLS.

Testing of the first engine had shown that the key to a more optimum engine cycle was to reduce the fan blade flow, thereby increasing fan rotor speed to obtain the same thrust. This became even more imperative with the vendor-fabricated improved fan blades. These blades had shown a further increase in fan airflow relative to the General Electric improved blades and a higher sfc by 0.6%. Although the intent was to produce identical blades, the process/tooling at the vendor had resulted in slight stagger changes in some sections of the airfoil.

A reduction in blade flow was accomplished with a set of prototype vendor-fabricated blades by modifying the part-span shroud interlocks. The modification produced a reduced incidence angle in the running condition, since the blade angle during engine operation is set by the blade-to-blade seating of the interlocks. The objective was 1.5° closure of the running stagger angle at the part-span shroud.

The restaggered (vendor-fabricated) improved fan blades were effective in reducing the fan flow at speed or increasing rotor speed at a given thrust. This effectively improved sfc at cruise equivalent power of 17,800 daN SLS thrust by 0.5%. Figures 70 through 72 show the effects of the various fan blades on SLS sfc improvement versus thrust, thrust versus fan speed, and fan efficiency versus fan airflow, respectively. The restaggered improved (vendor-fabricated) fan blades show a considerable reduction in engine thrust above SLS takeoff thrust levels due to the reduction in fan airflow. A loss in fan efficiency with the restaggering at higher flows is shown in Figure 72, although aerodynamic analysis would not predict a loss. Results of the fan blade evaluation are summarized on Figure 73, which shows the sfc improvement as related to fan airflow increase over the original fan blade at constant speed.

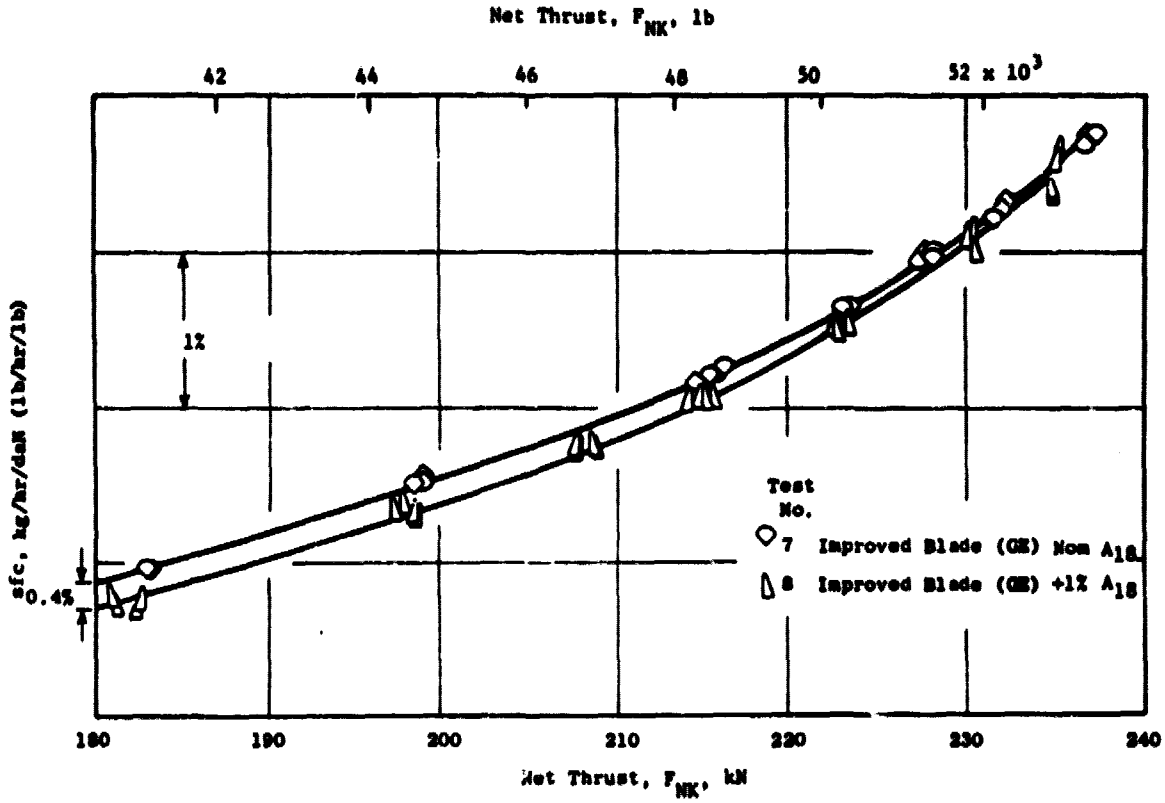

Figure 68. CF6-50 Engine: Effect of Fan Nozzle Area (A_{18}) on SFC Performance, Sea Level Static With Improved Fan.

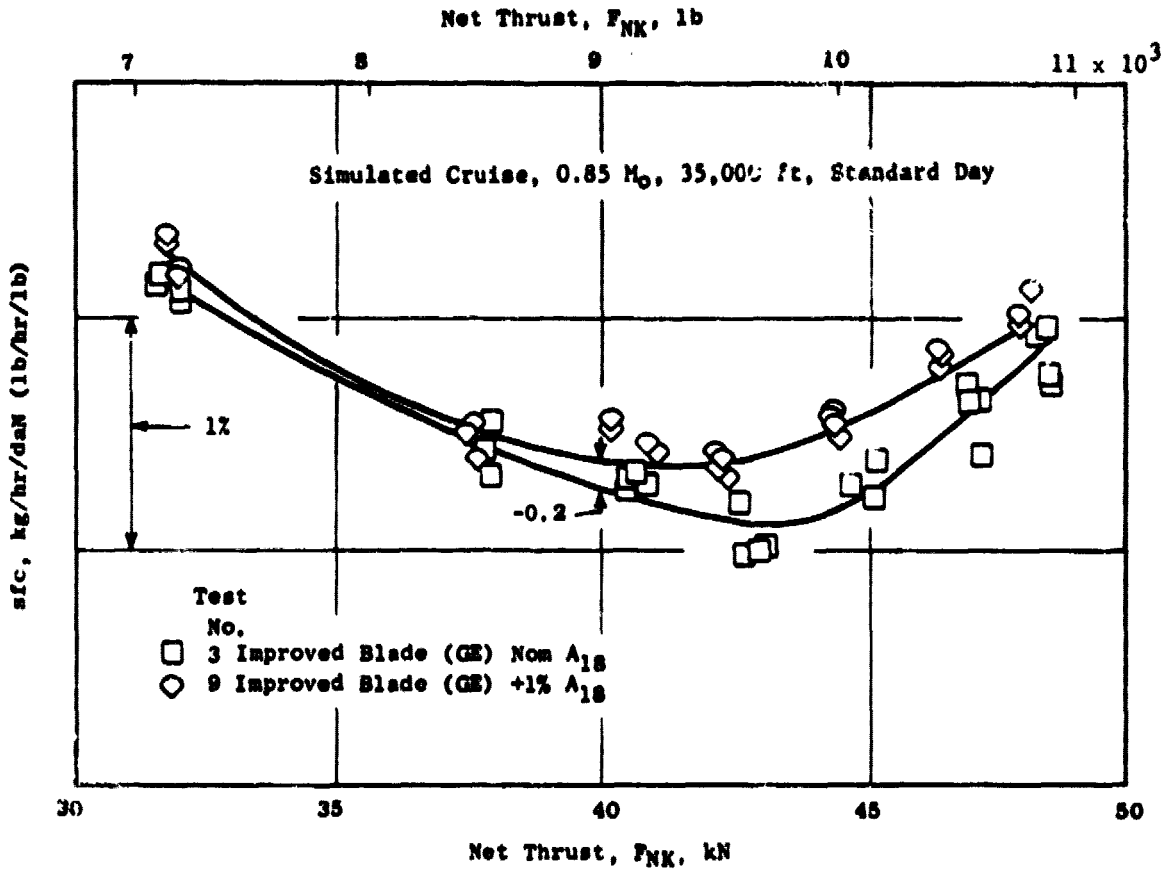

Figure 69. CF6-50 Engine: Effect of Fan Nozzle Area (A_{18}) on Simulated Altitude SFC Performance with Improved Fan.

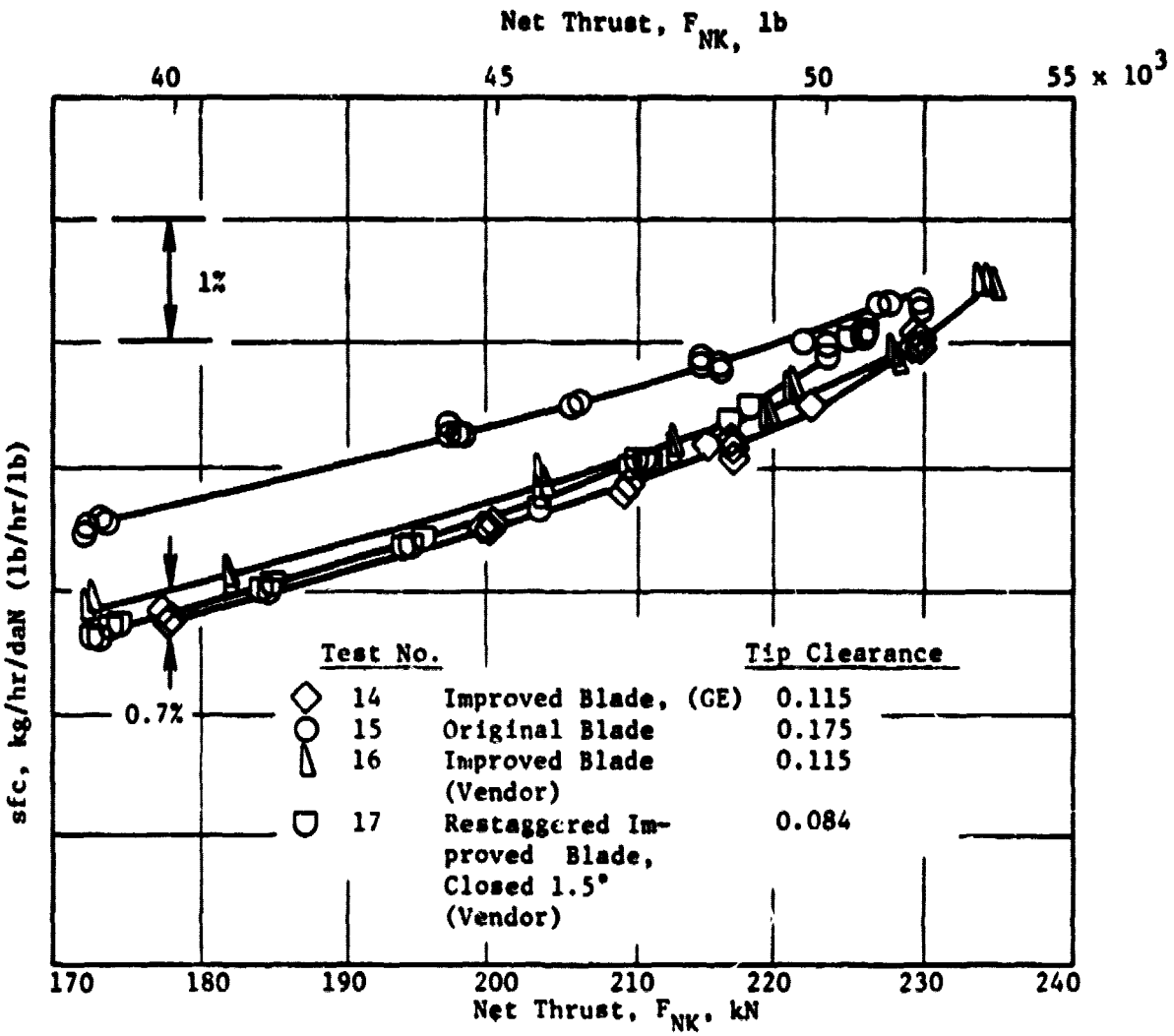

Figure 70. CF6-50 Engine No. 2: Effect of Various Fan Blades on SFC Performance, Sea Level Static, Nominal Fan Nozzle Area A_{18}.

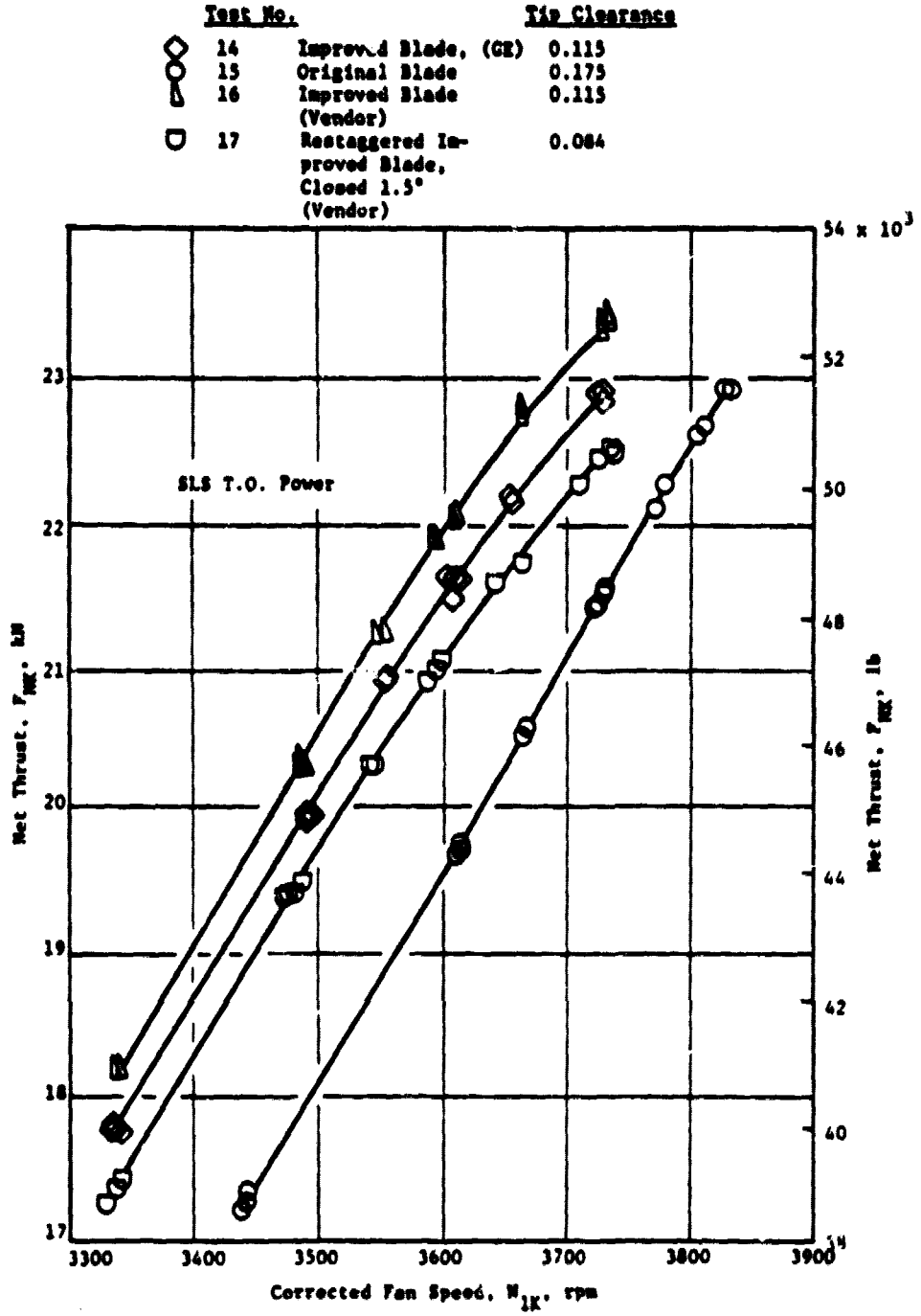

Figure 71. CF6-50 Engine No. 2: Effects of Various Fan Blades on Thrust Characteristics, Sea Level Static, Nominal Fan Nozzle Area.

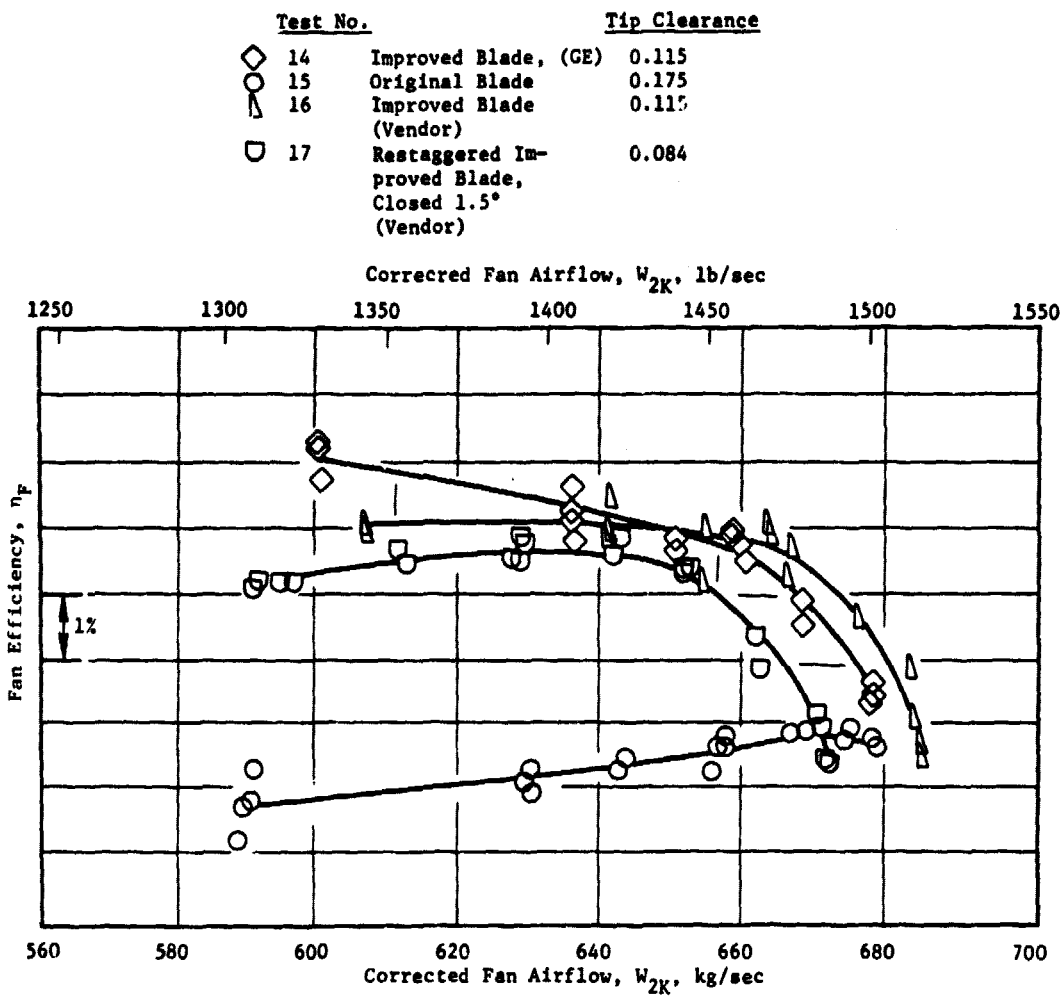

Figure 72. CF6-50 Engine No. 2: Effects of Various Fan Blades on Fan Efficiency, SLS, Nominal Fan Nozzle Area A_{18}.

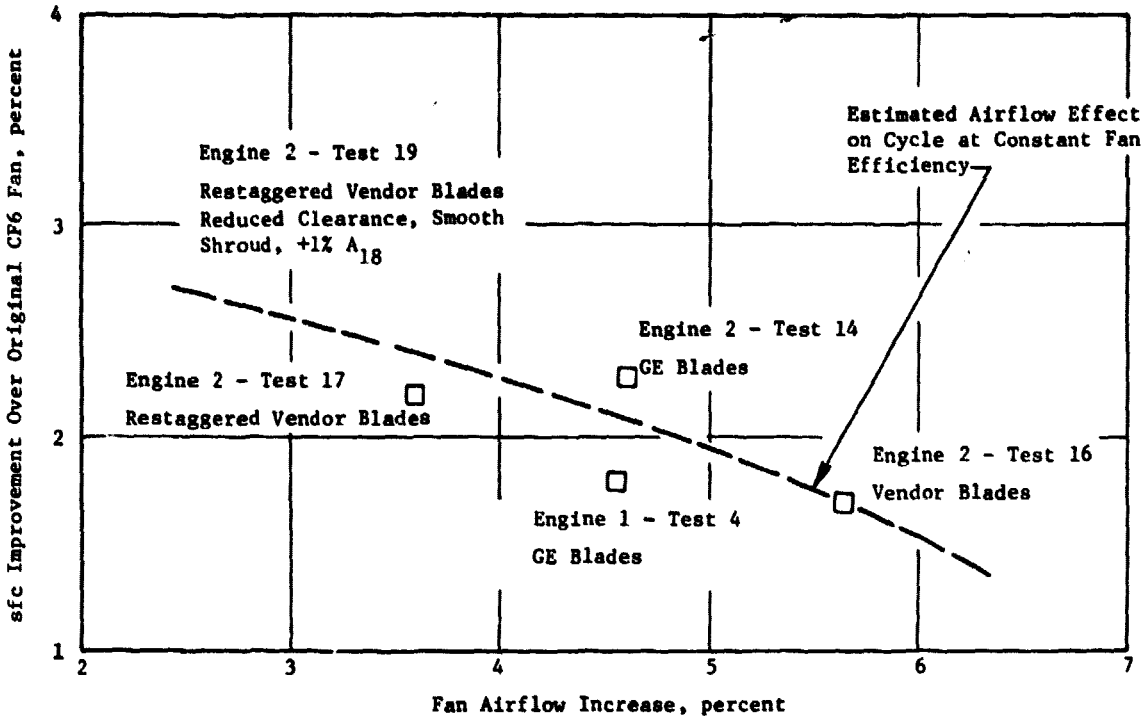

Figure 73. CF6-50 Engine SFC Improvement Versus Fan Airflow for Various Improved Fan Blades, SLS Thrust of 17,800 daN (40,000 Pounds), Nominal A_{18}.

Fan tip rub button testing on the second engine was initiated to determine if a further reduction in tip clearance was possible (Figure 74). This testing showed that the fan case stiffener had provided a significant improvement in casing roundness compared to the unstiffened case. This permits tightening grind clearances such that average running clearances are correspondingly reduced for improved performance without reducing minimum running clearances. Back-to-back testing with a further reduction in tip clearance of 0.090 mm (0.035 in.), along with a change in tip shroud material from open-celled honeycomb to a smooth surface "microballoon", showed a significant improvement in fan efficiency (1.2 points) and sfc (0.7%) at part power somewhat more than expected. Conversely, the performance improvements previously measured on an engine with the restaggered blade at the same clearance were somewhat less than expected, considering the airflow reduction achieved as shown in Figure 75. Although the performance increments measured for the further reduced tip clearance and for the blade restagger at the same clearance were inconsistent with expected improvements, these increments are small and within the capabilities of engine/data system repeatability. The net total effect of these changes, however, was consistent with predictions.

The final improved fan package includes the restaggered improved fan blade, a total of 2.5 mm (0.100 in.) reduction in tip clearance with the fan case stiffener and the smooth fan casing tip shroud.

7.6 APPLICATION OF RESULTS

Results of this testing and plans for further development have been coordinated with the aircraft manufacturers currently using CF6-50 model engines. Flight test programs directed toward recertification of the respective aircraft and a production engine program for the CF6-50C2 and E2 model engines have evolved from the fan development program. The first set of production-type fan blades having the desired stagger angle was tested back-to-back against a set of the modified restaggered blades in a production CF6-50E2 engine installed in a production test cell. This testing essentially showed the same performance for the two blade sets. A comparison of sfc performance for the third engine is shown on Figure 76.

The production CF6-50C2 and CF6-50E2 model engines are demonstrating the expected sfc improvements relative to the CF6-50C and CF6-50E models, and the performance results are presented in Section 11.0.

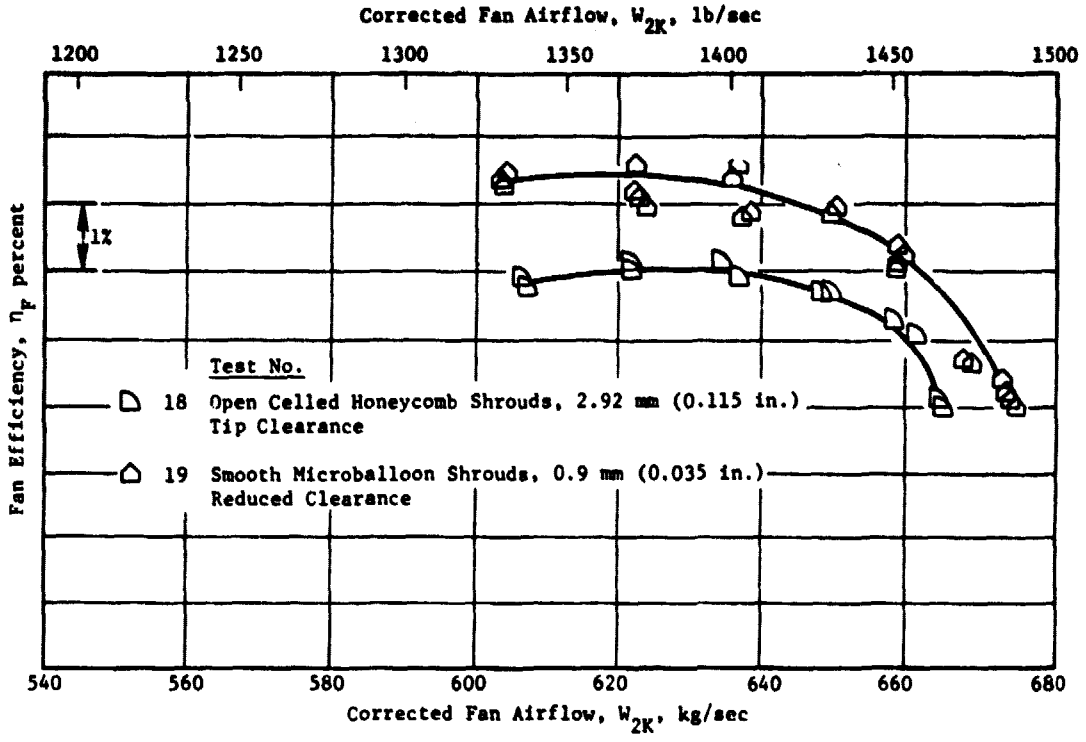

Figure 74. CF6-50 Engine No. 2: Effects of Fan Tip Clearance on Fan Efficiency, Sea Level Static, Nominal +1% Fan Nozzle Area with Restaggered Improved Vendor Fan Blades.

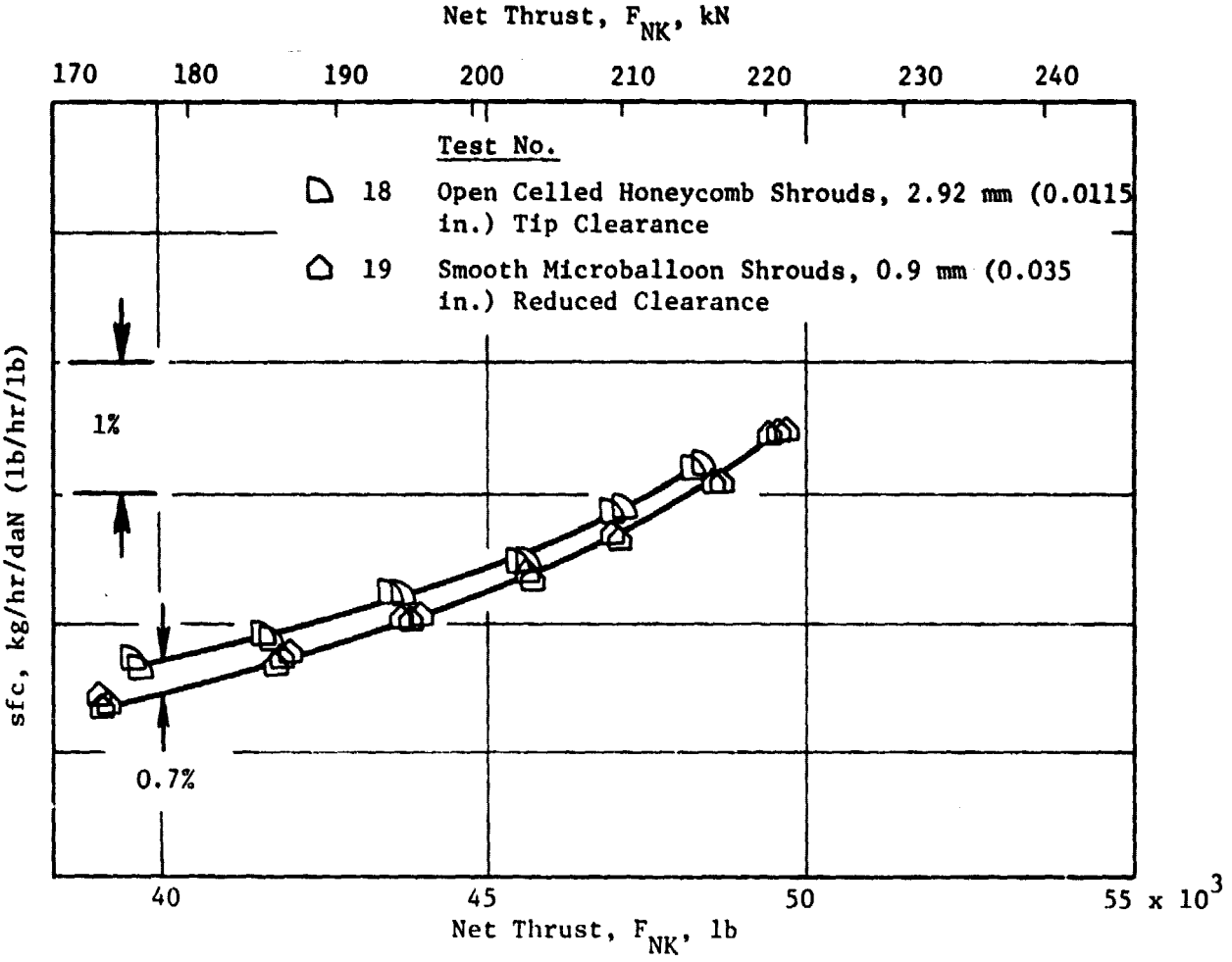

Figure 75. CF6-50 Engine No. 2: Effects of Shroud Tip Clearance on SFC Performance, Sea Level Static, Nominal +1% Fan Nozzle Area with Restaggered Improved Vendor Fan Blades.

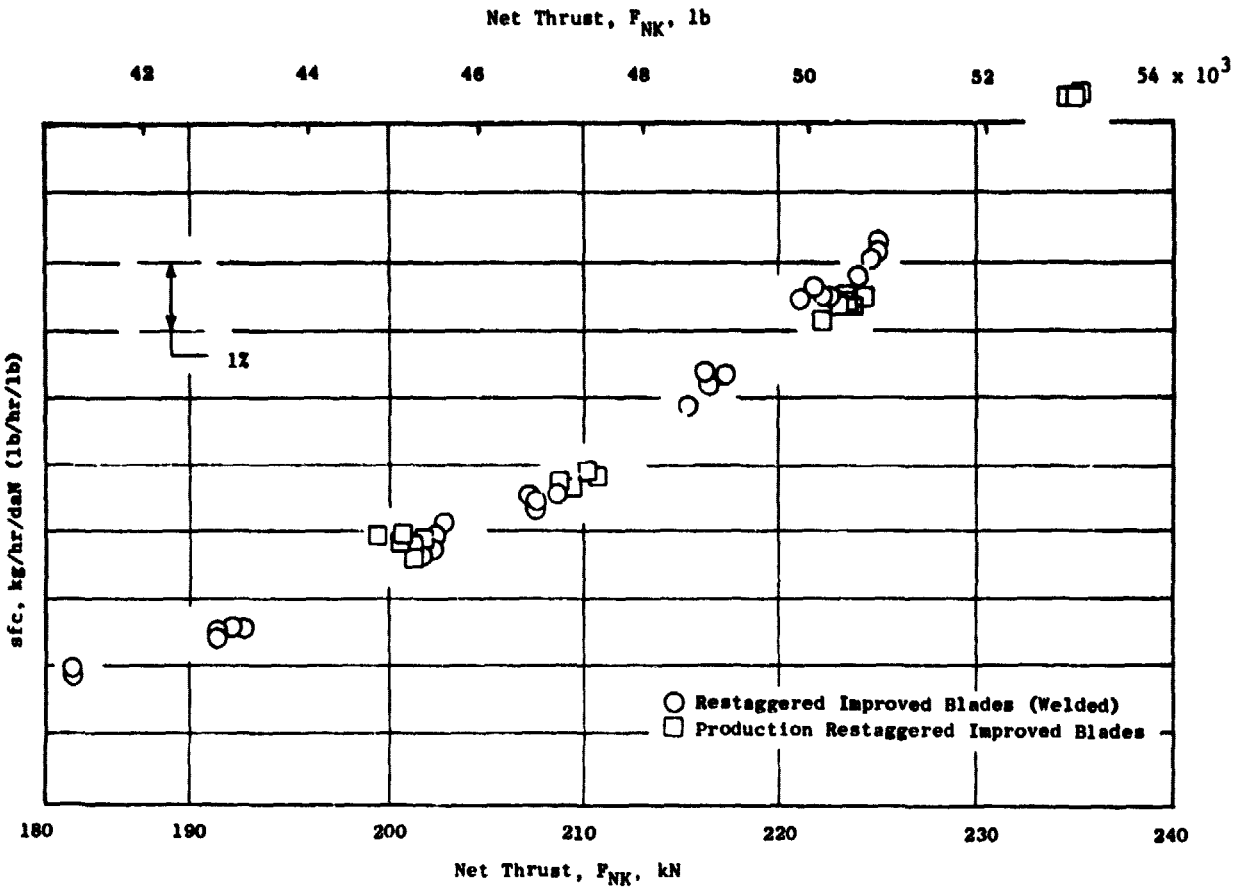

Figure 76. CF6-50 Engine 3: Back-to-Back Improved Fan Blade Performance.

8.0 ENGINE ACOUSTIC TEST

A series of static back-to-back acoustic tests was conducted on CF6-50 engine configurations with the original and the improved fans. Objectives of the acoustic test program and subsequent data analyses were to establish the acoustical effects of the improved fan performance improvement package on CF6-50 engine noise, and assess the impact of the subject engine modification on community noise levels for typical aircraft approach and takeoff flight conditions. This section describes the acoustic test facility, engine configurations, instrumentation, acoustic testing procedure, and data reduction methods utilized. Results are presented comparing noise levels of the original CF6 fan to those of the improved fan configuration.

Community noise exposure estimates are presented in terms of simulated effective perceived noise level (EPNL) determined from the static test data and typical aircraft operating characteristics for takeoff and approach flight conditions. These estimates were developed analytically assuming the static measurements to be flight levels.

8.1 ENGINE ACOUSTIC TEST FACILITY

The static back-to-back noise tests were performed in the outdoor performance/acoustic test facility. The site was paved with concrete extending a minimum of 6.1 m (20 ft) beyond the microphone positions. The acoustic field was free of obstructions for 45.7 m (150 ft) minimum distance beyond the far field microphone locations. The engine was mounted to a thrust frame supported by an open-trussed cantilever structure with the engine centerline located 3.96 m (13 ft) above the concrete as shown in Figure 77.

The engine was operator-controlled using a minicomputer-based engine and facility data monitoring system located in the control room complex. In addition to the real-time monitoring of engine performance parameters, the computer system provided real-time data acquisition and analysis for a maximum of 878 channels of steady-state engine performance data and ambient conditions. The data channels were continuously sampled and time-averaged for a 52-second interval for each engine power set point. Acoustic data acquisition was synchronized with the data monitoring system (DMS) data acquisition.

8.2 TEST CONFIGURATIONS

One production CF6-50C engine (Douglas configuration) and one production CF6-50E engine (Boeing configuration) were used for the acoustic tests. Both engines were fitted with a reference acoustic inlet with bellmouth lip, a long reversing core nozzle (LRCN), and current production fan and core duct acoustic treatment. The acoustic treatment is described below:

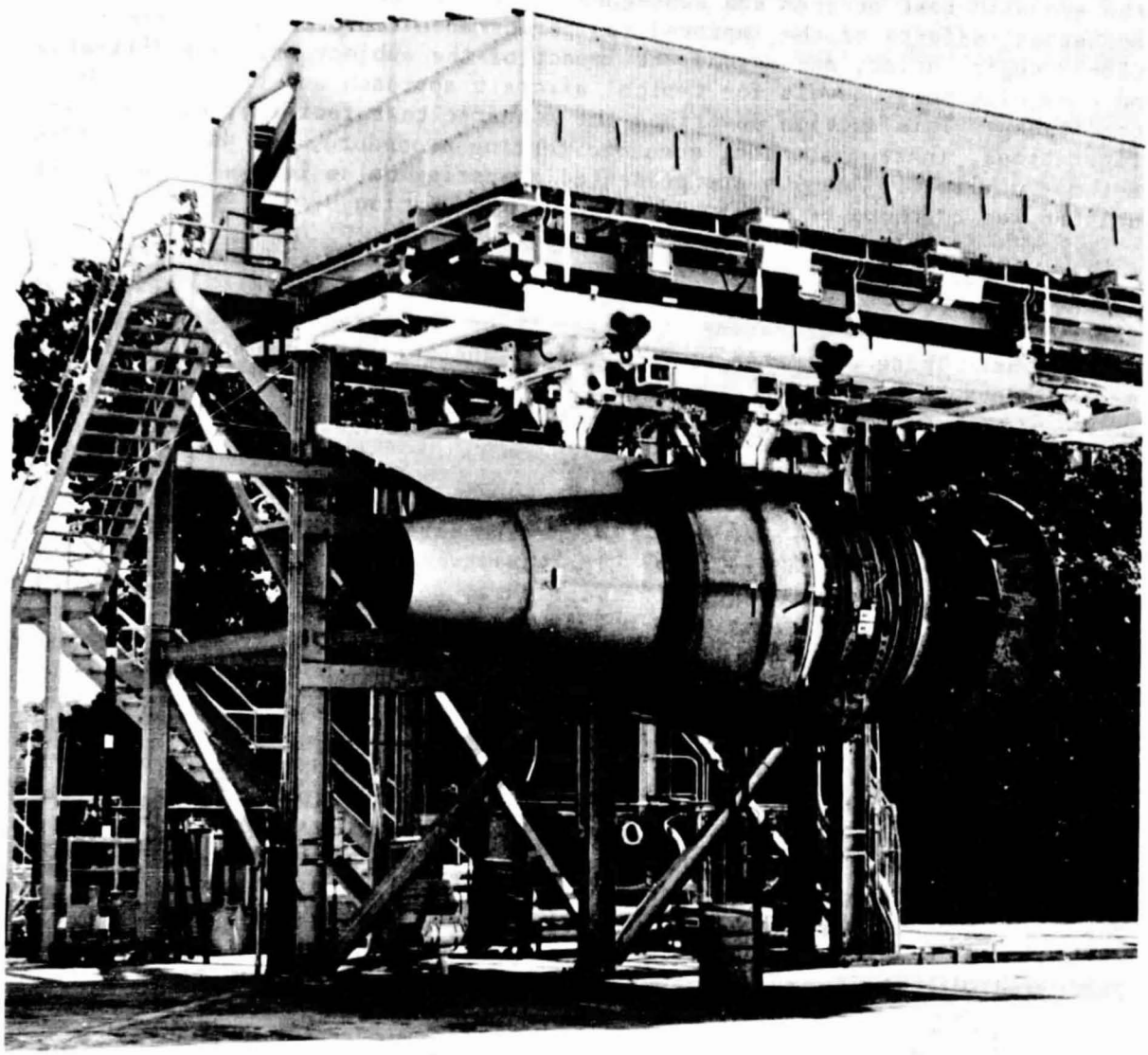

Figure 77. CF6-50 Engine Mounted on Thrust Stand for Acoustic Tests.

ORIGINAL PAGE IS
OF POOR QUALITY

Location	Treatment Type	Treatment Area
Fan Inlet	Single Degree of Freedom (SDOF)	5.57 m^2 (60 ft^2)
Fan Casing	Multiple Degree of Freedom (MDOF)	5.85 m^2 (61 ft^2)
Fan Exhaust Duct	Single Degree of Freedom (SDOF)	4.65 m^2 (50 ft^2)
	Multiple Degree of Freedom (MDOF)	4.37 m^2 (47 ft^2)
Long Reversing Core Nozzle	"Tophat" (SDOF)	1.94 m^2 (21 ft^2)

The engines were modified in order to run the configurations described in Table VII. All performance rakes were excluded from the fan inlet, fan exhaust duct, and core exhaust duct for these tests in order to preserve the acoustic characteristics of an aircraft installation.

For the baseline acoustic tests (No. 3 and 5), the CF6-50 engine was run with a set of original production fan blades. The fan casing tip shroud was open cell aluminum honeycomb and ground to the production minimum tip clearance of 4.45 mm (0.175 in.). For the fan blade tip clearance acoustic test (No. 1) with the original fan blades, the fan casing tip shroud was modified by installing microballoon epoxy in open cell aluminum honeycomb to provide a smooth casing tip shroud. The tip shroud was ground to provide a fan tip clearance of 3.30 mm (0.130 in.), a reduction of of 1.14 mm (0.045 in.).

For the improved fan acoustic tests (No. 2 and 4), the original production fan blades were replaced with a full set of restaggered improved fan blades. The smooth fan casing tip shrouds were ground to provide tighter fan tip clearances down to 1.90 mm (0.075 in.), a reduction of 2.54 mm (0.100 in.). Refer to Section 3.0 for a detailed description of the improved fan.

8.3 INSTRUMENTATION - ACOUSTIC

8.3.1 Far Field Microphones

Acoustic data were obtained from a set of microphone systems which consisted of the microphone, cathode follower, power supply, and pistonphone; no windscreens were used.

The far field microphones were positioned 3.96 m (13 ft) above the concrete surface and at 10° to 160° in 10° increments measured from the inlet direction. Additional microphones were positioned at 85°, 95°, 105°, 115°, and 125° at the same height. All microphones were located on a 45.73 m (150 ft) arc measured from the fan exhaust nozzle and oriented toward the source (normal incidence) at a sufficient offset distance from the microphone stands to minimize reflection effects. A sketch and photograph of the sound field are shown in Figures 78 and 79.

Table VII. CF6-50 Engine Test Configurations for Acoustic Tests.

Test No.	Configuration	Fan Blades	Casing Tip Shroud	Nominal Buildup Tip Clearance		Core Nozzle
				mm	in.	
1	Original Fan Reduced Tip Clearance	Original	Smooth Microballoon	3.30	0.130	LRCN*
2	Improved Fan	Restaggered Improved	Smooth Microballoon	2.29/1.78	0.090/0.070	LRCN
3	Original Fan Baseline	Original	Open Cell Honeycomb	4.45	0.175	LRCN
4	Improved Fan	Restaggered Improved	Smooth Microballoon	1.90	0.075	LRCN
5	Original Fan Baseline	Original	Open Cell Honeycomb	4.45	0.175	LRCN

*LRCN - Long Reversing Core Nozzle

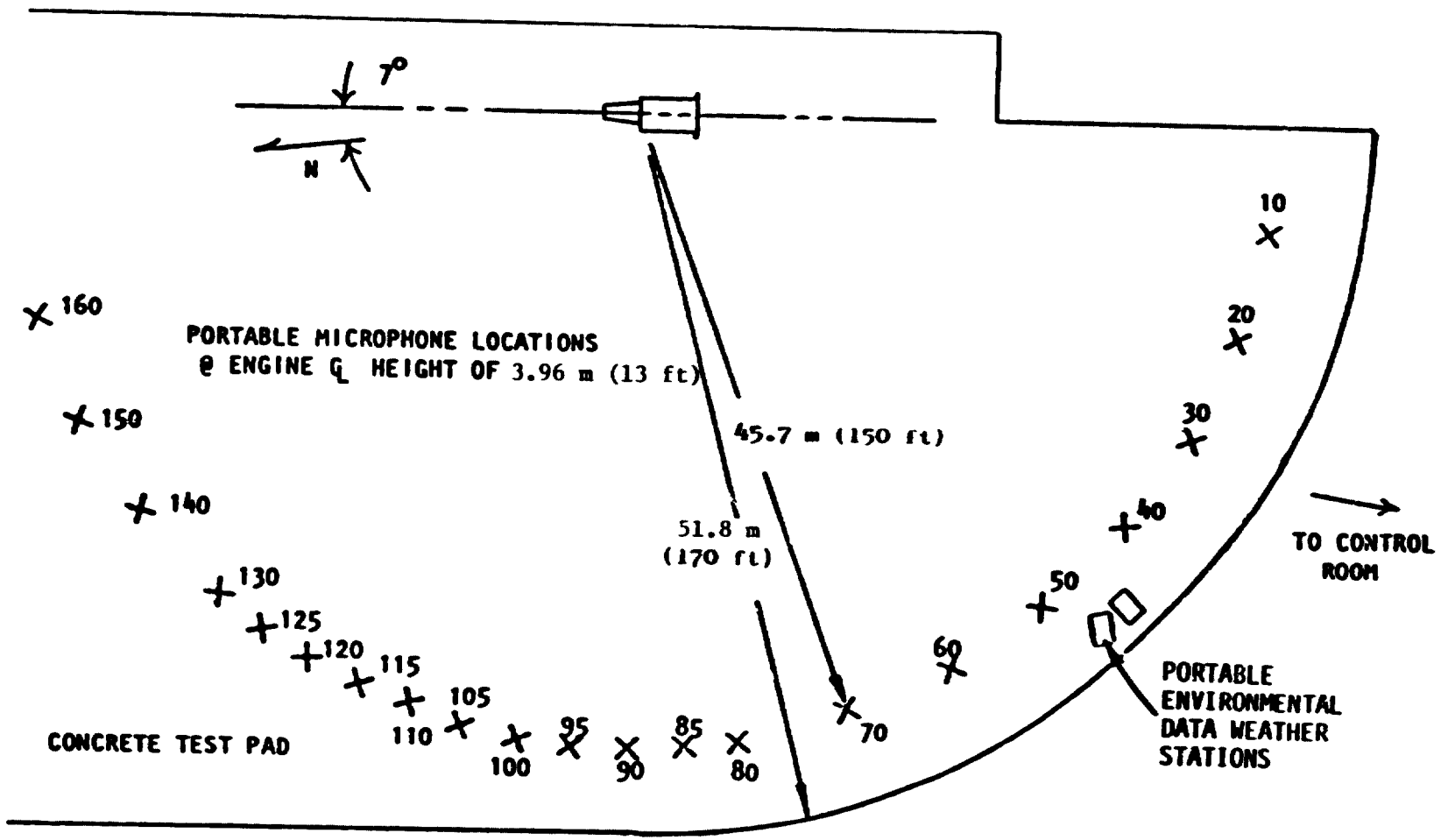

Figure 78. CF6-50 Sound Field Layout.

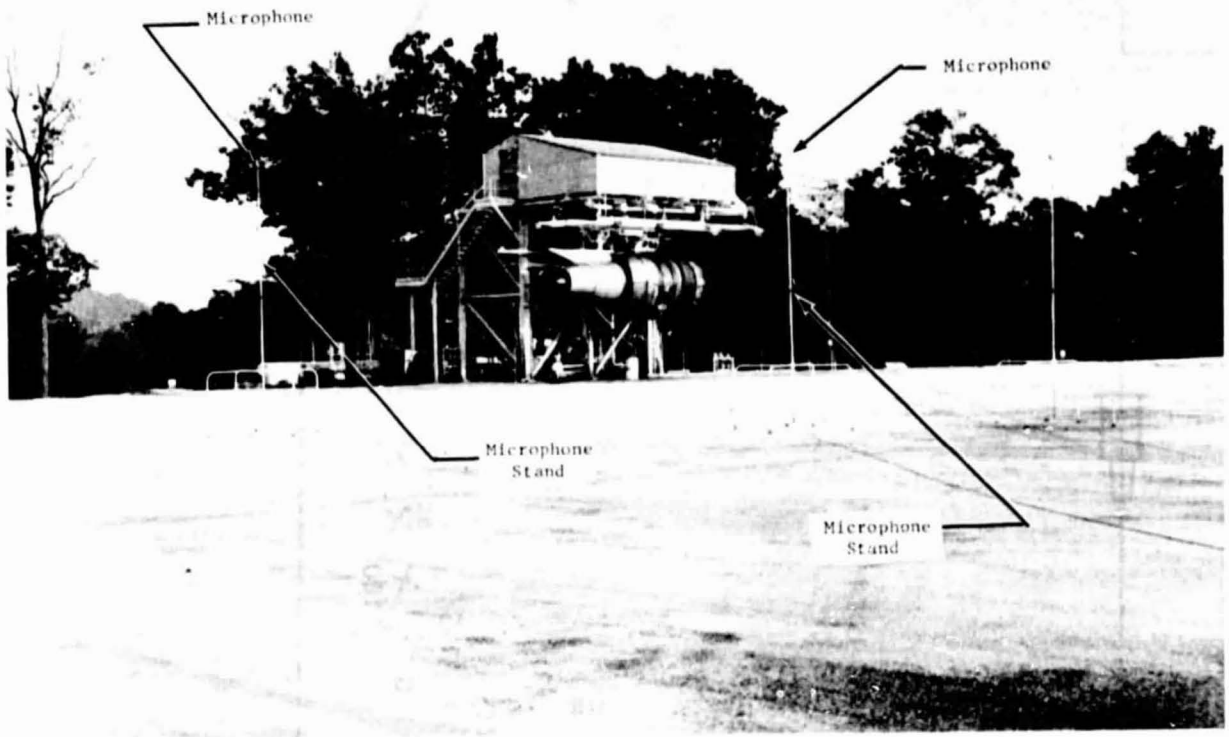

Figure 79. CF6-50 Engine Sound Field at Test Site.

8.3.2 Acoustic Data Recording

Acoustic data were recorded on magnetic tape at a tape speed of 76.2 cm/sec (30 in./sec). The recorder was set up for 40% carrier deviation (± 40%) at full scale record level. Signal amplification was provided by a General Electric-designed ac/dc preamplifier module. During testing, the tape recorder input and output were monitored to assure that adequate amplification was used and to assure proper operation of the recorder. Data were recorded for at least 2 minutes at each speed point.

8.3.3 Atmospheric Test Condition Instrumentation

Barometric pressure was recorded for each test point. Wind speed, direction, air temperature and dew point were all measured using a portable environmental data station (PEDS). Two of these stations were located approximately 45° from the inlet on a 51.2 m (168 ft) arc. The sensors were positioned at a 3.96 m (13.0 ft) height. Wind speed and direction, as measured on one of the PEDS, were recorded continuously on strip charts. The second PEDS incorporated General Electric designed wind speed and V cosθ wind direction instrumentation. These signals were also recorded continuously on strip charts. Ambient temperature was measured by aspirated resistance temperature devices. The dew point measurement was made with a hygrometer which sampled air from the 3.96 m (13.0 ft) location. All these measurements were also recorded on the DMS computer system.

8.4 TEST PROCEDURE AND DATA REDUCTION

8.4.1 Atmospheric Test Condition Limits

Atmospheric condition limits were set prior to the test which include water, snow, or ice cover on sound field, and no visible fog or precipitation. Any data recorded outside the limits listed below were discarded and no testing was permitted under conditions of:

Relative humidity		$20\% \leq RH \leq 95\%$
Temperature	263.6° K (15° F)	$\leq T_o \leq$ 305.2° K (90° F)
Headwind		$\leq$ 4.1 m/sec (8 kn) including gusts
Crosswind		$\leq$ 2.6 m/sec (5 kn) including gusts
Tailwind		0 m/sec
Gusts		$\leq$ 1.5 m/sec (3 kn)

8.4.2 Engine Test Conditions

Various engine configurations were run to obtain data for comparisons at the same corrected thrust over a range of conditions that encompassed the approach, cutback, and takeoff power ranges for aircraft powered by the CF6-50 engine. For each test configuration, the sequence shown in Table VIII was repeated twice in the same order for a total of three readings at each power setting. A shutdown of at least 30 minutes occurred between each test series. At each power setting, the engine was stabilized for at least 2 minutes prior to recording acoustic data. All performance parameters were determined from the DMS computer system and corrected to standard temperature, standard sea level pressure, zero humidity, and zero wind using measured ambient data for temperature, pressure, absolute humidity, and wind velocity and direction.

8.4.3 Calibration of Far Field Microphone Systems

Prior to each configuration test series, each system was calibrated to determine frequency response and sensitivity. Each microphone head was removed and a known voltage level of pink noise was input to the microphone preamplifier. The output signal from each amplifier was recorded on magnetic tape. Subsequent playback and processing through the data reduction system determined system frequency response corrections. The microphone cartridge response, as determined from the individual microphone laboratory calibration curves, was algebraically added to the former corrections to determine the overall system response for inclusion in the data reduction program.

The microphone cartridge was then replaced and a 124 dB pistonphone was applied to each microphone. The microphone sensitivity was compared to the most recent laboratory calibration data to assure compliance within ±1.5 dB. Any system falling outside this band was replaced. The microphone outputs were then normalized using variable attenuators in order to record the same voltage level with the pistonphone source input. At the conclusion of each test series, the pistonphone was reapplied, and the voltage level was recorded as a verification of microphone system integrity.

On several occasions throughout the test series, 2-minute recordings of ambient noise were made with "facility on" and "facility off". These recordings were made at gain settings used during the sound measurements to assure acceptable signal to noise ratios for the acoustic data.

8.4.4 Acoustic Data Reduction

Off-line acoustic data reduction was performed using an Automated One-third Octave Band Data Reduction System. The recorded data were played back on a 28-track system. In the automatic operating mode, control of the system was provided by means of a computer and operator-provided information. The data to be sampled were located by means of a time code reader, indexing from the time code signal recorded on the data tape. This tape-shuttling was continued for each data channel with sampling performed over the same time

Table VIII. CF6-50. Engine Nominal Test Conditions for Acoustic Tests.

Corrected Thrust, Fn/δ_2		Corrected Speed, N_{1k} (rpm)	
N	lb	Original Fan	Improved Fan
234,420	52,700	3875	3880
227,962	51,248	3850	3850
216,810	48,741	3780	3710
204,488	45,971	3700	3600
168,921	37,975	3450	3350
158,477	35,727	3370	3275
148,491	33,382	3290	3210
126,592	28,459	3100	3005
117,113	26,328	3010	2910
109,173	24,543	2930	2835
101,686	22,860	2850	2760
94,654	21,279	2770	2685
88,079	19,801	2690	2610
81,958	18,425	2610	2535
76,291	17,151	2530	2460
72,341	16,263	2470	2405
68,053	15,299	2400	2340
59,094	13,285	2230	2190
53,632	12,057	2100	2090

increment until all channels of a particular reading were processed. The system then advanced to the next data point, based on the operator-supplied time reference, and repeated the shuttling process. After the processing information (including reading identification, reading time, gain changes, etc.) was set up by the operator, the system ran without further operator assistance until a magnetic tape change was required.

All one-third octave band analyses were performed using a one-third octave band analyzer. An integration time of 32 seconds was used to provide adequate sampling of the low frequency portion of the data signal. The frequency range of the data reduction process was 50 Hz through 10 kHz. Each data channel output was passed through an interface to the minicomputer where data were corrected for both the frequency response of the acquisition and reduction system (as determined from the pink noise calibration) and for the microphone head response. The minicomputer was interfaced to a main frame computer to generate a file containing the one-third octave band data for further processing. The one-third octave band data were also punched on paper tape as a backup for the communication interface system.

Noise data at each point were processed using a digital computer program to normalize the data to a 298° K (77° F)/70% relative humidity, standard day and perform data extrapolations to various sideline distances. Overall sound pressure levels, PNL and PNLT, were computed for each angle at the sideline distances. The sound power level for each one-third octave band and overall sound power level were computed for each test point. These results were used for subsequent analysis and data comparisons.

8.4.5 Instrumentation Accuracy

The accuracy of any sound measurement is dependent on the accuracy of the acoustic data recording and reduction system which is dependent on the tolerance of each independent component in the system. A list of each component and the accuracy (3 σ tolerances) is presented below:

Component	3 σ Tolerance (± dB)
Microphone Cartridge Calibration	0.2 f < 10 kHz
Cathode Follower Amplifier	0.2
Pistonphone	0.2
Noise Generator	0.5
Power Supply	0.09
Variable Gain Amplifier	0.2
Tape Recorder	0.5
Tape Deck	0.5
1/3 OB Analyzer	0.25

Since these variations are independent of each other, the estimated variance of the sound level can be computed as the rms of the variances due to each component separately. The accuracy of the acoustic data recording and reduction system is then ± 1.0 dB.

The accuracy of the system does not define data reproducibility, which is dependent on many other factors. The intrinsic variation of acoustic data, due to meteorological conditions, source variation, random instrument error, etc., defines data sample variance about the "true" absolute level of the noise source under evaluation. Hence, the instrumentation accuracy defines the tolerance (systematic error) on a "true" noise level determined from test sample statistics (random error). Noise level differences obtained from static back-to-back testing remove any data bias introduced as a result of instrumentation systematic error.

8.5 TEST HISTORY

A production CF6-50E engine with the original CF6 production fan blades was modified to a reduced tip clearance and smooth shroud configuration and then tested. Upon completion of the clearance testing, the engine was converted to an improved fan configuration and various performance and acoustic tests were run. The engine was then converted to an original fan configuration with the original CF6 production fan blades, open cell aluminum honeycomb fan tip shroud, and production fan tip clearance. Checkout, power calibration, and acoustic tests were performed to provide an acoustic baseline for the original fan.

A production CF6-50C engine was converted to the final improved fan configuration and installed at the same test site. Checkout of the engine and facility was completed, followed by a power calibration of the engine and the acoustic testing. The engine was then modified to an original fan engine configuration and a baseline acoustic test series was completed.

8.6 TEST RESULTS AND DISCUSSION

8.6.1 Effect of Fan Tip Clearance on Acoustic Characteristics

Static acoustic tests were conducted to evaluate possible differences in engine noise produced by reducing fan tip clearance. Results are presented for the original production fan configuration with the production open cell honeycomb tip shroud with a minimum tip clearance of 4.45 mm (0.175 in.) in Test 3 (Table VII) and the original fan blades with a smooth microballoon casing tip shroud and a reduced clearance of 3.30 mm (0.130 in.) in Test 1.

The 45.7 m (150 ft) arc data were extrapolated to a reference sideline of 122 m (400 ft). Spherical divergence was used to correct for distance, and SAE Aerospace Recommended Practice ARP866A (Reference 3) was used to correct for atmospheric absorption. A 122 m (400 ft) sideline distance was selected

for data analysis, because it is representative of FAA certification altitude for approach engine power settings.

The use of longer sideline distances representing takeoff flight paths would tend to mask potential differences in high frequency fan noise that could be produced by the tip clearance/fan shroud modification. To facilitate data comparisons between the engine configurations, all data were averaged, and comparative plots were made. Data are presented for the power settings summarized in Table IX. Averaged one-third octave spectra at peak forward and peak aft angles are presented in Figures 80 through 85 for low and high approach, and cutback thrust levels. PNL directivity behavior comparing the engine configurations at these thrust levels are exhibited in Figures 86 through 88. PNL data at peak forward and peak aft angles are shown versus thrust in Figures 89 and 90.

No significant acoustic differences between the engine configurations are apparent in the spectral comparisons at peak angles. The perceived noise directivity behavior and thrust behavior comparisons do not exhibit any systematic differences in engine noise as a result of the tip clearance/fan shroud modification.

8.6.2 Improved Fan Acoustic Characteristics

Results comparing the original and improved fan configurations, obtained from two separate static back-to-back engine test series, are presented herein. Data analyses to evaluate small differences between the engine configurations are discussed.

Corrected thrust versus corrected fan speed (N_{1K}), as determined during the test series, are compared in Figure 91. Good agreement was maintained between repeat test runs for each engine configuration.

The 45.7 m (150 ft) arc data were extrapolated to reference sidelines of 122 m (400 ft) and 305 m (1000 ft). Spherical divergence was used to correct for distance, and ARP866A (Reference 3) was used to correct for atmosphere absorption. These reference distances were chosen because they are typical of FAA certification altitudes for approach and takeoff, respectively. To facilitate acoustic data comparisons between engine configurations, all data were averaged and comparative plots were made. Results are presented in terms of one-third octave band spectra at peak forward and peak aft angles, PNL directivity, and PNL as a function of thrust for peak forward and peak aft angles in Figures 92 through 107 at typical takeoff and approach power settings summarized in Table X. The small differences in acoustic characteristics between engine configurations were not systematic and were considered to be within normal data scatter for static engine noise testing with the exception of the 315-630 Hz band levels shown in Figure 96.

The spectrum level differences shown in Figure 96 between the improved and original fan engine configurations at 50° and 158 kN corrected thrust (cutback) are the result of multiple pure tones (MPT), i.e., "buzz saw" noise.

Table IX. Nominal Engine Power Settings Used for Data Presentation Comparing Reduced and Standard Tip Clearance Configurations.

Nominal Thrust		Flight Condition	Sideline Distance	
kN	lb		meters	feet
148.5	33,400	Cutback	122	400
88.0	19,900	High Approach	122	400
59.0	13,300	Low Approach	122	400

Table X. Nominal Engine Power Settings Used for Data Presentation Comparing Improved and Original Fan Engine Configurations.

Nominal Thrust		Flight Condition	Sideline Distance	
kN	lb		meters	feet
228	51,200	Takeoff (T/O)	305	1000
158	35,600	Cutback (C/B)	305	1000
88	19,800	High Approach	122	400
59	13,300	Low Approach	122	400

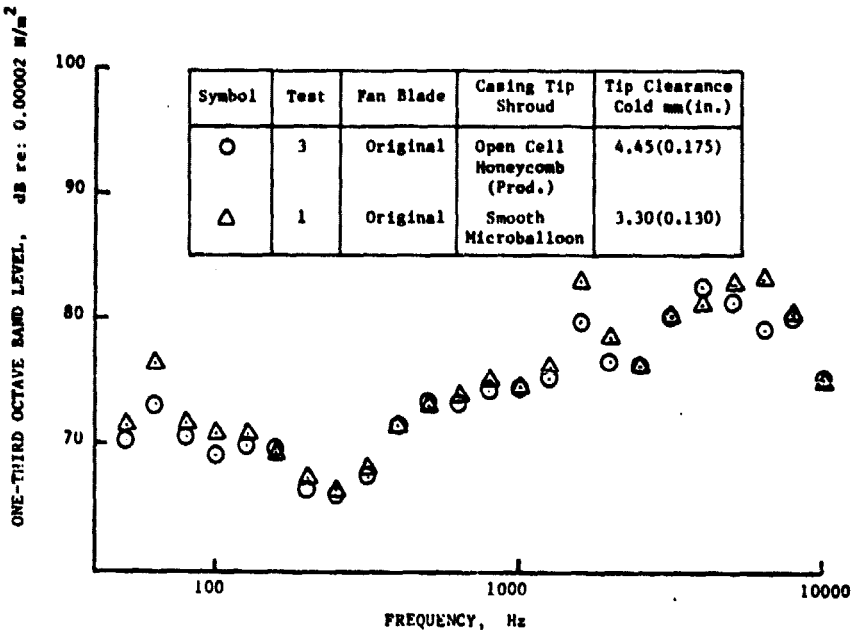

Figure 80. One-third Octave Spectrum Comparison of Original Fan With Original and Reduced Tip Clearance at 60° Peak Forward Angle (122 m Sideline and 59 KN Corrected Thrust - Low Approach).

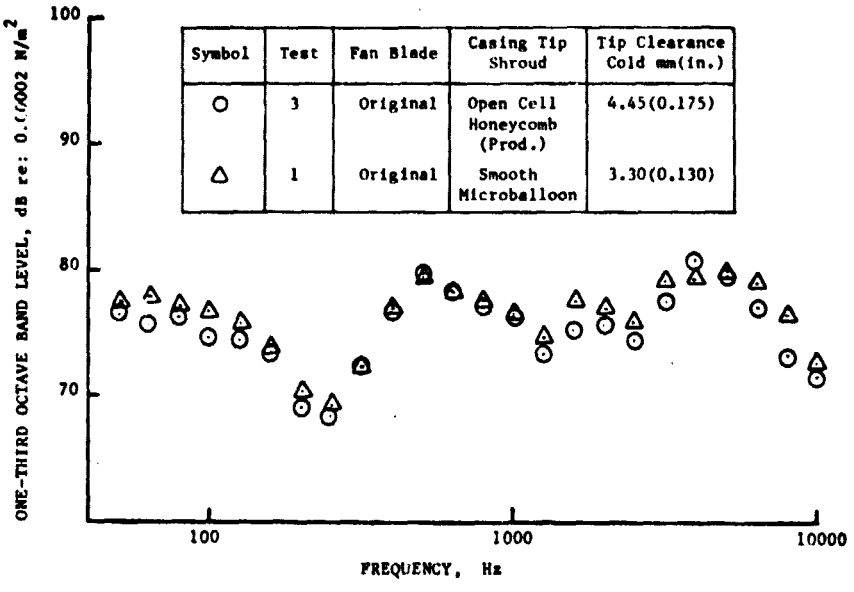

Figure 81. One-third Octave Spectrum Comparison of Original Fan With Original and Reduced Tip Clearance at 120° Peak Aft Angle (122 m Sideline and 59 KN Corrected Thrust - Low Approach).

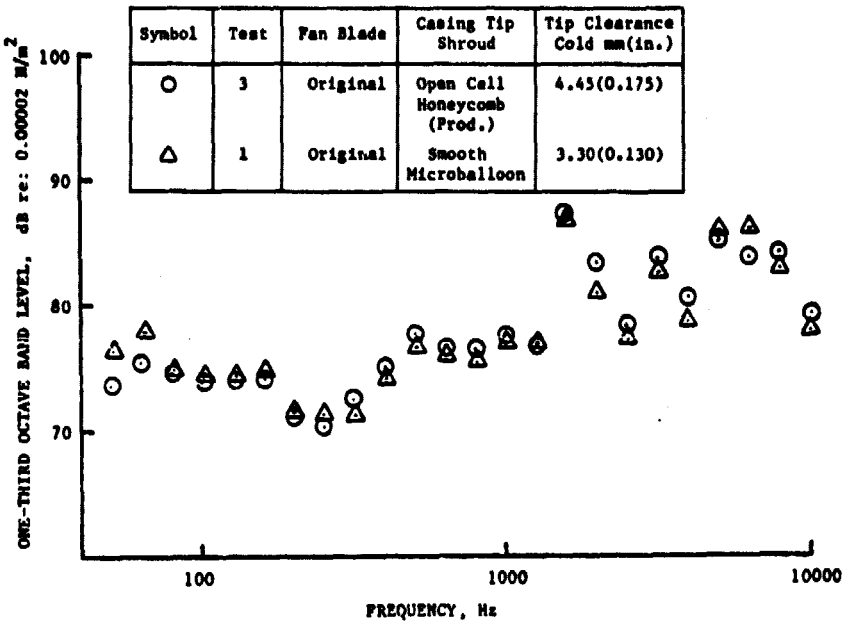

Figure 82. One-third Octave Spectrum Comparison of Original Fan With Original and Reduced Tip Clearance at 60° Peak Forward Angle (122 m Sideline and 88 KN Corrected Thrust - High Approach).

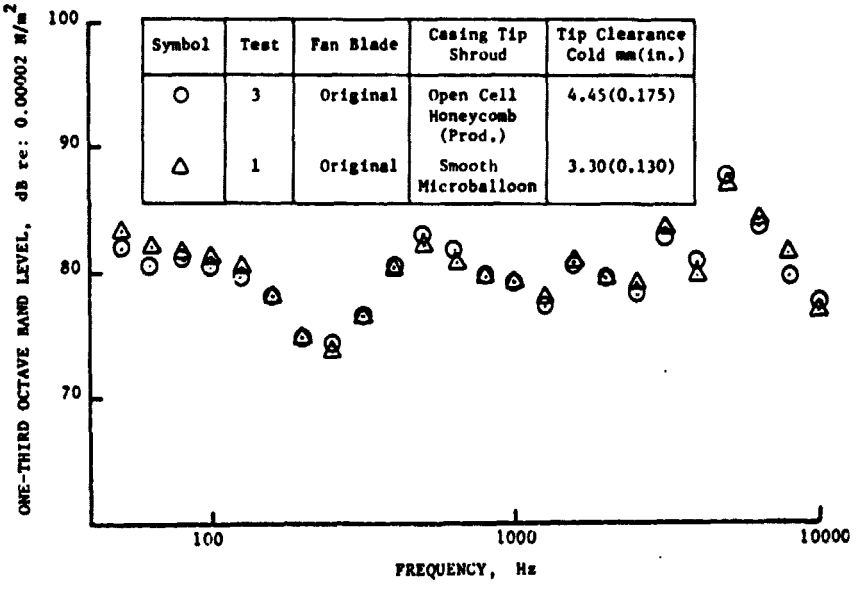

Figure 83. One-third Octave Spectrum Comparison of Original Fan With Original and Reduced Tip Clearance at 120° Peak Aft Angle (122 m Sideline and 88 KN Corrected Thrust - High Approach).

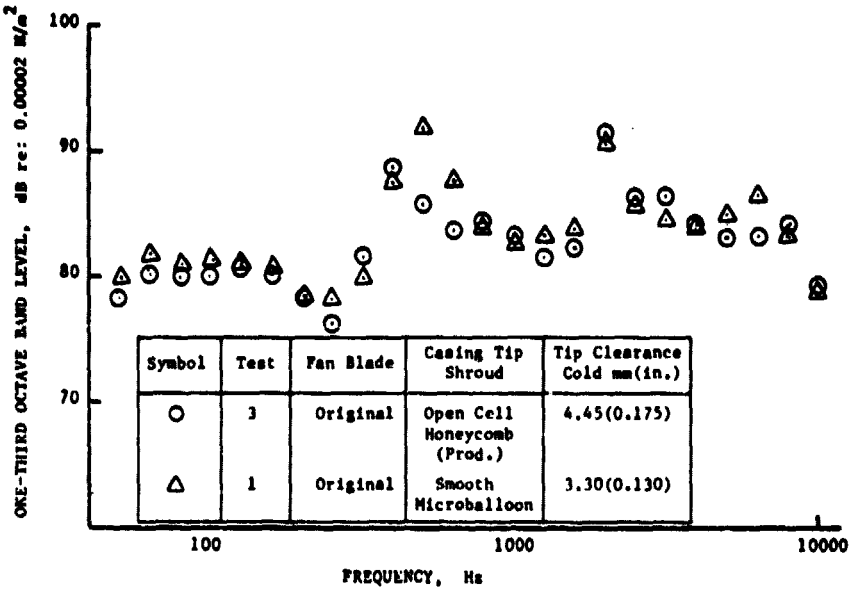

Figure 84. One-third Octave Spectrum Comparison of Original Fan with Original and Reduced Tip Clearance at 60° Peak Forward Angle (122 m Sideline and 148.5 KN Corrected Thrust - Cutback).

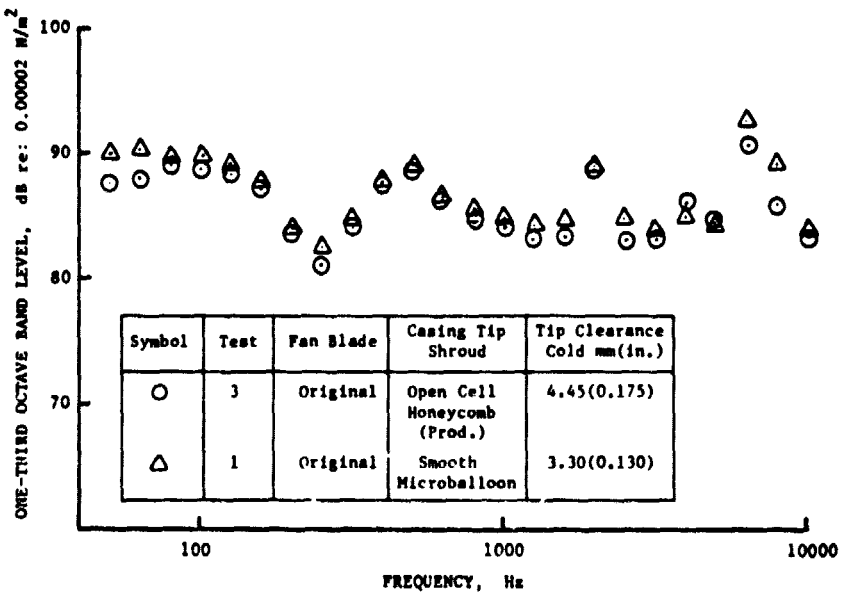

Figure 85. One-third Octave Spectrum Comparison of Original Fan With Original and Reduced Tip Clearance at 120° Peak Aft Angle (122 m Sideline and 148.5 KN Corrected Thrust - Cutback).

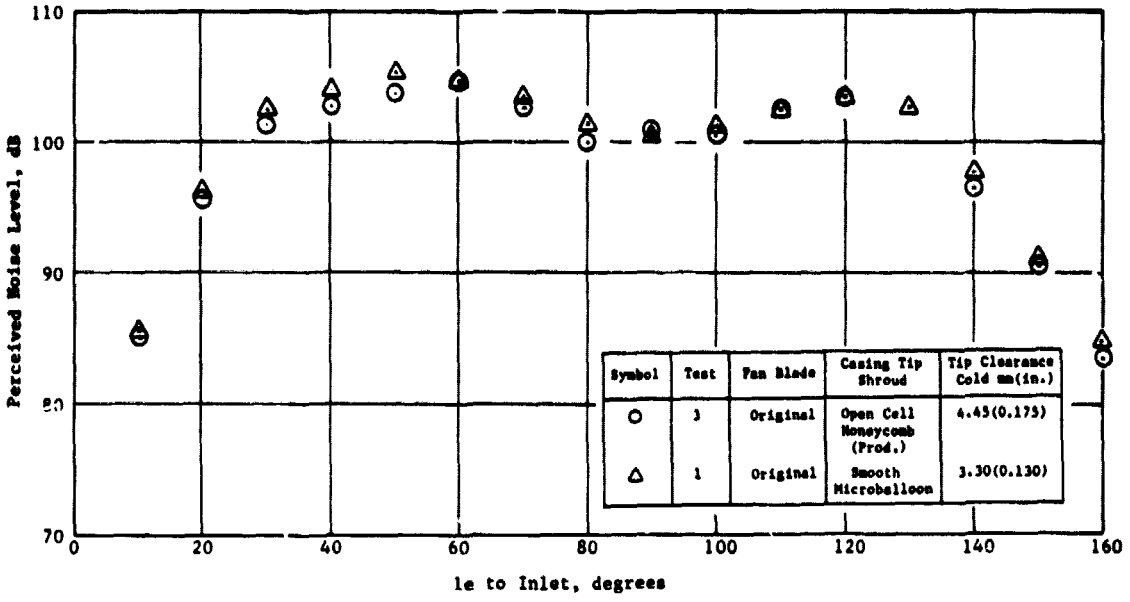

Figure 86. Influence of Reduced Fan Blade Tip Clearance on PNL Directivity (122 m Sideline and 59 kN Corrected Thrust - Low Approach).

Figure 87. Influence of Reduced Fan Blade Tip Clearance on PNL Directivity (122 m Sideline and 88 kN Corrected Thrust - High Approach).

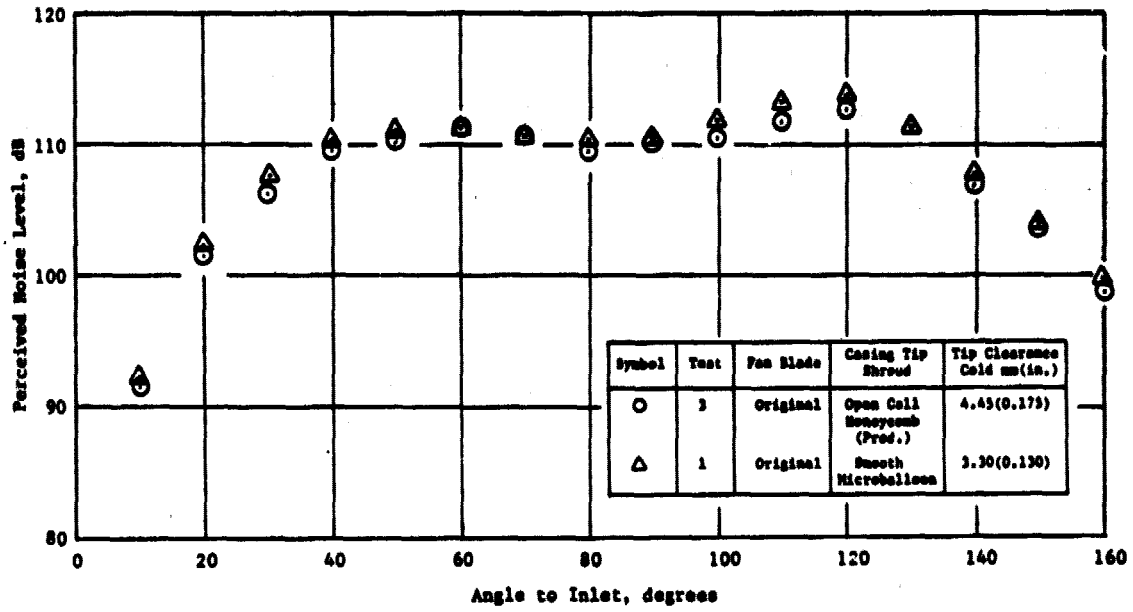

Figure 88. Influence of Reduced Fan Blade Tip Clearance on PNL Directivity (122 m Sideline and 148.5 kN Corrected Thrust - Cutback).

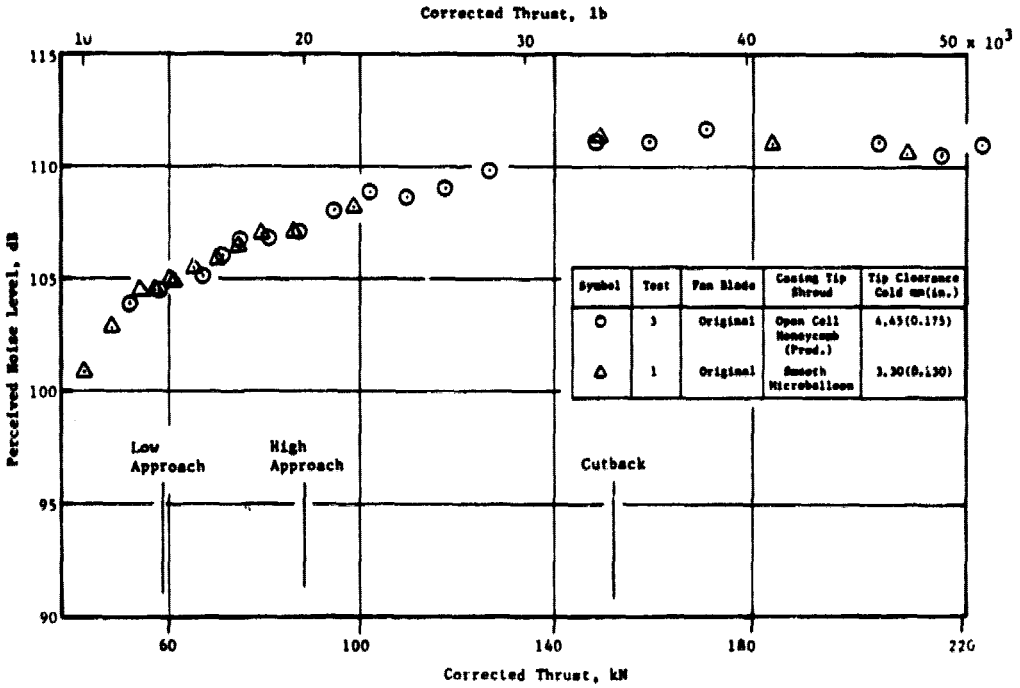

Figure 89. Influence of Reduced Fan Blade Tip Clearance on PNL as a Function of Corrected Thrust at 60° Peak Forward Angle at 122 m Sideline.

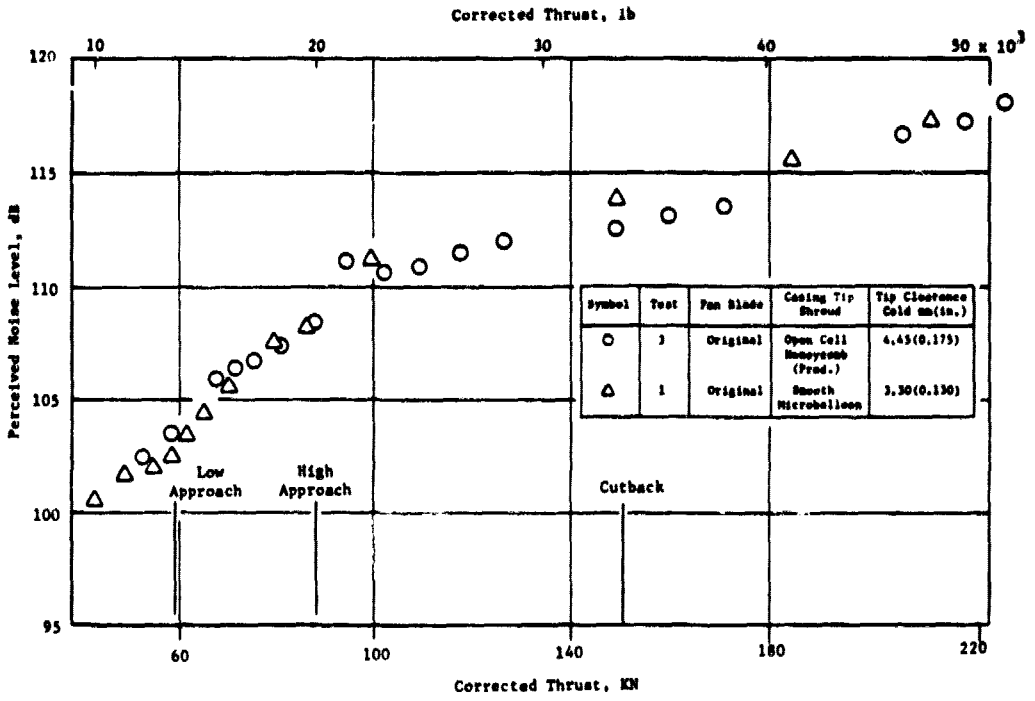

Figure 90. Influence of Reduced Fan Blade Tip Clearance on PNL as a Function of Corrected Thrust at 120° Peak Aft Angle at 122 m Sideline.

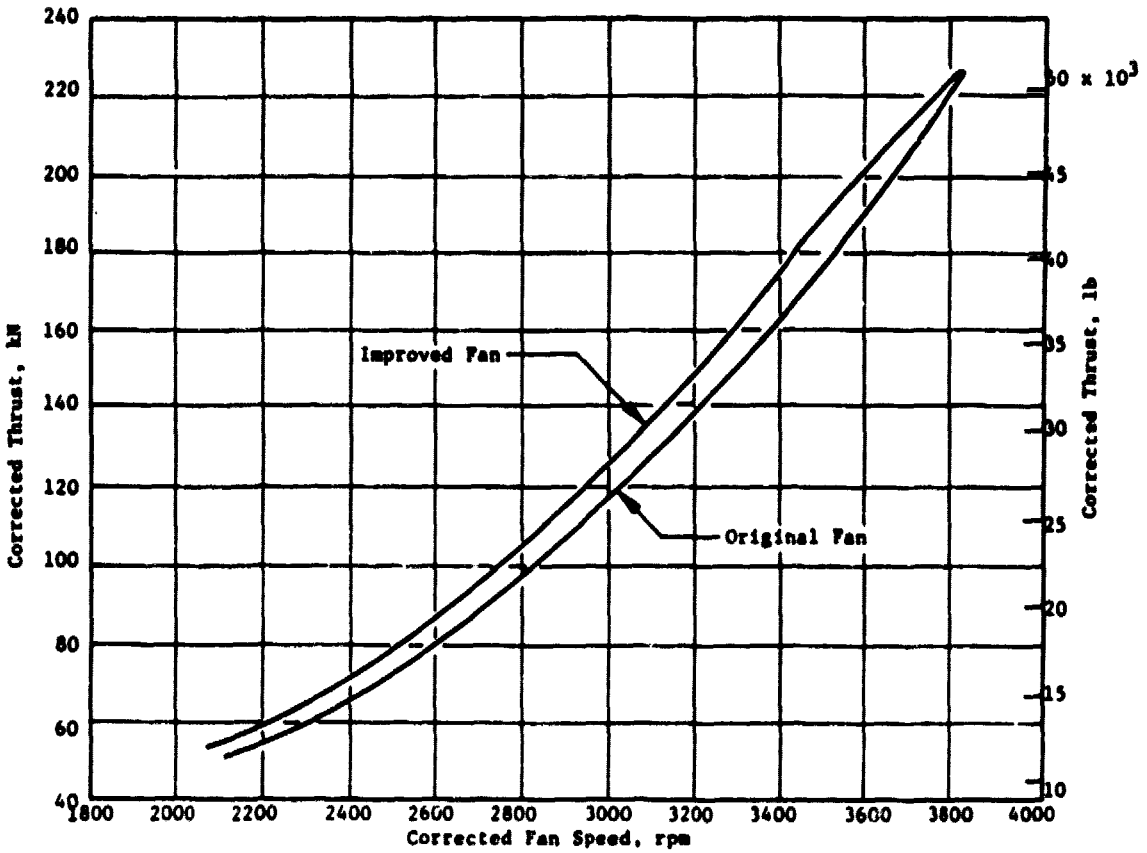

Figure 91. CF6-50 Engine Corrected Thrust/Corrected Speed Relationship with Original and Improved Fans.

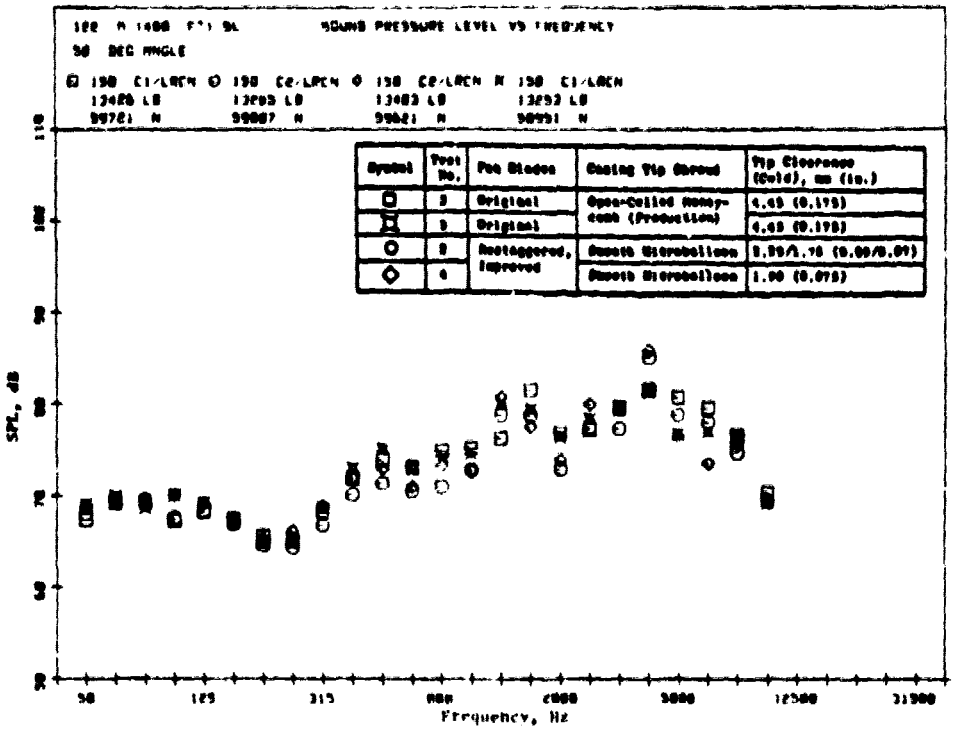

Figure 92. One-third Octave Spectrum Comparison of Improved and Original Fan at 50° Peak Forward Angle (122 m on Sideline and 59 KN Corrected Thrust - Low Approach).

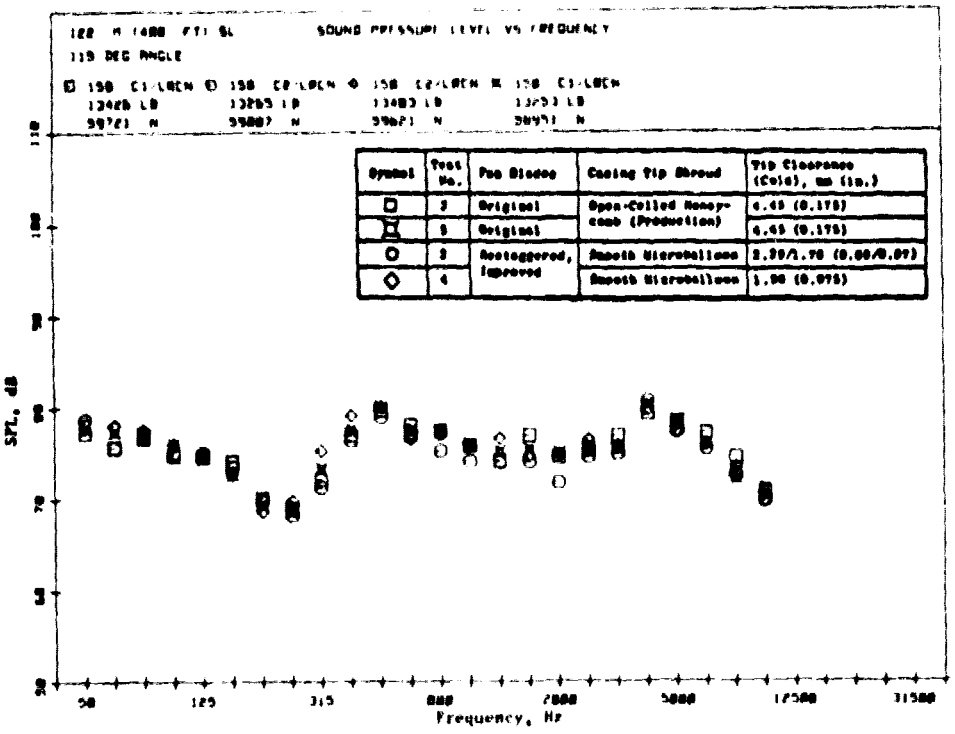

Figure 93. One-third Octave Spectrum Comparison of Improved and Original Fan at 115° Peak Aft Angle (122 m Sideline and 59 KN Corrected Thrust - Low Approach).

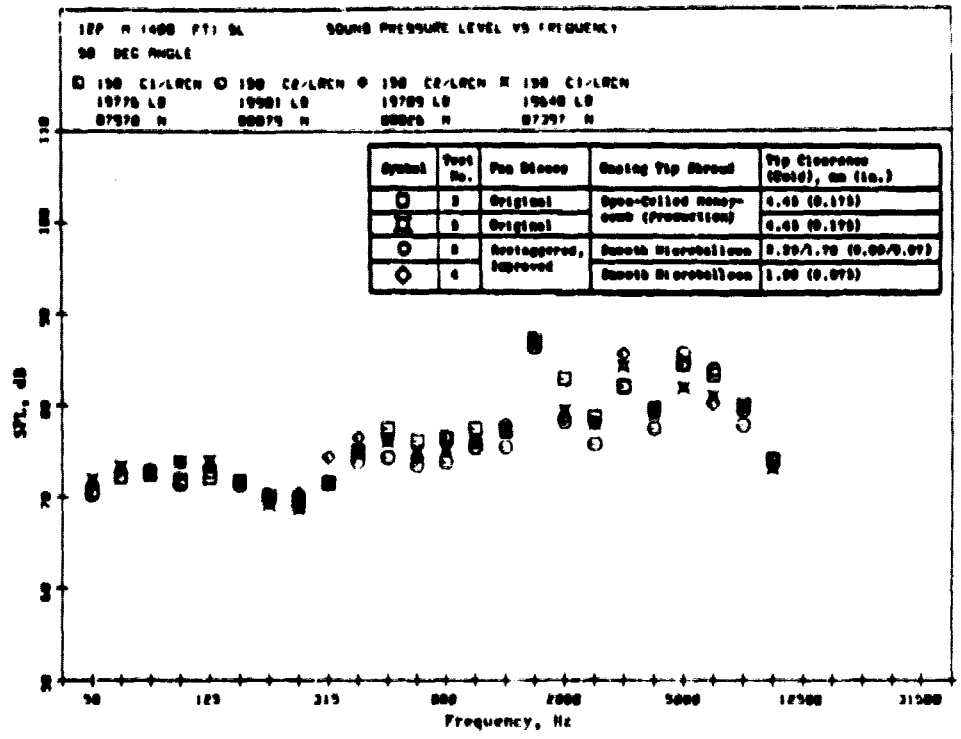

Figure 94. One-third Octave Spectrum Comparison of Improved and Original Fan at 50° Peak Forward Angle (122 m Sideline and 88 KN Corrected Thrust - High Approach).

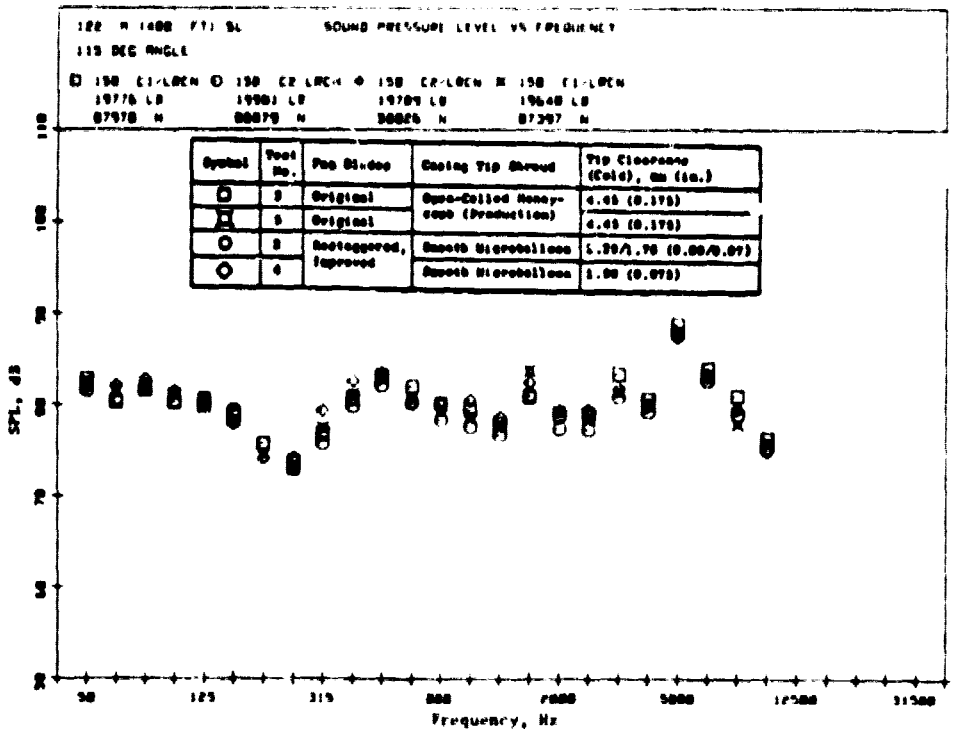

Figure 95. One-third Octave Spectrum Comparison of Improved and Original Fan at 115° Peak Aft Angle (122 m Sideline and 88 KN Corrected Thrust - High Approach).

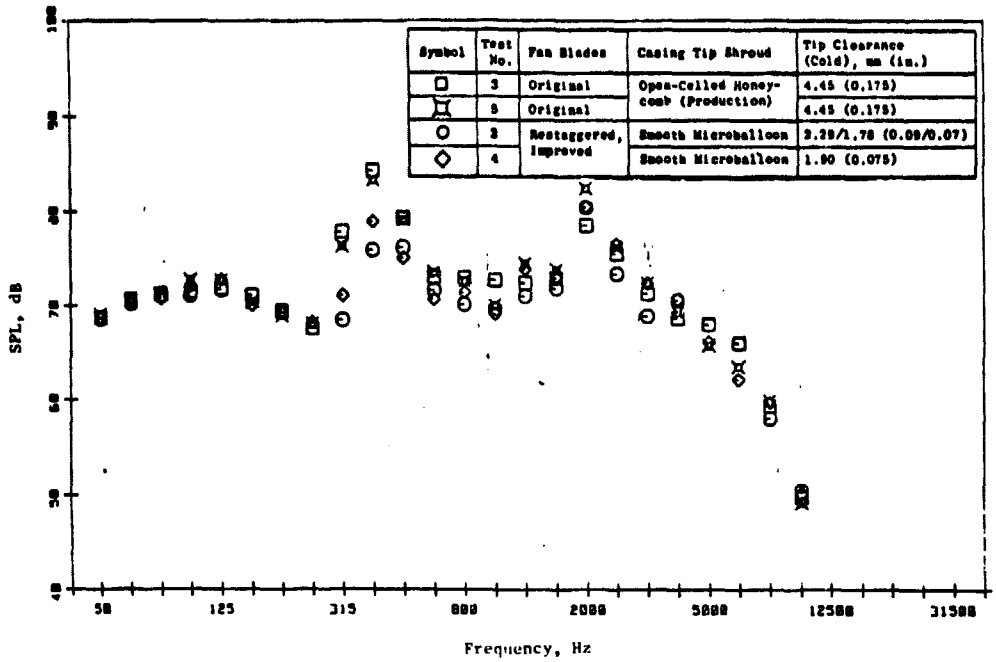

Figure 96. One-third Octave Spectrum Comparison of Improved and Original Fan at 50° Peak Forward Angle (305 m Sideline and 158 KN Corrected Thrust - Cutback).

ORIGINAL PAGE IS
OF POOR QUALITY

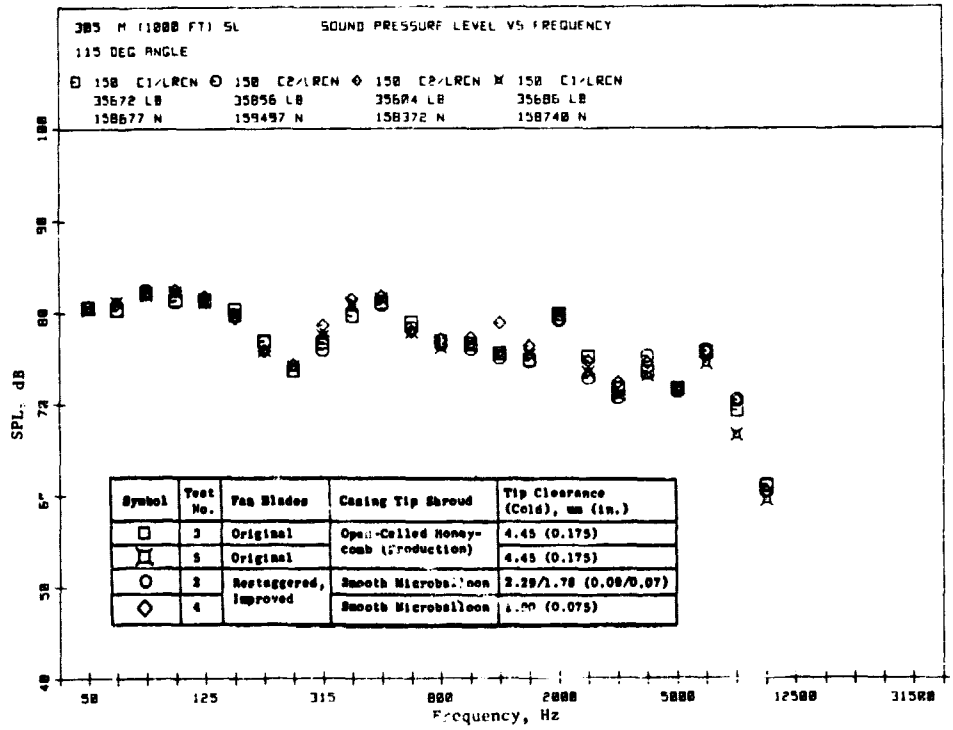

Figure 97. One-third Octave Spectrum Comparison of Advanced and Original Fan at 115° Peak Aft Angle (305 m Sideline and 158 KN Corrected Thrust - Cutback).

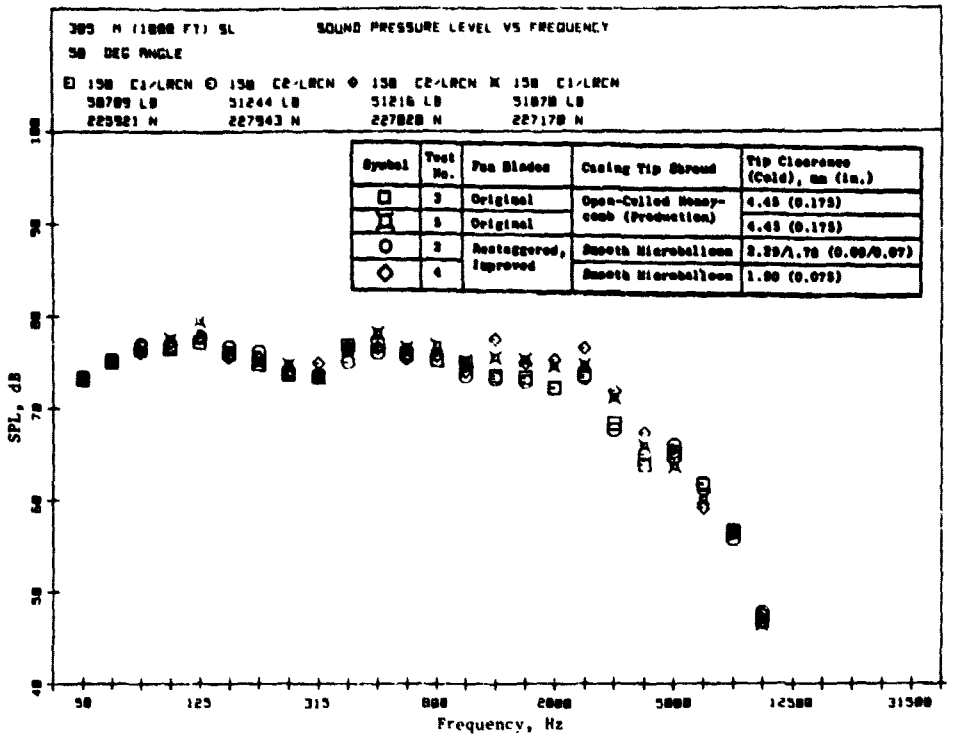

Figure 98. One-third Actave Spectrum Comparison of Improved and Original Fan at 50° Peak Forward Angle (305 m Sideline and 228 KN Corrected Thrust - Takeoff).

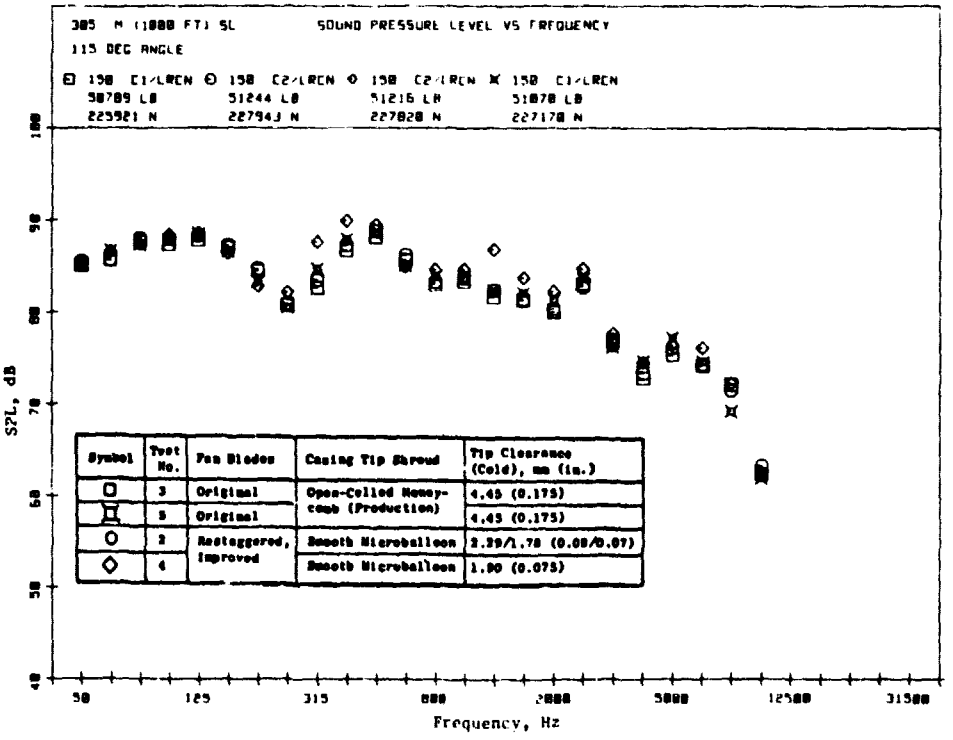

Figure 99. One-third Octave Spectrum Comparison of Improved and Original Fan at 115° Peak Aft Angle (305 m Sideline and 228 KN Corrected Thrust - Takeoff).

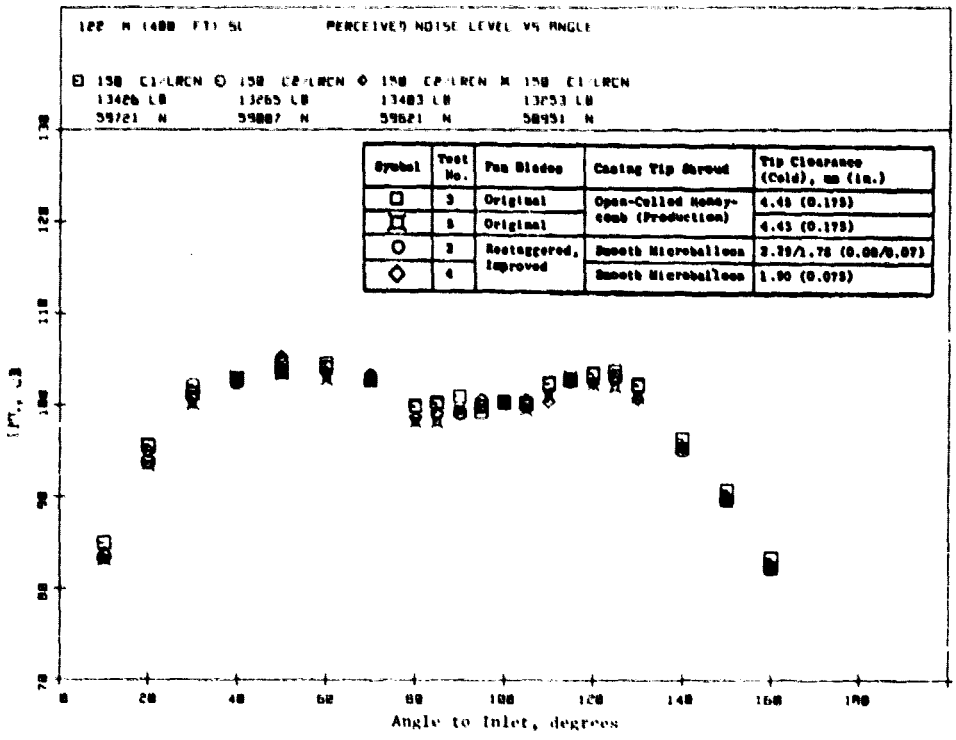

Figure 100. Perceived Noise Level Directivity Comparison of Improved and Original Fan (122 m Sideline and 59 KN Corrected Thrust - Low Approach).

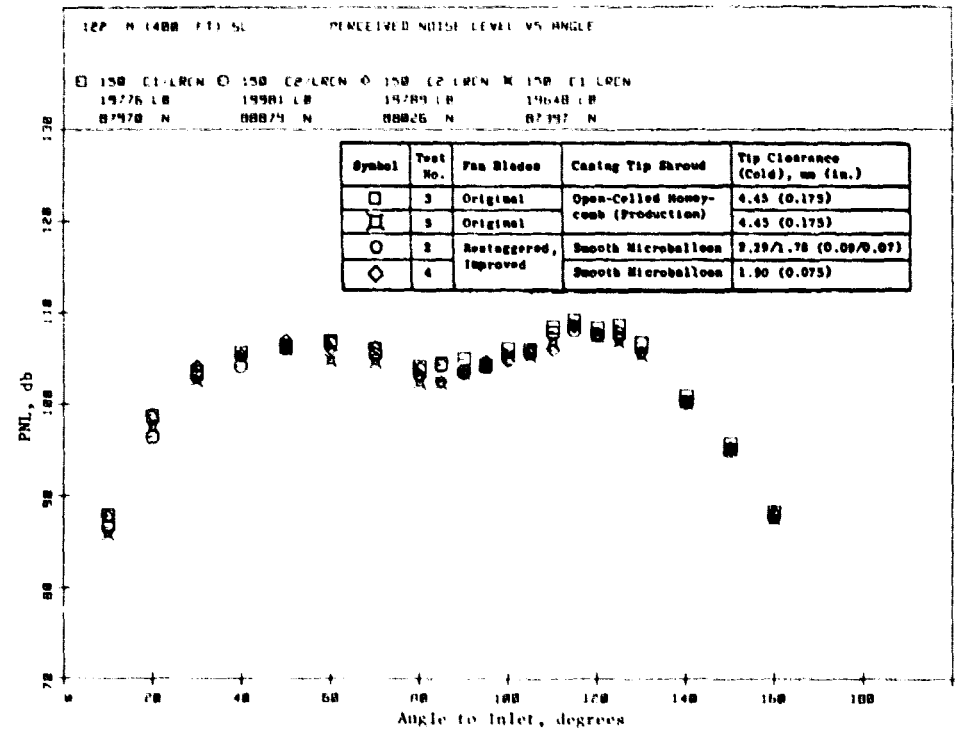

Figure 101. Perceived Noise Level Directivity Comparison of Improved and Original Fan (122 m Sideline and 88 KN Corrected Thrust - High Approach).

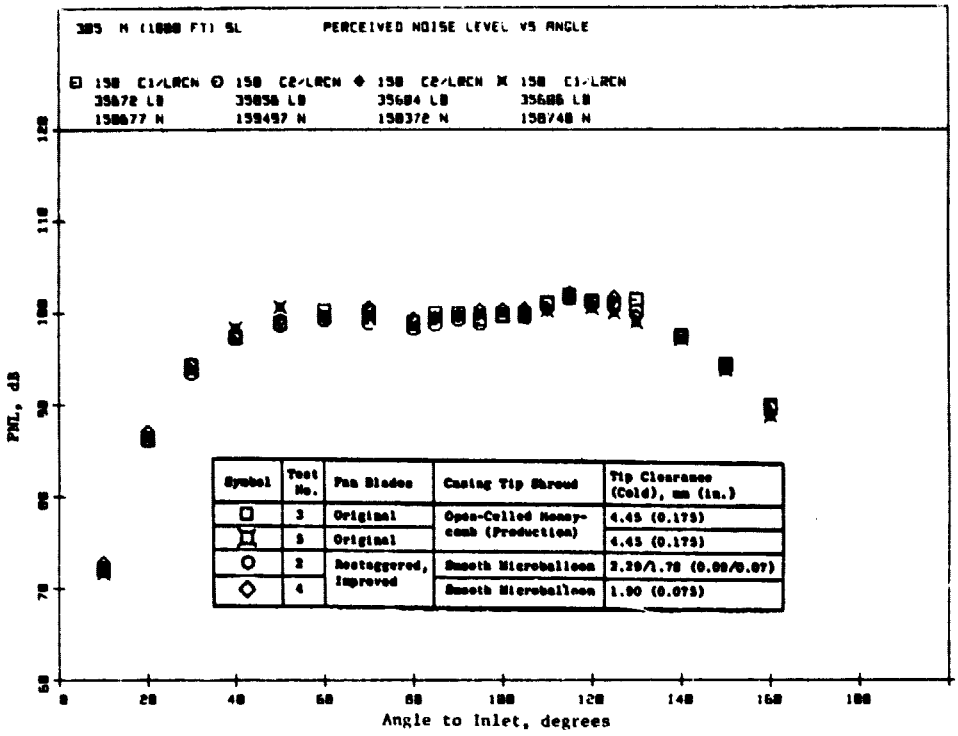

Figure 102. Perceived Noise Level Directivity Comparison of Improved and Original Fan (305 m Sideline and 158 KN Corrected Thrust - Cutback).

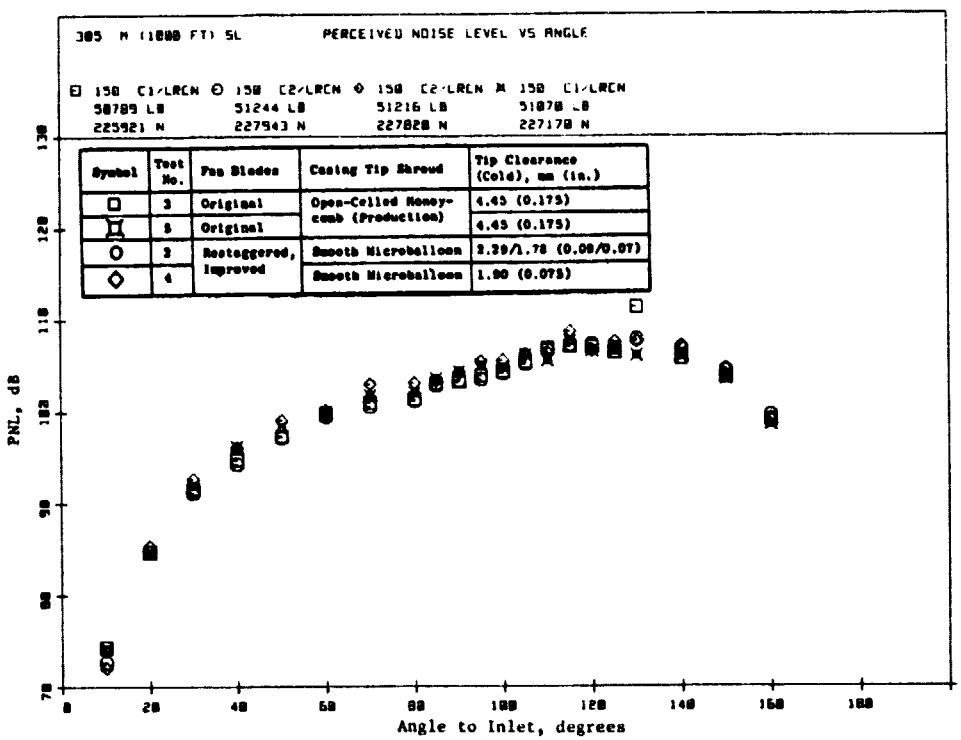

Figure 103. Perceived Noise Level Directivity Comparison of Improved and Original Fan (305 m Sideline and 228 KN Corrected Thrust - Takeoff).

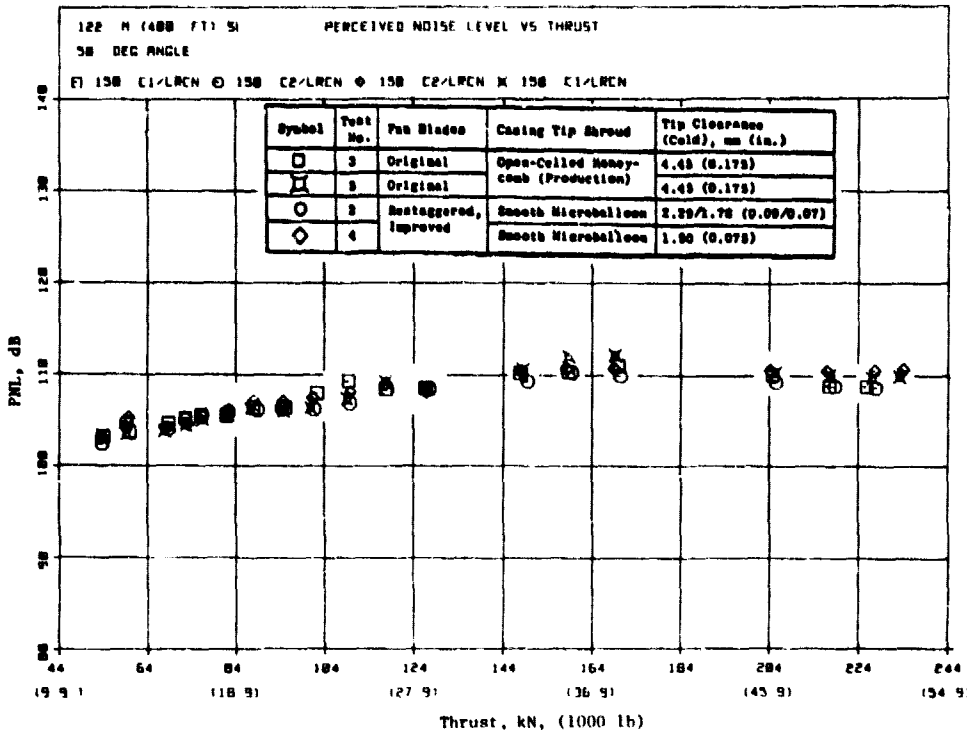

Figure 104. Perceived Noise Level Directivity Comparison of Improved and Original Fan as a Function of Thrust for 50° at 122 m Sideline.

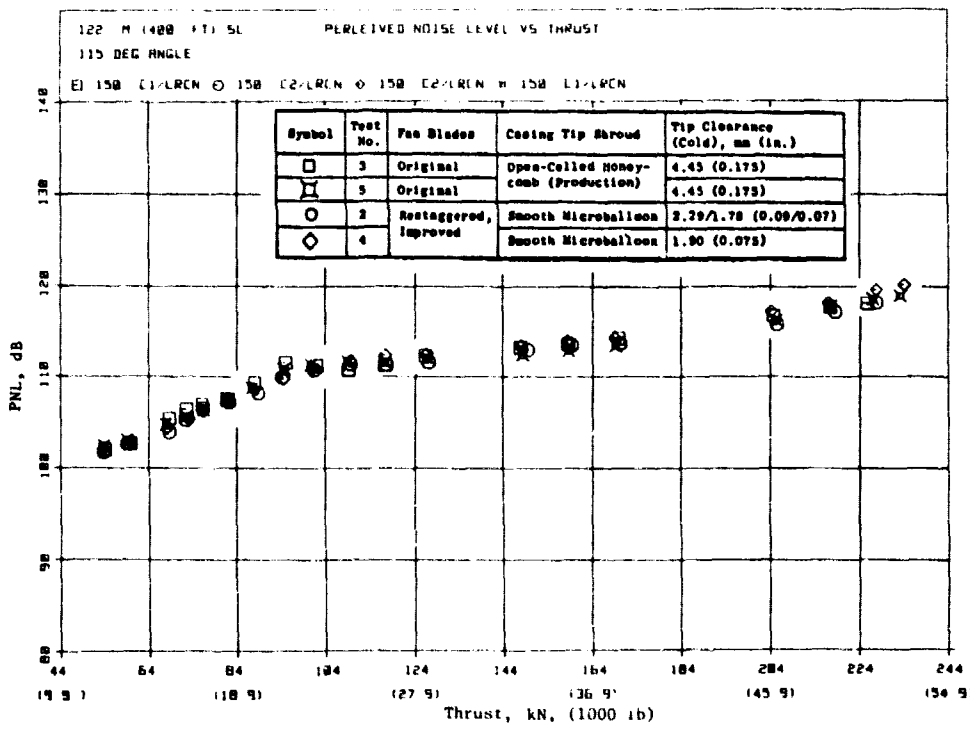

Figure 105. Perceived Noise Level Comparison of Improved and Original Fan as a Function of Thrust for 115° at 122 m Sideline.

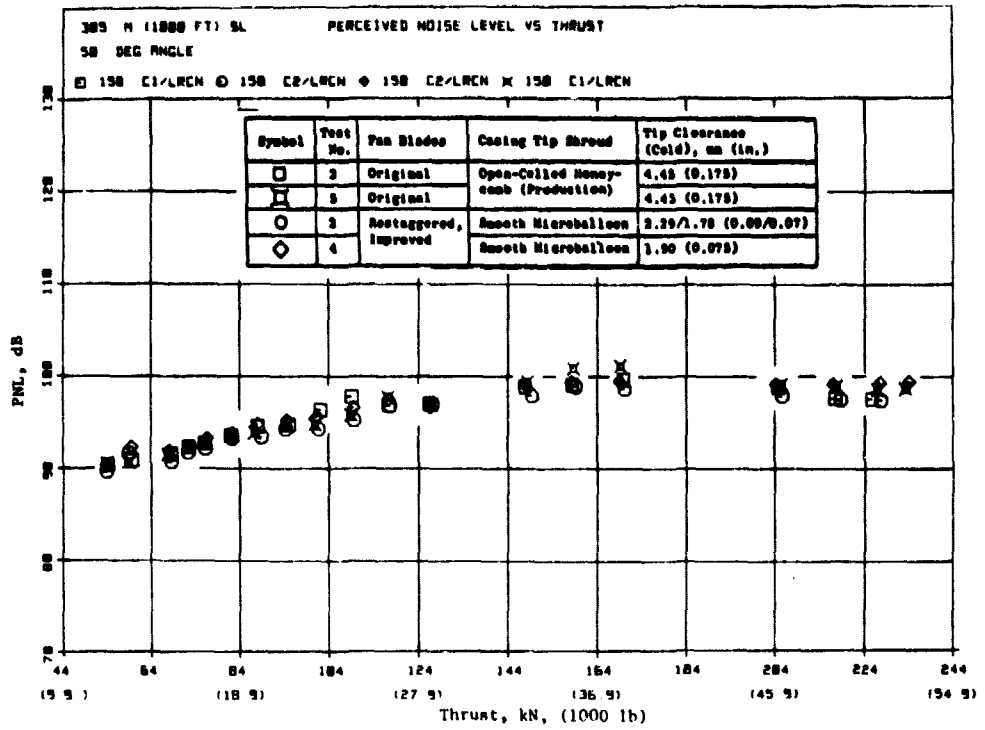

Figure 106. Perceived Noise Level Comparison of Improved and Original Fan as a Function of Thrust for 50° at 305 m Sideline.

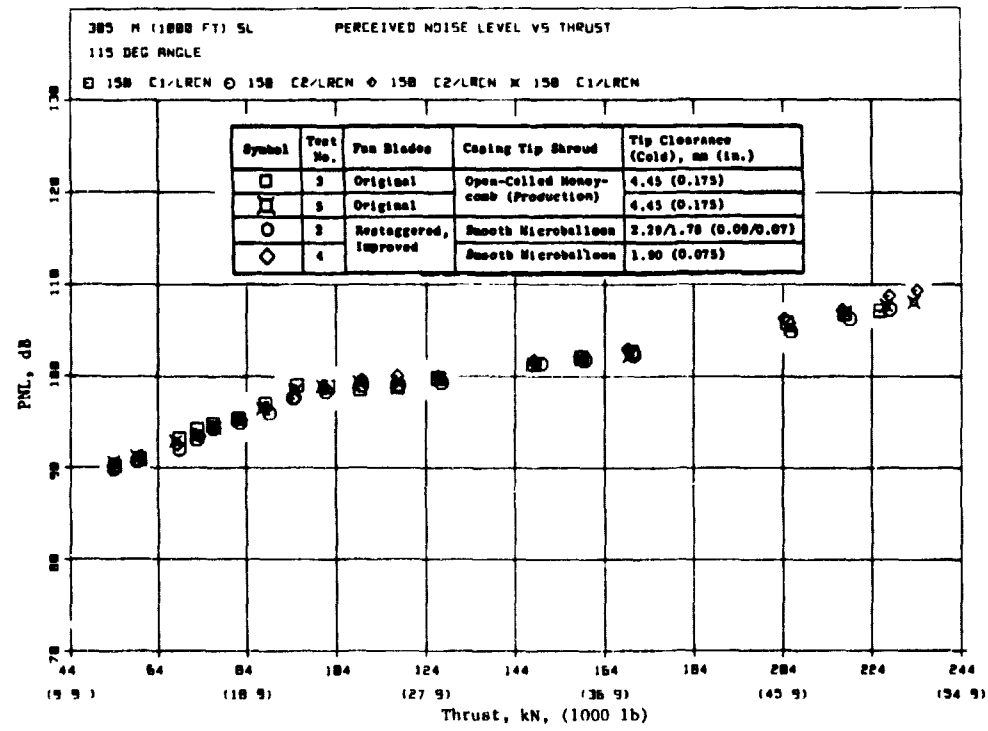

Figure 107. Perceived Noise Level Comparison of Improved and Original Fan as a Function of Thrust for 115° at 305 m Sideline.

MPT levels for the improved fan configuration are significantly reduced compared to the original fan engine configuration. These results do not affect PNL, hence EPNL, over the corrected speed range (3200-3700 rpm) where the MPT levels are a dominant feature of the forward quadrant one-third octave band spectra for the original fan configuration. However, the significant MPT level reduction should significantly reduce aircraft passenger compartment noise levels during aircraft takeoff and initial climbout.

To evaluate the impact of the improved fan configuration on CF6-50 engine community noise levels, simulated EPNL values were analytically obtained from the static engine noise. It was assumed that the static PNL data were measured flight levels recorded at typical aircraft velocities. No corrections were applied to estimate flight effects on engine noise. Simulated EPNL values were calculated at power settings typical of the DC-10-30, B747-200 and A300B aircraft for approach and takeoff operating conditions. These power conditions and associated altitudes and aircraft velocities are summarized in Table XI. Results from this analysis are exhibited in Figures 108 and 109 for approach and takeoff power conditions, respectively. Differences between the fan configuration data are not regarded as significant effects.

Based on the above analysis, no significant systematic differences in CF6-50 engine noise data that impact EPNL are apparent as a result of the fan modification. By analogy, noise levels of the CF6-50D engine with the advanced fan package are not projected to show any change. The CF6-6D engine uses the same fan as the CF6-50 engine and is very similar acoustically to that engine but with lower takeoff fan speed and thrust. Thus, use of the improved fan in the CF6-6D engine would have no effect on community noise of the DC-10-10 aircraft.

Table XI. Typical Flight Operating Conditions for CF6-50 Engine.

Condition	Thrust Range (Max./Min.) kN / 1000 lb	Altitude (Max./Min.) meters	Altitude (Max./Min.) feet	Flight Velocity (Max./Min.) m/sec	Flight Velocity (Max./Min.) knots
Takeoff (T/O)	230/200	52/46	610/305	2000/1000	103/93	200/180
Cutback (C/B)	170/150	38/34	610/305	2000/1000	103/93	200/180
High Approach	100/65	23/15	120/113	394/370	85/77	165/150
Low Approach	70/50	16/12	120/113	394/370	85/77	165/150

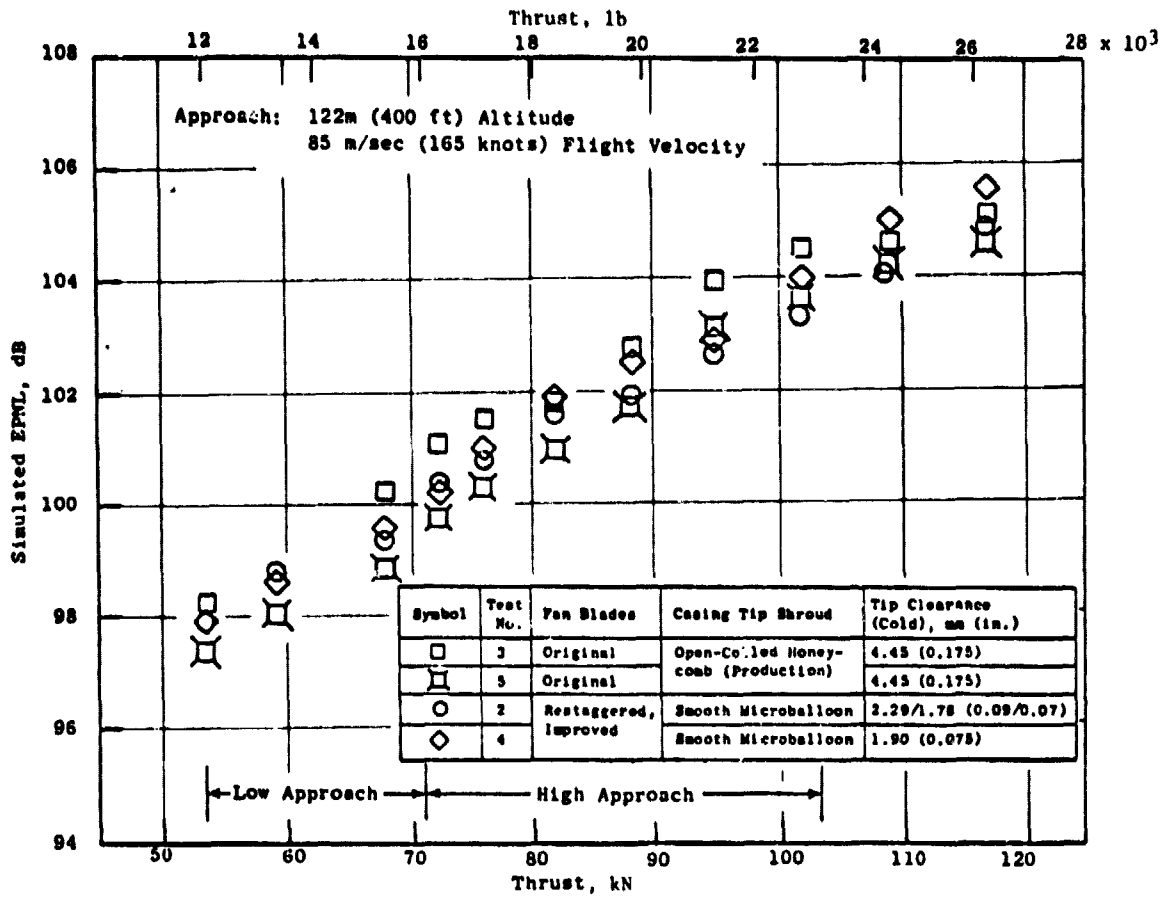

Figure 108. Noise Comparison of Original and Improved Fan Configurations at Approach Flight Conditions.

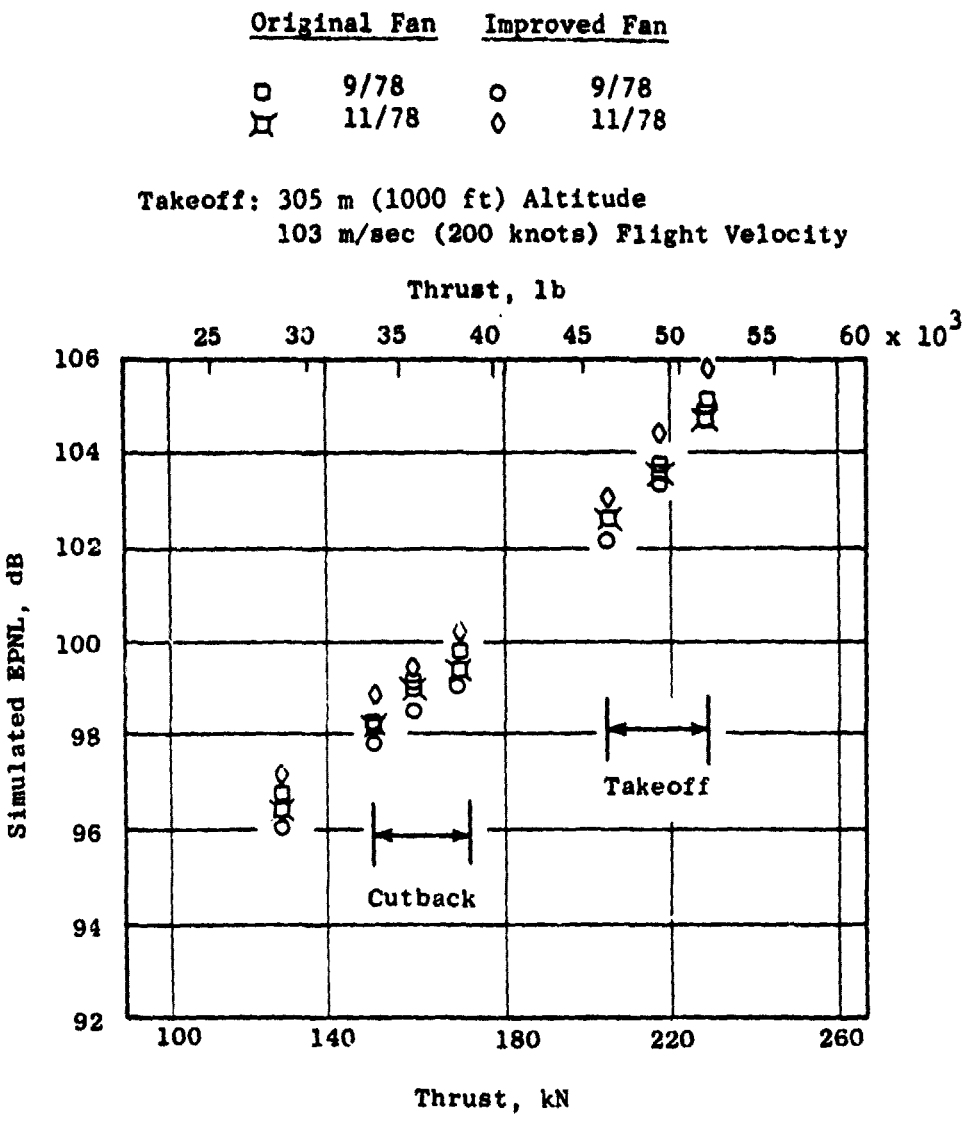

Figure 109. CF6-50 Engine Noise Comparison of Original and Improved Fan Configurations at Takeoff Flight Conditions.

9.0 ENGINE POWER MANAGEMENT TEST

The CF6-50 engine with the improved fan has a substantially different thrust versus fan speed characteristics than with the original CF6 production fan. Since the CF6-50 uses fan speed as the power setting parameter, the engine with the improved fan requires a redefinition of the power management fan speeds. The objectives of the power management testing were (1) to establish the sea level static thrust versus corrected fan speed characteristics of the CF6-50C2 and -50E2 engines installed in flight cowlings, and (2) to define the full scale exhaust nozzle coefficient correlations required to calculate in-flight thrust on the B747-200 and DC-10-30 aircraft at various flight conditions. The sea level and in-flight thrust versus fan speed characteristics are the basis for the ultimate definition of engine power management schedules.

In-flight thrust calculations for the CF6-50 engine are based on using nozzle thrust and flow coefficients obtained from scale model tests and modified for full scale effects. The full scale effects are defined by conducting engine performance tests in an outdoor test stand with the engine configured in the flight nozzle configuration and equipped with a bellmouth inlet to allow accurate engine airflow determination. Measured airflow and measured thrust were used to define full scale nozzle thrust and flow coefficients. The fan and core nozzle instrumentation used in the calculation of these coefficients is the same as used in the flight test programs to calculate in-flight thrust. Calculated in-flight thrust determined at various flight conditions was used to define the level of the power management parameter required to achieve guaranteed thrust.

9.1 ENGINE TEST FACILITIES

The power management test was conducted in the General Electric outdoor performance/acoustic test facility shown in Figure 110. An overhead thrust frame is provided for engine mounting. Instrumentation gathering equipment is located in the underground bunker and the overhead facility. Data are processed by a computer located in the adjacent blockhouse and displayed real-time. Data are also transmitted to Evendale for more sophisticated off-line and on-line reduction.

Additional power management tests of the same engine were subsequently conducted at an outdoor Boeing engine test facility.

9.2 TEST CONFIGURATION

The engine used for this test was CF6-50E2 engine (Boeing configuration), which was designed with the restaggered improved fan blades, the fan case stiffener, and a smooth microballoon except fan casing tip shroud. Fan blade tip clearance was 1.9 mm (0.075 in.).

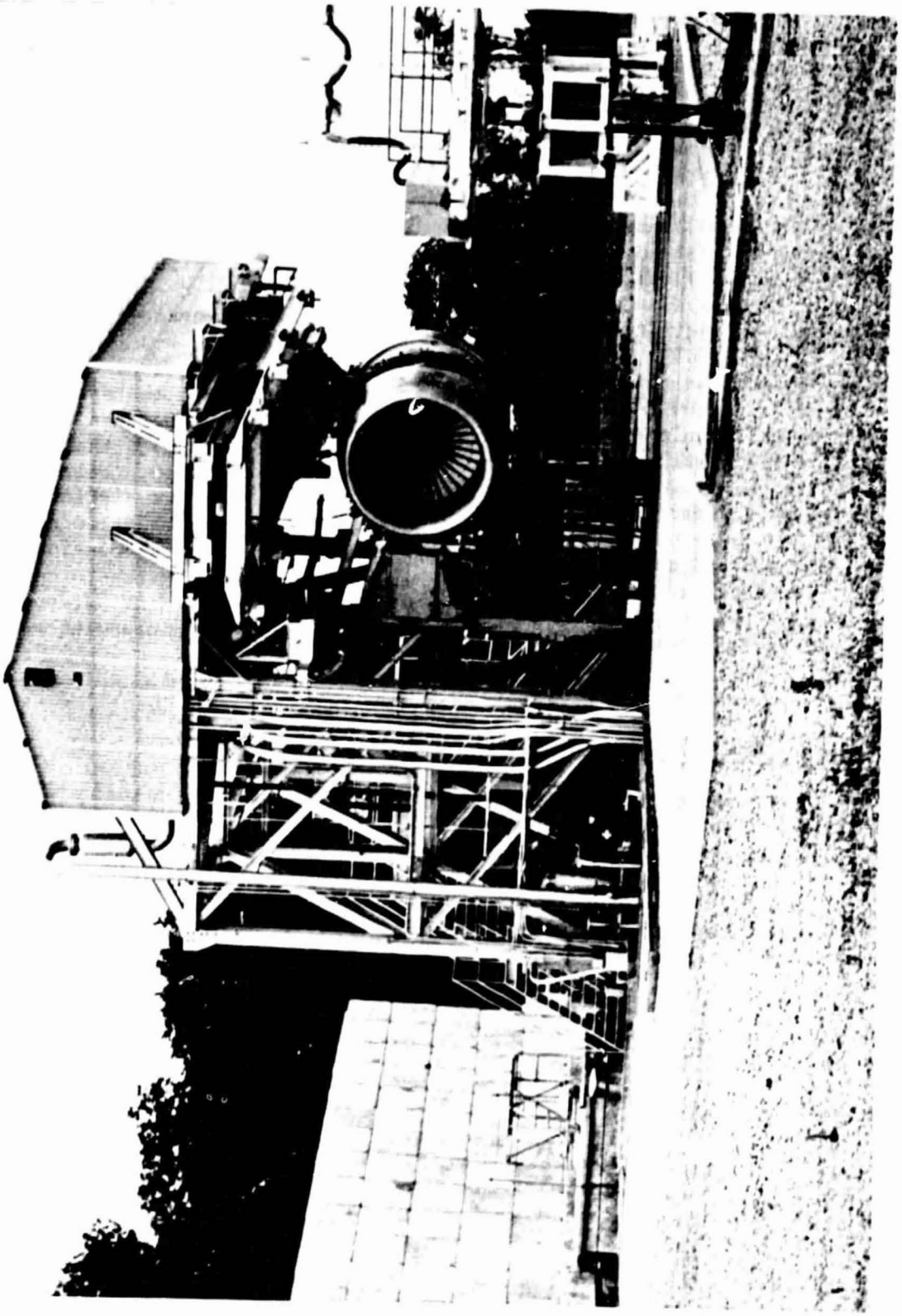

Figure 110. GE Engine Test Facility.

ORIGINAL PAGE IS
OF POOR QUALITY

9.3 INSTRUMENTATION

Instrumentation for the power management testing consisted of bellmouth inlet, fan discharge, and core engine discharge rakes to determine fan nozzle and core nozzle thrust and flow coefficients to be used to calculate in-flight thrust and flow. Standard engine safety instrumentation was also used.

A schematic diagram of the CF6-50 engine is shown in Figure 111 with the engine flow stations indicated, which conform to ARP755A station designations. Instrumentation for the power management test is shown on the CF6-50 engine cross section in Figure 112 and listed below:

- Barometric Pressure - Barometric pressure was taken using an electronic barometer.

- Humidity - Absolute humidity in grains of moisture per pound of dry air was recorded using a meter to determine dew point temperature.

- Inlet Total Pressure - Four six-element total pressure rakes located in the engine inlet at the fan face and measured with 0 to 10 psid transducers and pressure scanning valves were used. The angular locations of these rakes measured from the engine top vertical centerline 45°, 135°, 225°, and 315°.

- Inlet Static Pressure - Four six-element rakes identical to the total pressure rakes were used in the engine inlet at the fan face.

- Compressor Inlet Static Pressure - One static pressure tap located on the outer wall of the fan frame core flowpath was recorded. Measurements were made using a 0-15 psid transducer and pressure scanning valves.

- Compressor Inlet Temperature - One ungrounded copper-constantan thermocouple replacing one of the mounting bolts for the sensor was used.

- Compressor Discharge Temperature - One single element probe mounted in the condition monitoring port of the compressor rear frame was recorded. Sensor is a chromel-alumel (C/A) thermocouple.

- Compressor Discharge Pressure - One static pressure tap was located in a combustor borescope plug and measured on a 0-500 psid transducer.

- LP Turbine Inlet Total Pressure - One four-element probe was recorded on a 0-150 psid transdudcer.

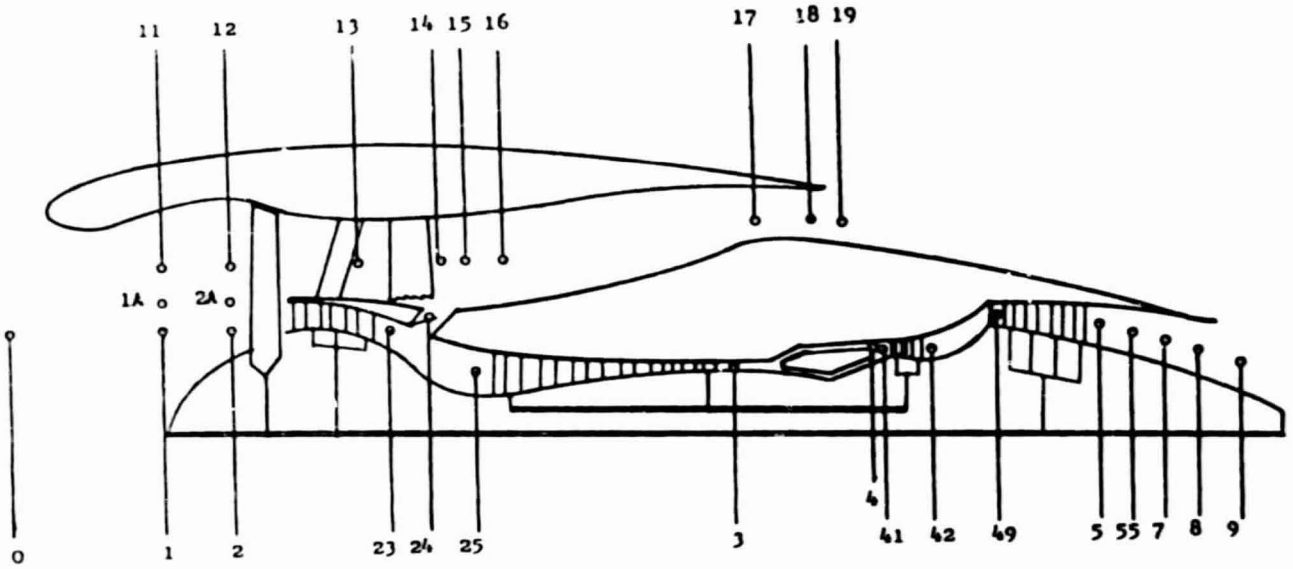

0 Ambient
1 Inlet discharge at fan hub
1A Average at inlet/engine interface
11 Inlet discharge at fan tip
12 Fan inlet at tip (includes acoustic treatment)
13 Fan discharge
14 Bypass duct inlet before booster bleed valve
15 Bypass duct inlet - includes booster bleed flow
16 Interface plane
17 Bypass stream at nozzle inlet
18 Bypass nozzle throat
19 Bypass stream at nozzle exit
2 Booster inlet
2A Flow weighted average at fan front face (includes acoustic treatment)

23 Booster discharge
24 Booster bleed valve
25 Compressor inlet
3 Compressor discharge
4 HP turbine first stage nozzle inlet
41 HP turbine rotor inlet
42 HP turbine discharge
49 LP turbine inlet
5 LP turbine exit
55 Interface plane (LP turbine rear frame exit)
7 Core stream at nozzle inlet
8 Core nozzle throat
9 Core stream at nozzle exit

Figure 111. CF6-50 Engine: Flow Station Designation.

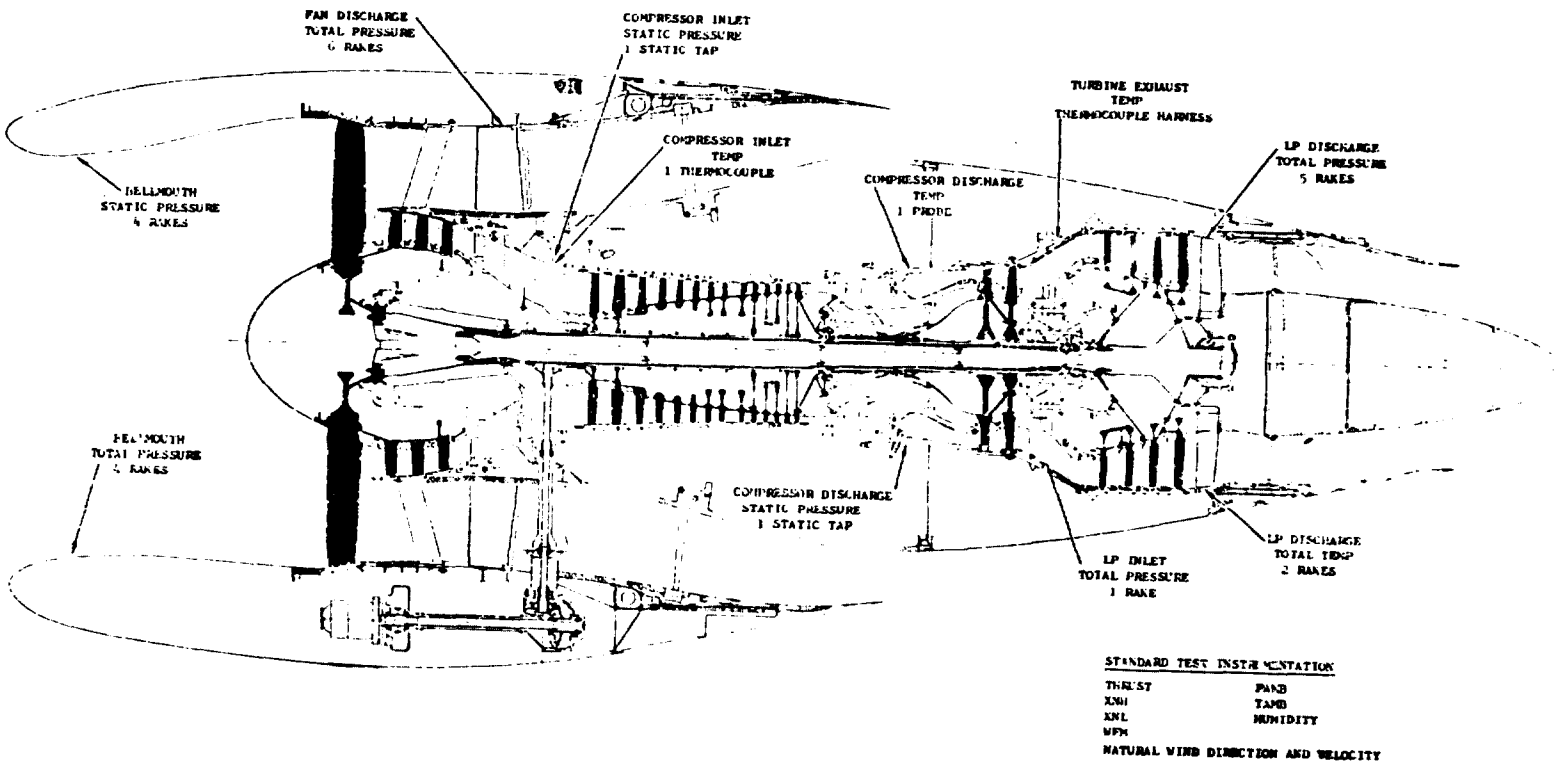

Figure 112. CF6-50 Engine: Instrumentation for Fan Power Management Test.

ORIGINAL PAGE IS
OF POOR QUALITY

- T49 Exhaust Gas Temperature - The LP turbine inlet temperature indicating system consisted of 11 dual immersion C/A thermcouple probes electrically averaged.

- LP Turbine Discharge Pressure - Four five-element rakes were manifolded together by immersion and located in the turbine rear frame. PT5 is measured with a 0-15 psid transducer and pressure scanning valves.

- LP Turbine Discharge Temperature - Two five-element rakes (C/A thermocouples) were located in the turbine rear frame. The signals were electrically averaged, providing one readout.

- Fan Discharge Pressure - Six seven-element rakes were manifolded by immersion and located in the fan frame. The measurement was made with a 0-15 psid transducer and pressure scanning valve.

- Fan Speed - LP rotor speed was recorded using two fan speed sensors.

- Core Speed - HP rotor speed was measured using a tachometer.

- Main Fuel Flow - Facility engine fuel flow was measured on a 1-1/2-inch diameter flowmeter.

- Verification Fuel Flow - Facility engine fuel flow was measured in series with the main fuel flowmeter.

- Fuel Temperature - Facility engine fuel temperature was measured at the flowmeters using a copper-constantan (C/C) thermocouple.

- Fuel Sample Specific Gravity - Specific gravity of the fuel sample was measured using a hydrometer.

- Fuel Sample Temperature - Fuel sample temperature was read during the specific gravity measurement.

- Fuel Lower Heating Valve - Lower heating valve of the fuel sample was determined by a bomb calorimeter.

- Load Cell Thrust - Thrust frame axial force was measured using a 50,000-pound (22,500 kg) load cell output.

- Variable Stator Position - LVDT readout was measured on a 0 to 5 volt scale.

- Variable Bleed Valve Position - LVDT readout was measured on a 0 to 5 volt scale.

- Wind Speed - Wind speed was measured by using a cup anemometer.

- Wind Direction - Wind direction was measured utilizing a light-weight airfoil vane with damping.

- Ambient Temperature - A resistance device was utilized.

9.4 TEST RESULTS AND DISCUSSION

Full scale fan nozzle thrust and flow coefficients were determined from the CF6-50E2 instrumented engine testing at the General Electric outdoor test site. Nozzle coefficient data were also obtained from indoor test cell back-to-back engine tests of the improved fan and other associated design improvements. Due to anomalies in the measured nozzle coefficient data, the same engine was transferred to the Boeing Tulalip outdoor engine test facility to repeat the power management test and correlate results. The CF6-50E2 engine was then installed on a B747-200 aircraft to correlate and verify preflight predictions and actual flight test power management.

Fan nozzle thrust and flow coefficients resulting from the General Electric testing along with additional testing done at the Boeing test facilty on the same engine are presented in Figures 113 and 114. Testing at Boeing was used in conjunction with the earlier results, because the Boeing data could be compared to previous results from another CF6-50 engine with the improved fan. Fan nozzle thrust coefficient (CFG28) and fan nozzle flow coefficient (CW28) are defined as follows:

$$CFG28 = \frac{\text{Total Engine Thrust - Core Engine Thrust}}{\text{Ideal Fan Thrust}}$$

$$CW28 = \frac{\text{Total Engine Bellmouth Flow - Core Flow}}{\text{Ideal Fan Flow}}$$

Prior to flight testing, a computer model (status deck) representation of the improved fan engine was constructed based on the production engine modified by the improved fan blade representation. The improve fan blade representation was based primarily on SLS full scale engine test results. This status deck became the basis for preflight predictions and preliminary flight test power management. Comparison of the actual flight test data to the pretest status deck prediction is presented on Figures 115 through 119 using data for the B747-200 aircraft as an example. The flight test data are compared to the status deck prediction at the identical flight condition that the flight data were taken. The status deck prediction is higher in thrust relative to the flight data at low power settings, crosses over, and is somewhat lower in thrust at high power settings, suggesting a basic difference in airflow versus cruise fan speed representation. The status deck was refined based on the flight test data.

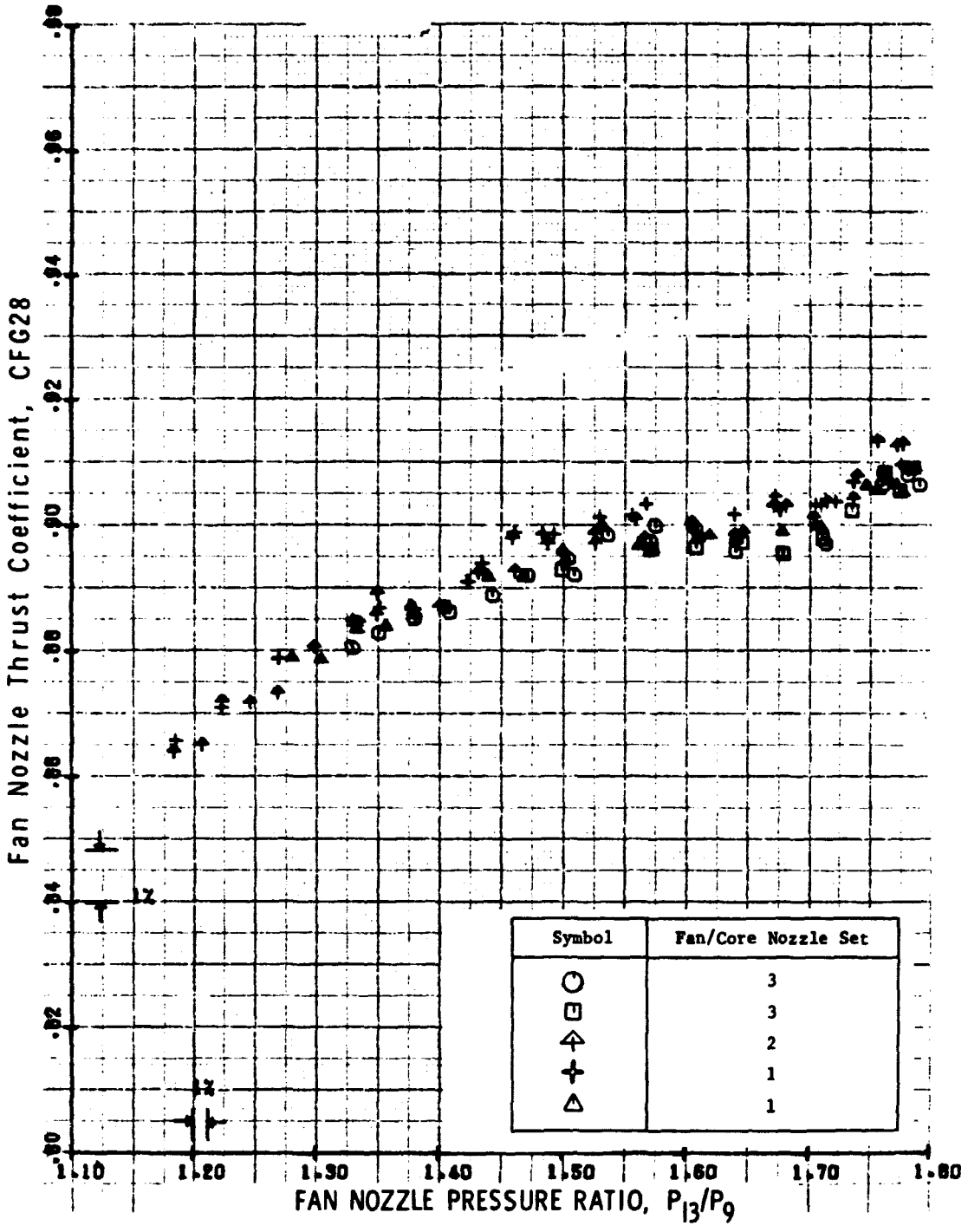

Figure 113. CF6-50 Engine with Improved Fan: Fan Nozzle Thrust Coefficient Versus Fan Nozzle Pressure Ratio.

ORIGINAL PAGE IS
OF POOR QUALITY

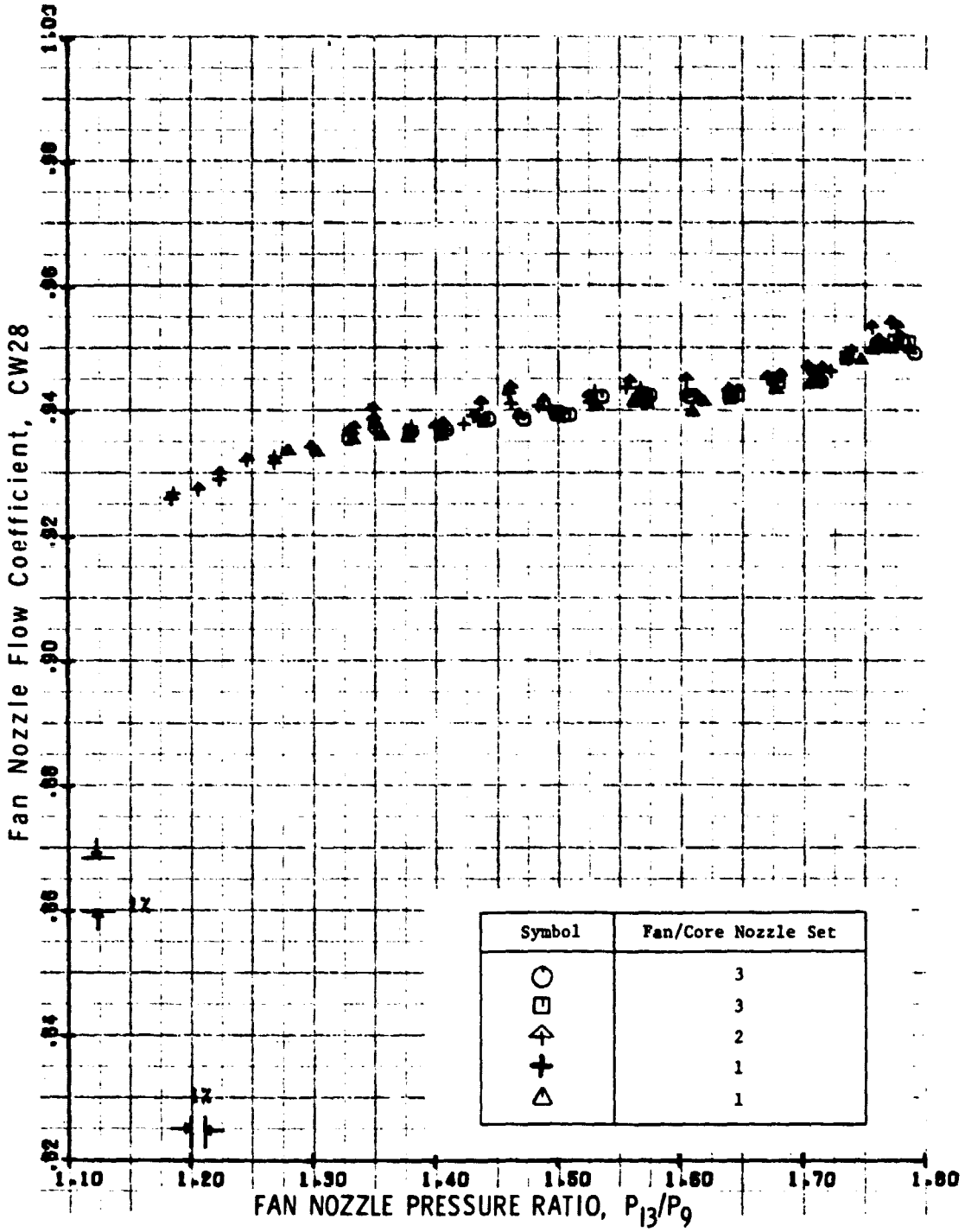

Figure 114. CF6-50 Engine with Improved Fan: Fan Nozzle Flow Coefficient Versus Fan Nozzle Pressure Ratio.

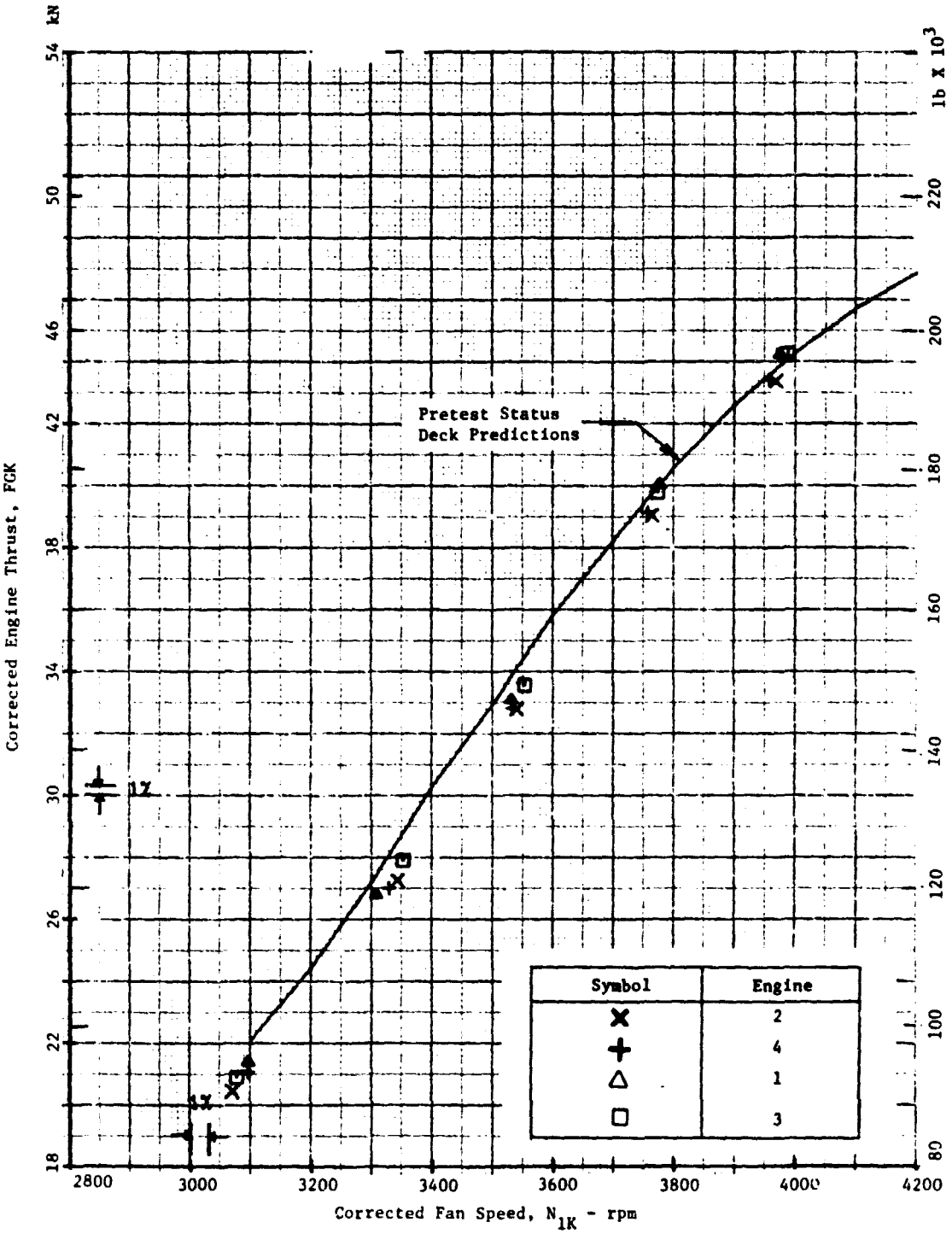

Figure 115. TBC Flight Test at 10,000/0.4 M_O; ATC Corrected Thrust Versus Corrected Fan Speed for CF6-50 Engine with Improved Fan.

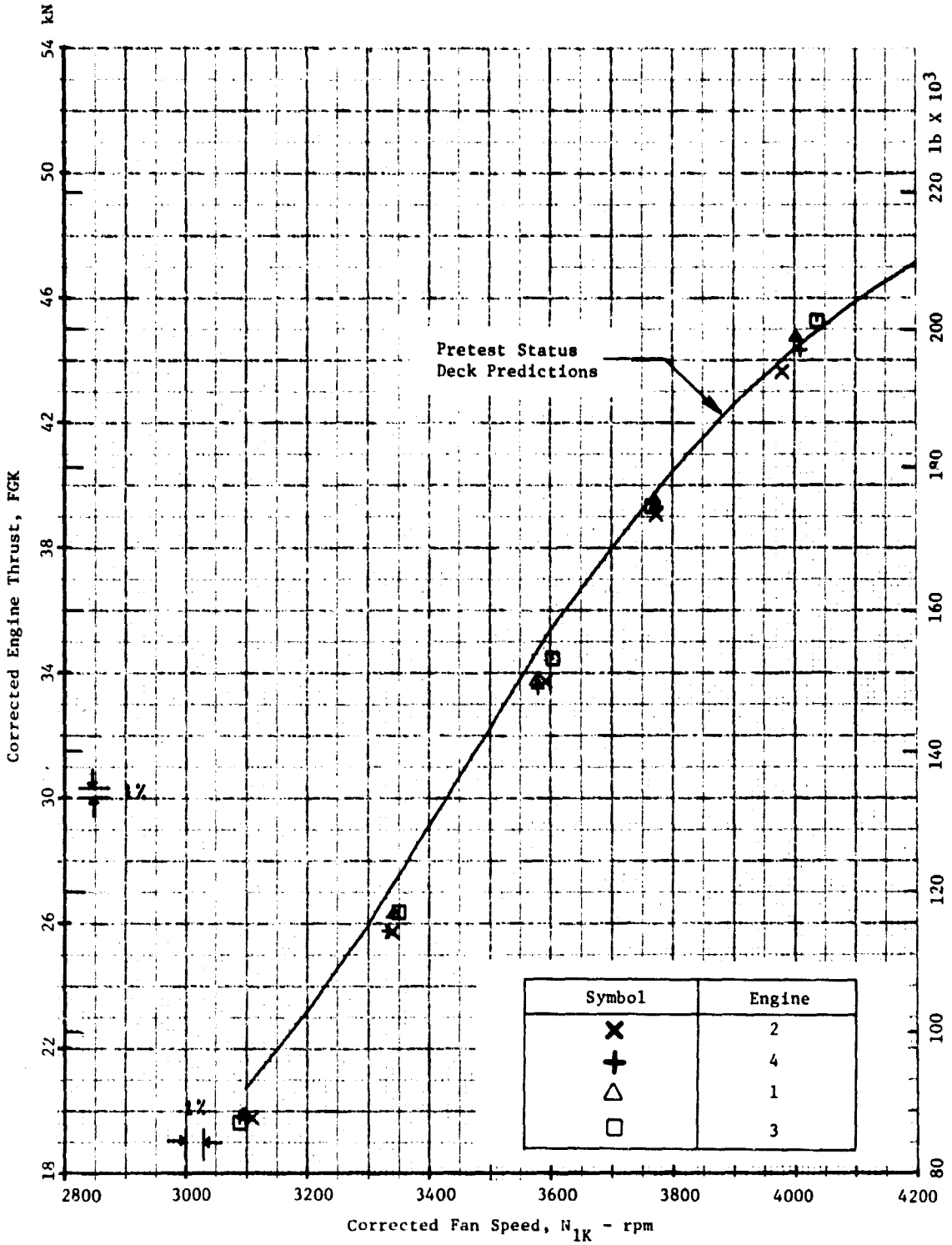

Figure 116. TBC B747 Flight Test at 20,000/0.6 M_O; ATC Corrected Thrust Versus Corrected Fan Speed for CF6-50 Engine with Improved Fan.

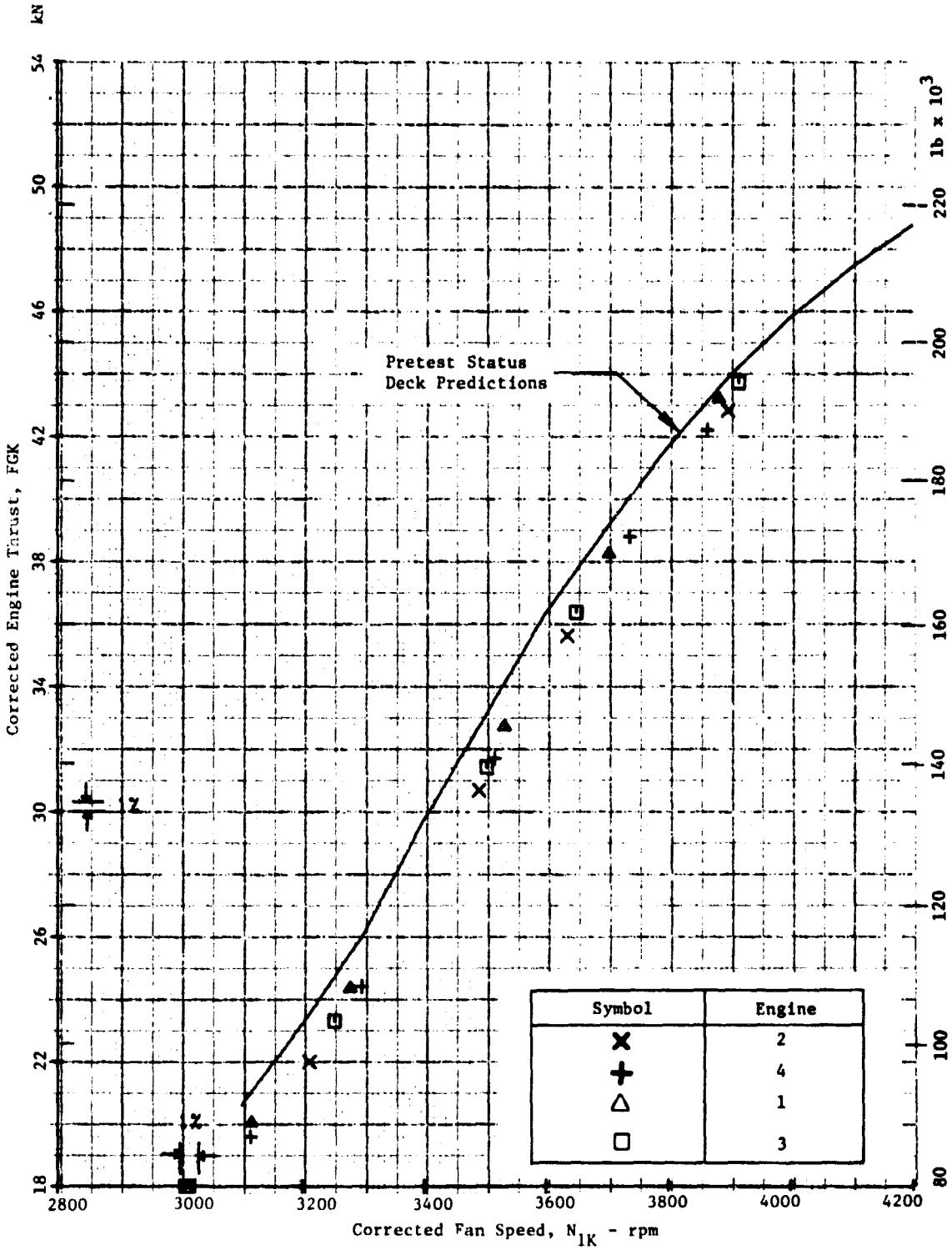

Figure 117. TBC B747 Flight Test at 25,000/0.7 M_o; ATC Corrected Thrust Versus Corrected Fan Speed for CF6-50 Engine with Improved Fan.

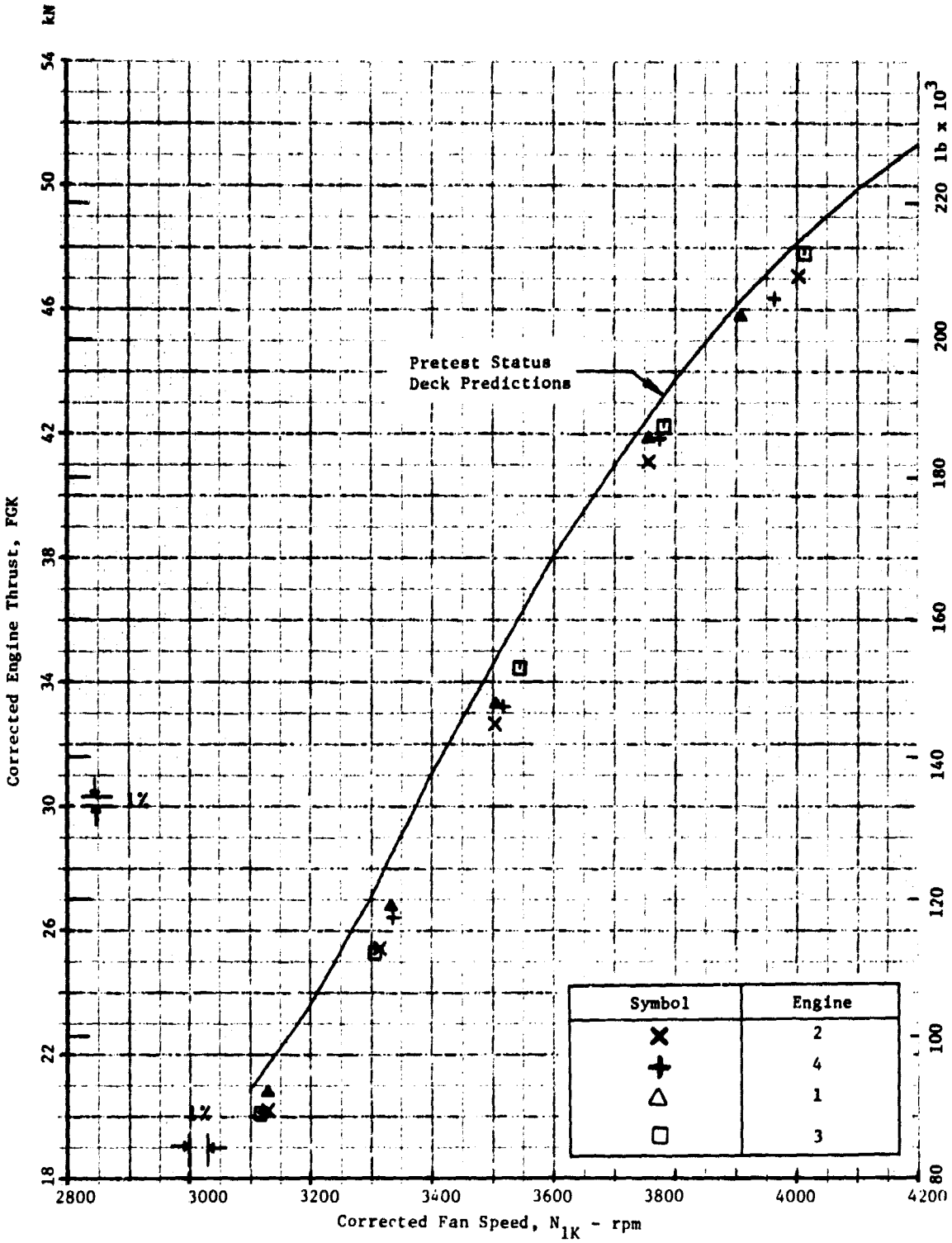

Figure 118. TBC B747 Flight Test at 30,000/0.8 M_0; ATC Corrected Thrust Versus Corrected Fan Speed for CF6-50 Engine with Improved Fan.

ORIGINAL PAGE IS
OF POOR QUALITY

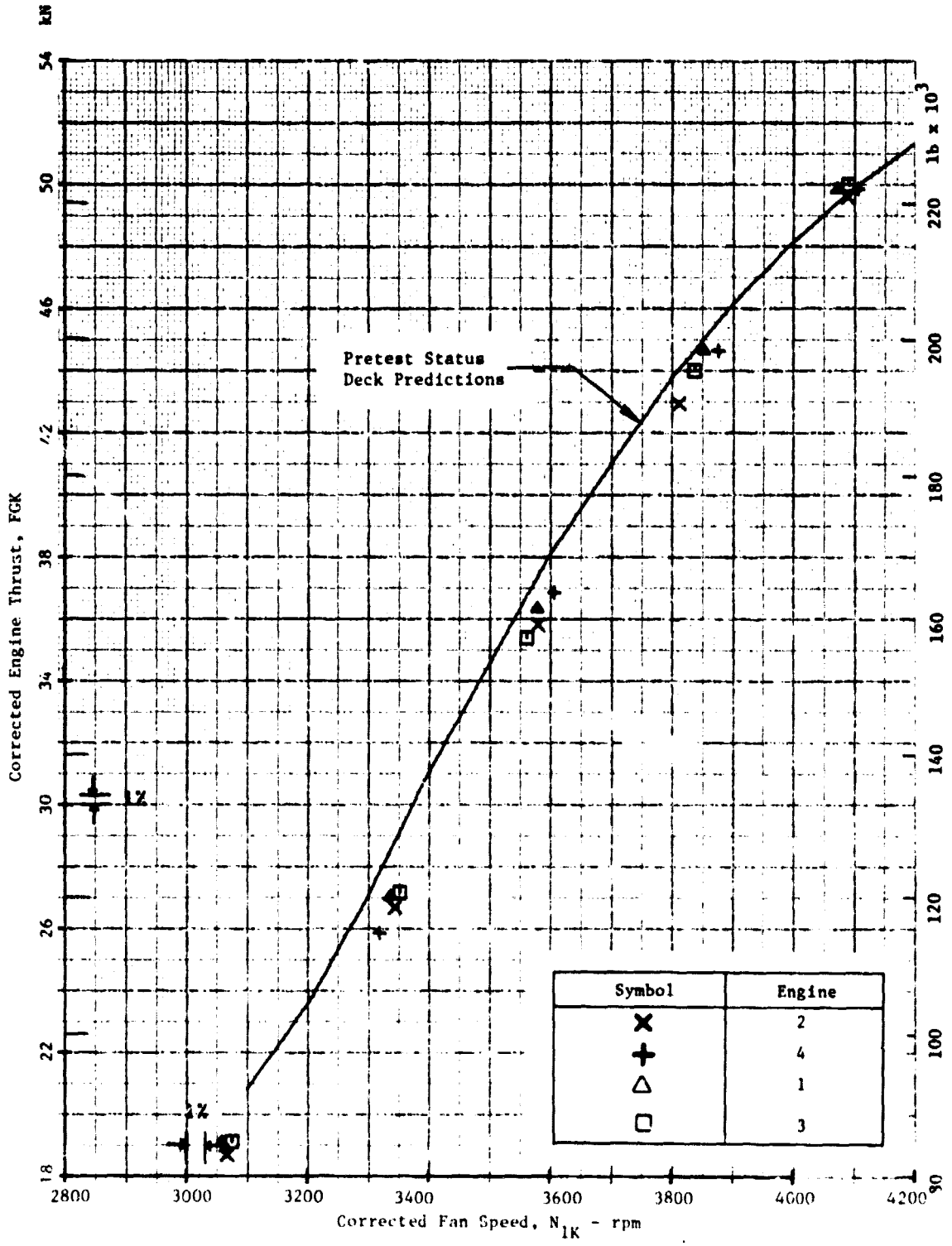

Figure 119. TBC B747 Flight Test at 35,000/0.85 M_o; ATC Corrected Thrust Versus Corrected Fan Speed for CF6-50 Engine with Improved Fan.

The data, as presented, were used to define the power management for the improved fan engine. Power management fan speeds are determined by entering the curves at the appropriate thrust level for each flight rating condition and determining the fan speed required based on the flight test data as shown in Figure 120. The resulting fan speeds are combined in a curve form for each rating (takeoff, maximum climb, maximum cruise, etc.). A typical end product power managament curve for takeoff is shown in Figure 121. The curve shows the altitude fan speed adjustment required for the improved fan as compared to the original CF6 production fan. As anticipated, the power management speeds required to achieve thrust for the improved fan engine are different than those required to obtain the same thrust on the baseline engine as shown in Figure 122. Since 1% delta fan speed is equivalent to approximately 2% delta thrust, the requirement for the new power management is evident from this figure.

This general procedure for power mangement definition was used for the DC-10, the B-747, and the A300 applications of the improved fan engine. A typical power management curve for the CF6-50E2 engine with the improve fan is presented in Figure 122 for a rolling takeoff of the B747-200 aircraft. The actual required fan speed at 0.1 M_o is shown as a function of the ambient temperature and altitude.

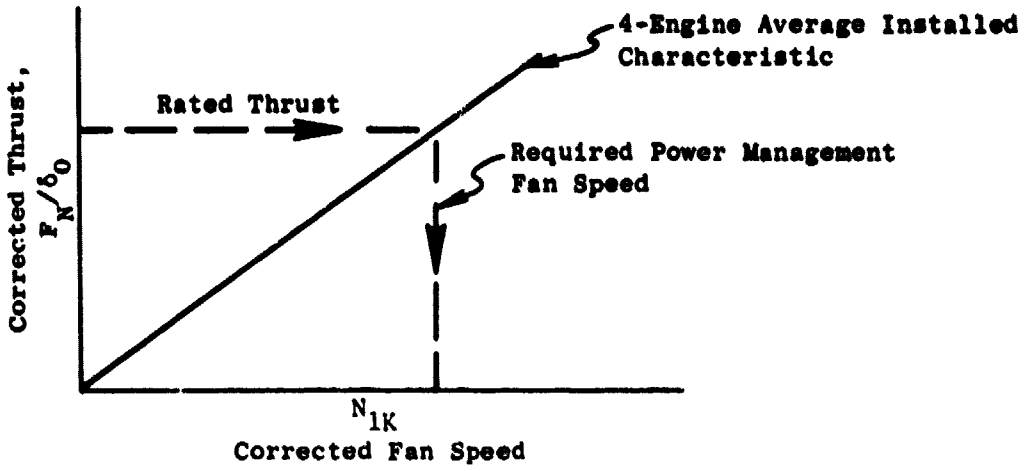

Figure 120. Typical Thrust Versus Corrected Fan Speed Characteristic.

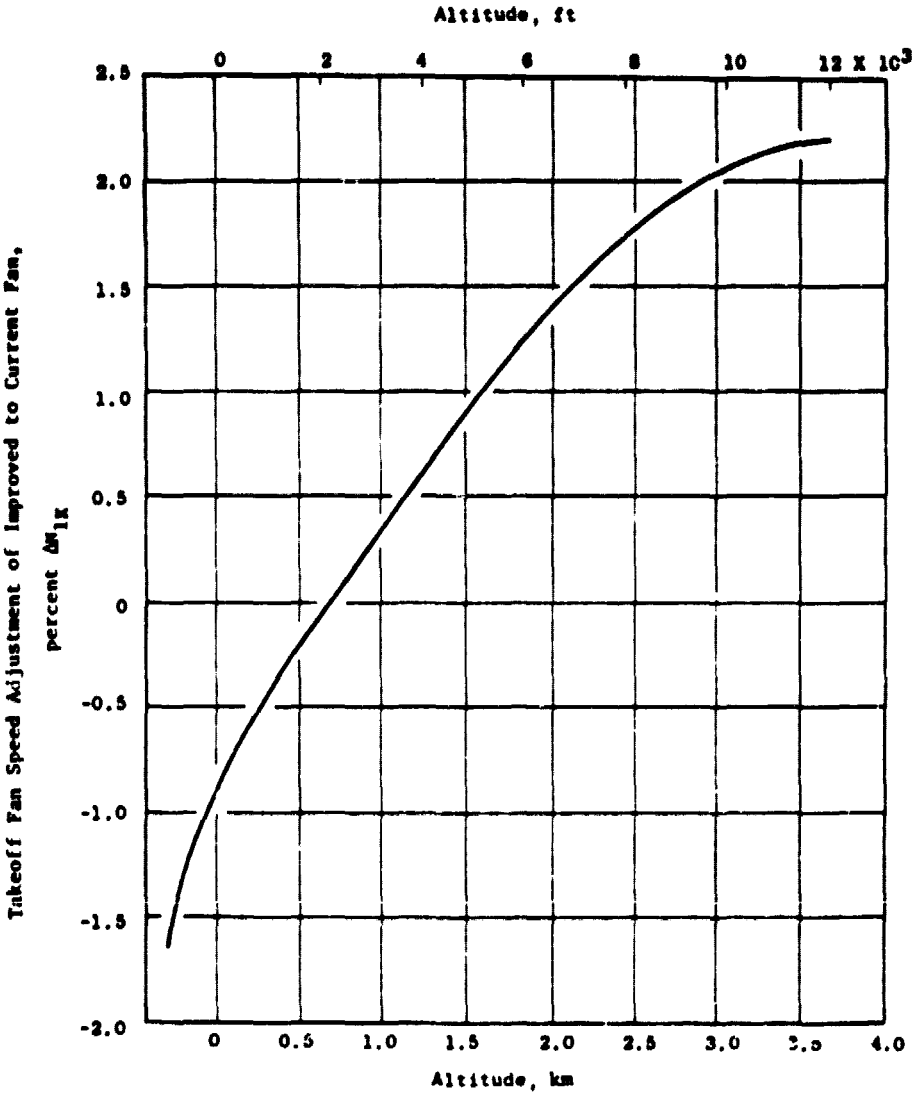

Figure 121. CF6-50 Engine Takeoff Power Management Curve: Fan Speed Adjustment Versus Altitude for the Improved Fan Compared to Current Baseline Fan.

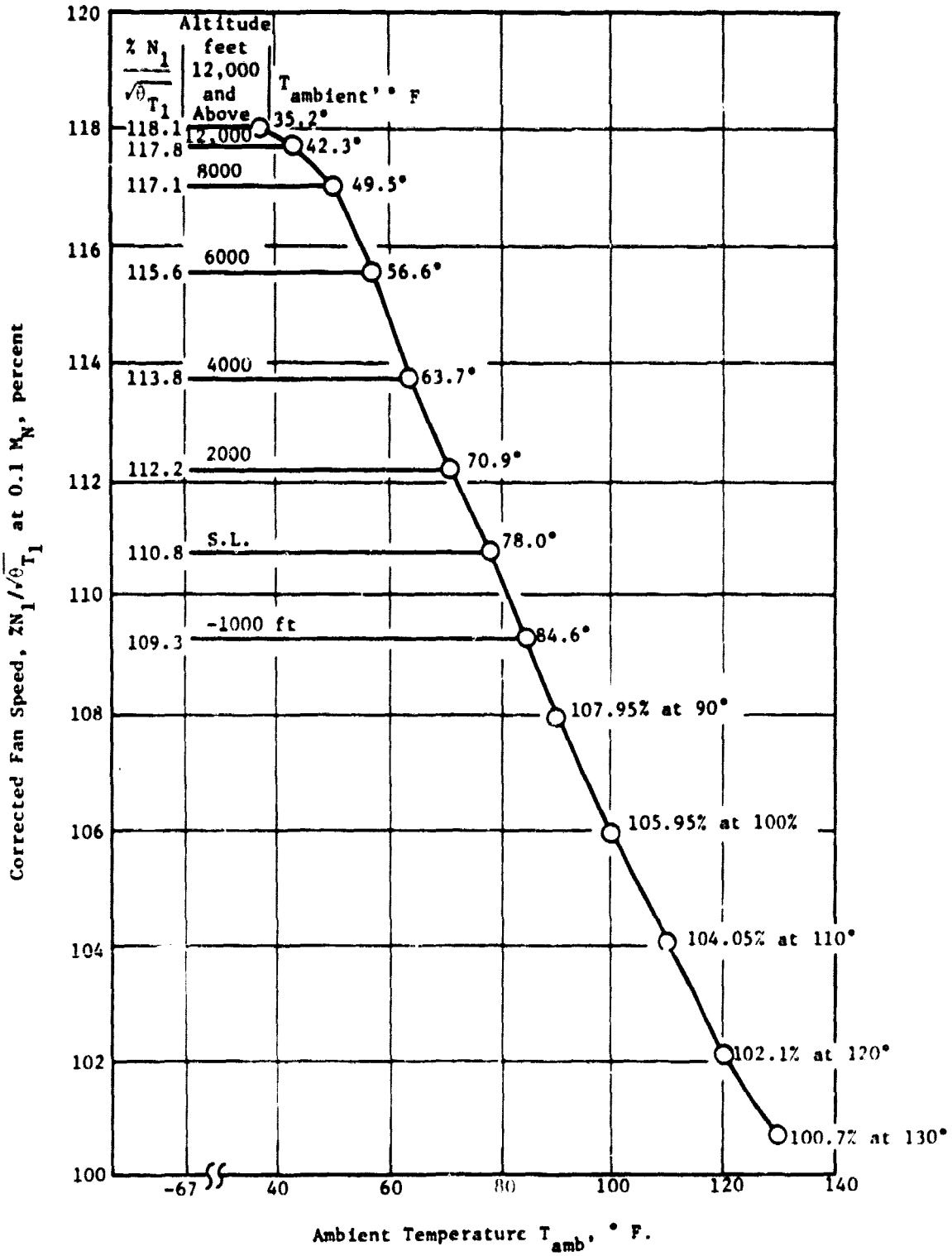

Figure 122. B747-200/CF6-50E2 Rolling Takeoff Fan Speed Versus Ambient Temperature.

10.0 ENGINE CYCLIC ENDURANCE TEST

Objectives of the cyclic endurance test were to demonstrate the life capability of the improved fan blades and the fan case stiffener; assess the wear characteristics of the fan blade part-span shrouds and dovetails; and assess fan blade leading edge deterioration and wear due to erosion.

In addition, a fan blade/shroud rub test was conducted to determine any indications of blade and casing interaction due to heavy rubs into the smooth microballoon tip shroud material.

10.1 TEST FACILITY, CONFIGURATION, AND INSTRUMENTATION

The cyclic endurance test was conducted at the General Electric outdoor test site (Figure 123). This site contains an outdoor frame structure with an overhead engine mounting. No provisions have been made on this site for thrust measurement. Automatic data handling in the adjacent control blockhouse was processed on the Evendale-based time-sharing computer.

The test vehicle for the cyclic endurance test was a CF6-50 engine (Figure 124). The final fan configuration consisted of restaggered improved fan blades, a fan case stiffener, a smooth microballoon fan casing tip shroud, and a reduced fan tip clearance of 2.16 mm (0.085 in.).

Instrumentation for this cyclic endurance test consisted of standard engine safety and monitoring instrumentation. Steady-state instrumentation included 86 pressures, 200 temperatures, fan and core speeds, and six liquid flows.

10.2 TEST DESCRIPTION

In order to simulate the most severe engine operating conditions during an actual flight mission, an abbreviated 15-minute simulated "C" cycle was defined as shown in Figure 125.

Initially, the engine was installed with improved fan blades, a fan case stiffener, aluminum honeycomb casing tip shrouds, and a reduced fan tip clearance of 2.92 mm (0.115 in.). Following a mechanical checkout and break-in run, cyclic testing was initiated. After completing 34 cycles, testing was interrupted to replace the open cell aluminum honeycomb Stage 1 fan shroud with a smooth shroud composed of microballoon-filled epoxy in Nomex honeycomb. The Stage 1 blade-to-case clearances were set to 0.61 mm (0.024 in.) minimum near the blade leading edge, and 0.84 mm (0.033 in.) minimum near the blade trailing edge. A series of slow accels and throttle bursts was made in increments up to 4040 rpm fan speed (approximately 106% of takeoff speed) to observe any indications of blade and casing interaction

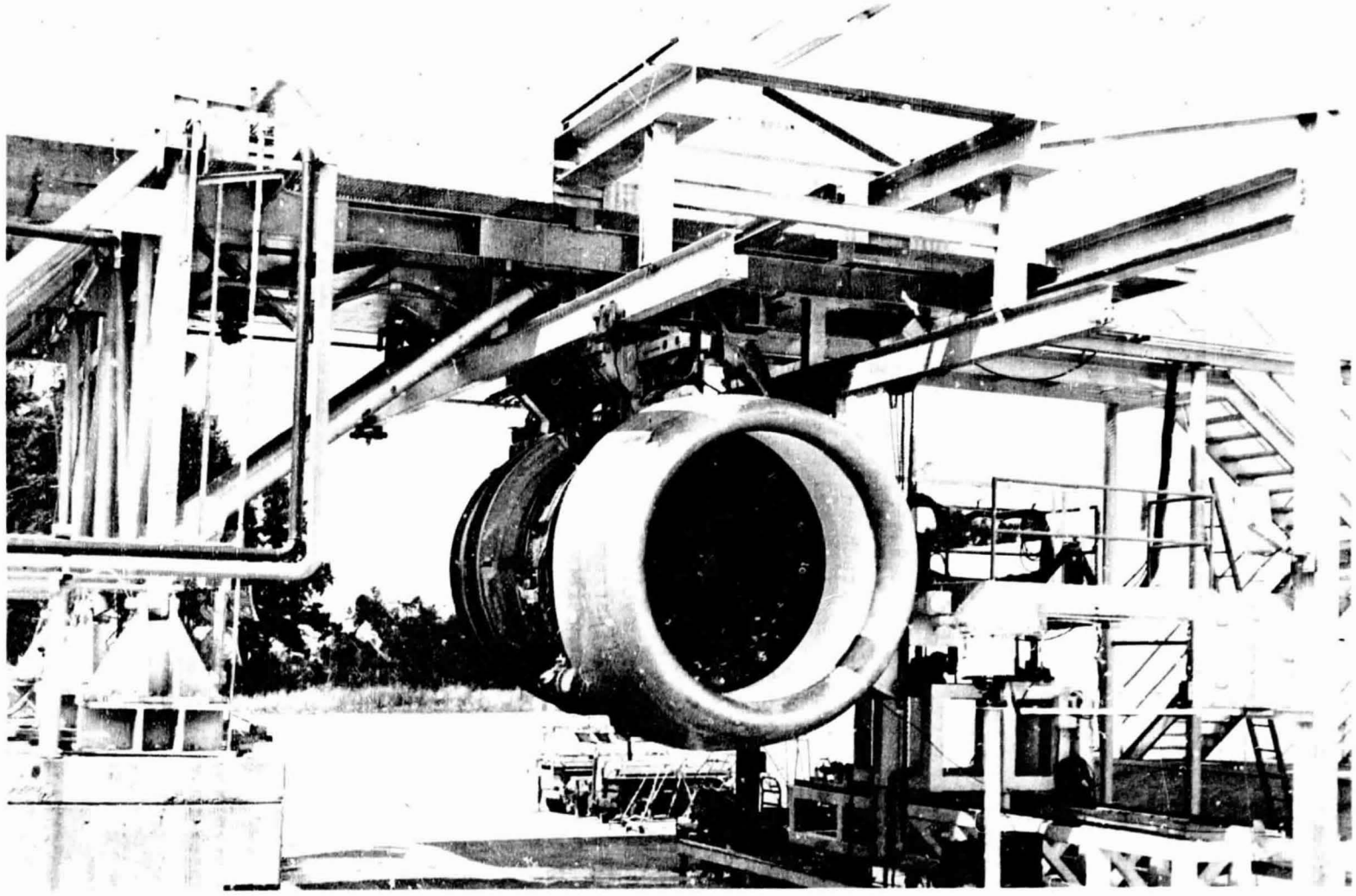

Figure 123. CF6-50 Engine Installed for Cyclic Endurance Test.

ORIGINAL PAGE IS
OF POOR QUALITY

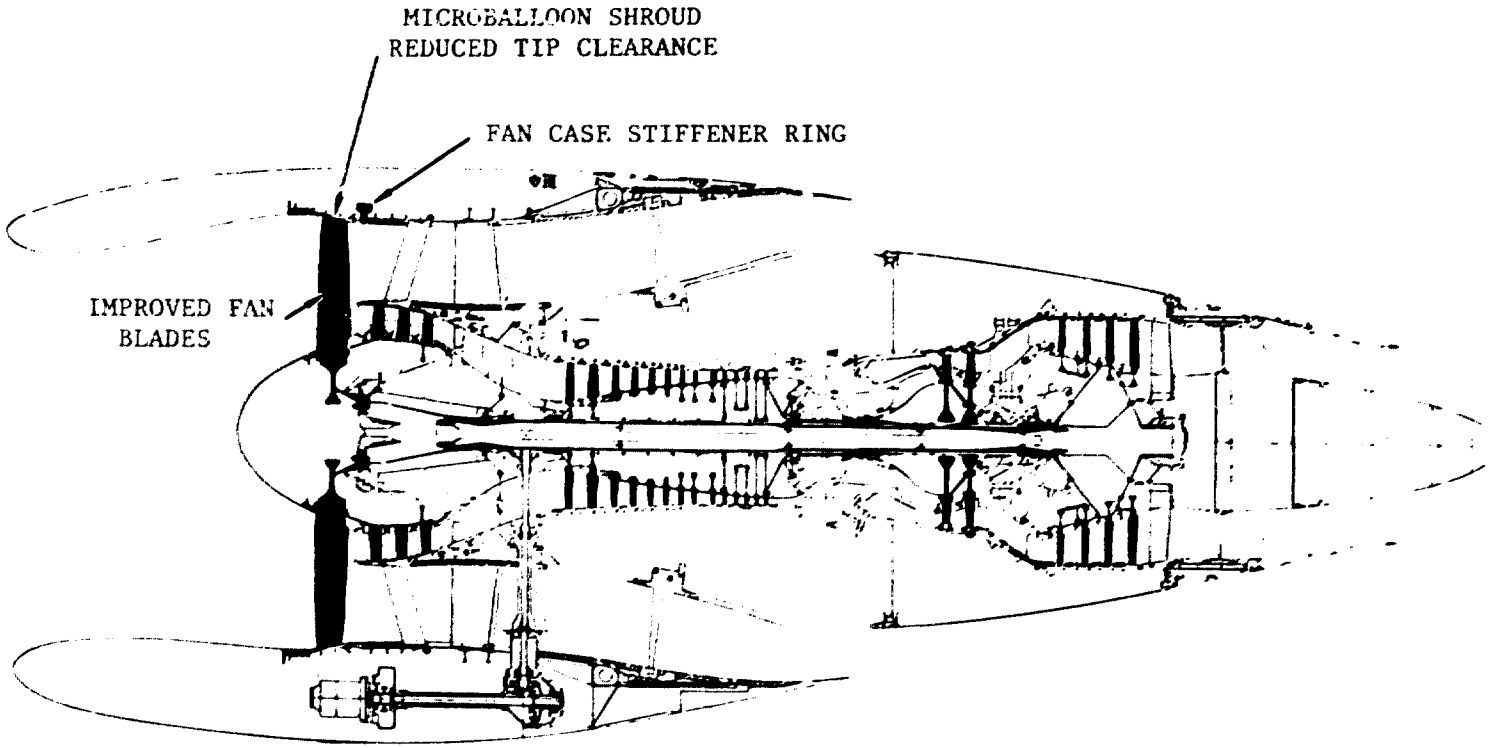

Figure 124. CF6-50 Engine: Fan Performance Improvement Concept.

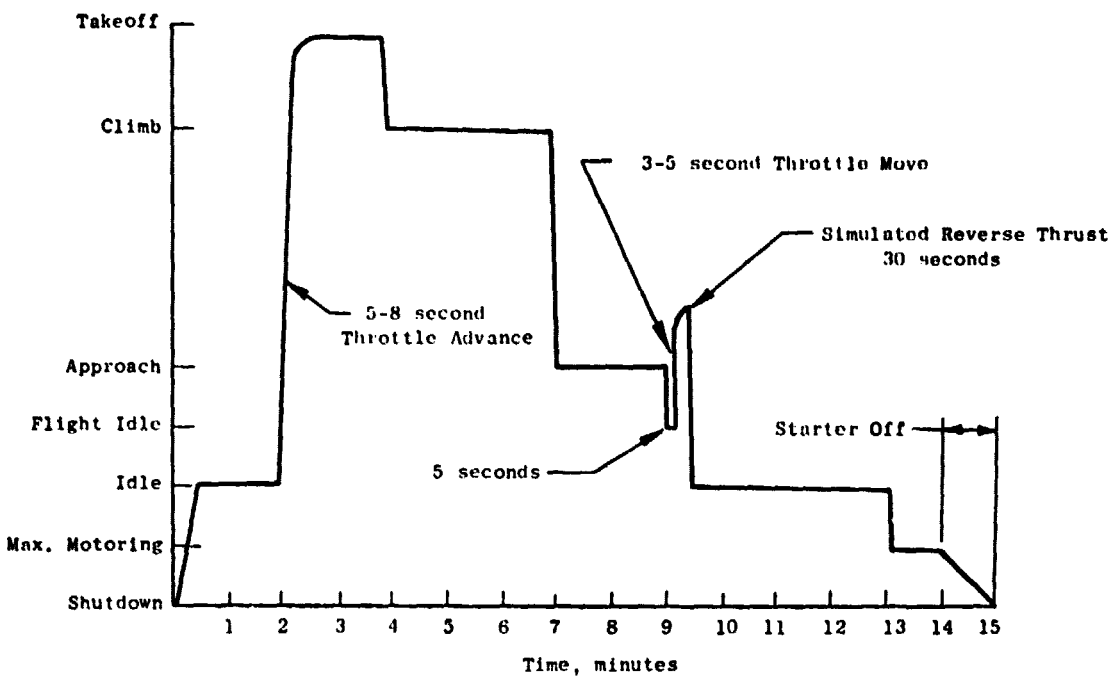

Figure 125. "C" Cycle Definition for Engine Cyclic Endurance Test to Simulate Actual Flight Mission.

due to heavy rubs into the microballon shroud material. No evidence of interaction was observed in visual examination of the shroud rub pattern, in the analysis of the outputs from the fan stator casing accelerometers which had been installed for this test, or in the high speed movies taken during the test. Figure 126 depicts rub depths incurred during the test.

Following this blade/shroud interaction test, the improved fan blades were removed and a new set of restaggered improved fan blades was installed, and fan tip clearance was reduced to 2.16 mm (0.085 in.). Endurance testing was resumed. After completing 1000 simulated "C" cycles, additional testing was performed to check out a new design main engine control prior to installing this control on flight test engines. Following this testing, the engine was returned to the development assembly area for teardown. The total number of cycles amounted to 1036.

During cyclic endurance testing, an effort was made to achieve various levels of peak exhaust gas temperature (EGT) at takeoff to simulate the distribution of takeoff temperatures seen in airline service. This "mission mix" was achieved by advancing the throttle beyond takeoff power or by engine bleed extraction, which generate the desired turbine temperatures at a given power setting. The mixture accomplished during this testing was:

	Takeoff EGT		
Type	°C	°F	Number of Cycles
M	<878	<1613	163
N	879-919	1614-1678	368
O	920-942	1679-1728	305
P	943-950	1729-1742	100
P_1	951-960	1743-1760	100
		Total	1036

10.3 TEST RESULTS AND DISCUSSION

The engine successfully completed more than 1000 "C" cycles of endurance testing on the improved fan blades and fan case stiffener. Visual inspection of the blades and stiffener showed them to be in excellent condition. Blade interlock surfaces show good contact areas and normal wear. Dovetail pressure faces still had Moly-Dag dry film lubricant present and showed the normal contact area. The blade tips indicated moderate rubs. There was no distress

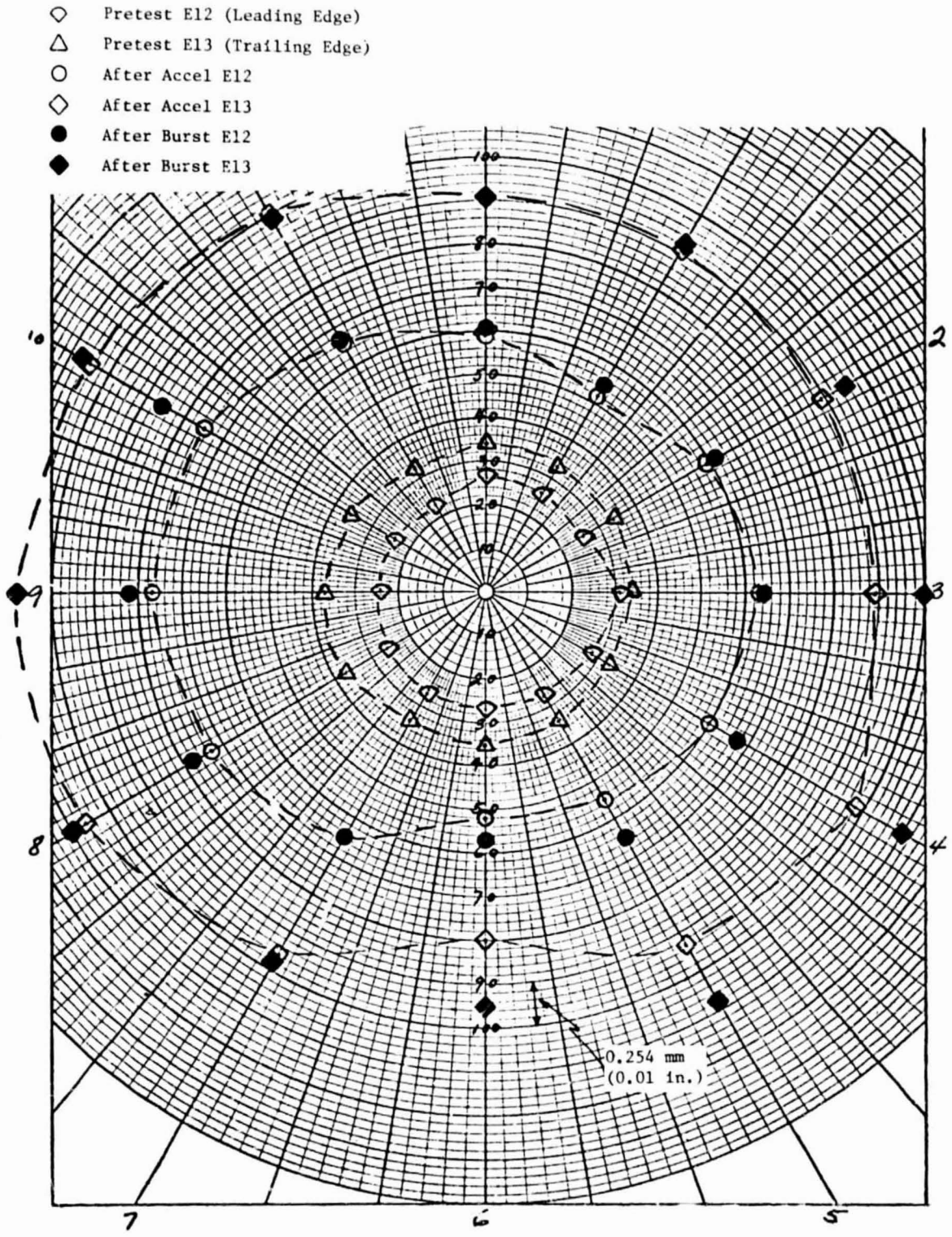

Figure 126. Smooth Microballoon Shroud Rub Patterns After Blade/Shroud Interaction Tests.

of the blade tips due to rubbing against the smooth microballoon fan casing tip shroud. There was a typical rub pattern on the tip of the blade, but no measurable amount of blade material lost. The fan blade leading edge showed no deterioration due to erosion or small particle pitting.

At the conclusion of the cyclic endurance testing, the fan blades were cleaned and fluorescent penetrant inspected. No cracks or distress of any kind were found from the fluorescent penetrant inspection. These results are comparable to results found on the original fan blades when tested in a similar manner. The endurance test results indicate that the improved fan blade would have mechanical performance in airline service equivalent to the original CF6 fan blade. There has been no low cycle fatigue limit on the original fan blade, and there has never been a fatigue failure of a fan blade in more than 12 million hours of airline service with approximately 18,000-20,000 hours on maximum high-time hardware.

Additional endurance testing outside the scope of this program has subsequently been performed to provide further design assurance for airline introduction. This additional testing has continued to confirm the mechanical integrity of the fan.

11.0 PRODUCTION ENGINE AND AIRCRAFT FLIGHT PERFORMANCE TESTS

The improved fan has been certified by the FAA in the CF6-50C2/E2 engines and is now in commercial service on the Boeing 747-200, Douglas DC-10-30, and Airbus Industrie A300B aircraft. CF6-50C2/E2 production engines have newly fabricated fan blades with the 1.5° restagger incorporated in the airfoil, the fan case stiffener, smooth microballoon casing tip shroud, fan tip clearance reduced 2.54 mm (0.100 in.), and a modified main engine control (closed stator vane schedule).

Testing of the average improved fan production engine in the Evendale production test cells has demonstrated sea level static sfc improvements relative to the current CF6-50 engine as shown in Figure 127. These improved fan engines demonstrated an average sfc improvement of 0.6% at sea level static takeoff power and 3.4% sfc improvement at thrust levels consistent with operation in the altitude cruise regime. This translates into an average cruise sfc improvement of 2.3%.

Flight test programs to demonstrate the cruise performance improvements of the CF6-50C2/E2 engines relative to the current models of the -50 engine were conducted on DC-10-30, B747-200, and A300B aircraft during 1978 and early 1979. Preliminary results substantiate an improvement in excess of 2.0% in cruise sfc throughout the normal cruise flight regime. About 0.2% of the improvement is attributed to the modified main engine control (closed stator vane schedule).

Sea level production engine testing and preliminary analysis of aircraft flight test result indicate that the objective cruise sfc performance improvement of 1.8% was demonstrated by the improved fan on the CF6-50 engine.

The improved fan will also be incorporated in the CF6-6D2C engine, and provides a basis for further improvements in other GE commercial engines, such as the CF6-80 and CF6-32 engines. Subsequent production engine tests of CF6-6D2C engines with the improved fan demonstrated an improvement in cruise sfc of 1.8% as compared to the predicted 1.6% (Reference 1).

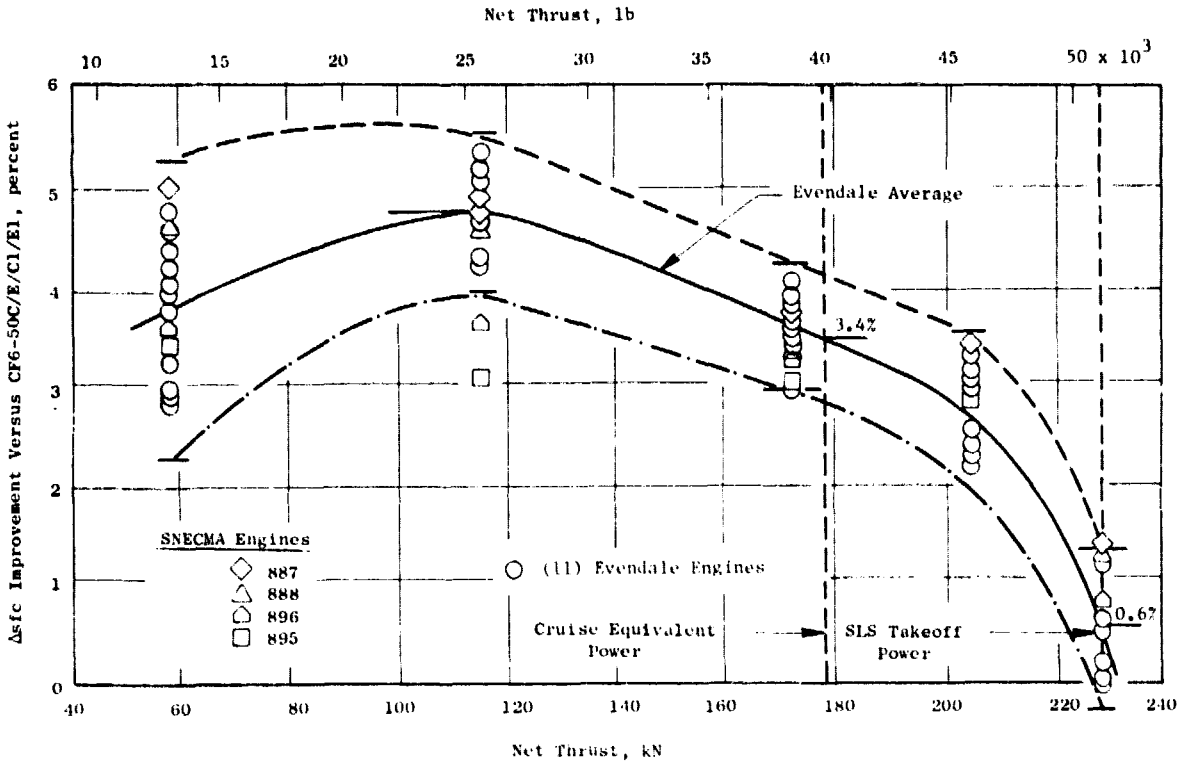

Figure 127. CF6-50C2 Production Engines SFC Improvement with Improved Fan.

12.0 ECONOMIC ASSESSMENT

The Fan Performance Improvement concept was evaluated by Boeing and Douglas during the Feasibility Analysis under Task 1 of this program (Reference 1). The initial new fan configuration consisted of improved fan blades, a fan case stiffener, a 1.50 mm (0.060 in.) reduction in fan tip clearance, and fan nozzle area change. This configuration was predicted to have a cruise sfc improvement of 1.8% for the CF6-50 engine on the DC-10-30 and B747-200 aircraft, and a cruise sfc improvement of 1.6% for the CF6-6 engine on the DC-10-10 aircraft.

Back-to-back sea level static engine performance tests demonstrated the predicted cruise sfc improvement of 1.8% with restaggered improved fan blades, the fan case stiffener, a smooth microballoon casing tip shroud, and the fan tip clearance reduced by 2.54 mm (0.100 in.). An additional improvement of 0.2% was obtained for a modification to the compressor variable stator vane (VSV) schedule. Flight tests of the improved fan with reduced clearance and a modified main engine control (closed stator vane schedule) conducted by Airbus Industrie, Boeing and Douglas on the A300B, B747-200 and DC-10-30, respectively, substantiated an improvement in excess of 2% in cruise sfc throughout the normal cruise flight regime.

The cruise sfc improvement of 1.8% for the CF6-50 and the CF6-6 engines due to the fan performance improvement results in the block fuel savings per aircraft shown in Table XII for the minimum fuel consumption mission analysis. Block fuel savings increase with increased range for all three aircraft. A 2.0% block fuel savings is projected for a new CF6 engine with the longest U.S. domestic and international mission ranges. The estimated annual fuel savings per aircraft for the above block fuel savings are also shown in Table XII, and indicates an annual fuel savings up to 1.37 million liters (0.36 million gallons) per aircraft.

Economic assessment of payback period (PBP) and return on investment (ROI) is summarized in Table XIII for the medium international fuel price of 14.53¢/l (55¢/gal) for the DC-10-30 and the medium domestic fuel price of 11.89¢/l (45¢/gal) for the DC-10-10 and the B747-200. Calculations indicate that the PBP for airlines to recover costs for the improved fan on a new CF6 engine is from 0.8 to 1.4 years. This low payback period makes the concept economically attractive to the airlines, so that introduction on new engines would be expected.

The new fan package has retrofit potential on an attrition basis. Such a retrofit would require new fan blades, a fan case stiffener, a new fan casing tip shroud, piping changes near the new fan case stiffener, and changes in engine power management.

Table XII. CF6 Engine with Improved Fan Aircraft - Fuel Savings/Analysis.

Aircraft (Engine)	Range		Block Fuel Savings/Aircraft		Annual Fuel Savings/Aircraft	
	km	miles	kg	%	ℓ/AC/yr	gal/AC/yr
DC-10-10 (CF6-6)	645	400	-134.2	-1.7	380,720	100,581
(Cruise Δsfc = -1.8%)	1690	1050	-294.0	-1.8	546,510	144,388
	3700	2300	-631.8	-2.0	[illegible],000	164,861
DC-10-30 (CF6-50)	805	500	-104.3	-1.1	270,440	71,450
(Cruise Δsfc = - 1.8%)	2735	1700	-412.8	-1.6	503,640	133,062
	6275	3900	-1157.6	-2.0	1,013,200	267,688
B747-200 (CF6-50)	770	480	-123.0	-1.1	365,610	96,595
(Cruise Δsfc = -1.8%)	3460	2150	-712.0	-1.7	669,910	176,991
	6195	3850	-1497.0	-2.0	1,369,580	361,844

Table XIII. CF6 Engine with Improved Fan - Economic Assessment of Payback Period and Return on Investment for New Buy.

(Medium Range, Medium Fuel Price, Minimum Fuel Analysis)

Aircraft Engine	Payback Period, years	Return on Investment, %
DC-10-10 (CF6-6) (Cruise Δsfc = -1.8%)	1.4	73
DC-10-30 (CF6-50) (Cruise Δsfc = -1.8%)	1.2	85
B747-200 (CF6-50) (Cruise Δsfc = -1.8%)	0.8	123

13.0 SUMMARY OF RESULTS

As part of the NASA-sponsored Engine Component Improvement Program, a new fan package has been developed to reduce fuel consumption in current CF6 turbofan engines for today's wide-bodied commericial aircraft. This new fan package consists of an improved CF6 fan blade, reduce fan tip clearances due to a fan case stiffener, and a smooth casing tip shroud (microballoon epoxy in open-cell aluminum honeycomb).

The new CF6 fan program was a 20-month effort that included component and full scale engine testing and monitoring of aircraft flight tests. Component tests consisted of a model fan rotor photoelastic stress test and a full-sized fan blade bench fatigue test. CF6-50 engine testing included back-to-back performance and acoustic tests, a power management test, a crosswind test, and a cyclic endurance test.

FAN ROTOR PHOTOELASTIC TEST

The photoelastic test of a 0.6 scale fan rotor with the improved fan blades showed no life limiting stresses, although some local stress levels were found to be higher than those determined by other means. In almost every instance, the finite element analysis predicts lower stresses than the photoelastic results. In general, the stress distributions are very similar to the ones obtained from finite element analysis. Evaluation of three different shank designs indicates that the standard half-pocket shank is a good compromise for light weight and low stress. Improved stress freezing procedures were developed for large-size fan blades due to some unforseen problems which were encountered, such as shroud "shingling", gravity load effects, and model defects.

FAN BLADE BENCH FATIGUE TEST

Bench fatigue test results with both the round bar test specimens and the finished airfoil demonstrated that the new fan blade design is equal in fatigue margin to the current CF6 fan blade. The current CF6 fan blade has never experienced a fatigue failure in over 12 million flight hours. The fatigue testing demonstrated that the new fan blade has no high stress risers that degrade the fatigue strength of the design. A substantial margin exists between measured engine stresses and the fatigue capability of the design.

ENGINE CROSSWIND TEST

Crosswind testing demonstrated that the new fan blade has similar crosswind/distortion characteristics to the original CF6 fan blade. Results indicate that the new fan blade can operate successfully without exceeding vibratory stress limits with both the DC-10-30 and B747 inlets at allowable takeoff crosswinds up to 35 knots.

ENGINE PERFORMANCE TEST

CF6-50 engine back-to-back sea level and simulated altitude performance tests demonstrated the predicted altitude cruise sfc improvement of 1.8% for the improved fan compared to the original fan. Over 20 engine tests were conducted in order to verify the predicted performance improvement. The final new fan package consists of:

- Improved fan blades restaggered to close blade about 1.5° at part-span shroud
- Reduction in fan tip clearance of 2.5 mm (0.100 in.)
- Fan case stiffener
- Smooth casing tip shroud (microballoons in open cell honeycomb).

Fan tests with tip rub buttons indicated that the fan case stiffener provided a significant improvement in fan casing roundness compared to the unstiffened case. This permits reduced operating fan tip clearances and improved fan efficiency. Fan efficiency increased about 4.5% for the improved fan blade with 1.5 mm (0.060 in.) reduced tip clearances, which was generally consistent with predictions. Restaggering the blade about 1.5° and reducing tip clearance an additional 1.0 mm (0.040 in.) resulted in a slight increase in fan efficiency at lower flow (cruise power range) and a slight decrease in fan efficiency at high flow (takeoff power).

The 1.0% increase in fan nozzle exit area did not provide a measurable improvement in cruise fuel consumption; and consequently, no change in the fan exit area is utilized in the new fan package, as finally developed.

Exhaust diffusers for the fan and primary nozzles provided an effective simulation of altitude cruise engine operating lines in a sea level test facility. Using normalized nozzle pressures and fuel flow data from the test runs with the diffusers is a viable method of obtaining cruise performance estimates.

ENGINE ACOUSTIC TEST

Back-to-back engine acoustic tests established that the use of the improved fan in the CF6-50 engines in the DC-10-30, B747-200 and A300B aircraft, or in the CF6-6 engines of the DC-10-10 aircraft, will have noise characteristics comparable to the original production fan. The FAA has accepted the acoustic equivalency of the two fans. The improved fan offers a significant reduction in multiple pure tones, or buzz saw noise, compared to the original fan and should significantly reduce aircraft passenger compartment noise levels during aircraft takeoff and initial climbout. Use of the original CF6 fan blade with a reduced fan tip clearance of about 1.14 mm (0.045 in.) and a smooth microballoon casing tip shroud will likewise have comparable community noise exposure to the original production fan.

ENGINE POWER MANAGEMENT TEST

Power management tests of the CF6-50 engine with the improved fan defined the fan speed/engine thrust relationship for the DC-10-30, B747-200, and A300B aircraft. Full scale fan nozzle thrust and flow coefficients were determined from instrumented engine ground tests and correlated with aircraft flight tests.

ENGINE CYCLIC TEST

The CF6-50 engine with the improved fan blades and fan case stiffener successfully completed over 1000 "C" cycles of cyclic endurance testing. the blades and stiffener were in excellent condition without any cracks or signs of distress. A separate blade/shroud rub test indicated that no evidence of blade and casing interaction due to heavy rubs into the smooth microballoon tip shroud material.

PRODUCTION ENGINE AND AIRCRAFT FLIGHT PERFORMANCE TESTS

As a direct result of the above tests and additional General Electric-sponsored efforts, the development and certification of the improved fan were continued, and the fan is now being introduced into airline service. DC-10, B747, and A300B aircraft flight tests were completed. Subsequent SLS production engine and aircraft flight tests confirmed the cruise sfc improvement of 1.8% for the improved fan. The improved fan has been certified by the FAA for use in the CF6-50C2/E2 engines and is now in commercial service on the Boeing 747-200, Douglas DC-10-30, and Airbus Industrie A300B aircraft.

Subsequent production engine tests of CF6-6D2C engines with the improved fan also demonstrated an improvement in cruise sfc of 1.8% as compared to the predicted 1.6%. The improved fan is also offered for CF6-6 retrofit.

ECONOMIC ASSESSMENT

Based on the demonstrated cruise sfc improvement of 1.8%, a 2.0% block fuel savings per aircraft is projected for a new CF6-50 engine with the improved fan for the longest U.S. domestic and international mission. The improved fan concept offers an annual fuel savings per aircraft up to 1.37 million liters (0.36 million gallons), depending on aircraft application and mission range. A low payback period of 0.8 to 1.4 years makes the concept economically attractive for the airlines to recover costs. The new fan package has retrofit potential on an attrition basis with new fan blades, a new fan case stiffener, a new fan casing tip shroud, minor piping changes, and changes in engine power management.

C-3

APPENDIX A

QUALITY ASSURANCE

INTRODUCTION

The quality program applied to this contract is a documented system throughout the design, manufacture, repair, overhaul, and modification cycle for gas turbine aircraft engines. The quality system has been constructed to comply with military specifications MIL-Q-9858A, MIL-I-45208, and MIL-C-45662 and Federal Aviation Regulations FAR-145 and applicable portion of FAR-21.

The quality system and its implementation are defined by a complete set of procedures which has been coordinated with the DOD and FAA and has their concurrence. In addition, the quality system as described in the quality program for this contract has been coordinated with NASA-Lewis Research Center. The following is a brief synopsis of the system.

QUALITY SYSTEM

The quality system is documented by operating procedures which coordinate the quality-related activities in the functional areas of Engineering, Manufacturing, Materials, Purchasing, and Engine Programs. The quality system is a single-standard system wherein all product lines are controlled by the common quality system. The actions and activities associated with determination of quality are recorded, and documentation is available for review.

Inherent in the system is the assurance of conformance to the quality requirements. This includes the performance of required inspections and tests. In addition, the system provides change control requirements which assure that design changes are incorporated into manufacturing, procurement and quality documentation, and into the products.

Measuring devices used for product acceptance and instrumentation used to control, record, monitor, or indicate results of readings during inspection and test are initially inspected and calibrated and periodically are reverified or recalibrated at a prescribed frequency. Such calibration is performed by technicians against standards which are traceable to the National Bureau of Standards. The gages are identified as a control number and are on a recall schedule for reverification and calibration. The calibration function maintains a record of the location of each gage and the date it requires recalibration. Instructions implement the provisions of MIL-C-45662 and the appropriate FAR requirements.

PRECEDING PAGE BLANK NOT FILMED

Work sent to outside vendors is subject to quality plans which provide for control and appraisal to assure conformance to the technical requirements. Purchase orders issued to vendors contain a technical description of the work to be performed and instructions relative to quality requirements.

Engine parts are inspected to documented quality plans which define the characteristics to be inspected, the gages and tools to be used, the conditions under which the inspection is to be performed, the sampling plan, laboratory and special process testing, and the identification and record requirements.

Work instructions are issued for compliance by operators, inspectors, testers, and mechanics. Component part manufacture provides for laboratory overview of all special and critical processes, including qualification and certification of personnel, equipment and processes.

When work is performed in accordance with work instructions, the operator/inspector records that the work has been performed. This is accomplished by the operator/inspector stamping or signing the operation sequence sheet to signify that the operation has been performed.

Various designs of stamps are used to indicate the inspection of status of work in process and finished items. Performance or acceptance of special processes is indicated by distinctive stamps assigned specifically to personnel performing the process or inspection. Administration of the stamp system and the issuance of stamps are functions of the Quality Operation. The stamps are applied to the paperwork identifying or denoting the items requiring control. When stamping of hardware occurs, only laboratory approved ink is used to assure against damage.

The type and location of other part marking are specified by the design engineer on the drawing to assure effects do not compromise design requirements and part quality.

Control of part handling, storage and delivery is maintained through the entire cycle. Engines and assemblies are stored in special dollies and transportation carts. Finished assembled parts are stored so as to preclude damage and contamination, openings are covered, lines capped and protective covers applied as required.

Nonconforming hardware is controlled by a system of material review at the component source. Both a Quality representative and an Engineering representative provide the accept (use-as-is or repair) decisions. Nonconformances are documented, including the disposition and corrective action if applicable to prevent recurrence.

The system provides for storage, retention for specified periods, and retrieval of nonconformance documentation. Documentation for components is filed in the area where the component is manufactured/inspected.

APPENDIX B

NOMENCLATURE

A_o	Stress Ratio (Alternating/Mean)
ALF	Aft Looking Forward
C/A	Chromel-Alumel
C/C	Copper-Constantan
CFG28	Fan Nozzle Thrust Coefficient
CW28	Fan Nozzle Flow Coefficient
DA	Double Amplitude
Dia	Diametral
DMS	Data Monitoring System
DOD	Department of Defense
EBU	Engine Buildup
EGT	Exhaust Gas Temperature, ° C (° F)
EPNL	Effective Perceived Noise Level, EPNdB
FAA	Federal Aviation Administration
FGK	Corrected Thrust, FN/δ_o, N (lb)
$FN/\delta 2$	Corrected Thrust, N (lb)
GE	General Electric
ID	Inner Diameter, mm (in.)
IDC	Inlet Distortion Circumferential
IDR	Inlet Distortion Radial
K_t	Stress Concentration Factor
LCF	Low Cycle Fatigue
LE	Leading Edge
LRCN	Long Reversing Core Nozzle
MDOF	Multiple Degree of Freedom
MPT	Multiple Pure Tones
N	Newton
N_1	Physical Fan Speed, rpm
N_{1K}	Corrected Fan Speed, rpm
NASA	National Aeronautical and Space Administration

P	Pressure, N/cm^2 ($lb/in.^2$)
P_o	Ambient Pressure, N/cm^2 ($lb/in.^2$)
PEDS	Portable Environmental Data Station
PNL	Perceived Noise Level, PNdB
PNLT	Perceived Noise Level, Tone Corrected, PNdB
REV	Revolution
RH	Relative Humidity, %
ROI	Return on Investment, %
rpm	Revolution per Minute
SA	Single Amplitude
SDOF	Single Degree of Freedom
sfc	Specific Fuel Consumption, kg/hr/N (lb/hr/lb)
SL	Side Line
SLS	Sea Level Static
SPL	Sound Pressure Level, dB re 2×10^{-5} N/m^2 ($lb/in.^2$)
T_1	Inlet Total Temperature, ° C, (° F)
T_{amb}	Ambient Temperature, ° C (° F)
TE	Trailing Edge
T_o	Ambient Temperature, ° C (° F)
$\theta^\bullet$	Polar Angle Referenced to Engine Centerline, Clockwise From Inlet, Degrees
σ	Standard Deviation

APPENDIX C

REFERENCES

1. Fasching, W.A., "CF6 Jet Engine Performance Improvement Program, Task I - Feasibility Analysis," NASA CR-159450 (GE R79AEG295), March 1979.

2. Patt, R.F. and Reemsynder, D.C., "CF6 Fan Performance Improvement," ASME Paper, March 1980.

3. Society of Automotive Engineers, Aerospace Recommended Practice ARP 866A, "Standard Values of Atmospheric Absorption as a Function of Temperature and Humidity for Use in Evaluating Aircraft Flyover Noise," Revised March 15, 1975.